



HAL
open science

Injectable and self-healing polysaccharide hydrogels via boronate ester bonds: relationships between the binding mode of boronic acids to saccharide moieties and the macroscopic mechanical properties

Tamiris Vilas Boas Figueiredo

► To cite this version:

Tamiris Vilas Boas Figueiredo. Injectable and self-healing polysaccharide hydrogels via boronate ester bonds: relationships between the binding mode of boronic acids to saccharide moieties and the macroscopic mechanical properties. *Polymers*. Université Grenoble Alpes, 2018. English. NNT : 2018GREAV048 . tel-03510315

HAL Id: tel-03510315

<https://theses.hal.science/tel-03510315>

Submitted on 4 Jan 2022

HAL is a multi-disciplinary open access archive for the deposit and dissemination of scientific research documents, whether they are published or not. The documents may come from teaching and research institutions in France or abroad, or from public or private research centers.

L'archive ouverte pluridisciplinaire **HAL**, est destinée au dépôt et à la diffusion de documents scientifiques de niveau recherche, publiés ou non, émanant des établissements d'enseignement et de recherche français ou étrangers, des laboratoires publics ou privés.

THÈSE

Pour obtenir le grade de

DOCTEUR DE LA COMMUNAUTE UNIVERSITE GRENOBLE ALPES

Spécialité : **Sciences des Polymères**

Arrêté ministériel : 25 mai 2016

Présentée par

Tamiris VILAS BOAS FIGUEIREDO

Thèse dirigée par **Rachel AUZELY-VELTY**

préparée au sein du **CERMAV**
dans l'**École Doctorale Chimie et Sciences du Vivant**

Injectable and self-healing polysaccharide hydrogels via boronate ester bonds: relationships between the binding mode of boronic acids to saccharide moieties and the macroscopic mechanical properties

Thèse soutenue publiquement le **5 décembre 2018**,
devant le jury composé de :

Monsieur François TOURNILHAC

Directeur de Recherche, CNRS, ESPCI Paris, Rapporteur

Monsieur Patrice WOISEL

Professeur des Universités, Université de Lille, Rapporteur

Monsieur Pierre SCHAAF

Professeur des Universités, Université de Strasbourg, Examineur

Madame Sandrine PY

Directeur de Recherche, CNRS, UGA, Président

Monsieur Christophe MARQUETTE

Directeur de Recherche, CNRS, Université Lyon 1, Examineur

Monsieur Craig HARRIS

Chercheur R&D, Nestlé Skin Health, Examineur

Madame Rachel AUZELY-VELTY

Professeur des Universités, UGA, Directeur de thèse

Madame Jing JING

Chercheur R&D, Nestlé Skin Health, Invité



A mes parents,

A mon frère,

A Guillaume

Je tiens d'abord à remercier tous les membres du jury pour le temps qu'ils ont consacré à évaluer mes travaux de thèse. Je remercie ainsi le Prof. Patrice Woisel et le Dr. François Tournilhac d'avoir accepté d'être rapporteurs de mon travail. Mes remerciements vont également au Prof. Pierre Schaaf et aux docteurs Sandrine Py, Christophe Marquette et Craig Harris pour leur participation au jury de thèse. La discussion très intéressante et enrichissante ainsi que les conseils apportés lors de la soutenance de thèse ont rendu ce moment captivant.

Ces travaux ont été réalisés au CERMAV, unité de recherche du CNRS associée à l'Université Grenoble Alpes. Je remercie sa directrice, Anne Imberty, de m'avoir accueilli au sein du laboratoire. Je remercie également Anne Imberty pour les études de modélisation réalisées tout au début de ma thèse, ainsi que pour ses conseils concernant la calorimétrie de titration isotherme.

J'adresse mes sincères remerciements à ma directrice de thèse, Rachel Auzély, qui m'a donné l'opportunité de réaliser cette thèse captivante en collaboration avec la société Galderma/Nestlé Skin Health, tout en me faisant confiance. Je tiens à la remercier pour ses encouragements dans mes projets de recherche depuis le Master 2 PTA. Je lui suis très reconnaissante pour sa disponibilité immédiate et pour nos nombreuses discussions qui ont été essentielles pour ma formation en tant que jeune chercheur. Enfin, un grand merci pour ses conseils précieux et toute son aide durant ces quatre ans de travail ensemble, et notamment pour son soutien pour la suite de ma carrière en recherche.

Je tiens également à remercier nos collaborateurs industriels de la société Galderma/Nestlé Skin Health qui a financé ce projet, basés sur les sites de R&D en France (Sophia Antipolis) et en Suède (Uppsala). Je les remercie pour cette excellente collaboration, marquée par des réunions et discussions scientifiques très enrichissantes. Je suis très reconnaissante, tout particulièrement, aux docteurs Jing Jing et Craig Harris pour leur forte implication dans ce projet, ainsi que pour leurs encouragements et leur sympathie admirable.

Mes remerciements vont également aux docteurs Vanina Cosenza et Yu Ogawa pour leurs études de modélisation moléculaire. Je les remercie énormément d'avoir partagé leurs connaissances précieuses sur les calculs théoriques qui m'ont indiscutablement permis d'évoluer scientifiquement.

Un grand merci à Isabelle Jeacomine pour son support avec la spectroscopie RMN tout au long de ces trois années. Je lui suis très reconnaissante pour sa forte implication dans cette thèse, notamment lors de l'implémentation d'analyses inédites au CERMAV et lors de la réalisation d'études de RMN à très hauts champs en collaboration avec la plateforme de RMN de l'IBS. Je tiens également à remercier Sonia Ortega pour son aide concernant la purification de dérivés de maltose par chromatographie (HPLC) et pour son support technique au laboratoire. Je remercie également les étudiants de Master 2, François Bulteau et Baptiste Quienne, qui ont réalisé les études biologiques sur les hydrogels d'acide hyaluronique en collaboration avec Grenoble Institut de Neurosciences (GIN), sous la direction du Prof. Rachel Auzély et des docteurs Claire Rome et Olivier Detante.

C'est aussi grâce à l'ensemble des personnes du CERMAV, permanents et non-permanents, que ces années se sont si bien passées ! Je souhaite exprimer toute ma gratitude à ceux et celles avec qui j'ai pu tisser des liens et partager des moments uniques.

Je remercie Eric Bayma, Pierre Sailler et Patrick Perez pour leur sympathie et leur bonne humeur quotidienne. Mes remerciements vont également à Martine Morales pour son grand cœur et sa gentillesse. Je tiens aussi à remercier Bruno Jean pour son accueil chaleureux lors de mon premier séjour au CERMAV en octobre 2012, ainsi que pour ses conseils et son attention depuis toujours. Un grand merci à Martine Broué, Sandrine Coindet, Kristina Slavcheva, Isabelle Caldara, Marie-France Métral, Christine Lancelot-Pin, Valérie Chazalet,

Emilie Gillon, Stéphanie Pradeau, Laurine Buon, Christophe Travelet, Sylvain Cottaz, Sami Halila, William Helbert, Sophie Drouillard, Bernard Priem, Cyril Bras, Christelle Breton pour leur gentillesse et pour quelques petits moments que nous avons pu partager au cours de ces années...

Un grand merci également aux non-permanents (doctorants, post-doctorants, stagiaires, CDD) des différents étages et différentes équipes : Charlène, Mathilde, Lauric, Julien, Clémentine, Yotam, Pierre, Yanis, Agustin, Khanh, Lea, Harisoa, Mélanie L., Rubal, Félix P., Milène, João, Félix C., Mickaël, Laurent P., Yingjie, Laurent G., Yoko, Johanna... Merci pour tous les moments d'échange vécus au laboratoire, à la cafétéria ou à l'extérieur, toujours avec de beaux sourires !

Je tiens tout particulièrement à remercier toutes les personnes de l'équipe « Structure et Modifications des Polysaccharides » pour tous les moments inoubliables partagés tout au long de ces années. Merci à Anna Szarpak pour les échanges lors des réunions d'équipe. Merci à Talitha Stefanello pour son aide au laboratoire lors de mon arrivée dans l'équipe en Master 2. Et un grand et chaleureux merci aux « jeunes du labo » qui ont sans doute rendu tous les jours plus agréables et joyeux : Marlène, Robin, Lisa, Fatma, Maxime Michelas et Maxime Leprince (mes co-bureaux du 110) ; Thaysa, Juliana et Takeshi (mes co-bureaux de l'aquarium) ; Dominte, François, Laurianne, Francielle, Vanina, Mariana, Claire, Simon, Baptiste, Raphaël.

Direction Bahia-B Brésil pour remercier également mes ami(e)s de l'autre côté de l'Atlantique ! Je remercie tous ceux et celles qui ont été à mes côtés malgré la distance. Merci à ma grande amie Flávia et à mon grand ami Vitor pour leur amitié et leur soutien depuis le lycée. Merci à mes copains et copines de la faculté de pharmacie et de mon premier laboratoire de recherche : Livia, Camylla, Ana Carla, Luana, Thamires, Denilson, Carolina, Jania, Márcio, Luciane, Gleice, Leonardo... Et merci également aux copains et copines du Master, Friaume, Benoît, Soline, Jordan M., Jordan D., pour les bons moments que nous partageons toujours.

Je remercie infiniment mon père, ma mère et mon frère pour leur soutien dans tous mes projets de vie. Je les remercie (et je leur serai éternellement reconnaissante) pour m'avoir donné la chance de poursuivre mes études en France depuis le Master. Si j'ai eu cette opportunité en or, c'est grâce à leur dévouement sans faille et leur générosité. Malgré la distance, c'est grâce à leur précieux support quotidien que je dois ma réussite. (Eu agradeço infinitamente meu pai, minha mãe e meu irmão pelo apoio em todos os meus projetos de vida. Agradeço-lhes muito (e serei eternamente grata a eles) por terem me dado a chance de continuar mes estudos na França desde o mestrado. Se eu tive essa oportunidade de ouro, foi graças à dedicação inabalável e à generosidade deles. Apesar da distância, eu devo meu sucesso ao precioso apoio diário deles.)

Et je remercie Guillaume de tout mon cœur, mon compagnon de vie et d'aventures, qui m'a soutenu tous les jours de cette thèse et depuis le Master. Merci énormément d'avoir été à mes côtés dans tous les moments, toujours à l'écoute et prêt à m'apporter sa force et ses encouragements. Je le remercie infiniment pour son dévouement quotidien et pour sa compagnie. Merci encore pour m'avoir fait découvrir la randonnée en montagne et l'univers montagnard, ainsi que la beauté et la douceur de vivre de ce pays. Enfin, merci beaucoup pour m'avoir accueilli aussi chaleureusement au sein de sa famille que je tiens également à remercier pour le soutien et pour tous les moments partagés en famille.

Merci à tous et à très bientôt !

Table of contents

General introduction	6
Chapter 1:	
<u>Self-healing hydrogels crosslinked by dynamic covalent boronate ester bonds: a literature review</u>	14
1. Introduction.....	14
2. Boronic acids and boronate ester chemistry.....	15
3. Design of reversible hydrogels crosslinked by boronate ester bonds.....	17
3.1. Hydrogels crosslinked via phenylboronic acid-diol complexation.....	18
3.2. Hydrogels crosslinked via benzoboroxole-diol complexation.....	27
4. Current biomedical applications of boronate-crosslinked hydrogels.....	32
4.1. Controlled release of bioactive molecules.....	32
4.2. Injectable hydrogels for 3D cell encapsulation.....	40
4.3. Other applications.....	44
5. Conclusions and future perspectives.....	46
6. References.....	47
Chapter 2:	
<u>Mechanistic insight into the macroscopic mechanical properties of boronate-crosslinked hyaluronic acid hydrogels in relation to the structure of the small molecular crosslinkers</u>	55
1. Introduction.....	56
2. Results.....	58
2.1. Modification of hyaluronic acid with phenylboronic acid, benzoboroxole and carbohydrate molecules.....	58
2.2. Synthesis of the boronate ester-crosslinked networks and rheological characterization.....	59
2.3. Relationships between the macroscopic mechanical properties of the HA networks and the small molecule crosslinkers.....	61
2.4. Influence of the pH on the HA-PBA (BOR)/HA-saccharide hydrogel networks.....	66

Table of contents

2.5. Determination of the structures of the boronic acid complexes with maltose and fructose grafted on HA.....	68
3. Discussion.....	74
4. Conclusion.....	78
5. Experimental section.....	79
6. References.....	84
Supporting information.....	89

Chapter 3:

<u>Self-crosslinking smart hydrogels through multivalent interactions between benzoboroxole derivatives and diols from hyaluronic acid.....</u>	141
1. Introduction.....	141
2. Results.....	143
2.1. Synthesis of benzoboroxole-modified HA and behavior in aqueous solution at neutral pH.....	143
2.2. Effect of molar mass and environmental parameters on the dynamic mechanical properties of HA-DMF6ABOR and HA-DM7ABOR conjugates.....	147
3. Discussion about the outstanding capability of DMF6ABOR and DM7ABOR to bind HA sugar units.....	155
4. Conclusion.....	158
5. Experimental section.....	159
6. References.....	162
Supporting information.....	165

Chapter 4:

<u>Injectable self-healing hyaluronic acid hydrogels based on boronate ester crosslinks between benzoxaborin derivatives and saccharides.....</u>	206
1. Introduction.....	206
2. Results.....	209
3. Conclusion.....	217
4. Experimental section.....	217
5. References.....	220
Supporting Information.....	223

Table of contents

General conclusions and perspectives	248
Appendix - List of Abbreviations	253

GENERAL INTRODUCTION

General introduction

Injectable and self-healing hydrogels have recently drawn great attention in the fields of tissue engineering and regenerative medicine for minimally invasive delivery of cells and in the filling of irregular defects.^{1,2} These hydrogels have been considered as an alternative to traditional injectable gels, which are produced by *in situ* crosslinking of polymer chains using environmental triggers (pH, temperature, ionic strength), cross-linking chemicals or UV-light.³⁻⁵ Potential drawbacks are indeed related to these conventional crosslinking approaches, such as potential adverse effects on cell viability and/or low gelation kinetics. For this reason, recent advances in biomaterials research have encouraged the design of new injectable hydrogels showing shear-thinning and self-healing properties. Such gels can be pre-formed into syringes, show viscous flow under shear stress (i.e. shear-thinning) and rapid recovery when the applied stress is removed (i.e. self-healing).⁶ The capability of these polymer networks to autonomously repair their structure and functionalities upon mechanical damage is due to the dynamic nature of their crosslinks. Among reversible polymeric assemblies, hydrogels crosslinked through dynamic covalent boronate ester bonds have emerged as promising injectable materials for drug delivery and tissue engineering mainly because of their self-healing ability.⁷⁻¹⁰ This property is related to the dynamic covalent nature of boronate-diol complexes allowing hydrogels to reconfigure their covalent structure, and thereby to self-repair without any external stimuli after rupture.^{1,11,12} Moreover, the selective formation of boronate esters offers the possibility to adapt the mechanical properties of hydrogels by tuning the self-assembly properties of their small-molecule partners (i.e. by varying the boronic acid and/or the diol (or polyol) crosslinking moieties, which allows tunable binding strength and dynamics of the reversible crosslinks).

Given the exciting potential benefit of using boronic acid-containing polymers to construct dynamic covalent hydrogels, we explored this attractive strategy to design injectable boronate-crosslinked hydrogels based on hyaluronic acid (HA) for aesthetic and other biomedical applications in the framework of a collaboration between CERMAV and Galderma/Nestlé Skin Health. HA is a naturally occurring polysaccharide in the body which belongs to the glycosaminoglycan family and as such, it is an attractive building block for hydrogel design. Conventional hydrogel formulations currently employed as dermal fillers are covalently crosslinked by reaction of HA with 1,4-butanediol diglycidyl ether (BDDE).¹³ However, these permanently crosslinked gels allows clinicians to apply significant extrusion forces during injection, which can result in an inconvenient over-injection of the fillers and formation of bumps, as well as in a traumatic process for the patient(s). Therefore, the idea of designing gels that can be easily broken under shear stress, and that are able to reform instantaneously after injection in the skin, due to self-healing properties, may address this demand. In addition,

the dynamic nature of the crosslinks in these innovative hydrogels may endow fillers with new properties such as high malleability.

This provided the basis of the concept on which this PhD thesis was constructed, focusing on the design of injectable self-healing HA hydrogels crosslinked by reversible covalent boronate ester bonds. The synthesis of these materials was based on the expertise of the “*Structure and Modification of Polysaccharides*” group in CERMAV, with regard to the synthesis and characterization of hydrogels derived from HA. In addition to its attractive biocompatible and biodegradable properties, this biopolymer is widely used for hydrogel design due to its numerous sites for modification with reactive groups.¹⁴ Among different reversible HA assemblies developed by the group (mainly including non-covalent hydrophobic or host-guest interactions),^{15–17} a first autonomous self-healing hydrogel based on HA was successfully prepared in physiological conditions via formation of dynamic covalent boronate ester crosslinks.¹⁸ In these networks, hydrogel properties are closely tied to the structure of the small-molecule crosslinkers, i.e. the phenylboronic acid (PBA) and maltose derivatives grafted on HA.

Given the advantages offered by such hydrogels for biomedical applications, this attractive approach prompted us to design novel hydrogels with optimized properties by exploring the effect of the nature of the boronic acid moiety as well as the sugar molecule grafted onto the HA backbone on the gel properties (Figure 1a). Among arylboronic acid derivatives, *o*-hydroxymethylphenylboronic acid (commonly known as benzoboroxole, BOR) was selected in addition to PBA (Figure 1b) as the binding site for sugar moieties (Figure 1c) not only because of its efficient binding capability at physiological pH compared to PBA, but also for its ability to complex sugars locked in their pyranose form (i.e. glycopyranosides).^{19–21} These particular features are related to the strained structure of the five-membered oxaborole ring, which results in a lower pK_a compared to “classical” arylboronic acids. However, in contrast to PBA from which several substituted derivatives have been synthesized and investigated for the construction of dynamic polymeric assemblies, to date, no study on the effect of BOR substitution on boronate ester crosslinking has been produced (Figure 1d).

Finally, in addition to benzoboroxole, its six-membered ring homologue, *o*-hydroxyethylphenylboronic acid (benzoxaborin, 2,1-BORIN, Figure 1c) was explored as a new carbohydrate binding site for the formation of reversible HA networks. Besides 2,1-BORIN, we also investigated a new original benzoxaborin-like derivative (1,2-BORIN, Figure 1c) grafted on HA. Following the identification of the successful strategies allowing formation of promising hydrogels with attractive injectable and self-healing properties, we further investigated the mechanisms of reversible covalent complexation of the different grafted arylboronic acid derivatives with saccharide moieties. This consisted in studying the dynamic rheological

General introduction

behavior of the polymer networks in various environmental conditions combined with studies about the binding modes and self-assembly properties of the small-molecule partners.

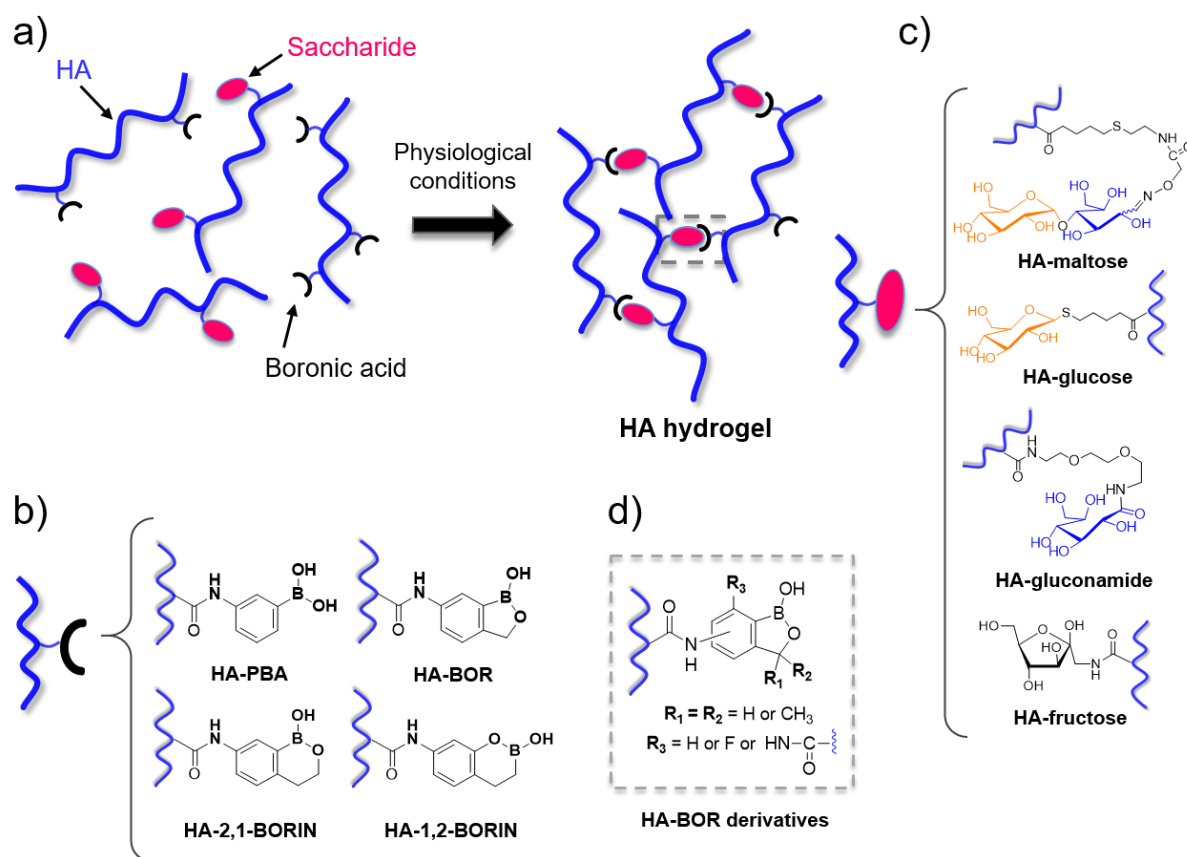


Figure 1. (a) Design of injectable self-healing hyaluronic acid hydrogels crosslinked through arylboronic acid-diol (polyol) complexation by combining a HA conjugate modified with (b) arylboronic acid moieties, i.e. phenylboronic acid (PBA), benzoboroxole (BOR) or benzoxaborin (BORIN) derivatives, and (c) a HA partner bearing different saccharide residues. (d) BOR derivatives used to investigate the effect of BOR substitution on boronate ester crosslinking.

These studies revealed original properties for the new boronate-crosslinked HA hydrogels developed, ranging from self-healing capability to stimuli-responsive behaviors triggered by pH and addition of free sugars (e.g. D-glucose, D-fructose).

The thesis manuscript is divided into four chapters.

The first chapter sets out a bibliographic analysis of self-healing hydrogels crosslinked via dynamic covalent boronate ester bonds.

The second chapter deals with the effect of the nature of the boronic acid moiety (PBA or BOR) as well as of the sugar molecule grafted onto the HA backbone on the dynamic properties of HA assemblies. Our main aim was to explore the relative importance of the effect of dynamics and thermodynamics of molecular crosslinks on the viscoelastic properties of HA

networks. To this end, we set out on a structural study using NMR and computational analysis to gain a better understanding of the binding mode of PBA and BOR toward different saccharide moieties grafted on HA. The findings from this study offer interesting new perspectives for the rational design of adaptable hydrogel scaffolds using arylboronic acid-polyol complexes.

The third chapter reports on the design of innovative self-crosslinking HA hydrogels through multivalent interactions between benzoboroxole derivatives grafted on HA and diols from the polysaccharide chains. These new systems were produced from custom-made derivatives of benzoboroxole. Among the ten BOR derivatives tested for engineering HA hydrogels, we identified two BOR derivatives that showed unprecedented binding capability toward HA diols, leading to the formation of self-healing hydrogels with extremely slow dynamics. The mechanism of reversible covalent complexation of the grafted BOR moieties with HA was further investigated by combining dynamic rheological studies and molecular dynamics.

Finally, the fourth chapter describes a first demonstration of the applicability of dynamic benzoxaborin-saccharide complexation as a reversible covalent crosslinking method to form HA networks. To assess the effect of the structure of the arylboronic acid group on the efficiency of boronate crosslinking formation, we compared the rheological properties of HA assemblies based on a HA-fructose conjugate combined with HA bearing 2,1-BORIN, BOR or PBA moieties in addition to a new 1,2-BORIN derivative. With this study, we demonstrate the ability of this original benzoxaborin-like derivative to complex saccharide moieties allowing injectable and self-healing hydrogels in physiological conditions.

These three chapters describing the synthesis and study of new boronate-crosslinked HA hydrogels will be submitted to specific peer-reviewed journals in the near future.

References

- (1) Taylor, D. L.; in het Panhuis, M. Self-Healing Hydrogels. *Adv. Mater.* **2016**, *28* (41), 9060–9093.
- (2) Wang, H.; Heilshorn, S. C. Adaptable Hydrogel Networks with Reversible Linkages for Tissue Engineering. *Adv. Mater.* **2015**, *27* (25), 3717–3736.
- (3) Patenaude, M.; Smeets, N. M. B.; Hoare, T. Designing Injectable, Covalently Cross-Linked Hydrogels for Biomedical Applications. *Macromol. Rapid Commun.* **2014**, *35* (6), 598–617.
- (4) Yang, J.-A.; Yeom, J.; Hwang, B. W.; Hoffman, A. S.; Hahn, S. K. In Situ-Forming Injectable Hydrogels for Regenerative Medicine. *Prog. Polym. Sci.* **2014**, *39* (12), 1973–1986.

- (5) Sivashanmugam, A.; Arun Kumar, R.; Vishnu Priya, M.; Nair, S. V.; Jayakumar, R. An Overview of Injectable Polymeric Hydrogels for Tissue Engineering. *Eur. Polym. J.* **2015**, *72*, 543–565.
- (6) Loebel, C.; Rodell, C. B.; Chen, M. H.; Burdick, J. A. Shear-Thinning and Self-Healing Hydrogels as Injectable Therapeutics and for 3D-Printing. *Nat. Protoc.* **2017**, *12* (8), 1521–1541.
- (7) Yesilyurt, V.; Webber, M. J.; Appel, E. A.; Godwin, C.; Langer, R.; Anderson, D. G. Injectable Self-Healing Glucose-Responsive Hydrogels with PH-Regulated Mechanical Properties. *Adv. Mater.* **2016**, *28* (1), 86–91.
- (8) Chen, Y.; Wang, W.; Wu, D.; Nagao, M.; Hall, D. G.; Thundat, T.; Narain, R. Injectable Self-Healing Zwitterionic Hydrogels Based on Dynamic Benzoxaborole–Sugar Interactions with Tunable Mechanical Properties. *Biomacromolecules* **2018**, *19* (2), 596–605.
- (9) Chen, Y.; Diaz-Dussan, D.; Wu, D.; Wang, W.; Peng, Y.-Y.; Asha, A. B.; Hall, D. G.; Ishihara, K.; Narain, R. Bioinspired Self-Healing Hydrogel Based on Benzoxaborole-Catechol Dynamic Covalent Chemistry for 3D Cell Encapsulation. *ACS Macro Lett.* **2018**, *7* (8), 904–908.
- (10) Wang, Y.; Li, L.; Kotsuchibashi, Y.; Vshyvenko, S.; Liu, Y.; Hall, D.; Zeng, H.; Narain, R. Self-Healing and Injectable Shear Thinning Hydrogels Based on Dynamic Oxaborole-Diol Covalent Cross-Linking. *ACS Biomater. Sci. Eng.* **2016**, *2* (12), 2315–2323.
- (11) Wei, Z.; Yang, J. H.; Zhou, J.; Xu, F.; Zrínyi, M.; Dussault, P. H.; Osada, Y.; Chen, Y. M. Self-Healing Gels Based on Constitutional Dynamic Chemistry and Their Potential Applications. *Chem Soc Rev* **2014**, *43* (23), 8114–8131.
- (12) Wang, Y.; Adokoh, C. K.; Narain, R. Recent Development and Biomedical Applications of Self-Healing Hydrogels. *Expert Opin. Drug Deliv.* **2018**, *15* (1), 77–91.
- (13) Edsman, K.; Nord, L. I.; Öhrlund, Å.; Lärkner, H.; Kenne, A. H. Gel Properties of Hyaluronic Acid Dermal Fillers. *Dermatol. Surg.* **2012**, *38* (7pt2), 1170–1179.
- (14) Highley, C. B.; Prestwich, G. D.; Burdick, J. A. Recent Advances in Hyaluronic Acid Hydrogels for Biomedical Applications. *Curr. Opin. Biotechnol.* **2016**, *40*, 35–40.
- (15) Creuzet, C.; Kadi, S.; Rinaudo, M.; Auzély-Velty, R. New Associative Systems Based on Alkylated Hyaluronic Acid. Synthesis and Aqueous Solution Properties. *Polymer* **2006**, *47* (8), 2706–2713.
- (16) Kadi, S.; Cui, D.; Bayma, E.; Boudou, T.; Nicolas, C.; Glinel, K.; Picart, C.; Auzély-Velty, R. Alkylamino Hydrazide Derivatives of Hyaluronic Acid: Synthesis, Characterization in Semidilute Aqueous Solutions, and Assembly into Thin Multilayer Films. *Biomacromolecules* **2009**, *10* (10), 2875–2884.
- (17) Charlot, A.; Auzély-Velty, R. Novel Hyaluronic Acid Based Supramolecular Assemblies Stabilized by Multivalent Specific Interactions: Rheological Behavior in Aqueous Solution. *Macromolecules* **2007**, *40* (26), 9555–9563.
- (18) Tarus, D.; Hachet, E.; Messenger, L.; Catargi, B.; Ravaine, V.; Auzély-Velty, R. Readily Prepared Dynamic Hydrogels by Combining Phenyl Boronic Acid- and Maltose-Modified Anionic Polysaccharides at Neutral PH. *Macromol. Rapid Commun.* **2014**, *35* (24), 2089–2095.
- (19) Dowlut, M.; Hall, D. G. An Improved Class of Sugar-Binding Boronic Acids, Soluble and Capable of Complexing Glycosides in Neutral Water. *J. Am. Chem. Soc.* **2006**, *128* (13), 4226–4227.

General introduction

- (20) Bérubé, M.; Dowlut, M.; Hall, D. G. Benzoboroxoles as Efficient Glycopyranoside-Binding Agents in Physiological Conditions: Structure and Selectivity of Complex Formation. *J. Org. Chem.* **2008**, 73 (17), 6471–6479.
- (21) Peters, J. A. Interactions between Boric Acid Derivatives and Saccharides in Aqueous Media: Structures and Stabilities of Resulting Esters. *Coord. Chem. Rev.* **2014**, 268, 1–22.

CHAPTER 1

Self-healing hydrogels crosslinked by dynamic covalent boronate ester bonds: a literature review

Self-healing hydrogels crosslinked by dynamic covalent boronate ester bonds: a literature review

1. Introduction

Hydrogels are soft materials with tunable physical and chemical properties that have been widely used for biomedical applications, including regenerative medicine, tissue engineering, drug delivery and aesthetics.^{1,2} These materials are particularly attractive for sophisticated *in vivo* applications, because of their highly hydrated structure composed of crosslinked hydrophilic polymers that imparts a biomimetic microenvironment, mechanical similarity to natural tissues and high moldability.³ However, even though traditional polymer gels formed via conventional covalent crosslinking exhibit high elastic properties, they often present limited lifetime due to loss or deterioration of their mechanical properties when subjected to damages at the macro- or microscale.⁴ To overcome this challenge, increased attention has been paid, over the past decade, to develop a new class of hydrogels that are able to autonomously self-heal upon damage, allowing them to recover their original mechanical properties.⁵

In these networks, the self-healing nature of their constituting polymers is mediated by reversible crosslinks based on noncovalent interactions and/or dynamic covalent chemistry. Physically-crosslinked gels are capable of re-establish networks through reversible physical associations, such as hydrogen bond, ionic, hydrophobic and host-guest interactions.⁶ Dynamic covalent hydrogels are networks possessing adaptable linkages that can be reversibly broken and re-formed, with a slower kinetics than physical crosslinks.^{7,8} Consequently, hydrogels based on dynamic covalent reactions can self-heal in response to mechanical stress similar to physically-crosslinked gels, but they are more stable.

Among a number of dynamic covalent bonds used to fabricate functional materials, boronate esters have emerged as promising reversible covalent crosslinks for the design of self-healing hydrogels.^{4,9} In these materials, polymer crosslinking is often achieved via formation of boronate ester bonds between two assembling polymers: a boronic acid-containing polymer and a polymer bearing functional diols or polyols (Figure 1a). The introduction of boronate linkages endows a hydrogel with new functions besides self-healing capacity, such as pH and saccharide responsiveness. These attractive properties make boronate-crosslinked gels highly suitable for application in glucose sensing and self-regulated insulin release.⁹ More recently, such hydrogels have been investigated as injectable biomaterials taking advantage of their self-healing properties (Figure 1b). They can, indeed, be pre-formed into syringes, extruded under shear stress, and rapidly re-form when the applied

stress is removed.¹⁰ For these reasons, successful design of boronate-based hydrogels has found great interest for various applications, including their use as soft injectable devices for the delivery of bioactive (macro)molecules^{11–14} and 3D cell encapsulation,^{11,15–18} and, more recently, as self-adhesive matrices for 3D bioprinting of tissue scaffolds.¹⁹

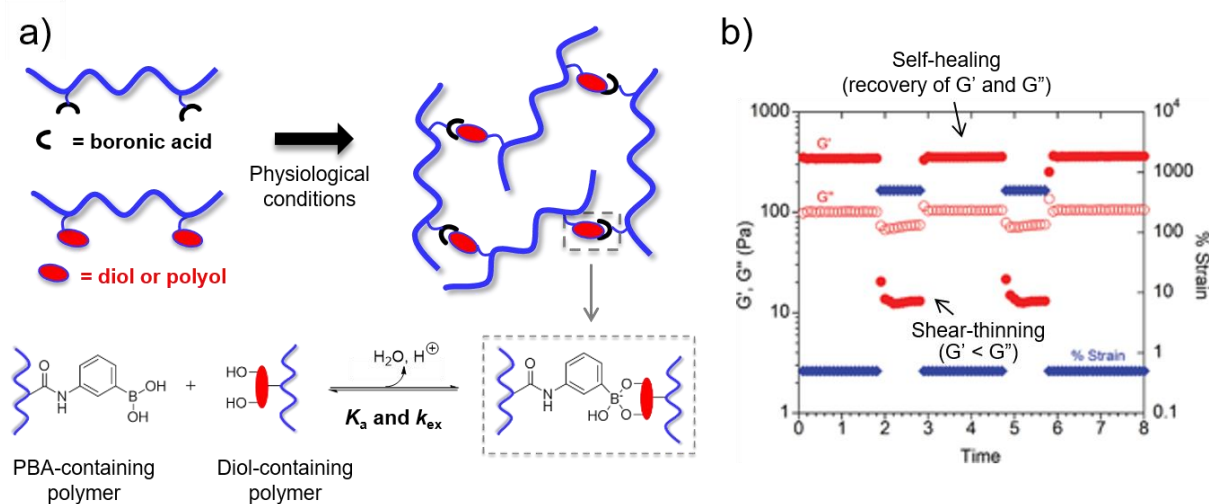


Figure 1. Reversible hydrogels crosslinked by dynamic covalent boronate ester chemistry. (a) Gel formation by usually combining two polymer partners functionalized either with boronic acid or diol (polyol) moieties. (b) Typical rheological behavior of shear-thinning and self-healing gels: viscous flow under high stress application ($G' < G''$) and recovery of the rheological moduli when stress is removed (reproduced from Guvendiren *et al.*²⁰).

In this literature review, the recent advances made in reversible boronate-crosslinked hydrogels are discussed, focusing on hydrogel design and on the relationship between their macroscopic mechanical behavior and the properties of their small-molecule crosslinkers. First, for a better understanding of the dynamic behavior of such gels, we briefly outline the fundamentals of boronic acid chemistry and boronate ester formation. Then, we describe the different strategies used to design hydrogels with tunable viscoelasticity and macromolecular architectures. Finally, we focus on the potential of boronate-crosslinked gels as injectable biomaterials by highlighting their biomedical applications and new perspectives for their future development.

2. Boronic acids and boronate ester chemistry

Boronic acids are mild Lewis acids that can usually react with 1,2- and 1,3-diols to form boronate esters, allowing intermolecular interactions with a number of biologically important species (e.g. saccharides, dopamine, glycoproteins). Boronate ester bonds are known to be reversibly formed and broken through a kinetically controlled equilibrium between the reactants

(i.e. free diol and boronic acid) and the product (i.e. boronate ester), due to a low-energy transition state between them (Figure 1a).²¹ This reversible mechanism is strongly associated with the affinity constant (K_a) of a boronic acid towards a specific diol (or polyol), and with the exchange rate constant (k_{ex}) between the ester formed and the free species. In this regard, the dynamic properties of boronate-crosslinked polymer networks were indeed found to be closely related to k_{ex} , which can be tuned according to the structure of the boronate ester crosslinks.²²

Furthermore, boronate ester formation is strongly influenced by the pH of the medium and the pK_a of the molecular partners (i.e. boronic acid and diol).²³ Indeed, the transesterification reaction is expected to be favored at pH values about half-way between the pK_a of the boronic acid and the pK_a of the diol.²⁴ However, most of boronic acids used for biomedical applications, in particular phenylboronic acid (PBA), have a pK_a in the range of 8-9.²⁴ Obviously, the acidity of boronic acids depends on the charge density about the boron atom, which explains the lower pK_a of PBA (8.8)²⁴ compared to boric acid (9.2)²⁵ (Figure 2a and 2b). On the other hand, diol-containing molecules that are commonly used in the reaction with boronic acids have pK_a values above 8, such as aliphatic diols (e.g. 10.7 for poly(vinyl alcohol)),²⁶ catechol-based molecules (e.g. 8.9 for dopamine),²⁷ and saccharides (e.g. 12.4 for glucose).²⁸ Therefore, from the pK_a values of PBA and known diol-containing molecules, optimal pH values for boronate ester formation would be expected in a large range of 8.0-11.0.

For this reason, many efforts have been made to improve diol-binding affinity at physiological pH, due to the great potential of arylboronic acids for biomedical applications (e.g. carbohydrate sensing, drug development, functional materials). To this end, great attention has been paid to the synthetic manipulation of the PBA structure in order to reduce its pK_a , such as by adding electron-withdrawing groups on the phenyl ring (i.e. fluorine, nitro).²⁹⁻³¹ Moreover, *ortho*-substituted PBA derivatives have attracted special attention due to their increased acidity induced by the substituent in the *ortho* position relative to the boronic center. Indeed, Wulff and coworkers initially showed that the addition of a nitrogen center (e.g. secondary or tertiary amines) adjacent to boron can facilitate ester formation (Figure 2c).^{32,33} In the case of these *o*-aminoalkylphenylboronic acids, it is believed that the improved binding properties are due to the formation of an intramolecular B-N dative bond, which promotes the dissociation of the neutral boronic acid species in its anionic tetrahedral form, contributing to form more stable boronate esters at neutral pH.²¹

More recently, *o*-hydroxymethylphenylboronic acid (commonly known as benzoboroxole or benzoxaborole, Figure 2d) has gained increased interest due to its better solubility in water and a considerably lower pK_a (7.3), compared to PBA.^{34,35} This lower pK_a is a consequence of the ring strain in the five-membered oxaborole cycle containing an intramolecular B-O bond, which distorts the geometry about boron in the neutral trigonal acid, leading to a more favorable

ionization.³⁴ Ring strain in benzoboroxole is relieved due to its conversion to its tetrahedral anionic form, which is partially responsible for its excellent sugar-binding capability in particular towards non-reducing saccharides locked in their pyranose form (i.e. glycopyranosides).^{25,36,37} On the other hand, its homologue benzoxaborin (Figure 2e) possesses a six-membered ring that does not induce such ring strain and distortion about the boron atom, leading to a higher pK_a (8.4).²⁵ This slightly lower value of pK_a of benzoxaborin compared to unsubstituted PBA is explained by the reduced flexibility of the heterocyclic B-O bond of the former, which may increase the electronic deficiency about the boron atom.³⁴

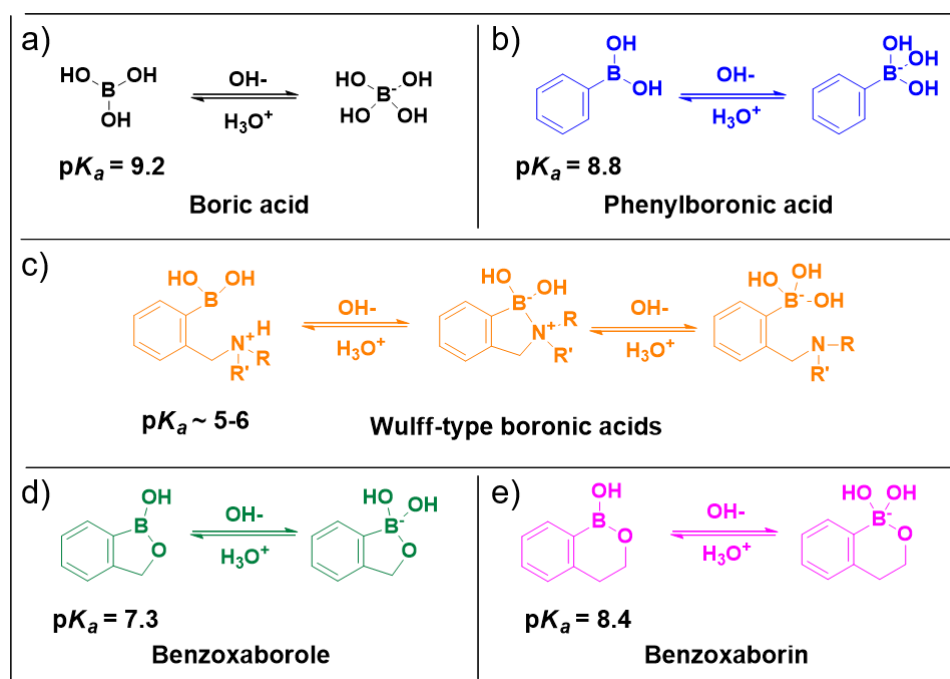


Figure 2. Boric acid, phenylboronic acid (PBA) and *ortho*-substituted PBA derivatives with their respective pK_a values in water at 25 °C.^{25,33,34,38}

3. Design of reversible hydrogels crosslinked by boronate ester bonds

Taking advantage of the versatile properties associated with the selective reaction of boronic acids with diol-containing molecules, dynamic boronate ester bonds have extensively been explored for the design of reversibly crosslinked hydrogels. Boronate ester crosslinks can, indeed, endow hydrogels with tunable viscoelasticity, which hold promise as biomaterials that can recapitulate many dynamic mechanical properties found in native tissues.¹⁵ More than six decades ago, boronate ester-like gels were fabricated for the first time upon mixing poly(vinyl alcohol) with borax, a tetrahydroxy boron species (Figure 2a).³⁹ Then, many synthetic polyhydroxy polymers (e.g. poly(glyceryl methacrylate))⁴⁰ and some polysaccharides (e.g. galactomannan and guar)^{41–43} have also been used to form gel networks via borate-polyol

crosslinking. These systems were found to show attractive transient properties and self-healing ability after mechanical disruption due to the reversible nature of the reaction between borate ions and diol-containing macromolecules. Nevertheless, a limitation of such gels is related to their formation only at basic pH (8-9), near the pK_a of boric acid (9.2).²⁵ Compared to borax, PBA derivatives with lower pK_a values can be grafted on polymer chains and form crosslinks with diol-containing polymers more effectively at physiological pH, allowing for a multipoint and stronger interaction in the gel network.

Taking advantages of the advances made in developing PBA derivatives with improved affinity toward saccharides at neutral pH, boronate-crosslinked gels have undergone significant developments in recent years. This has led to the production of hydrogel networks with tunable mechanical strength and relaxation dynamics by varying the nature of their small-molecule crosslinkers (i.e. boronic acid and/or diol moieties), and that additionally can possess different macromolecular architectures depending on the nature of the polymer backbone and the synthetic approach used for their preparation.

Like other gels, boronate-crosslinked hydrogels can be designed on various scales, the most common being macroscopic networks. There exists an extensive body of literature on the synthesis of this type of gels, that are formed by combining two synthetic polymers partners bearing either PBA or diol functional moieties (e.g. poly(acrylamide), poly(ethylene glycol), poly(methacrylate), poly(vinyl alcohol)). By contrast, to date, only few studies have focused on the use of polysaccharides, such as alginate and hyaluronic acid to engineer such hydrogels taking advantage of their biocompatibility and biodegradability.

Regardless, there is a need to understand the relationships between the composition, structure and properties of these hydrogels for their rational design in biomaterials engineering. For this reason, the following sections are focused on the advances made in the design of boronate-crosslinked gels, with special attention to the relationships between their macroscopic mechanical properties and the fundamentals of their boronic acid-diol interactions. First, we present examples of hydrogel synthesis from the association of standard (unmodified) PBA with varied diol-containing molecules. Then, attention is paid to the optimization of hydrogel viscoelastic properties at physiological pH using chemically modified PBA derivatives, such as PBA with electron-withdrawing or *ortho* substituents in the phenyl ring, in particular benzoboroxole. Such an approach allows for designing hydrogels with adaptable dynamic behavior by tuning the properties of their small-molecule partners (e.g. boronic acid-diol affinity (K_a), exchange dynamics (k_{ex})).

3.1. Hydrogels crosslinked via phenylboronic acid-diol complexation

A number of literature examples have explored hydrogel formation via interaction of standard PBA grafted on polymer backbones of different natures combined with various diol-containing polymers. The first example of interpolymer complex based on phenylboronate-diol crosslinking was reported by Kitano *et al.*⁴⁴ By mixing a poly(vinyl alcohol) solution and an alkali solution of poly(N-vinylpyrrolidone-co-3-acrylamidophenylboronic acid), a hydrogel was formed above a critical concentration. However, a disadvantage of these networks regarding biomedical applications is that they are obtained only at pH values above pH 8-9, near the pK_a of 3-aminophenylboronic acid (3-APBA, $pK_a = 8.8$)⁴⁵ used for the synthesis of 3-acrylamidophenylboronic acid.

Alternatively, Kiser and co-workers used salicylhydroxamic acid (SHA) to prepare dynamic hydrogels at physiological pH through formation of boronate ester crosslinks between synthetic polymer partners bearing 4-carboxyphenylboronic acid derivatives ($pK_a = 8.4$)⁴⁶ or SHA moieties (Figure 3a). The choice of SHA was based on its higher affinity for PBA at lower values of pH in comparison with other known diols, allowing crosslinking formation at pH 4-5 (almost four pH units below the pK_a of PBA) and at neutral pH. Indeed, systems with frequency-dependent viscoelastic responses (i.e. crossover of the storage (G') and loss (G'') moduli at a determined frequency, ω_c) were synthesized using two different polymer backbones based on neutral 2-hydroxypropylmethacrylamide (HPMA) or anionic acrylic acid (AA) (Figure 3b).⁴⁷ Interestingly, the authors could readily adjust the viscoelastic properties of the polymer networks as a function of pH by varying the nature of the polymer backbone used. When using neutral HPMA, crosslinking formation was achieved at mildly acidic pH, characterized by a viscoelastic network (Figure 3c). However, when the binding constant between PBA and SHA was too high due to pH increase to 7.6, gels were brittle and showed a slower dynamics due to the long-lived crosslinks and poor chain mobility (Figure 3d). On the other hand, the use of negatively charged poly(acrylic acid) as polymer backbone (AA-based assembly) only provided formation of crosslinks at higher pH (pH 7.6, Figure 3d). A similar behavior was observed when using a sulfonated polymer backbone, demonstrating that the use of polyelectrolytes allow a lower binding constant between PBA and SHA moieties (Figure 3e).⁴⁸ The authors attributed this unexpected behavior to an altered PBA-SHA equilibrium induced by the Donnan effect generated by an increased acidic microenvironment. The charge-induced faster dynamics of these viscoelastic networks could be effectively screened by addition of ions in solution, leading to a leftward shift of ω_c (Figure 3f).

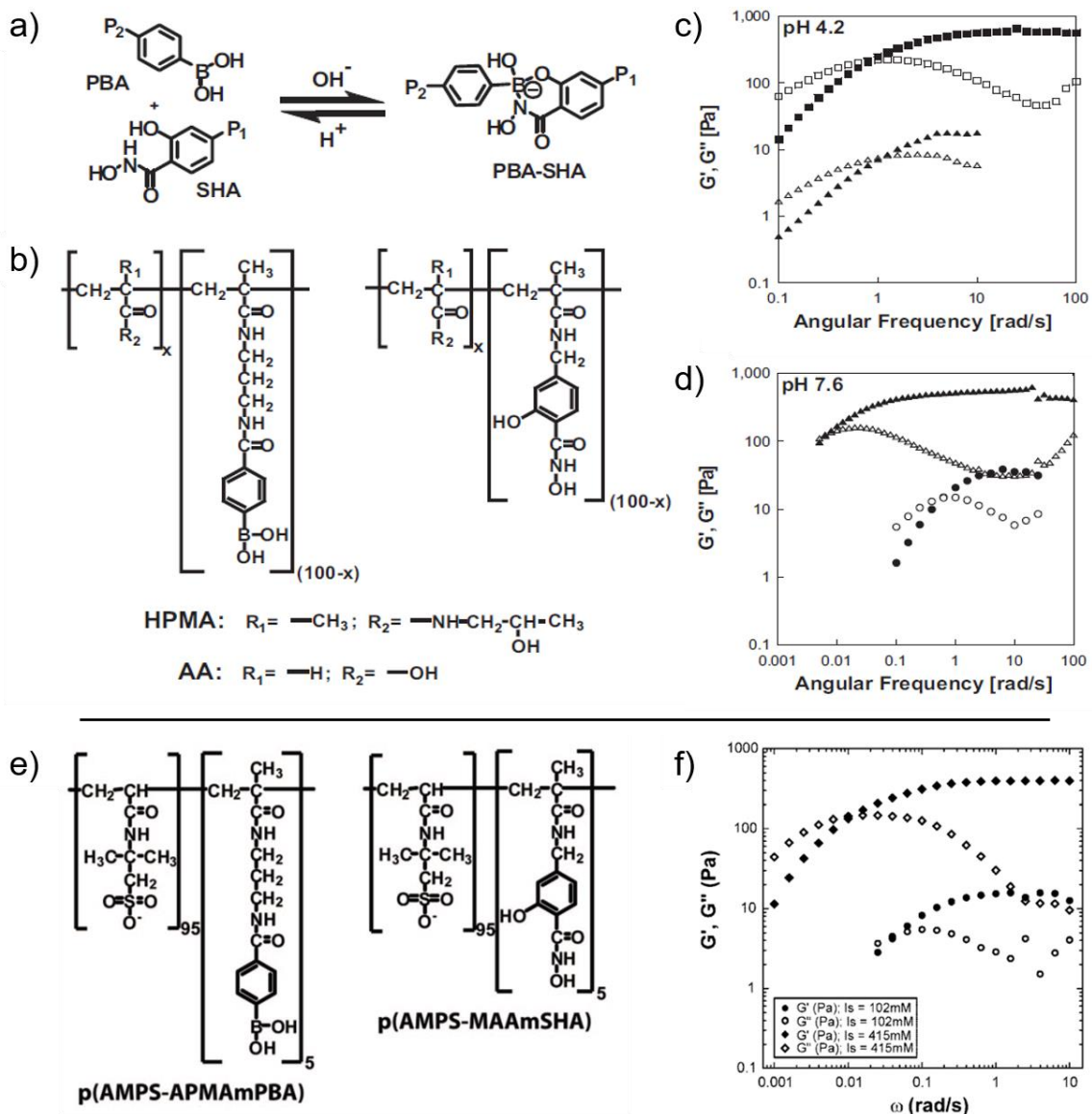


Figure 3. Viscoelastic PBA-SHA polymer networks. (a) Reversible formation of boronate ester crosslinks between a SHA-containing polymer (P1) and a PBA-containing polymer (P2) under pH-dependent equilibrium. (b) Linear polymers bearing either PBA or SHA moieties: 2-hydroxypropylmethacrylamide (HPMA) or acrylic acid (AA) that can be synthesized at controlled molar ratios. Dynamic rheology of PBA-SHA crosslinked networks at 25 °C: frequency dependence of G' (filled symbols) and G'' (empty symbols) of (c) the HPMA-based systems at 50 mg/mL⁻¹ (▲) or 100 mg/mL⁻¹ (■) at pH 4.2; and of (d) HPMA- (▲) and AA-based (●) networks at 50 mg/mL⁻¹ at pH 7.6. (e) Linear polymers containing either PBA or SHA moieties synthesized with a polysulfonate (AMPS) backbone, and (f) frequency-dependent viscoelastic behavior of the PBA-SHA crosslinked network formed at pH 7.6 at varied ionic strengths. Note the higher ω_c and increased moduli of the polysulfonate-backed network when increasing ionic strength (Is). PBA/SHA molar ratio used in all polymer networks of 1:1. Reproduced from Roberts *et al.*^{47,48}

The use of PBA-catechol complexation for hydrogel synthesis was also explored by combining a dopamine functionalized 4-armed poly(ethylene glycol) (PEG) and a 4-armed

PEG modified with 4-carboxyphenylboronic acid.⁴⁹ Hydrogel formation was observed within 10 s upon mixing solutions of these two PEG partners but only at pH 9.

Another strategy was used by He *et al.* to prepare a PEG hydrogel crosslinked via PBA-catechol complexation. By combining a branched catechol derivatized PEG (cPEG) with a difunctional PBA derivative, 1,3-benzenediboronic acid (BDDBA), they obtained a network exhibiting a gel-like behavior ($G' > G''$ within the frequency window explored), but only at pH 9.⁵⁰ This hydrogel displayed self-healing properties due to the dynamic nature of the boronate ester linkages and was highly sensitive to pH as it was disintegrated when immersed in pH 7.4 buffer.

In a similar approach, Tao Chen and co-workers developed supramolecular networks using alginate modified with 3-APBA in combination with an alginate-dopamine conjugate or PVA.^{51–53} Hydrogels were obtained under alkaline conditions by mixing the two polymeric partners. They exhibited a pH-dependent behavior due to the reversible crosslinks formed between PBA and dopamine or PVA diols. Moreover, additional crosslinking of the networks through alginate-calcium ionic interactions afforded gels with a great potential for shape memory applications, endowed with self-healing and adhesive properties (*for more details, see section 4.3*).

More recently, a self-crosslinking polysaccharide hydrogel was obtained under basic aqueous conditions from alginate functionalized with 3-APBA moieties that can reversibly bind the vicinal diols of the alginate pyranose rings.⁵⁴ This work is the first report on a straightforward synthesis of alginate hydrogels achieved without the need of additional diol-containing crosslinker molecules and/or divalent cations.⁵² The addition of 1 M NaOH to an aqueous solution of alginate-PBA led to immediate formation of soft gel networks (Figure 4a), which were shown to self-heal within minutes when cleaved in two fragments and placed back in contact (Figure 4b). Interesting further studies demonstrated the progressive self-healing of a scratch made on an alginate-PBA gel film monitored by optical microscopy, showing a decrease of the scratch size after 7 min and a totally repaired surface within 30 min (Figure 4c). In addition, oscillatory shear experiments confirmed the recovery of the rheological properties of the alginate-PBA network after three cycles of strain-induced breakdowns, consisting in the application of a high strain (500 %) to ensure gel rupture ($G' < G''$), followed by application of a low strain (5 %) (Figure 4d). Clearly, this is an original and promising approach for hydrogel formation via direct complexation between boronic acid moieties and saccharide units grafted on the biopolymer chain. While offering economy of raw materials and a simpler methodology for gel synthesis, such an approach may also benefit from the unique properties of natural polysaccharides, such as biocompatibility and biodegradability.

Nevertheless, the fact that gel formation in these systems is achieved at basic pH may represent a limitation for their use for biomedical applications.

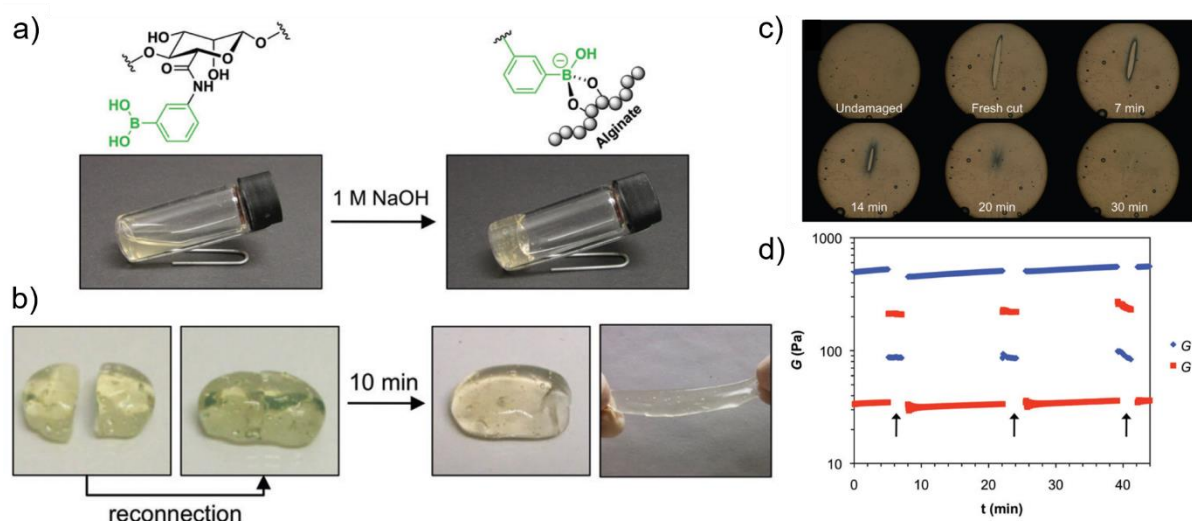


Figure 4. (a) Hydrogel formation under alkaline conditions of an alginate a PBA-modified conjugate via reversible crosslinking between PBA grafted moieties and vicinal diols of alginate pyranose rings. (b) Qualitative test illustrating the self-healing behavior of the alginate-PBA bulk hydrogel. (c) Self-healing process of a scratch made on an alginate-PBA hydrogel film monitored by optical microscopy. (d) Stress recovery of the gel (G') after three cycles of recovery from stress-induced breakdowns. Arrows indicate the application of increased shear strain (500 %) for 2 min, intercalated with G' recovery at a low strain (5 %) applied for 5 min. Reproduced from Pettignano *et al.*⁵⁴

The position of the amino substituent on the aromatic ring of aminophenylboronic acid was demonstrated to have strong effect on boronic-diol complexation. In the case of 2-acrylamidophenylboronic acid, the participation of the amide group at the *ortho*-position of the the boronic acid group through an intramolecular B-O-coordinated interaction was found to induce boron changes from the trigonal planar form to the anionic tetrahedral form, favoring binding with glucose (Figure 5a).⁵⁵ By using this 2-APBA-based monomer to prepare boronic acid-containing copolymers, Deng *et al.* showed the ability to obtain hydrogels at neutral and acidic pH via boronate ester formation with a dopamine-containing polyacrylamide or PVA (Figure 5b and c).⁵⁶ Qualitative assessment of the self-healing ability of gels prepared at pH 4 via cut/heal tests demonstrated their ability to heal within 60 min (Figure 5d).

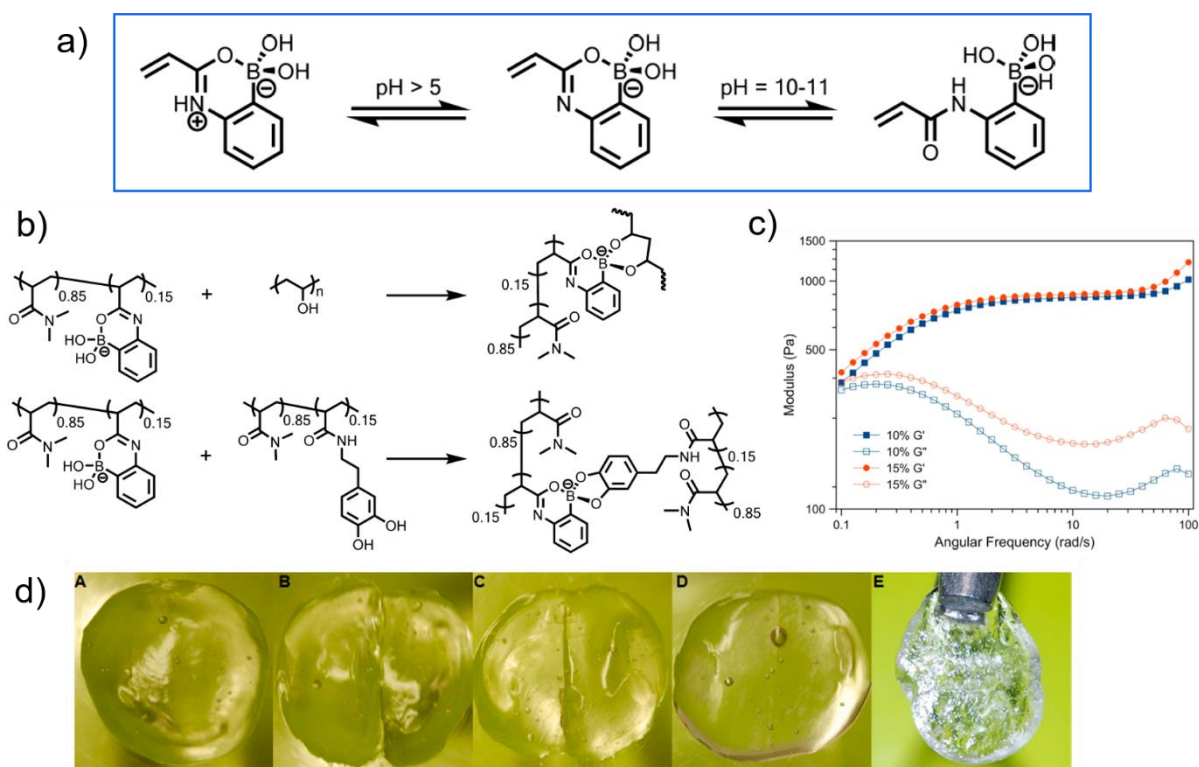


Figure 5. (a) Equilibrium of 2-acrylamidophenylboronic acid (2APBA) in water. Intramolecular B-O bond formation leads to the tetrahedral geometry of the boron atom that promotes boronate ester formation in a wider pH range. (b) Hydrogel formation using a 2APBA-containing polyacrylamide combined with PVA or with a dopamine-containing polyacrylamide partner. (c) Frequency dependence of G' and G'' of hydrogels formed with PVA at pH 4.0 (polymers containing 10 mol % and 15 mol % of the 2APBA monomer). (d) Self-healing of a hydrogel formed by crosslinking a 2APBA-containing polymer (at 10 mol % of 2APBA) and PVA: (A) intact gel; (B) cut gel; (C) gel halves placed in contact immediately after cutting; (D) healed gel within 60 min; (E) healed gel suspended under its own weight. Reproduced from Deng *et al.*⁵⁶

Yesilyurt *et al.* showed the ability to tune the dynamic mechanical properties of boronate-ester crosslinked PEG networks at physiological pH as a function of the pK_a of the PBA moiety grafted on the PEG derivative (Figure 6a).¹¹ In this work, the three hydrogels networks, obtained by boronate ester bond formation between the different PBA moieties and glucose units in the ring-opened form grafted on a four-arm PEG, exhibited a viscoelastic behavior in the frequency window explored, with the crossover frequency (ω_c) correlating with the rank of pK_a values (7.8, 7.2, and 6.5-6.7). The dynamic behavior of these materials make them promising candidates as injectable systems for the delivery of protein therapeutics, including insulin, as well as for three-dimensional (3D) cell culture (*details in section 4.1 and 4.2*).

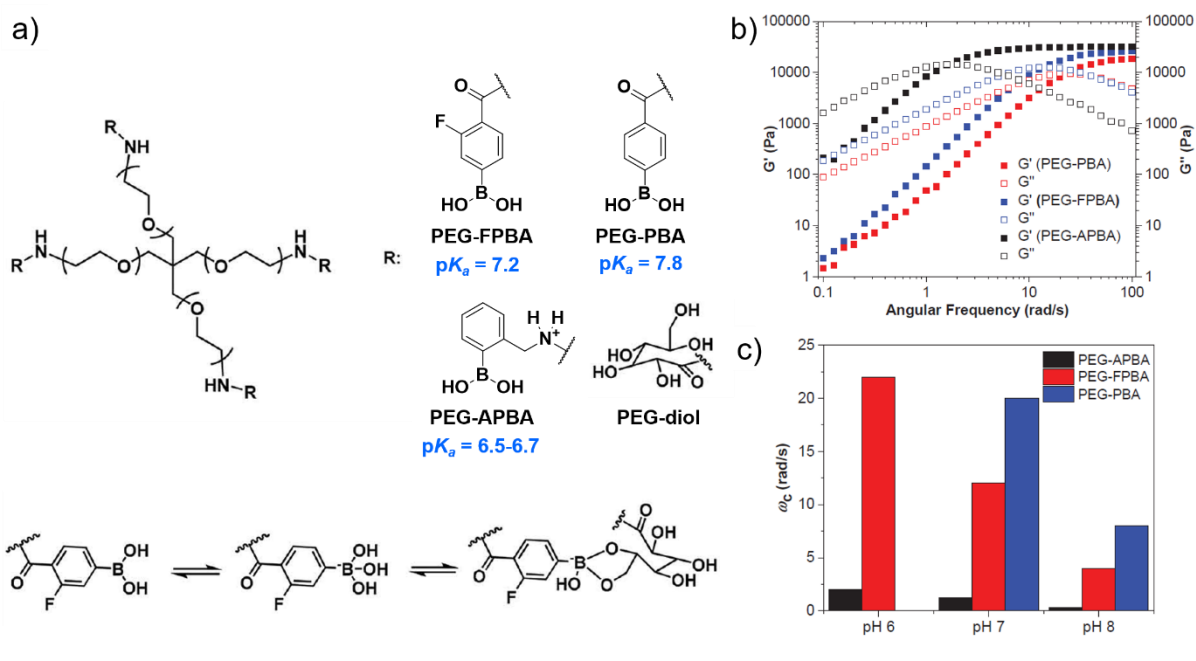


Figure 6. (a) Scheme of hydrogel formation between four-arm PEG derivatives modified with PBA derivatives and four-arm PEG bearing glucose-like moieties (values of pK_a of the three PBA derivatives are indicated below each chemical structure). (b) Dynamic oscillatory measurements of the frequency dependence of G' and G'' at 37 °C and at pH 7. (c) Crossover frequencies (ω_c) of the viscoelastic networks at pH 6, 7 and 8, obtained from frequency sweep experiments at 37 °C. Reproduced from Yesilyurt *et al.*¹¹

On the other hand, the results obtained by the same authors in another study on poly(acrylamide) networks assembled via complexation between 3-APBA ($pK_a = 8.8$) and the glucose unit did not confirm this trend, as a gel-like behavior ($G' > G''$ in the frequency window explored) was observed at physiological pH (Figure 7).¹³ As mentioned above, it is generally believed that the pH needs to be above the pK_a of the phenylboronic acid derivative to see meaningful binding.²⁴ The efficient boronate ester crosslinking observed at neutral pH indicates that other factors specific to each boronic acid/diol complex (conformational changes, interactions such as binding by a third hydroxyl)²⁴ can affect the binding as previously described for boronate complexes between small molecules.²⁴ The synthetic route to the synthetic polymer hydrogel included the radical copolymerization of 3-acrylamidophenylboronic acid and a Boc-protected monomer using azobis-(isobutyronitrile) (AIBN) as an initiator (Figure 7b). Then, the intermediate copolymer BC was subsequently treated by two reaction steps to give the final copolymer BG bearing PBA and glucose-like molecules in the same chain (Figure 7b). This simple strategy offered the possibility to easily vary the ratio of PBA and glucose moieties in the synthetic hydrogels. The frequency dependence of G' and G'' of the network prepared from a polymer containing an equal ratio of PBA to glucose-like molecules was characteristic of a typical hydrogel, with nearly linear and parallel G' and G'' curves and a dominant elastic modulus across the range of frequencies

measured (Figure 7c). Further investigation of the glucose-responsiveness of the hydrogel showed its ability to release an important amount of rhodamine B used as a model drug, when immersed in PBS containing glucose at different concentrations (1 and 20 g/L) (Figure 7d). Based on these results, the authors suggested potential application of these hydrogels as sensors to monitor blood glucose levels.

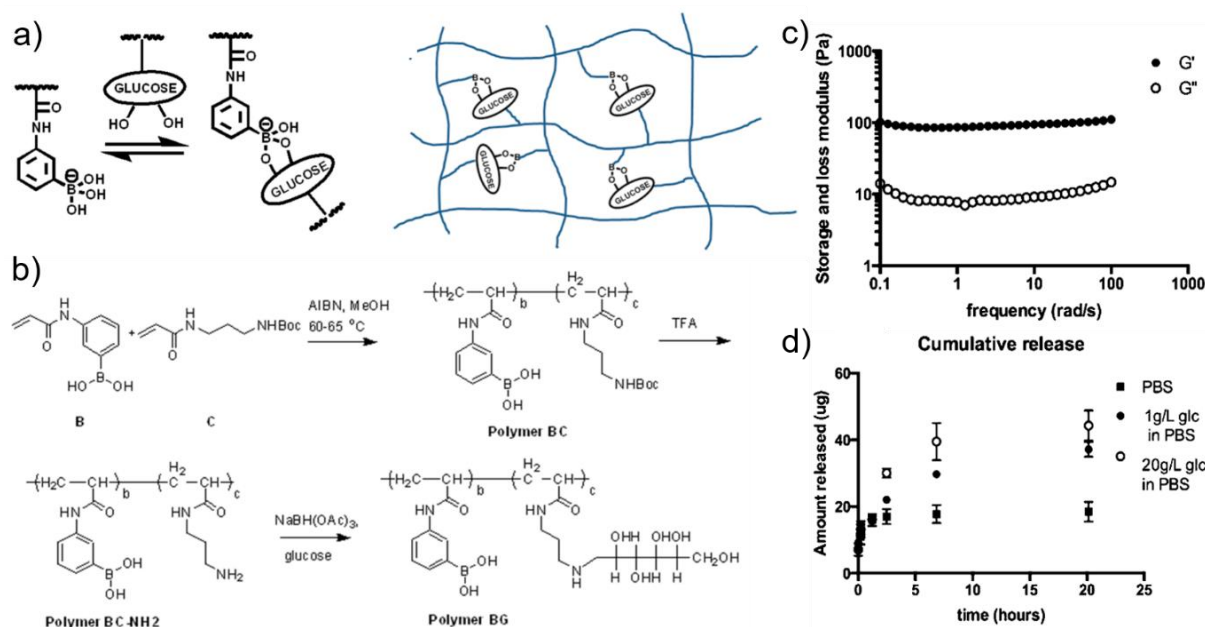


Figure 7. Design and synthesis of an injectable hydrogel based on the self-assembly of one single polymeric component via complexation between PBA and glucose-like moieties introduced within the same polymer chain. (a) Illustration of PBA-glucose complexation on the synthetic polymer chains. (b) Synthetic routes to polymer BG, which can self-assemble into an injectable and glucose-responsive hydrogel. (c) Frequency dependence of G' and G'' for the hydrogel (strain of 2 %). (d) Glucose responsiveness of the hydrogel *in vitro*, with a release of a higher amount of rhodamine B in a 20 g/L D-glucose solution than that in 1 g/L D-glucose and control PBS solutions (hydrogel prepared from a BG polymer containing 50 % PBA/50 % glucose moieties). Reproduced from Dong *et al.*¹³

Interestingly, Tarus *et al.* also reported formation of hydrogels at physiological pH via boronate ester crosslinking of hyaluronic acid (HA) modified with either 3-APBA or a maltose derivative with the glucose unit linked to HA in the opened form (Figure 8a).⁵⁷ The hydrogel networks were formed almost instantaneously upon mixing the two HA partners in physiological conditions and exhibited a gel-like behavior (with $G' > G''$ within the whole range of frequencies covered, Figure 8b). Moreover, at pH ranging from 6.5 to 9.5, the mixture of the two polymer partners gave rise to networks with impacted ω_c and G' in the plateau region (Figure 8c). The increase of the relaxation time of the network (associated with ω_c) and of the density of crosslinking (associated with G') at alkaline pH was related to the increase of the PBA/diol affinity. This study also showed the possibility to tune the rheological properties by

varying the polymer concentration and the molar ratio between PBA and maltose moieties. Furthermore, the self-healing ability of the HA-PBA/HA-maltose network was demonstrated by measuring the recovery of G' after exposure of the hydrogel to high oscillatory stress (Figure 8d). After being stressed, the gel could recover its original mechanical properties immediately, and no loss of G' was observed after a series of five breaks.

Given the soft nature of the hydrogels designed and the wide distribution of HA in the brain, the authors highlighted their potential of application as soft matrices for neuronal regeneration. Similar gel networks were also obtained using carboxymethylcellulose, which demonstrates the flexibility of this synthetic approach for the design of injectable biomimetic scaffolds.

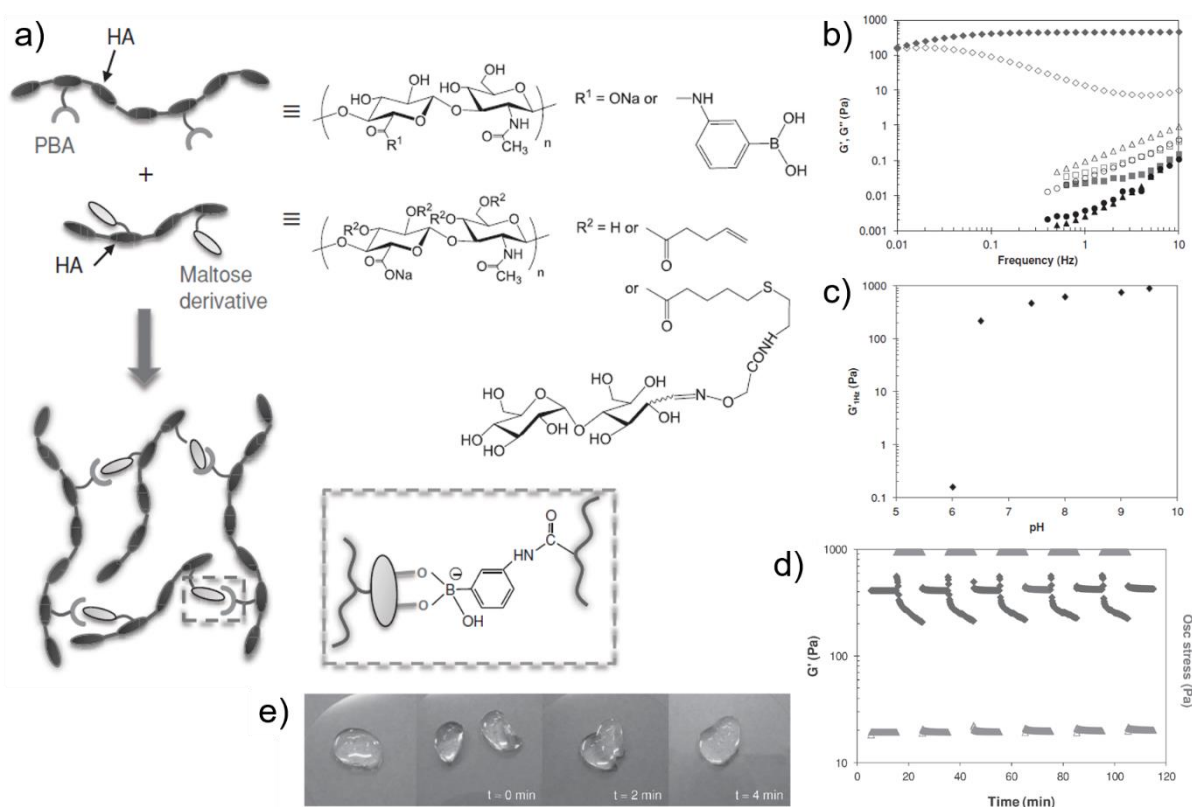


Figure 8. (a) Formation of dynamic covalent hydrogels at physiological pH by simply mixing HA modified with PBA (HA-PBA) and a HA conjugate grafted with a maltose derivative (HA-maltose). (b) Dependence on frequency of G' (filled symbols) and G'' (open symbols) of the HA-PBA/HA-maltose mixture (\blacklozenge), and of solutions of native HA (\bullet), HA-PBA (\blacksquare), and HA-maltose (\blacktriangle) at pH 7.4. (c) Variation of G' at 1 Hz with the pH for the HA-PBA/HA-maltose mixture. Self-healing properties of the hydrogel: (d) stress recovery after five cycles of recovery from stress-induced breakdowns at pH 7.4. An oscillatory stress above the linear viscoelastic region was applied for 10 min followed by linear recovery measurements for 10 min; and (e) qualitative recovery test showing that after cutting a piece of gel into two fragments and putting them back into contact, the separated pieces were allowed to heal in a few minutes. Total polymer concentration (C_p) of $15 \text{ g}\cdot\text{L}^{-1}$; PBA/maltose molar ratio of 1:1; measurement frequency of 1 Hz. Reproduced from Tarus *et al.*⁵⁷

Recently, a similar approach was applied to form hydrogels at neutral pH by combining PVA and hyaluronic acid (HA) bearing 2-APBA moieties.¹⁹ In addition to boronate ester crosslinking, ionotropic crosslinking of alginate in the presence of calcium was used to form an interpenetrating hydrogel network (IPN) with enhanced mechanical properties (higher G' modulus) and self-healing ability. These improved properties enabled the use of these gels as self-adhesive materials for additive manufacturing of hydrogel microchannels to produce cell scaffolds (see section 4.3).

3.2. Hydrogels crosslinked via benzoboroxole-diol complexation

Among aryl boronic acids, benzoboroxole (*o*-hydroxymethylphenylboronic acid, Figure 2d) has attracted increasing interest for hydrogel design over the last five years because of its efficient carbohydrate-binding capability at physiological pH but also for its ability to complex sugars locked in their pyranose form (i.e. glycopyranosides).^{25,36,37} As previously mentioned, compared to classical PBA, BOR has a lower pK_a (7.3), which is a contributing factor explaining its exceptional carbohydrate-binding behavior.

This particular property has been successfully used by Narain and co-workers to prepare self-healing networks at physiological pH by combining synthetic copolymers containing benzoboroxole moieties and glucose or lactose derivatives in the open-chain form,^{17,18,58,59} as well as dopamine.¹⁶ In their earlier work on the subject, they prepared thermoresponsive networks using a statistical copolymer of *N*-isopropylacrylamide (NIPAAm) and 5-methacrylamido-1,2-benzoxaborole mixed with synthetic glycopolymers containing glucose- or lactose-like moieties.^{58,59} However, as this procedure required extensive efforts on polymer synthesis and purification, a simpler and straightforward route was developed to synthesize one single copolymer from monomers based on benzoboroxole and on a glucose-like derivative, in addition to acrylamide, via one-pot free-radical copolymerization at pH 8-9 (Figure 9a).¹⁸ Such an approach allowed to tailor the hydrogel properties by easily tuning the molar ratio of the benzoboroxole and glucose-like units (i.e. 5, 10 or 20 mol % of benzoboroxole/sugar).

Dynamic rheological analysis showed viscoelastic behaviors for the networks with an increase of ω_c at pH 7.4 as the benzoboroxole/sugar molar ratio increased (Figure 9b and c). Though the values of ω_c correlated with the materials pH responsiveness (decrease of ω_c as the pH increased), it can be noted that the network containing a higher amount of benzoboroxole (i.e. 20 mol % of benzoboroxole/sugar) displayed lower dynamic moduli at pH 8 than the network with a 10 % benzoboroxole/sugar ratio. This unexpected behavior was attributed to imperfections in the former network due to free chains or formation of primary

loops. Then, studies of self-healing ability at physiological pH mainly focused on hydrogels containing lower benzoboroxole/sugar mole ratios (i.e. 5 or 10 mol %), taking into account their better properties. Qualitative cut/heal tests together with rheological analysis demonstrated this property by applying increasing strains until gel failure ($G' < G''$), and recording the recovery under reduced strain (Figure 9d). Strain-induced breakdown experiments also demonstrated the ability of the networks to disintegrate into a quasi-liquid state when sheared with a strain over 100 %, due to the dissociation of the polymer chains, and to completely restore G' and G'' once strain was reduced to 1 % (Figure 9e).

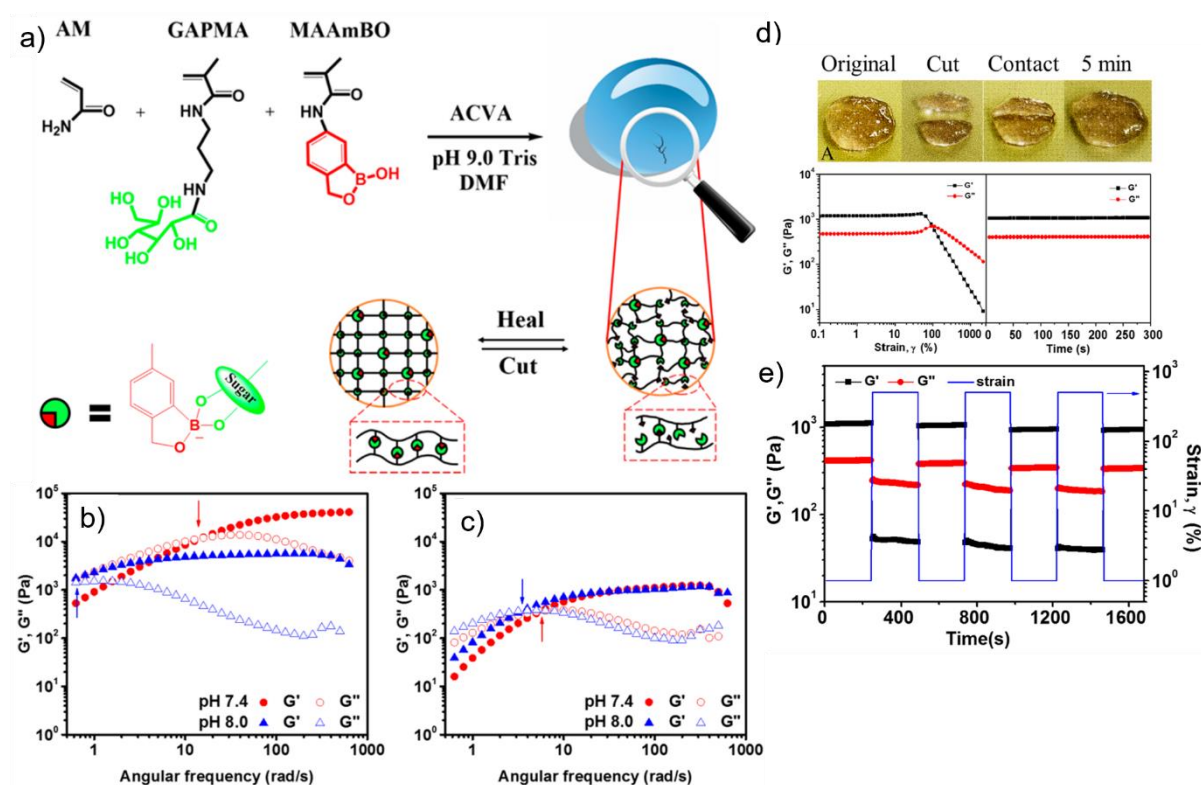


Figure 9. (a) Synthesis of polymer gel networks by one-pot radical copolymerization of monomers of benzoboroxole (MAAmBO), a glucose-like derivative (GAPMA) and acrylamide (AM). Dynamic rheological analysis exhibiting the viscoelastic behavior of the systems containing (b) 10 mol % or (c) 20 mol % of benzoboroxole/sugar ratio at pH 7.4 and 8.0. Arrows indicate ω_c , which only shifted towards higher frequencies in the first case, increasing gel strength. Self-healing behavior of the network containing 5 mol % of benzoboroxole-glucose content: (d) qualitative healing within 5 min, and G' and G'' dependence on strain (from 1 to 2500 % strain), followed by the rheological moduli recovery at 1 % strain as a function of time; (e) strain-induced breakdowns recorded during three cycles of strain changes between 1 and 500 %. Reproduced from Wang *et al.*¹⁸

As the biocompatibility of those hydrogels was unsatisfied, Narain and co-workers recently developed gel networks using 2-methacryloyloxyethyl phosphorylcholine (MPC)-based zwitterionic polymers, which possess cell membrane bioinspired molecular structures.¹⁷ Indeed, hydrogels made from these polymers have been reported as biocompatible platforms

for wound dressing, cell culture, and tissue engineering.^{60–62} Thus, hydrogel assemblies were obtained by combining two polymers partners synthesized by RAFT polymerization, containing benzoboroxole or glucose-like moieties, with varied sugar/benzoboroxole molar ratios (i.e. 20, 50 and 80 mol %, Figure 10a). The sugar content was varied with the purpose to tune the gel network mechanical properties due to varied cross-linking densities.

Furthermore, rheological analyses showed that, regardless of the sugar content, all mixtures showed a frequency-dependent viscoelastic behavior at different pH (7.4, 8.4 and 9.4, Figure 10c, d and e). As expected, both sugar content and pH influenced the mechanical properties, with lower ω_c observed for the viscoelastic networks with higher sugar contents and higher pH values. It was also found that the influence of glucose-like content on ω_c at higher pH values (8.4 and 9.4) was less significant than that at pH 7.4, which could be explained by the increased binding affinity of benzoboroxole for the glucose derivative at higher pH. Therefore, by varying both the molar concentration of sugar in the mixtures and the pH, G' values ranging from 261 Pa (20 mol % sugar/benzoboroxole, pH 7.4) to 2638 Pa (80 mol % sugar/benzoboroxole, pH 9.4) could be obtained. This indicated the great potential of this methodology for designing hydrogels with tailored mechanical properties as mimetic ECM for cell culture and tissue engineering.

Furthermore, this synthetic approach was also applied to design biocompatible hydrogels crosslinked via benzoboroxole-catechol complexation at physiological pH (Figure 10f).¹⁶ This work demonstrated, for the first time, the formation of boronate ester crosslinks using catechol-containing molecules at neutral pH. Despite a number of studies have reported on gel formation by combining catechol-containing polymers with PBA-modified polymers or borax,^{50,63–65} most of these systems were prepared at pH higher than 8. Herein, viscoelastic networks were obtained by mixing two zwitterionic polymers containing benzoboroxole or dopamine moieties at pH 7.4 (Figure 10g). The ω_c value remained constant while the elastic modulus increased as the total polymer concentration was increased in the mixture (i.e. (7.5, 10 and 12.5 wt %, Figure 10h and i). Moreover, the benzoboroxole-catechol interaction could be weakened, leading to gel disintegration, by reducing pH or adding free D-fructose for which boronic acids have high affinity (e.g. $336\text{--}606\text{ M}^{-1}$ for benzoboroxole and $128\text{--}160\text{ M}^{-1}$ for PBA)^{36,38,66} (Figure 10l).

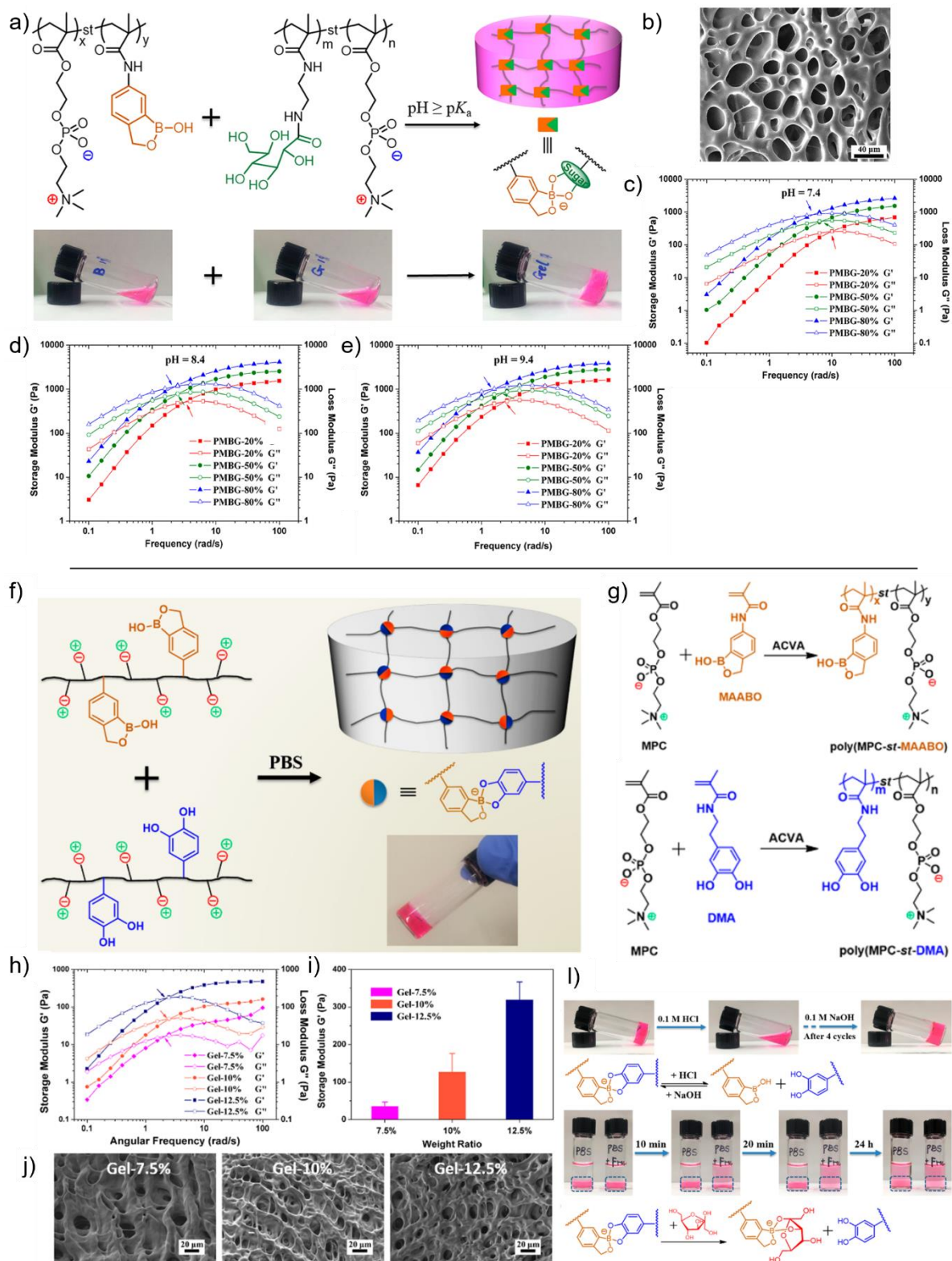


Figure 10. (a) Scheme illustrating zwitterionic polymer networks formed by combining two copolymers modified with benzoboroxole and a glucose-like derivative. (b) SEM image of the polymer assembly at pH 7.4 (at 50 % sugar/benzoboroxole molar ratio). Dynamic oscillatory frequency sweeps of hydrogel mixtures at different sugar/benzoboroxole ratios, formed at (c) pH 7.4, (d) pH 8.4, and (e) pH 9.4. (f) Scheme illustrating the preparation of bioinspired zwitterionic hydrogels based on dynamic benzoboroxole-catechol complexation, and (g) synthetic routes for the benzoboroxole- and dopamine-containing copolymers. (h)

Frequency dependence of G' and G'' for the viscoelastic polymer networks prepared at different concentrations (7.5, 10 and 12.5 wt %), and (i) increase of G' with the increased polymer concentration in the assemblies. (j) SEM images of hydrogels with different weight ratios. (l) Reversible gel-sol-gel transition by changing pH and schematic illustration for reversible pH responsiveness (top); hydrogel stability in PBS only (left vial) and in PBS with 50 mM of fructose (right vial) and scheme illustrating gel disassembly by fructose competition (bottom). Reproduced from Chen *et al.*^{16,17}

It is important to note that, in these studies, all polymeric assemblies developed exhibited a viscoelastic behavior (crossover of G' and G'' seen within the tested frequencies) regardless of the nature of the diol-containing molecule used to form boronate ester crosslinks with benzoboroxole.

The only example in literature that shows formation of a polymer network exhibiting a gel-like behavior ($G' > G''$) in the frequency window explored) consists of a mixture of an acrylamide-based copolymer containing benzoboroxole residues and a synthetic glycopolymer bearing mannopyranoside moieties (PMan, Figure 11a). By contrast, when PMan was replaced by glucopyranoside- or galactopyranoside-containing polymers (PGlc and PGal, respectively), only viscous or viscoelastic solutions were obtained, depending on the total polymer concentration used (5 or 10 wt %, respectively, Figure 11b). Obviously, the different capability of these glycopolymers to form gel networks was attributed to their specific ability to interact with benzoboroxole. However, low values of K_a were measured for the interaction of methyl glycopyranosides with benzoboroxole (24 M^{-1} for methyl α -D-mannopyranoside, 22 M^{-1} for methyl α -D-glucopyranoside and 29 M^{-1} for methyl α -D-galactopyranoside), which are slightly lower than that of reducing α -D-glucose (31 M^{-1}). This indicates that, in these systems, the binding constants are not determinant factors controlling hydrogel strength. Therefore, some explanation based on the number of different possible complex structures for benzoboroxole with the glycopyranosides was proposed (Figure 11c).³⁷ The authors attributed the formation of a slow relaxing hydrogel using PMan to the existence of two different binding modes of benzoboroxole toward the mannopyranoside unit, which involve two independent diol pairs. Nevertheless, more work is warranted to assess the relationship between the dynamic mechanical behavior of benzoboroxole-based networks and the properties of the small-molecule crosslinkers.

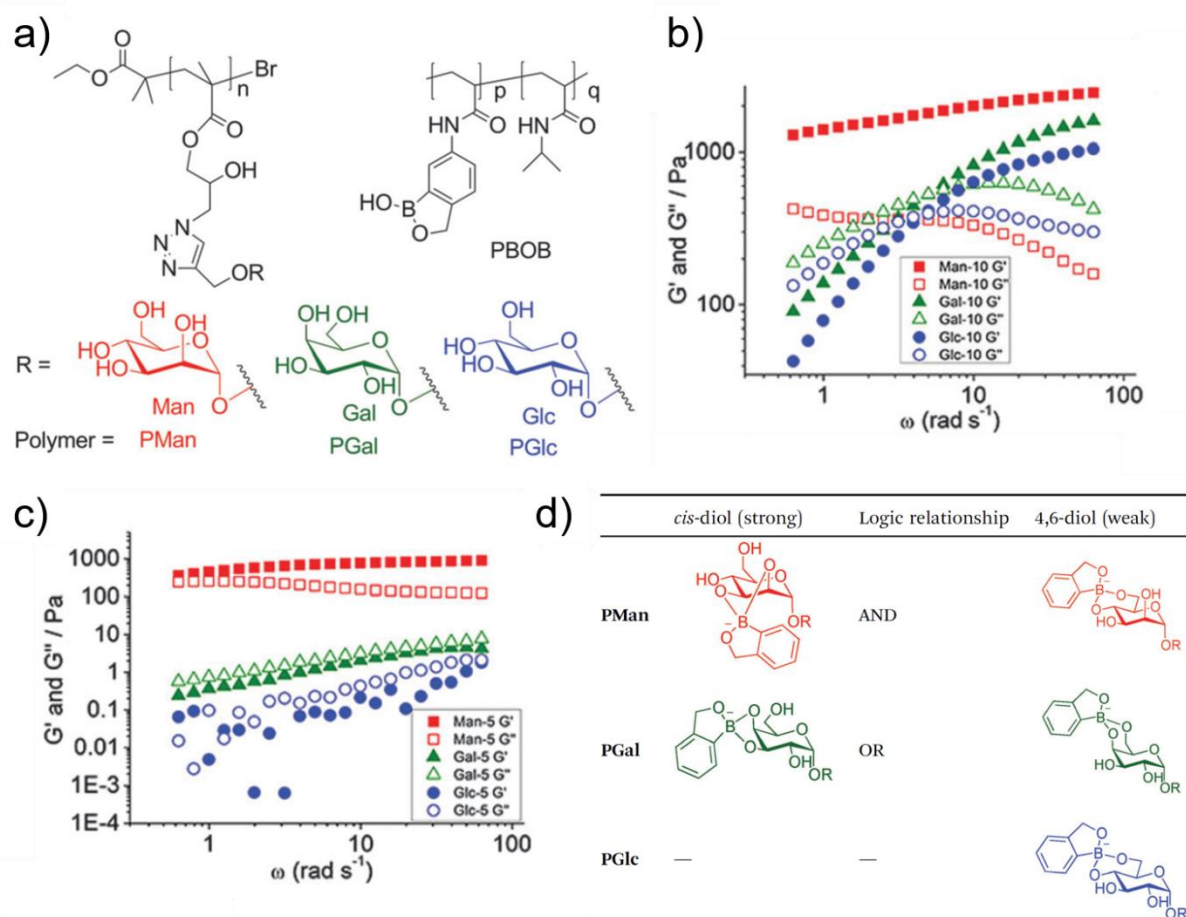


Figure 11. (a) Chemical structures of the benzoboroxole-based copolymer (PBOB) and of the synthetic glycopolymers bearing pendent mannopyranoside (PMan), galactopyranoside (PGal) and glucopyranoside (PGlc) units. Frequency dependence of G' and G'' at 20 °C of the polymer assemblies at a total polymer concentration of (b) 10 wt % and (c) 5 wt %. (d) Possible binding modes of benzoboroxole with mannopyranoside, galactopyranoside and glucopyranoside. Reproduced from Lin *et al.*⁶⁷

4. Current biomedical applications of boronate-crosslinked hydrogels

4.1. Controlled release of bioactive molecules

For many years, boronic acid-containing hydrogels have been developed for drug release applications, taking advantage of their stimuli-responsiveness allowing for fine control over the drug release rate.⁴ A major challenge in this field is to design self-regulated insulin release hydrogels by exploiting their glucose-sensitivity. More recently, increased attention has also been paid to the delivery of other bioactive molecules, such as anti-HIV drugs,^{68,69} anti-cancer drugs,^{12,14,70} and adenosine triphosphate (ATP).⁷¹

The incorporation of such molecules into the hydrogel is usually performed by passive diffusion into the pre-formed gel matrices (i.e. post-loading), or during hydrogel formation by mixing the polymer solutions containing the active molecule (i.e. *in situ* loading). Inert

molecules (with no specific interaction with the polymer networks and boronic functional groups), can be loaded simply by physical entrapment, whereas those with diol functionality can also be incorporated via boronate ester binding with boronic acid moieties in the hydrogel matrix.^{72–75}

A method to release insulin from boronate-crosslinked hydrogel films were demonstrated using layer-by-layer films fabricated from PVA mixed with an acrylamide-based copolymer containing PBA moieties.^{76,77} Because of the reversible nature of the phenylboronate ester crosslinks, the layer-by-layer hydrogel was able to disintegrate gradually when immersed in aqueous solutions.⁷⁷ This gradual disassembly of the network allowed encapsulated insulin to be released into the aqueous media with a release rate that increased when the glucose concentration in the media was increased. This property revealed the potential of application of the system as a platform for self-regulated insulin release. Indeed, in such system, free glucose may react with PBA groups by binding with free pendant PBA moieties or by competing with PVA diols complexed with PBA sites (hydrogel crosslinks). While the former leads to the formation of hydrophilic negatively charged phenylboronate groups, the later results in a decreased crosslinking density. Both reactions thus promote hydrogel film disassembly, and thereby, insulin release.

Recently, strategies were developed to improve the applicability of boronate-crosslinked hydrogels possessing self-healing properties in this field. Based on the idea that glucose could competitively bind to boronic acid moieties in other boronic acid-diol systems, it is reasonable to use free glucose to control the drug release behavior of hydrogels. In this context, a previously described PEG-based hydrogel network designed by Yesilyurt *et al.* (i.e. based on a four-arm PEG derivative modified with FPBA (PEG-FPBA) that forms a viscoelastic network with a four-arm PEG containing glucose-like moieties) showed ability to incorporate insulin, globulin G (IgG) and bovine serum albumin (BSA) as model proteins, by loading them into solutions of the PEG precursors prior to hydrogel formation.¹¹ Both BSA and insulin had an initial burst release before controlled release was observed. This was not observed for the larger IgG (Figure 12). The release rate of protein from the hydrogel correlated with protein molecular weight, with 77 % of insulin released within the first 48 h against only 30 % of IgG released within 10 days. The authors attributed this protein size-dependent release effect to the mesh size of the hydrogel network. Indeed, this explains why the release kinetics of insulin was hardly affected, as this macromolecule was poorly sensitive to the mesh size of the hydrogel. By contrast, in the case of IgG, free glucose in solution disassembled the polymer network, changing the mesh size of the hydrogel and accelerating the release kinetics. This protein demonstrated size-selective release from the hydrogel, showing a release of 13 %

within 48 h in glucose-free PBS buffer, whereas a release of 46 % and 65 % were observed in a buffer of 4 mg.mL⁻¹ glucose and 12 mg.mL⁻¹ glucose, respectively.

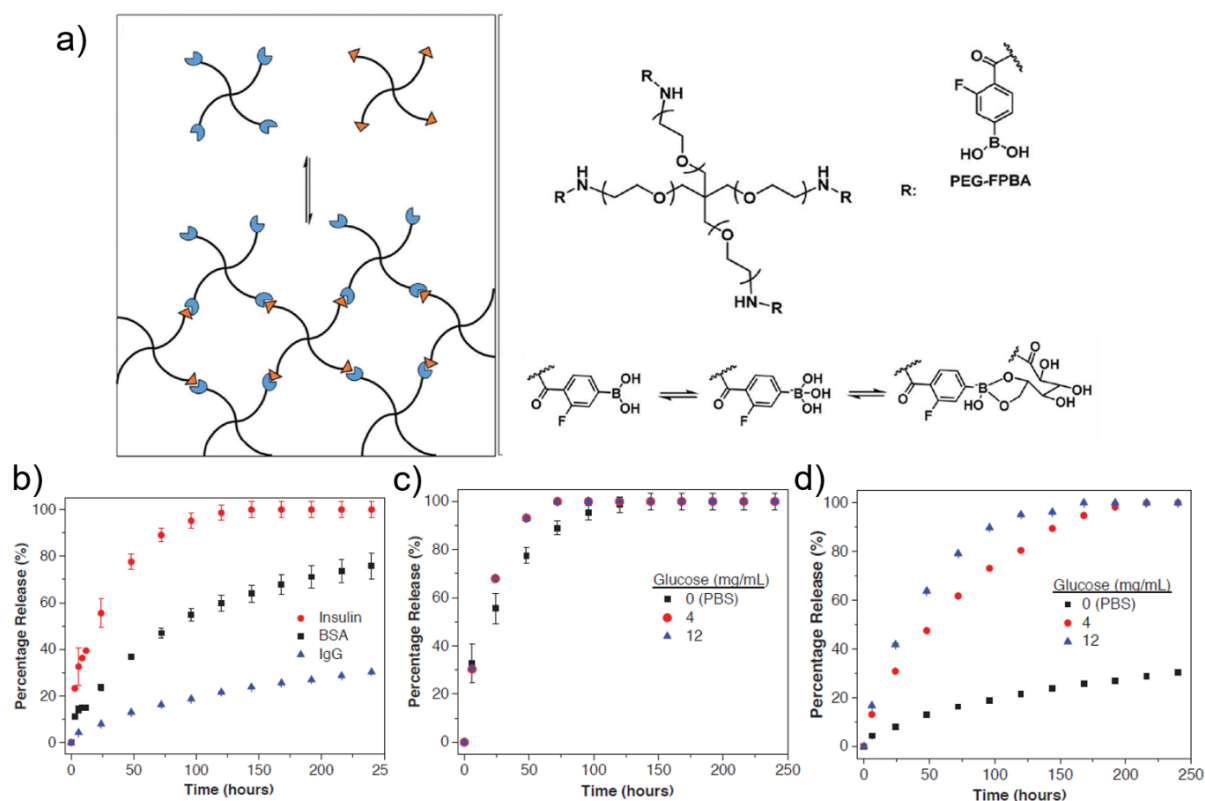


Figure 12. (a) Viscoelastic network formed by combining FPBA-containing four-arm PEG derivative and four-arm PEG bearing glucose-like moieties. Release profiles of proteins (insulin, IgG and BSA) from the PEG assembly formed at pH 7: (b) release profiles in PBS buffer, and release of (c) insulin and (d) IgG at different glucose concentrations. Reproduced from Yesilyurt *et al.*¹¹

In the majority of hydrogels based on PBA-diol crosslinking used as insulin-delivery systems, the gels experience an early drug release mainly due to their large pore size and high water content, which may decrease the therapeutic efficacy of insulin. To address this problem and increase the performance of these hydrogels, one strategy that has recently been used is to modify their morphology by incorporating micro/nanostructured fillers into the macrogel network. This allows formation of nanocomposite hydrogels capable of encapsulating insulin inside the micro/nanostructures while retaining their rheological properties. For example, a microparticle-viscoelastic hydrogel (MP-gel) hybrid system was designed for fast glucose-responsive delivery at physiological conditions. The system was based on PBA-modified porous poly(lactic-co-glycolic acid) (PLGA) microparticles that were bound to a dopamine-modified hyaluronic acid (DOP-HA) conjugate via PBA-catechol interaction.⁷⁸ This complexation enabled a dense and hydrophilic gel layer of DOP-HA on the particle surface

under neutral conditions, with particles serving as an insulin reservoir and as a crosslinker for the HA chains (Figure 13a). The formation of boronate ester crosslinks led to a soft injectable nanocomposite system exhibiting a viscoelastic behavior (Figure 13b), as well as shear-thinning properties (Figure 13c) and tissue-adhesive functionality for long-lasting adherence. The study of insulin release from the MP-viscoelastic gel at 37 °C (pH 7.4) showed that the system was able to load 35.6 % of the drug with an encapsulation efficacy of 45.8 %, due to its large pore surface area. At low glucose concentration, DOP-HA could remain tightly attached to the MPs surface, acting as a barrier for insulin diffusion. However, when increasing the glucose concentration, the particles were disconnected from the DOP-HA macrogel layer due to the displacement of DOP by glucose at the PBA binding sites, enabling a fast release of the encapsulated insulin from the particles.

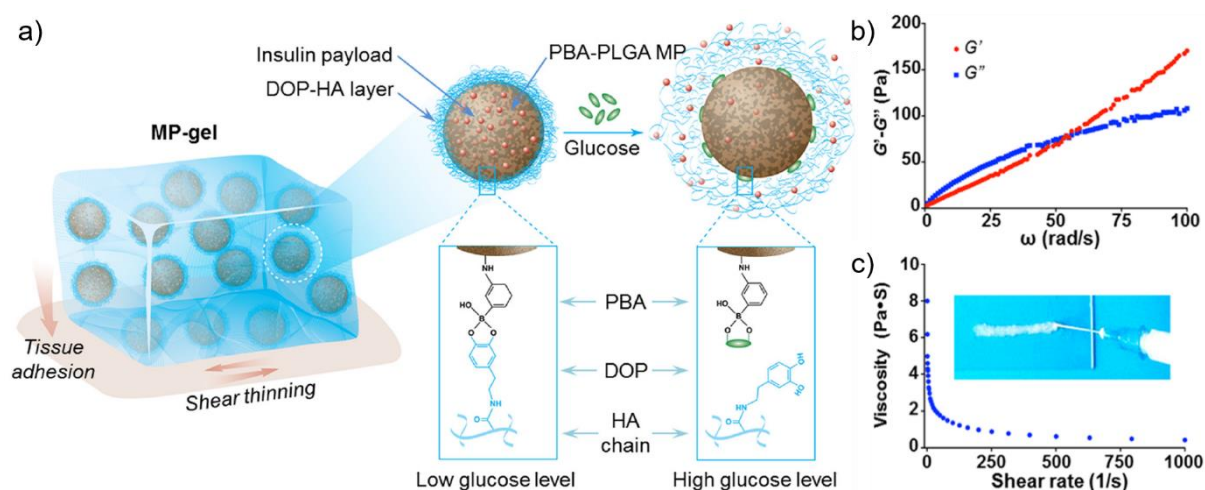


Figure 13. (a) Schematic illustration of a microparticle-hydrogel hybrid formulation (MP-gel) based on the interaction of PBA-modified porous poly(lactic-co-glycolic acid) (PLGA) microparticles (PBA-PLGA MPs) with a dopamine-grafted hyaluronic acid (DOP-HA) conjugate via PBA-catechol crosslinking. In the design, the particles serve as both the insulin reservoir and the crosslinker of HA chains. At a low glucose level, DOP-HA remains bound to the PBA-PLGA MPs, forming a dense hydrophilic layer which acts as a diffusion barrier to avoid insulin release. At a high glucose concentration, DOP-HA chains dissociate from the particles surface, leading to a faster insulin release. Rheological analysis of the MP-viscoelastic nanocomposite at 25 °C, pH 7.4: (b) frequency dependence of G' and G'' ; and (c) viscosity and shear-thinning behavior (inset shows the injection of the MP-viscoelastic gel through a 23-gauge needle). Reproduced from Zhao *et al.*⁷⁸

Besides insulin-delivery gels, Kiser and co-workers also demonstrated the potential of boronate-based hydrogels as innovative therapeutics for HIV-1 prevention.^{68,69} As discussed above, the HPMA-based networks crosslinked via PBA-SHA complexation exhibit pH-dependent viscoelastic properties and behave as viscoelastic solutions at pH 4-5.⁴⁷ Thus, inspired by the ability of the cervicovaginal mucus to impede the movement of HIV virions at acidic pH, the authors demonstrated the improved barrier properties of these polymer networks

over the naturally occurring cervicovaginal mucus by inhibiting viral transport at acidic and neutral pH (Figure 14a).⁶⁹ Indeed, at pH 4.8, the crosslinked polymers formed a transient network with a characteristic relaxation time of 0.9 s and elastic modulus of 11 Pa (Figure 14b). With the introduction of semen which possesses a slightly alkaline pH, high buffering capacity and large volume, the pH of the lumen environment containing the PBA-SHA gel could be neutralized. Therefore, with the increase of pH, the viscoelastic assembly became a densely crosslinked elastic network, with a characteristic relaxation time greater than 60 s and an elastic modulus of 1800 Pa (Figure 14b and c). This polymer hydrogel matrix could thereby act as a physical barrier, significantly impeding HIV migration, as revealed by transport assay. Additionally, these crosslinked polymers did not induce symptoms of toxicity or irritation in either human vaginal explants or in a mouse model. On the basis of these results, the PBA-SHA assembly appears, indeed, as a promising candidate to be used as drug delivery vehicles of anti-HIV drugs, providing additional protection for women exposed to the HIV virus.

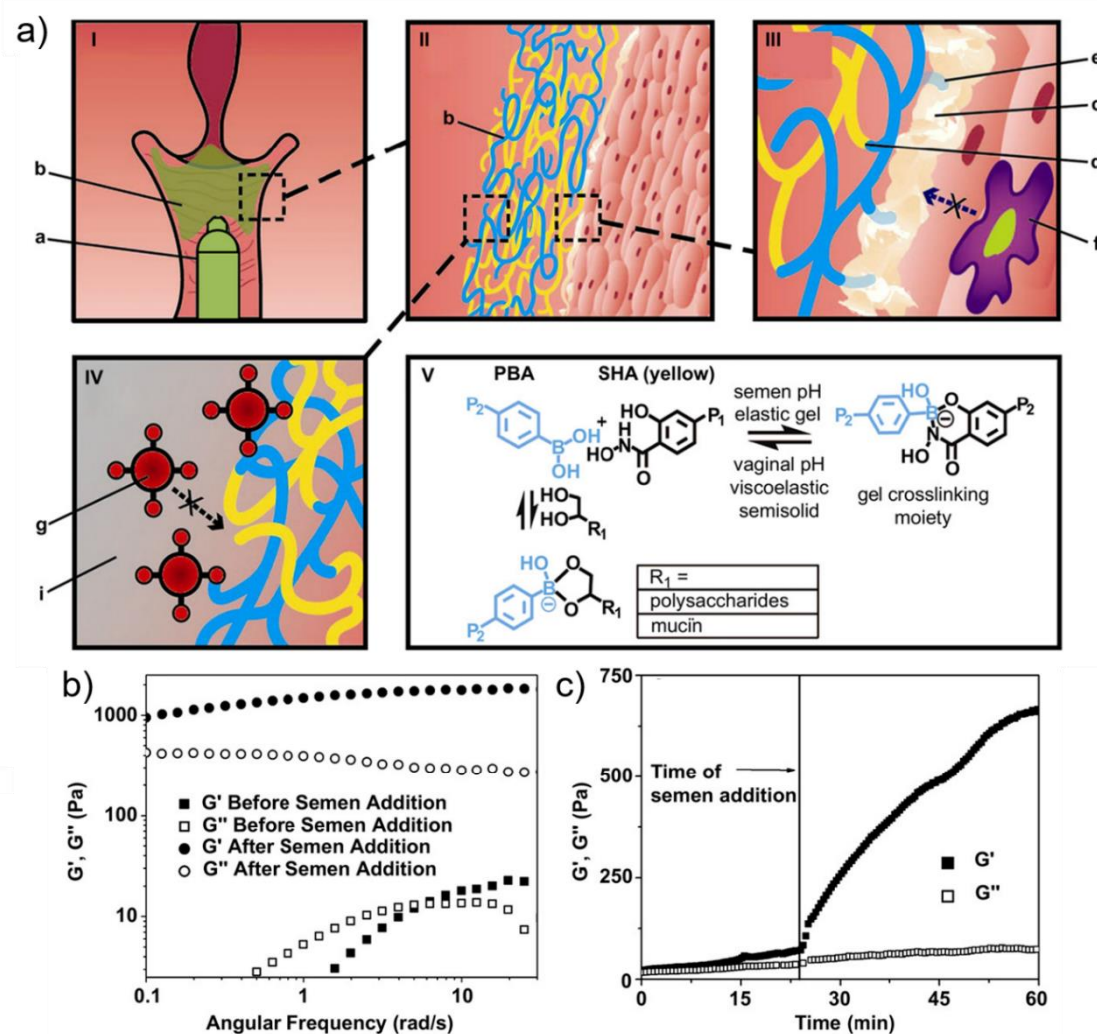


Figure 14. (a) Scheme illustrating the use of the PBA-SHA crosslinked hydrogel as a microbicide drug delivery system. (I) An applicator (a) is used to apply the weak viscoelastic

polymer network in the vaginal tract (b). (II) The polymer matrix forms a physical barrier between the vaginal mucosa and the environment. (III) The network formed consists of crosslinks between the two HPMA-based polymers (d) and diol-containing molecules present on the epithelial surface (c) and in cervical mucus (e). (IV) Upon insemination, vaginal pH is neutralized and the polymer system becomes a densely crosslinked elastic hydrogel, inhibiting diffusion of virions (g) to the vaginal mucosa. (V) pH-dependent equilibrium between PBA-SHA crosslinked structures and their free species that creates a pH-responsive polymer network that is transient and viscoelastic at vaginal acidic pH and is elastic and solid-like at the seminal pH. (b) Oscillatory measurements of frequency dependence of G' and G'' of the polymer network before and after semen addition at 37 °C. (c) Increase of the rheological moduli of the PBA-SHA polymer system due to the introduction of human semen at 37 °C. Reproduced from Mahalingam *et al.*⁶⁹

An interesting approach was described for the application of boronate-crosslinked hydrogels for the controlled release of anticancer drugs. This included hydrogel formation using a PBA-modified acrylamide copolymer which was directly crosslinked by gossypol, an anticancer drug containing diol functionality (Figure 15a). In contrast to previous hydrogel systems, where drugs were encapsulated in the crosslinked matrices, in the present system gossypol acts as a crosslinker itself. Indeed, hydrogels could be formed at physiological pH upon addition of gossypol at different molar concentrations (Figure 15b and c). Moreover, because lactic acid exists in cancer cells in elevated amounts, as well as formic acid, and the cancer cell environment is acidic, the release of gossypol from the hydrogel matrix was evaluated under these conditions. The polymer network could be dissociated in an acidic environment (pH 4.5), and its dissociation was enhanced in the presence of lactic acid (an α -hydroxy carboxylic acid) as compared to formic acid (Figure 15d and e). The enhanced dissociation of the hydrogel by lactic acid was attributed to the effective separation of the boronate ester bridging groups through the formation of a stabilized complex between the boronic acid substituent and lactic acid. These results suggested that the gossypol-crosslinked hydrogel may, indeed, act as a functional carrier of the chemotherapeutic drug, revealing its controlled release properties under acidic conditions available in cancer cells.

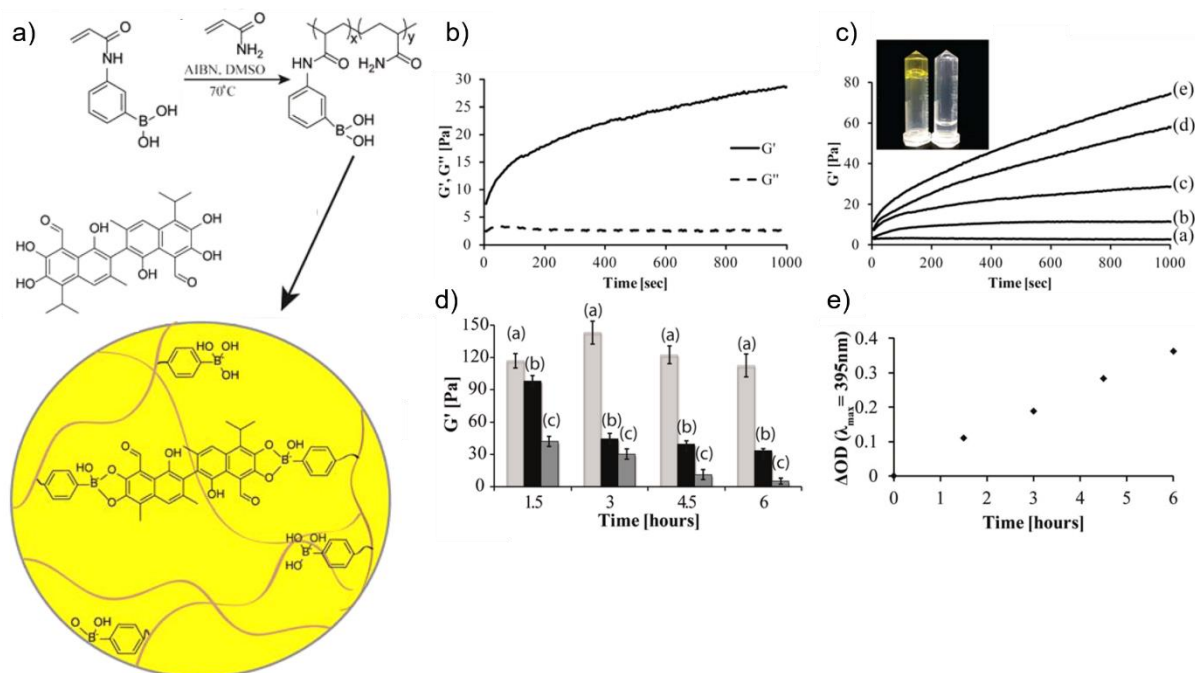


Figure 15. (a) Synthesis of PBA-containing polyacrylamide copolymer and its crosslinking with gossypol to form a hydrogel. (b) Time-dependent G' and G'' upon formation of the gossypol-crosslinked network. (c) Time-dependent changes in the storage modulus generated in the presence of various concentrations of gossypol ((a) 210 μM , (b) 440 μM , (c) 880 μM , (d) 1.8 mM, and (e) 3.5 mM; inset showing images of the gossypol crosslinked hydrogel (left) and of the polymer solution in the absence of gossypol (right). (d) Effect of adding formic acid and lactic acid in the values of G' of the network ((a) PBS buffer pH 7.4 as a control, (b) 200 mM formic acid pH 4.5, and (c) 200 mM lactic acid pH 4.5). (e) Time-dependent release of gossypol from the PBA-gossypol crosslinked hydrogel in the presence of 200 mM lactic acid at pH 4.5. Reproduced from Heleg-Shabtai *et al.*¹²

More recently, Huang *et al.* used a similar strategy to develop injectable hydrogels formed at physiological conditions using PEG derivatives modified with different boronic acids as polymer backbones and plant derived polyphenols (i.e. ellagic acid (EA), epigallocatechin gallate (EGCG), tannic acid (TA), nordihydroguaiaretic acid (NDGA), rutin trihydrate (RT), rosmarinic acid (RA) and carminic acid (CA)) as crosslinkers (Figure 16a).¹⁴ In addition to their recent emergence as building blocks for functional materials, plant polyphenols have, indeed, found growing interest due to their complex bioactivities and antioxidant behavior. However, these therapeutic molecules present limitations for their clinical translation, including poor bioavailability, rapid metabolism, and poor membrane permeability, requiring an efficient delivery method. Therefore, when EA and EGCG polyphenols were used as crosslinkers of boronic acid-modified PEG precursors with different architectures, stable boronate-crosslinked viscoelastic assemblies could be formed at physiological pH (Figure 16b, c and d). Taking advantage of the pH-dependent behavior of boronate ester crosslinks, polymer networks could be prepared *in situ* by injecting a slightly acidic solution of boronic acid-PEG derivative (i.e. PEG8H-BA4) and a polyphenol solution into pH 7.4 PBS buffer. This method provided long-

term steady state release of bioactive EA from the polymer matrix, which suggests the possibility to use an injectable hydrogel for localized delivery of bioactive polyphenols (Figure 16e). Moreover, the kinetics of EA release from the PEG-boronic acid assembly demonstrated *in vitro* cytotoxic effects of released EA on CAL-27 human oral cancer cells (Figure 16f).

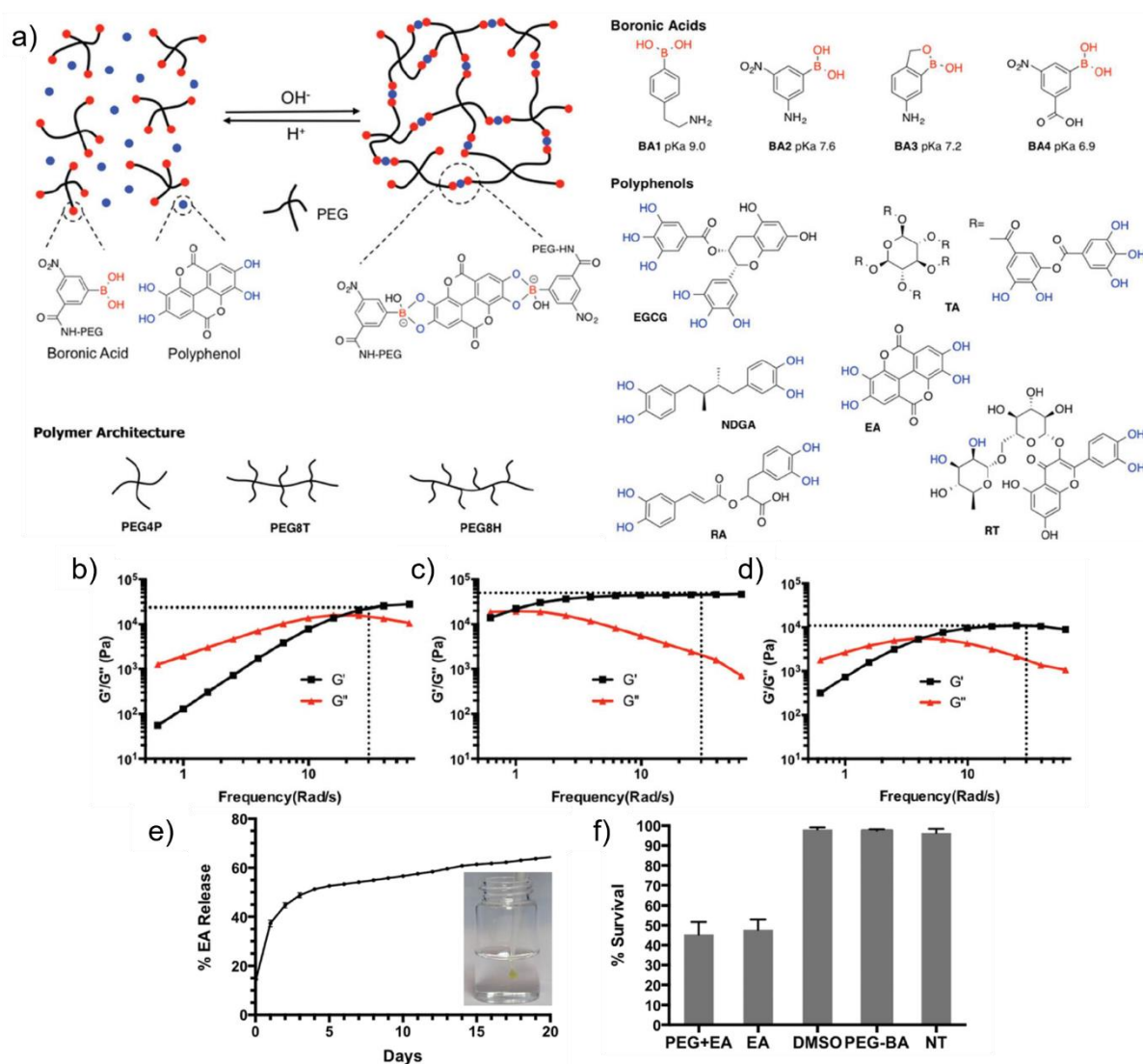


Figure 16. (a) Schematic illustration of pH responsive complexation between boronic acid functionalized PEG and polyphenols resulting in formation of a hydrogel network; architectures of PEG polymers and chemical structures of boronic acids and polyphenols (vicinal diols capable of boronate ester formation are shown in blue). Frequency dependence of G' and G'' for PEG networks crosslinked with EGCG and EA at pH 7.4: (b) PEG4P-BA1-EGCG; (c) PEG8H-BA4-EGCG; and (d) PEG8H-BA4-EA. (e) Release of EA from the PEG8H-BA4-EA polymer assembly in buffer (inset shows *in situ* gel formation upon injection of an acidic solution of the PEG8H-BA4 polymer precursor and EA into excess buffer at pH 7.4). (f) CAL27 cell survival rate upon exposure to PEG8H-BA4-EA gel, showing similar survival rates for both PEG8H-BA4-EA and EA groups, whereas nearly 100 % survival was found for DMSO, PEG8H-BA4 and untreated (NT) groups. Reproduced from Huang *et al.*¹⁴

4.2. Injectable hydrogels for 3D cell encapsulation

Boronate-crosslinked hydrogels have also emerged as promising injectable scaffolds for 3D culture and growth of cells, with applications in tissue engineering and regenerative medicine. The dynamic nature of boronate ester crosslinks endows hydrogels with reversible mechanical properties, usually accompanied by self-healing ability. In addition, the selective formation of boronate esters between boronic acids and diol-containing molecules provide systems with less interference from many functional groups that are present in complex biochemical environments.^{79,80}

Although such hydrogels have been widely investigated, only few studies report on their design to be used as stable 3D cell culture platforms^{4,11,16,47} because of the relatively weak interaction of common boronic acids with diol-containing molecules at physiological pH. In this context, the PEG-based viscoelastic assemblies designed by Yesilyurt *et al.* showed a good cytocompatibility as 3D substrates for 3T3 fibroblasts.¹¹ The presence of cells during network formation did not inhibit boronate ester crosslinking between PEG modified with glucose derivatives and PEG-FPBA partner and cells were dispersed homogeneously within the viscoelastic hydrogel network. Live/Dead staining demonstrated that most of cells encapsulated remained viable within 72 h, indicating minimal cytotoxicity in response to the material or its *in situ* crosslinking (Figure 17a). However, it is important to notice that when cells were dispersed in a pre-formed hydrogel and subsequently extruded through a syringe (21 gauge needle), cell viability was not preserved due to the high shear rates necessary to induce shear-thinning in the gel.

Narain and co-workers also demonstrated the applicability of 2-methacryloyloxyethyl phosphorylcholine (MPC)-based viscoelastic network crosslinked via benzoboroxole-dopamine interaction as a support for 3D cell encapsulation.¹⁶ This included loading of HeLa cells in the hydrogel, cultured with low glucose DMEM medium for 24 h. Live/Dead studies also showed that the majority of cells remained viable, with a cell viability of approximately 86 % (Figure 17b). Such promising results may be related to the nontoxic polymeric matrix (biocompatible MPC) and the porous network structure.

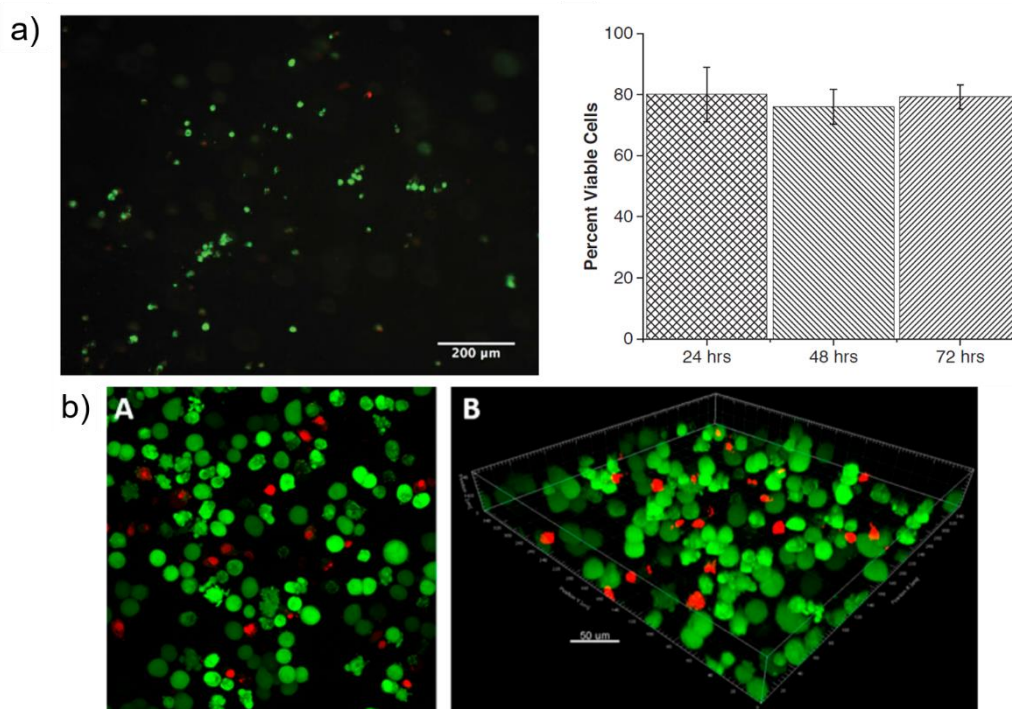


Figure 17. (a) Live/Dead assay image of 3T3 fibroblasts encapsulated within a PEG-FPBA hydrogel for 72 h (scale bar of 200 μm) and cell viability quantified at different time points (24–72 h). Reproduced from Yesilyurt *et al.*¹¹ (b) Live/dead assay of HeLa cells cultured in a hydrogel crosslinked via benzoboroxole-dopamine complexation for 24 h: (A) 2D and (B) 3D images obtained from fluorescent confocal microscopy. Green color represents live cells and red color represents dead cells. Reproduced from Chen *et al.*¹⁶

Inspired by previous studies, Tang *et al.* more recently designed adaptable hydrogels for 3D cell culture. This consisted of combining octa-arm PEG derivatives bearing catechol-based molecules (i.e. catechol derivative and nitro-dopamine, ND) and octa-arm PEG conjugates modified with either 2-fluorophenylboronic acid¹¹ (FPBA), benzoboroxole⁵⁹ (BX) or a Wulff-type *o*-aminomethylphenylboronic acid³¹ (WBA, Figure 18a) which formed viscoelastic networks at physiological pH. Rheological analysis showed that the frequency-dependent viscoelastic properties of the assemblies could be effectively controlled through small molecule design, with a higher plateau modulus observed for the PEG-FPBA network correlating with a higher affinity of FPBA for ND (Figure 18b). Furthermore, the different values of ω_c were also attributed by the authors to be similarly dependent on the boronic acid structure, with the slowest relaxation observed for the strongest FPBA-ND bonds, and the fastest relaxation related to the weakest WBA-ND bonds. Though the dissociation rate constants of the boronate bonds were not measured, the authors suggested that network relaxation time is governed by the small-molecule dissociation time, as previously reported in studies on coordinatively crosslinked polymer networks and metallohydrogels.^{81,82} However, due to the fast dynamics of the PEG assemblies based on boronate crosslinks formed with ND, these materials were found to

completely disassemble within less than 4 h at 37 °C when placed in a sink of cell culture media (often containing excess monosaccharides, such as low glucose Dulbecco's modified Eagle's medium, DMEM).

Thus, to overcome the limitation of rapid gel erosion, the FPBA-ND system was additionally crosslinked by a secondary orthogonal mechanism based on azide-alkyne cycloaddition (SPAAC) leading to covalent bonds formation (Figure 18c). This strategy resulted in a more stable network while presenting a relatively fast dynamics. The hybrid hydrogel showed a good cytocompatibility when encapsulated with hMSCs (human mesenchymal stem cells) cultured in growth media for 7 days. For a control, the same cells were encapsulated in a purely elastic hydrogel only crosslinked via the permanent covalent SPAAC chemistry, with an elastic modulus quite similar to that of the hybrid gel (14 kPa and 16.5 kPa, respectively). Cells in both gels showed a high viability 1 day after encapsulation (Figure 18d and e). Most of cells remained viable (over 90 %) in the hybrid gel network (stress-relaxing gel), with a significant fraction of cells that had spread within this material. On the other hand, cell viability decreased in the SPAAC elastic control (81 %), and the cells remained rounded. These results suggested that the stress relaxation found in boronate-crosslinked hydrogels may be, indeed, a contributing factor to maintain cell viability and allow cell–matrix interactions and spreading.

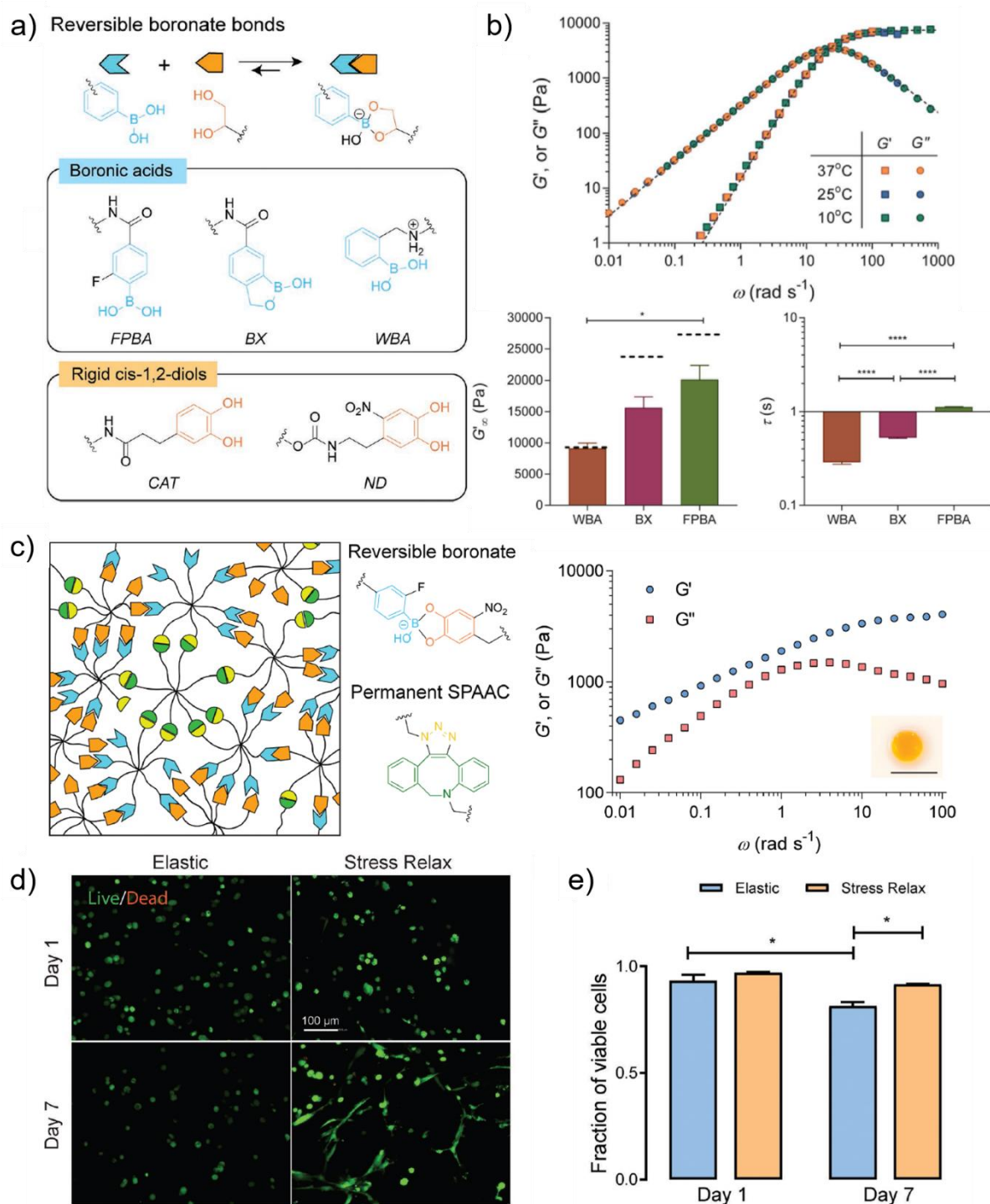


Figure 18. (a) Adaptable PEG networks based on dynamic covalent boronate ester crosslinks formed between 2-fluorophenylboronic acid (FPBA), benzoboroxole (BX), or a Wulff-type-like boronic acid (WBA) and catechol (CAT) or nitro-dopamine (ND). (b) Tunable rheological properties of the PEG assemblies based on boronic acid-ND crosslinks, showing frequency-dependent viscoelastic properties at 37 °C. Comparison of the plateau modulus (G') of the systems (black dashed lines show the theoretical moduli theoretically estimated with basis on the small molecule equilibrium constants), and comparison of ω_c values ($n \geq 3$). (c) Design of stable hybrid hydrogels exhibiting fast relaxation dynamics. Scheme illustrating the hybrid network containing both reversible boronate bonds and permanent covalent SPAAC bonds, and the frequency dependence of G' and G'' at 37 °C of this hydrogel after

being swollen in hMSC growth media for 7 days (low glucose DMEM supplemented with 10 % fetal bovine serum (FBS), 100 U.mL⁻¹ penicillin, 100 µg.mL⁻¹ streptomycin, and 1 µg.mL⁻¹ fungizone; inset photograph shows gel appearance after being swollen in media for 7 days, demonstrating gel stability; scale bar 1 cm). (d) Cytocompatibility of boronate-based hydrogels: representative maximum intensity projection images of cells in elastic and stress relaxing hydrogels on day 1 and day 7 (cells were stained with calcein AM (green, live) and ethidium homodimer (red, dead); scale bar of 100 µm), and quantification of cellular viability (error bars represent the standard errors of the mean; statistical analysis from one-way ANOVA test, * indicating $p < 0.05$). Reproduced from Tang *et al.*¹⁵

4.3. Other applications

Because of their sensitivity to glucose and other saccharides, boronic acid-containing hydrogels have also been exploited as sensing materials in electrochemical sensor design. For example, Kikuchi *et al.* prepared an interpolymer complex gel from PVA and a copolymer containing both PBA and tertiary amine moieties and casted the gel on a platinum electrode.⁸³ The gel-coated electrode was sensitive to external glucose concentrations, showing an increased swelling degree due to glucose addition. This allowed to increase diffusion of ion species and thus of current changes. Interestingly, the current changes were proportional to glucose concentration in the range of 0-300 mg.dL⁻¹, which corresponds well to physiological blood glucose levels.

Furthermore, a hydrogel obtained by combining a phospholipid polymer (i.e. 2-methacryloyloxyethyl phosphorylcholine) containing PBA units and PVA was successfully applied in microfluidic chips, on which various cell-based applications, such as cytotoxicity assays, can be performed.^{84,85} Indeed, cells could be homogeneously encapsulated in the *in situ*-formed gel, and kept a spherical morphology without forming cell aggregates. In addition, they could be released from the gel matrix by adding glucose. The recovered cells demonstrated good adhesion to tissue culture polystyrene and proliferate well on the surface. As the gel allowed for spontaneous encapsulation and mild preservation of living cells, the chips did not require an additional off-chip culture medium support for cell maintenance, making the system simpler, safer, and more independent.

In addition, Tao Chen and co-workers designed boronate-crosslinked hydrogels exhibiting shape-memory capability by mixing PBA-grafted alginate and alginate modified with dopamine residues or PVA, under alkaline conditions.⁵¹⁻⁵³ Apart from its reaction with the diol-containing polymers, alginate-PBA also formed ionotropic network with calcium ions, which can be extracted from the hydrogels and thus contribute to the shape memory ability. As expected, the gels showed a pH-induced shape-memory behavior. In acidic conditions (pH 6), the PBA-diol bonds could dissociate and be reformed at a higher pH value (pH 10.6), stabilising a temporary shape. Alginate-calcium interactions behave as permanent cross-links, allowing to

capture the hydrogel shape not only under slightly acidic conditions but also in a 0.2 M glucose solution.⁵³

More recently, an interpenetrating network (IPN) hydrogel was formed using a hyaluronic acid derivative bearing 2-aminophenylboronic acid moieties (HA-2APBA) combined with PVA, in addition to alginate-calcium crosslinks.¹⁹ The IPN hydrogel exhibited self-healing, self-adhesive properties and bulk and interfacial mechanical stabilities required for the direct additive manufacturing (3D printing) of hydrogel microchannels for prevascular network fabrication.¹⁹ Indeed, using the patterning technique, the hydrogel could be assembled into hollow perfusion channels by simple contact within few minutes due to its self-adhesive properties (Figure 19a and b). As these channels showed resistance to fluid perfusion while retaining their dimensions (Figure 19b), and supported endothelial cell growth and proliferation (Figure 19c), these materials may provide a simple route to produce customized cell scaffolds. This study emphasizes the potential of self-healing hydrogels based on boronate ester crosslinks for designing innovative biomaterials for modern biomedical applications, such as 3D bioprinting.

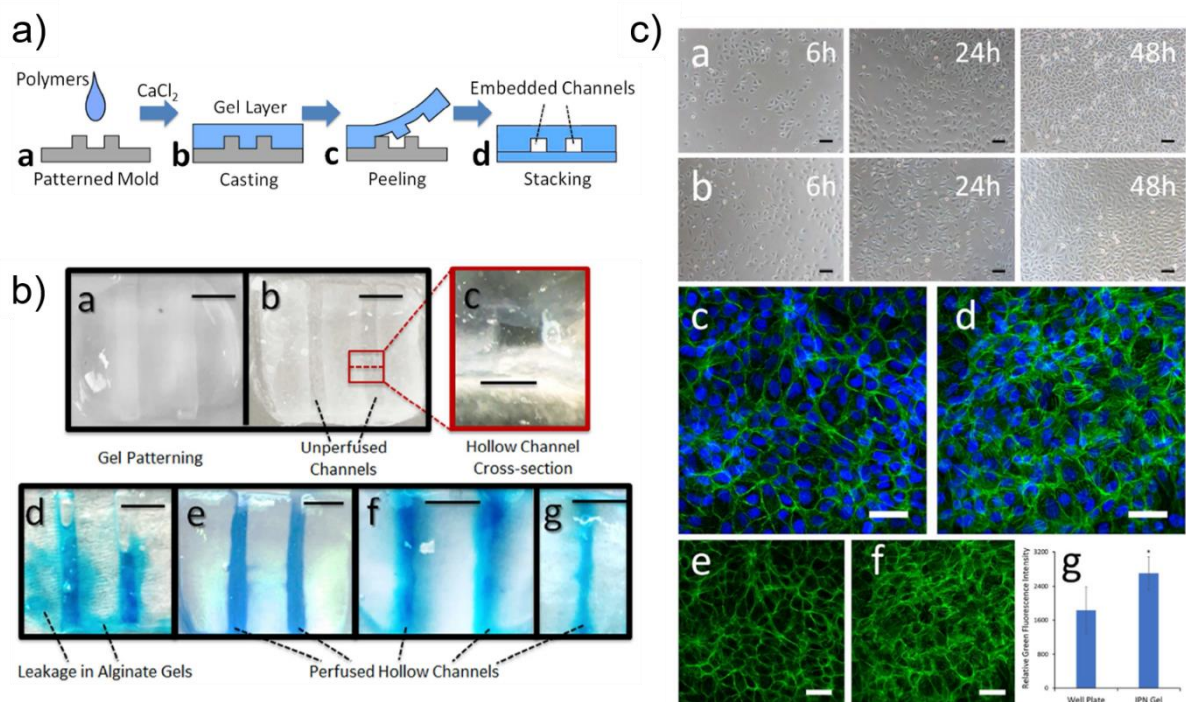


Figure 19. (a) Fabrication of integrated hollow channels using HA-2APBA/PVA + alginate-calcium IPN hydrogel in four steps: a) the precursor polymers (HA-2APBA/PVA and alginate) were mixed and spread across the mold; b) the cast hydrogel attached to the mold was immersed in a calcium chloride bath to crosslink free alginate and form the IPN gel; c) the patterned IPN gel film was peeled from the mold while retaining the templated structure and then d) placed on a flat gel sheet and allowed to self-adhere to bond the channels. (b) Structure and functionality of additively manufactured self-adhered channels using the IPN hydrogel: a) gels can be patterned using a 3D printed mold; b) hollow channel structures can

be formed by adhering the patterned gel to a flat gel support; c) a cross-section of a 2 mm × 2 mm hollow channel shows no interface between the top and bottom gel layers, indicating self-adhesion; d) perfusion of water (dyed blue) through channels fabricated from alginate-calcium alone leak due to the lack of interfacial adhesion; e) perfusion of water through channels fabricated from the IPN hydrogel confirms functional adhesion at the interface via autonomous self-healing; f) hollow channel IPN gel samples stored in air at 100 % relative humidity for 3 days could be successfully perfused without visible leaking; and g) hollow channel IPN gel stored in water for 3 days could be perfused without leaking (scale bars of 5 mm, except c (2 mm)). (c) Morphology of HUVECs (human umbilical vein endothelial cells) cultured on a) a polystyrene well plate and b) the IPN gel; fluorescent staining of F-actin (green) and nucleus (blue) in HUVECs cultured for 48 h on (c, e) a polystyrene well plate and (d, f) the IPN gel (scale bars of 50 μm). g) Relative green fluorescence intensity of e) and f) measured by ImageJ 1.51k software. Reproduced from Deng *et al.*¹⁹

5. Conclusions and future perspectives

The design of hydrogels crosslinked via boronic acid-diol complexation has found real progress in the past few years for many biomedical purposes. Through the selective binding of different arylboronic acids to a variety of diol-containing molecules, such gels can be engineered to have readily adjusted mechanical properties matching those required for each specific application. Taken together, the boronate-crosslinked hydrogels described in this literature review illustrate that such materials can indeed be rationally designed by tuning their small-molecule structure and properties. Such a strategy has been successfully used to produce hydrogels with optimized rheological properties at physiological pH, mainly by using PBA derivatives with improved binding capabilities at this pH. Moreover, the possibility to tune the macromolecular architecture (e.g. nature of polymer backbone, macromolecular structure) and/or the morphology (such as in micro/nanostructured composite gels) also allows the development of multiple hydrogel formulations with well-defined properties.

Nevertheless, advances in hydrogel design have essentially been proved by physico-chemical studies and the biocompatibility and biodegradability of these materials are other issues that need to be addressed. Indeed, while many hydrogels have shown limited toxicity in simple cytotoxicity assays, there remains a relative lack of true *in vivo* evaluation. Nevertheless, the use of boronate-crosslinked gels in the biomedical field has evolved, likely as a result of the advantageous synergy between boronic acid reactivity and biological composition. Over the past years, a major objective for the development of such gels has been the fabrication of glucose sensing and self-regulated insulin release systems. More recently, these biomaterials have emerged as promising candidates to be applied for modern therapies, in particular for tissue engineering and regenerative medicine. In this regard, great attention is currently focused on their use as injectable scaffolds that serve as a support for 3D cell encapsulation or even for the fabrication of complexed tissue scaffolds by 3D bioprinting.

Beyond these applications, boronate-crosslinked hydrogels will likely find much wider use in the medical field.

6. References

- (1) Ratner, B. D.; Bryant, S. J. Biomaterials: Where We Have Been and Where We Are Going. *Annu. Rev. Biomed. Eng.* **2004**, *6*, 41–75.
- (2) Edsman, K.; Nord, L. I.; Öhrlund, Å.; Lärkner, H.; Kenne, A. H. Gel Properties of Hyaluronic Acid Dermal Fillers: *Dermatol. Surg.* **2012**, *38* (7pt2), 1170–1179.
- (3) Li, Y.; Rodrigues, J.; Tomás, H. Injectable and Biodegradable Hydrogels: Gelation, Biodegradation and Biomedical Applications. *Chem Soc Rev* **2012**, *41* (6), 2193–2221.
- (4) Guan, Y.; Zhang, Y. Boronic Acid-Containing Hydrogels: Synthesis and Their Applications. *Chem. Soc. Rev.* **2013**, *42* (20), 8106.
- (5) Taylor, D. L.; in het Panhuis, M. Self-Healing Hydrogels. *Adv. Mater.* **2016**, *28* (41), 9060–9093.
- (6) Wei, Z.; Yang, J. H.; Zhou, J.; Xu, F.; Zrínyi, M.; Dussault, P. H.; Osada, Y.; Chen, Y. M. Self-Healing Gels Based on Constitutional Dynamic Chemistry and Their Potential Applications. *Chem Soc Rev* **2014**, *43* (23), 8114–8131.
- (7) Wang, H.; Heilshorn, S. C. Adaptable Hydrogel Networks with Reversible Linkages for Tissue Engineering. *Adv. Mater.* **2015**, *27* (25), 3717–3736.
- (8) Jin, Y.; Yu, C.; Denman, R. J.; Zhang, W. Recent Advances in Dynamic Covalent Chemistry. *Chem. Soc. Rev.* **2013**, *42* (16), 6634.
- (9) Elshaarani, T.; Yu, H.; Wang, L.; Zain-ul-Abdin, Z.-A.; Ullah, R. S.; Haroon, M.; Khan, R. U.; Fahad, S.; Khan, A.; Nazir, A.; et al. Synthesis of Hydrogel-Bearing Phenylboronic Acid Moieties and Their Applications in Glucose Sensing and Insulin Delivery. *J. Mater. Chem. B* **2018**, *6* (23), 3831–3854.
- (10) Chen, M. H.; Wang, L. L.; Chung, J. J.; Kim, Y.-H.; Atluri, P.; Burdick, J. A. Methods To Assess Shear-Thinning Hydrogels for Application As Injectable Biomaterials. *ACS Biomater. Sci. Eng.* **2017**, *3* (12), 3146–3160.
- (11) Yesilyurt, V.; Webber, M. J.; Appel, E. A.; Godwin, C.; Langer, R.; Anderson, D. G. Injectable Self-Healing Glucose-Responsive Hydrogels with PH-Regulated Mechanical Properties. *Adv. Mater.* **2016**, *28* (1), 86–91.
- (12) Heleg-Shabtai, V.; Aizen, R.; Orbach, R.; Aleman-Garcia, M. A.; Willner, I. Gossypol-Cross-Linked Boronic Acid-Modified Hydrogels: A Functional Matrix for the Controlled Release of an Anticancer Drug. *Langmuir* **2015**, *31* (7), 2237–2242.
- (13) Dong, Y.; Wang, W.; Veiseh, O.; Appel, E. A.; Xue, K.; Webber, M. J.; Tang, B. C.; Yang, X.-W.; Weir, G. C.; Langer, R.; et al. Injectable and Glucose-Responsive Hydrogels Based on Boronic Acid–Glucose Complexation. *Langmuir* **2016**, *32* (34), 8743–8747.
- (14) Huang, Z.; Delparastan, P.; Burch, P.; Cheng, J.; Cao, Y.; Messersmith, P. B. Injectable Dynamic Covalent Hydrogels of Boronic Acid Polymers Cross-Linked by Bioactive Plant-Derived Polyphenols. *Biomater. Sci.* **2018**, *6* (9), 2487–2495.
- (15) Tang, S.; Ma, H.; Tu, H.-C.; Wang, H.-R.; Lin, P.-C.; Anseth, K. S. Adaptable Fast Relaxing Boronate-Based Hydrogels for Probing Cell-Matrix Interactions. *Adv. Sci.* **2018**, 1800638.

- (16) Chen, Y.; Diaz-Dussan, D.; Wu, D.; Wang, W.; Peng, Y.-Y.; Asha, A. B.; Hall, D. G.; Ishihara, K.; Narain, R. Bioinspired Self-Healing Hydrogel Based on Benzoxaborole-Catechol Dynamic Covalent Chemistry for 3D Cell Encapsulation. *ACS Macro Lett.* **2018**, *7* (8), 904–908.
- (17) Chen, Y.; Wang, W.; Wu, D.; Nagao, M.; Hall, D. G.; Thundat, T.; Narain, R. Injectable Self-Healing Zwitterionic Hydrogels Based on Dynamic Benzoxaborole–Sugar Interactions with Tunable Mechanical Properties. *Biomacromolecules* **2018**, *19* (2), 596–605.
- (18) Wang, Y.; Li, L.; Kotsuchibashi, Y.; Vshyvenko, S.; Liu, Y.; Hall, D.; Zeng, H.; Narain, R. Self-Healing and Injectable Shear Thinning Hydrogels Based on Dynamic Oxaborole-Diol Covalent Cross-Linking. *ACS Biomater. Sci. Eng.* **2016**, *2* (12), 2315–2323.
- (19) Deng, X.; Attalla, R.; Sadowski, L. P.; Chen, M.; Majcher, M. J.; Urosev, I.; Yin, D.-C.; Selvaganapathy, P. R.; Filipe, C. D. M.; Hoare, T. Autonomously Self-Adhesive Hydrogels as Building Blocks for Additive Manufacturing. *Biomacromolecules* **2018**, *19* (1), 62–70.
- (20) Guvendiren, M.; Lu, H. D.; Burdick, J. A. Shear-Thinning Hydrogels for Biomedical Applications. *Soft Matter* **2012**, *8* (2), 260–272.
- (21) Brooks, W. L. A.; Sumerlin, B. S. Synthesis and Applications of Boronic Acid-Containing Polymers: From Materials to Medicine. *Chem. Rev.* **2016**, *116* (3), 1375–1397.
- (22) Cromwell, O. R.; Chung, J.; Guan, Z. Malleable and Self-Healing Covalent Polymer Networks through Tunable Dynamic Boronic Ester Bonds. *J. Am. Chem. Soc.* **2015**, *137* (20), 6492–6495.
- (23) Hall, D. G. Structure, Properties, and Preparation of Boronic Acid Derivatives. Overview of Their Reactions and Applications. In *Boronic Acids*; Hall, D. G., Ed.; Wiley-VCH Verlag GmbH & Co. KGaA: Weinheim, FRG, 2006; pp 1–99.
- (24) Yan, J.; Springsteen, G.; Deeter, S.; Wang, B. The Relationship among PK_a, PH, and Binding Constants in the Interactions between Boronic Acids and Diols—It Is Not as Simple as It Appears. *Tetrahedron* **2004**, *60* (49), 11205–11209.
- (25) Peters, J. A. Interactions between Boric Acid Derivatives and Saccharides in Aqueous Media: Structures and Stabilities of Resulting Esters. *Coord. Chem. Rev.* **2014**, *268*, 1–22.
- (26) Hosny, W. M.; Khalaf-Alaa, P. A. Potentiometric Study and Biological Activity of Some Metal Ion Complexes of Polyvinyl Alcohol (PVA). *Int J Electrochem Sci* **2013**, *8*, 14.
- (27) Lewis, G. P. The Importance of Ionization in the Activity of Sympathomimetic Amines. *Br. J. Pharmacol. Chemother.* **1954**, *9* (4), 488–493.
- (28) Martínez-Aguirre, M. A.; Villamil-Ramos, R.; Guerrero-Alvarez, J. A.; Yatsimirsky, A. K. Substituent Effects and PH Profiles for Stability Constants of Arylboronic Acid Diol Esters. *J. Org. Chem.* **2013**, *78* (10), 4674–4684.
- (29) Li, D.; Chen, Y.; Liu, Z. Boronate Affinity Materials for Separation and Molecular Recognition: Structure, Properties and Applications. *Chem. Soc. Rev.* **2015**, *44* (22), 8097–8123.
- (30) Mulla, H. R.; Agard, N. J.; Basu, A. 3-Methoxycarbonyl-5-Nitrophenyl Boronic Acid: High Affinity Diol Recognition at Neutral PH. *Bioorg. Med. Chem. Lett.* **2004**, *14* (1), 25–27.
- (31) Zhang, C.; Losego, M. D.; Braun, P. V. Hydrogel-Based Glucose Sensors: Effects of Phenylboronic Acid Chemical Structure on Response. *Chem. Mater.* **2013**, *25* (15), 3239–3250.

- (32) Wulff, G. Selective Binding to Polymers via Covalent Bonds. The Construction of Chiral Cavities as Specific Receptor Sites. *Pure Appl. Chem.* **1982**, *54* (11), 2093–2102.
- (33) Wiskur, S. L.; Lavigne, J. J.; Ait-Haddou, H.; Lynch, V.; Chiu, Y. H.; Canary, J. W.; Anslyn, E. V. PKa Values and Geometries of Secondary and Tertiary Amines Complexed to Boronic Acids: Implications for Sensor Design. *Org. Lett.* **2001**, *3* (9), 1311–1314.
- (34) Tomsho, J. W.; Pal, A.; Hall, D. G.; Benkovic, S. J. Ring Structure and Aromatic Substituent Effects on the p K_a of the Benzoxaborole Pharmacophore. *ACS Med. Chem. Lett.* **2012**, *3* (1), 48–52.
- (35) Adamczyk-Woźniak, A.; Borys, K. M.; Sporzyński, A. Recent Developments in the Chemistry and Biological Applications of Benzoxaboroles. *Chem. Rev.* **2015**, *115*, 5224–5247.
- (36) Dowlut, M.; Hall, D. G. An Improved Class of Sugar-Binding Boronic Acids, Soluble and Capable of Complexing Glycosides in Neutral Water. *J. Am. Chem. Soc.* **2006**, *128* (13), 4226–4227.
- (37) Bérubé, M.; Dowlut, M.; Hall, D. G. Benzoboroxoles as Efficient Glycopyranoside-Binding Agents in Physiological Conditions: Structure and Selectivity of Complex Formation. *J. Org. Chem.* **2008**, *73* (17), 6471–6479.
- (38) Springsteen, G.; Wang, B. A Detailed Examination of Boronic Acid–Diol Complexation. *Tetrahedron* **2002**, *58* (26), 5291–5300.
- (39) Deuel, von H.; Neukom, H. Über die reaktion von borsäure und borax mit polysacchariden und anderen hochmolekularen polyoxy-verbindungen. *Makromol. Chem.* **1949**, *3* (1), 13–30.
- (40) Pezron, E.; Leibler, L.; Ricard, A.; Lafuma, F.; Audebert, R. Complex Formation in Polymer-Ion Solution. 1. Polymer Concentration Effects. *Macromolecules* **1989**, *22* (3), 1169–1174.
- (41) Pezron, E.; Ricard, A.; Leibler, L. Rheology of Galactomannan-Borax Gels. *J. Polym. Sci. Part B Polym. Phys.* **1990**, *28* (13), 2445–2461.
- (42) Pezron, E.; Ricard, A.; Lafuma, F.; Audebert, R. Reversible Gel Formation Induced by Ion Complexation. 1. Borax-Galactomannan Interactions. *Macromolecules* **1988**, *21* (4), 1121–1125.
- (43) Kesavan, S.; Prud'homme, R. K. Rheology of Guar and (Hydroxypropyl) Guar Crosslinked by Borate. *Macromolecules* **1992**, *25* (7), 2026–2032.
- (44) Kitano, S.; Kataoka, K.; Koyama, Y.; Okano, T.; Sakurai, Y. Glucose-Responsive Complex Formation between Poly(Vinyl Alcohol) and Poly(N-Vinyl-2-Pyrrolidone) with Pendent Phenylboronic Acid Moieties. *Makromol. Chem., Rapid Commun.* **1991**, *12*, 227–233.
- (45) Li, M.; Fossey, J. S.; James, T. D. *Boron: Sensing, Synthesis and Supramolecular Self-Assembly*; RSC Publishing: Cambridge, UK, 2015.
- (46) Soundararajan, S.; Badawi, M.; Kohlrust, C. M.; Hageman, J. H. Boronic Acids for Affinity Chromatography: Spectral Methods for Determinations of Ionization and Diol-Binding Constants. *Anal. Biochem.* **1989**, *178* (1), 125–134.
- (47) Roberts, M. C.; Hanson, M. C.; Massey, A. P.; Karren, E. A.; Kiser, P. F. Dynamically Restructuring Hydrogel Networks Formed with Reversible Covalent Crosslinks. *Adv. Mater.* **2007**, *19* (18), 2503–2507.
- (48) Roberts, M. C.; Mahalingam, A.; Hanson, M. C.; Kiser, P. F. Chemorheology of Phenylboronate–Salicylhydroxamate Cross-Linked Hydrogel Networks with a Sulfonated Polymer Backbone. *Macromolecules* **2008**, *41* (22), 8832–8840.

- (49) Shan, M.; Gong, C.; Li, B.; Wu, G. A PH, Glucose, and Dopamine Triple-Responsive, Self-Healable Adhesive Hydrogel Formed by Phenylborate–Catechol Complexation. *Polym. Chem.* **2017**, *8* (19), 2997–3005.
- (50) He, L.; Fullenkamp, D. E.; Rivera, J. G.; Messersmith, P. B. PH Responsive Self-Healing Hydrogels Formed by Boronate–Catechol Complexation. *Chem. Commun.* **2011**, *47* (26), 7497.
- (51) Li, Z.; Lu, W.; Ngai, T.; Le, X.; Zheng, J.; Zhao, N.; Huang, Y.; Wen, X.; Zhang, J.; Chen, T. Mussel-Inspired Multifunctional Supramolecular Hydrogels with Self-Healing, Shape Memory and Adhesive Properties. *Polym. Chem.* **2016**, *7* (34), 5343–5346.
- (52) Meng, H.; Xiao, P.; Gu, J.; Wen, X.; Xu, J.; Zhao, C.; Zhang, J.; Chen, T. Self-Healable Macro-/Microscopic Shape Memory Hydrogels Based on Supramolecular Interactions. *Chem Commun* **2014**, *50* (82), 12277–12280.
- (53) Meng, H.; Zheng, J.; Wen, X.; Cai, Z.; Zhang, J.; Chen, T. PH- and Sugar-Induced Shape Memory Hydrogel Based on Reversible Phenylboronic Acid-Diol Ester Bonds. *Macromol. Rapid Commun.* **2015**, *36* (6), 533–537.
- (54) Pettignano, A.; Grijalvo, S.; Häring, M.; Eritja, R.; Tanchoux, N.; Quignard, F.; Díaz Díaz, D. Boronic Acid-Modified Alginate Enables Direct Formation of Injectable, Self-Healing and Multistimuli-Responsive Hydrogels. *Chem. Commun.* **2017**, *53* (23), 3350–3353.
- (55) Yang, X.; Lee, M.-C.; Sartain, F.; Pan, X.; Lowe, C. R. Designed Boronate Ligands for Glucose-Selective Holographic Sensors. *Chem. – Eur. J.* **2006**, *12* (33), 8491–8497.
- (56) Deng, C. C.; Brooks, W. L. A.; Abboud, K. A.; Sumerlin, B. S. Boronic Acid-Based Hydrogels Undergo Self-Healing at Neutral and Acidic PH. *ACS Macro Lett.* **2015**, *4* (2), 220–224.
- (57) Tarus, D.; Hachet, E.; Messenger, L.; Catargi, B.; Ravaine, V.; Auzély-Velty, R. Readily Prepared Dynamic Hydrogels by Combining Phenyl Boronic Acid- and Maltose-Modified Anionic Polysaccharides at Neutral PH. *Macromol. Rapid Commun.* **2014**, *35* (24), 2089–2095.
- (58) Kotsuchibashi, Y.; Ebara, M.; Sato, T.; Wang, Y.; Rajender, R.; Hall, D. G.; Narain, R.; Aoyagi, T. Spatiotemporal Control of Synergistic Gel Disintegration Consisting of Boroxole- and Glyco-Based Polymers via Photoinduced Proton Transfer. *J. Phys. Chem. B* **2015**, *119* (6), 2323–2329.
- (59) Kotsuchibashi, Y.; Agustin, R. V. C.; Lu, J.-Y.; Hall, D. G.; Narain, R. Temperature, PH, and Glucose Responsive Gels via Simple Mixing of Boroxole- and Glyco-Based Polymers. *ACS Macro Lett.* **2013**, *2* (3), 260–264.
- (60) Page, S. M.; Parelkar, S.; Gerasimenko, A.; Shin, D. Y.; Peyton, S. R.; Emrick, T. Promoting Cell Adhesion on Slippery Phosphorylcholine Hydrogel Surfaces. *J. Mater. Chem. B* **2014**, *2* (6), 620–624.
- (61) Su, T.; Liu, Y.; He, H.; Li, J.; Lv, Y.; Zhang, L.; Sun, Y.; Hu, C. Strong Bioinspired Polymer Hydrogel with Tunable Stiffness and Toughness for Mimicking the Extracellular Matrix. *ACS Macro Lett.* **2016**, *5* (11), 1217–1221.
- (62) Harvey, A. C.; Madsen, J.; Douglas, C. W. I.; MacNeil, S.; Armes, S. P. Antimicrobial Graft Copolymer Gels. *Biomacromolecules* **2016**, *17* (8), 2710–2718.
- (63) Li, L.; Smitthipong, W.; Zeng, H. Mussel-Inspired Hydrogels for Biomedical and Environmental Applications. *Polym. Chem.* **2014**, *6* (3), 353–358.
- (64) Vatankhah-Varnoosfaderani, M.; Hashmi, S.; GhavamiNejad, A.; Stadler, F. J. Rapid Self-Healing and Triple Stimuli Responsiveness of a Supramolecular Polymer Gel Based on Boron–Catechol Interactions in a Novel Water-Soluble Mussel-Inspired Copolymer. *Polym. Chem.* **2013**, *5* (2), 512–523.

- (65) Guo, R.; Su, Q.; Zhang, J.; Dong, A.; Lin, C.; Zhang, J. Facile Access to Multisensitive and Self-Healing Hydrogels with Reversible and Dynamic Boronic Ester and Disulfide Linkages. *Biomacromolecules* **2017**, *18* (4), 1356–1364.
- (66) Ellis, G. A.; Palte, M. J.; Raines, R. T. Boronate-Mediated Biologic Delivery. *J. Am. Chem. Soc.* **2012**, *134* (8), 3631–3634.
- (67) Lin, M.; Sun, P.; Chen, G.; Jiang, M. The Glyco-Stereoisomerism Effect on Hydrogelation of Polymers Interacting via Dynamic Covalent Bonds. *Chem Commun* **2014**, *50* (68), 9779–9782.
- (68) Jay, J. I.; Shukair, S.; Langheinrich, K.; Hanson, M. C.; Cianci, G. C.; Johnson, T. J.; Clark, M. R.; Hope, T. J.; Kiser, P. F. Modulation of Viscoelasticity and HIV Transport as a Function of PH in a Reversibly Crosslinked Hydrogel. *Adv. Funct. Mater.* **2009**, *19* (18), 2969–2977.
- (69) Mahalingam, A.; Jay, J. I.; Langheinrich, K.; Shukair, S.; McRaven, M. D.; Rohan, L. C.; Herold, B. C.; Hope, T. J.; Kiser, P. F. Inhibition of the Transport of HIV in Vitro Using a PH-Responsive Synthetic Mucin-like Polymer System. *Biomaterials* **2011**, *32* (33), 8343–8355.
- (70) Venkatesh, V.; Mishra, N. K.; Romero-Canelón, I.; Vernooij, R. R.; Shi, H.; Coverdale, J. P. C.; Habtemariam, A.; Verma, S.; Sadler, P. J. Supramolecular Photoactivatable Anticancer Hydrogels. *J. Am. Chem. Soc.* **2017**, *139* (16), 5656–5659.
- (71) Polikarpov, N.; Appelhans, D.; Welzel, P.; Kaufmann, A.; Dhanapal, P.; Bellmann, C.; Voit, B. Tailoring Uptake and Release of ATP by Dendritic Glycopolymer/PNIPAAm Hydrogel Hybrids: First Approaches towards Multicompartment Release Systems. *New J. Chem.* **2012**, *36* (2), 438–451.
- (72) Shiino, D.; Murata, Y.; Kubo, A.; Kim, Y. J.; Kataoka, K.; Koyama, Y.; Kikuchi, A.; Yokoyama, M.; Sakurai, Y.; Okano, T. Amine Containing Phenylboronic Acid Gel for Glucose-Responsive Insulin Release under Physiological PH. *J. Controlled Release* **1995**, *37* (3), 269–276.
- (73) Shiino, D.; Murata, Y.; Kataoka, K.; Koyama, Y.; Yokoyama, M.; Okano, T.; Sakurai, Y. Preparation and Characterization of a Glucose-Responsive Insulin-Releasing Polymer Device. *Biomaterials* **1994**, *15* (2), 121–128.
- (74) Ge, H.; Ding, Y.; Ma, C.; Zhang, G. Temperature-Controlled Release of Diols from N-Isopropylacrylamide-Co-Acrylamidophenylboronic Acid Microgels. *J. Phys. Chem. B* **2006**, *110* (41), 20635–20639.
- (75) Liu, P.; Luo, Q.; Guan, Y.; Zhang, Y. Drug Release Kinetics from Monolayer Films of Glucose-Sensitive Microgel. *Polymer* **2010**, *51* (12), 2668–2675.
- (76) Zhang, X.; Guan, Y.; Zhang, Y. Dynamically Bonded Layer-by-Layer Films for Self-Regulated Insulin Release. *J. Mater. Chem.* **2012**, *22* (32), 16299–16305.
- (77) Ding, Z.; Guan, Y.; Zhang, Y.; Zhu, X. X. Layer-by-Layer Multilayer Films Linked with Reversible Boronate Ester Bonds with Glucose-Sensitivity under Physiological Conditions. *Soft Matter* **2009**, *5* (11), 2302.
- (78) Zhao, F.; Wu, D.; Yao, D.; Guo, R.; Wang, W.; Dong, A.; Kong, D.; Zhang, J. An Injectable Particle-Hydrogel Hybrid System for Glucose-Regulatory Insulin Delivery. *Acta Biomater.* **2017**, *64*, 334–345.
- (79) Seifert, H. M.; Ramirez Trejo, K.; Anslyn, E. V. Four Simultaneously Dynamic Covalent Reactions. Experimental Proof of Orthogonality. *J. Am. Chem. Soc.* **2016**, *138* (34), 10916–10924.
- (80) Lascano, S.; Zhang, K.-D.; Wehlauch, R.; Gademann, K.; Sakai, N.; Matile, S. The Third Orthogonal Dynamic Covalent Bond. *Chem. Sci.* **2016**, *7* (7), 4720–4724.

- (81) Yount, W. C.; Loveless, D. M.; Craig, S. L. Small-Molecule Dynamics and Mechanisms Underlying the Macroscopic Mechanical Properties of Coordinatively Cross-Linked Polymer Networks. *J. Am. Chem. Soc.* **2005**, *127* (41), 14488–14496.
- (82) Tang, S.; Olsen, B. D. Relaxation Processes in Supramolecular Metallogels Based on Histidine–Nickel Coordination Bonds. *Macromolecules* **2016**, *49* (23), 9163–9175.
- (83) Kikuchi, A.; Suzuki, K.; Okabayashi, O.; Hoshino, H.; Kataoka, K.; Sakurai, Y.; Okano, T. Glucose-Sensing Electrode Coated with Polymer Complex Gel Containing Phenylboronic Acid. *Anal. Chem.* **1996**, *68* (5), 823–828.
- (84) Xu, Y.; Sato, K.; Mawatari, K.; Konno, T.; Jang, K.; Ishihara, K.; Kitamori, T. A Microfluidic Hydrogel Capable of Cell Preservation without Perfusion Culture under Cell-Based Assay Conditions. *Adv. Mater.* **2010**, *22* (28), 3017–3021.
- (85) Xu, Y.; Jang, K.; Konno, T.; Ishihara, K.; Mawatari, K.; Kitamori, T. The Biological Performance of Cell-Containing Phospholipid Polymer Hydrogels in Bulk and Microscale Form. *Biomaterials* **2010**, *31* (34), 8839–8846.

CHAPTER 2

Mechanistic insight into the macroscopic mechanical properties of boronate-crosslinked hyaluronic acid hydrogels in relation to the structure of the small molecular crosslinkers

T. Figueiredo, V. Cosenza, Y. Ogawa, I. Jeacomine, S. Ortega, J.-G. Boiteau, T. Gerfaud, J. Olsson, A. Imberty, J. Jing, C. Harris, R. Auzély-Velty

Mechanistic insight into the macroscopic mechanical properties of boronate-crosslinked hyaluronic acid hydrogels in relation to the structure of the small molecular crosslinkers

Abstract

The use of boronic acid-containing polymers to construct dynamic covalent hydrogels is an attractive strategy in injectable biomaterial design. Here, we provide a detailed mechanistic study on the mode of boronate ester crosslinking between hyaluronic acid (HA) modified with two different arylboronic acids (HA-phenylboronic acid (HA-PBA) or HA-benzoboroxole (HA-BOR) conjugates) and HA functionalized with different saccharide units (HA-fructose, -maltose, or -gluconamide derivatives). A careful analysis of the frequency-dependent dynamic mechanical moduli of the networks crosslinked via PBA-saccharide or BOR-saccharide complexation in relation to the dynamics and thermodynamics of the small molecular crosslinkers revealed surprising differences between the networks based on HA-PBA and those based on HA-BOR. PBA thus showed strikingly high affinity for the maltose and gluconamide derivatives (possessing a glucose unit in the ring-opened form) grafted onto HA as well as fructose, resulting in hydrogel networks with slow dynamics and relatively high elastic (storage) moduli. By contrast, the dynamics of the HA-BOR/HA-maltose (gluconamide) networks appeared to be much faster and the elastic (storage) moduli, lower, in comparison to the HA-PBA-based networks as well as to the HA-BOR/HA-fructose assembly. These differences were found to be closely linked to the molecular exchange dynamics and thermodynamics of the small molecular crosslinkers. From these results, we set out on a structural study using NMR and computational analysis to gain a better understanding of the binding mode of PBA and BOR toward the different saccharide moieties grafted on HA. With this study, we demonstrate that the slow dynamics and relatively high elastic moduli observed for the HA-PBA/HA-maltose (gluconamide) (fructose) networks is related to the original and previously unobserved formation of stable tridentate complexes with PBA grafted on HA. These findings offer interesting new perspectives for the rational design of adaptable hydrogel scaffolds using tricovalent aryl boronic acid-polyol complexes.

1. Introduction

Injectable hydrogels that are capable of autonomous healing upon damage have recently drawn great attention in the fields of tissue engineering and regenerative medicine for minimally invasive delivery of cells and in the filling of irregular defects.¹⁻² These hydrogels have been considered as an alternative to traditional injectable hydrogels, which are produced by in situ cross-linking of polymer chains using environmental triggers (pH, temperature, ionic strength), cross-linking chemicals or UV-light.³⁻⁵ There are indeed some potential drawbacks to these crosslinking approaches, which include potential adverse effects on cell viability and/or low gelation kinetics. Compared with traditional injectable hydrogels, self-healing autonomous hydrogels possess adaptable linkages that can be broken and re-formed in a reversible manner without external triggers. This feature is conducive to the homogeneous entrapment of cells *ex vivo* under physiological conditions. The mechanisms to form adaptable linkages include physical associations (hydrogen bonding, ionic, hydrophobic or host-guest interactions) and dynamic covalent chemistry.^{1-2, 6} Compared to physical associations, dynamic covalent reactions usually have slower bond cleavage kinetics.^{2, 7} Consequently, hydrogels based on dynamic covalent chemistry can self-heal in response to mechanical stress similar to physically crosslinked networks, but they are more stable.

As one of the dynamic covalent bonds, the boronate ester bond has been successfully used by our group to prepare autonomous self-healing hydrogels based on hyaluronic acid (HA), a polysaccharide that is ubiquitous in the human body.⁸ These gels are formed almost instantaneously in aqueous media at physiological pH by simply mixing solutions of HA derivatives modified with phenylboronic acid (PBA) and maltose moieties (HA-PBA et HA-maltose, Figure 1). Indeed, these groups react readily with each other to form interchain reversible boronate ester bonds. Although the association constant (K_a) of natural maltose with PBA at physiological pH is quite low ($K_a \sim 2.5$ L/mol),⁹ dynamic rheological measurements of the HA-PBA/HA-maltose mixture showed formation of an elastic hydrogel network (storage modulus (G') > loss modulus (G'')) within the whole range of frequencies covered).⁸ This is in contrast with networks based on host-guest (HG) interactions between HA derivatives modified with β -cyclodextrin (β -CD), as host molecule, and adamantane (AD), as guest molecule, previously investigated by our group¹⁰⁻¹¹ and others.¹²⁻¹³ Indeed, a viscoelastic behavior (crossover of G' and G'' seen within the tested frequencies) was observed for these HG hydrogel networks, while the K_a value of the β -CD/AD complex is relatively high ($K_a \sim 80000$ L/mol).

In a study on supramolecular networks based on metal-ligand interactions performed in 2005, Yount et al. showed that it is the dynamics of molecular crosslinks, much more so than

their thermodynamics, which are specifically and quantitatively responsible for the bulk viscoelastic properties of the supramolecular network.¹⁴ The concept of "strong means slow" introduced by these authors has been supported more recently by an independent study on a diol-containing polycyclooctene polymer cross-linked by boronic ester bonds. Cromwell et al. found that the dynamic properties of these boronate ester-crosslinked polymer networks are closely related to the transesterification kinetics and thereby, can be tuned according to the structure of the telechelic diboronic ester crosslinker.¹⁵

These results, together with the exciting potential benefit of boronate ester-crosslinked hydrogels based on HA in the biomedical field, prompted us to explore the effect of the nature of the boronic acid moiety as well as the sugar molecule grafted onto the HA backbone on the bulk network properties. Among arylboronic acid derivatives, benzoboroxole (BOR) was selected in addition to PBA as the binding site for sugar molecules grafted on HA because of its efficient carbohydrate binding capability at physiological pH compared to PBA.¹⁶⁻¹⁷ The relatively high Lewis acidity and strained cyclic structure of BOR are likely contributing factors for its capability to bind saccharides at neutral pH, including carbohydrates locked in their pyranose form for which PBA has virtually no affinity.¹⁸ Surprisingly, our previous results indicated effective binding of PBA to the maltose derivative introduced on HA, which consists of a terminal α -D-glucopyranoside unit linked to a ring-opened glucose unit.⁸ These factors led us to investigate formation of networks from HA derivatives modified with single glucose units locked in the pyranose form (referred to as HA-glucose) or in the ring-opened form (referred to as HA-gluconamide), in comparison to HA modified with the maltose derivative (Figure 1). Moreover, taking into account the higher affinity of boronic acids towards D-fructose over D-glucose, we also selected fructose as the binding site for PBA and BOR grafted on HA in our effort to determine the relative importance of the effect of dynamics and thermodynamics of molecular crosslinks on the viscoelastic properties of the networks (Figure 1). Despite the growing interest in boronate ester bond-based self-healing hydrogels, the relationship between the properties of the boronate esters crosslinks and the mechanical behavior of the networks, while being indispensable for their applicability, has not previously been investigated.

The studies here establish the high binding affinity of PBA for glucose units in the ring-opened form (such as in the maltose and gluconamide derivatives) as well as for fructose grafted onto HA, resulting in hydrogel networks with slow dynamics and relatively high elastic (storage) moduli. This finding is in contrast to the viscoelastic behavior observed for the HA-BOR/HA-maltose (gluconamide) networks, which correlates with the fast dynamics of the BOR/maltose (gluconamide) complex. Yet, a distinct macroscopic mechanical behavior is observed for the HA-BOR/HA-fructose mixture, showing dynamic properties similar to those

of the HA-PBA/HA-fructose network. Based on these results, we set out on a structural study to gain a better understanding of this unexpected difference in macroscopic mechanical properties in relation to the structure of the small molecular crosslinkers. With this study, we provide a comprehensive picture, from a structural perspective, of the binding mode of PBA and BOR to the different saccharide derivatives using NMR and computational analysis.

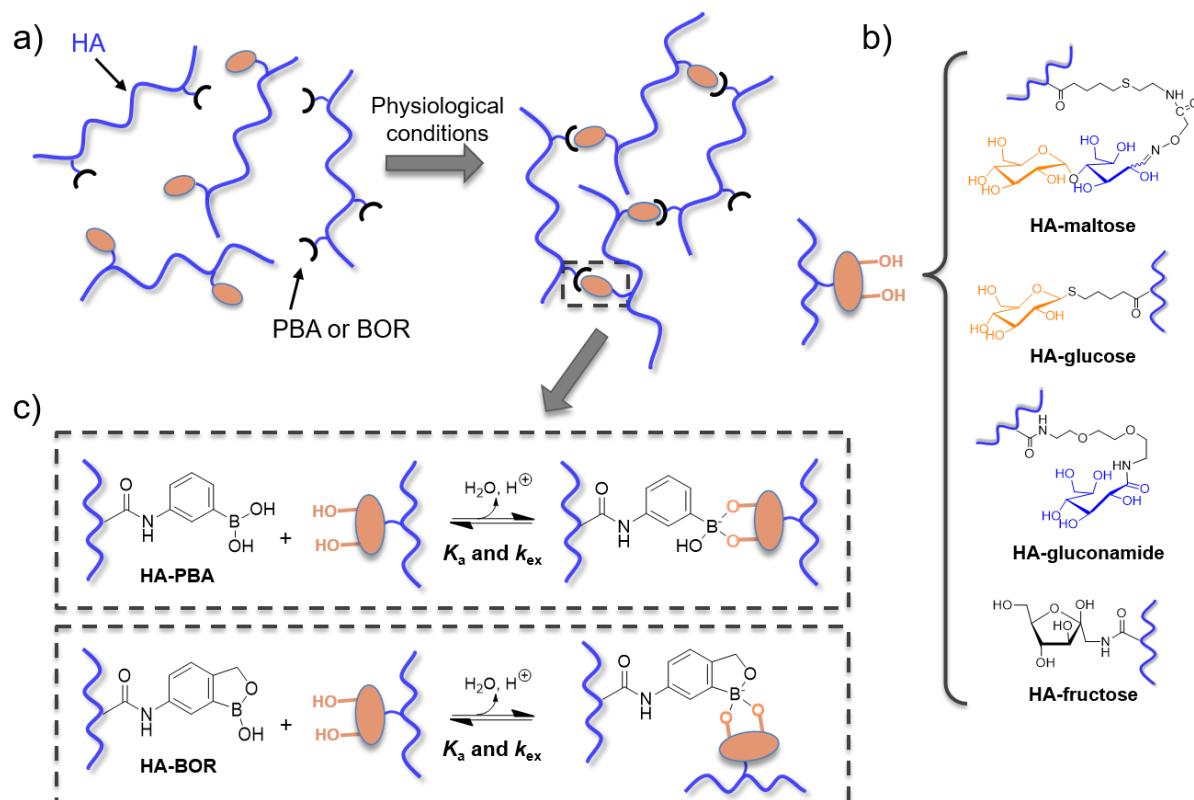


Figure 1. (a) Self-healing hyaluronic acid hydrogels crosslinked via tunable dynamic boronate ester bonds. (b) HA-saccharide derivatives investigated as partners of HA-PBA and HA-BOR to form hydrogel networks. (c) Mechanism of boronate ester bond formation according to literature.

2. Results

2.1 Modification of hyaluronic acid with phenylboronic acid, benzoboroxole and carbohydrate molecules

To properly compare the effect of the boronate ester cross-linker on the dynamic rheological properties of the HA networks, all HA derivatives were synthesized from the same initial HA sample, possessing a weight average molar mass M_w of 100 kg/mol, and with a similar degree of substitution (DS, average number of substituting group per repeating disaccharide unit). The syntheses of HA-maltose and HA-glucose were performed via thiol-ene coupling reactions between a maltose-thiol derivative and commercially available

thioglucose, respectively, and HA possessing alkene groups (HA-pentenoate)¹⁹ (Figure S1, Supporting Information). The maltose-thiol was prepared from a carboxylic acid derivative of maltose (maltose-COOH, Figure S1) as previously described.⁸ During the coupling reactions with HA-pentenoate, the thiol-to-ene ratios were adjusted to obtain a DS of 0.1 to 0.15 for the HA derivatives. Successful grafting of the saccharides onto HA was confirmed by ¹H NMR spectroscopy which also allowed determination of the DS (Figure S2).

The HA-PBA, HA-BOR, HA-fructose and HA-gluconamide derivatives were prepared by an amide coupling reaction carried out in aqueous solution between 3-aminophenylboronic acid (APBA), 6-amino-1-hydroxy-2,1-benzoxaborolane (6-aminobenzoboroxole, ABOR), 1-amino-1-deoxy-D-fructose (fructosamine) and a glucose derivative in the ring-opened form (1-amino-DOOA-gluconamide), respectively, and HA, using 4-(4,6-dimethoxy-1,3,5-triazin-2-yl)-4-methylmorpholinium chloride (DMTMM) as a coupling agent (Figure S3).²⁰ For the synthesis of the 1-amino-DOOA-gluconamide, D-gluconolactone was reacted with Boc-1-amino-3,6-dioxo-8-octanamine (Boc-DOOA) according to a previously reported procedure, affording Boc-1-amino-DOOA-gluconamide (Figure S3).²¹ The DS of the HA conjugates was controlled by the amount of amine to carboxylic acid. Using DMTMM/HA and amine/HA molar ratios of 1 and 0.15 to 0.2, respectively, we obtained HA derivatives with a DS of 0.1 to 0.15 from ¹H or ¹³C NMR analysis (Figure S4-S6). In the case of HA-fructose and HA-gluconamide, the DS was also estimated from the reaction kinetics performed using 2,4,6-Trinitrobenzene Sulfonic Acid (TNBS) to quantify the free primary amines in the reaction medium as a function of time (Figure S7).

2.2. Synthesis of the boronate ester-crosslinked networks and rheological characterization

The different HA-based networks were produced by mixing thoroughly aqueous solutions of HA-PBA (or HA-BOR) and HA bearing saccharide moieties (HA-maltose, HA-fructose, HA-glucose or HA-gluconamide) at physiological pH, at a total polymer concentration ($C_p = 15$ g/L) higher than the overlap concentration of initial HA ($C^* \approx 3$ g/L) and with a molar ratio of PBA (BOR)-to-grafted saccharide of 1. Visual observations by inverting the vials of the different mixtures suggested hydrogel formation for those based on HA-PBA (BOR)/HA-fructose and HA-PBA/HA-maltose (gluconamide). Of note, gel formation was observed almost instantaneously after mixing. By contrast, the mixtures based on HA-BOR/HA-maltose (gluconamide) and HA-PBA (BOR)/HA-glucose were found to flow down in the inverted vial.

Dynamic rheological experiments confirmed the gel-like behavior ($G' > G''$) in the frequency window explored for the formulations based on HA-PBA (BOR)/HA-fructose (Figure 2a), HA-PBA/HA-maltose (Figure 2b) and HA-PBA/HA-gluconamide (Figure 2c). By contrast, HA-PBA and HA-BOR alone exhibited a viscous behavior with G' and G'' values similar to initial HA (Figure S8), confirming selective boronate ester crosslinking between PBA (BOR) and the sugar moieties grafted on HA. Quite surprisingly, in spite of the reported low binding constant of PBA with natural maltose ($K_a \sim 2.5$ L/mol)⁹ compared to the K_a values of PBA and BOR with D-fructose ($K_a \sim 128$ and ~ 336 L/mol, respectively)^{9, 22} at physiological pH, the value of G' in the plateau region of the HA-PBA/HA-maltose network ($G'_{1\text{Hz}} = 648$ Pa) is higher than the G' values of HA-PBA/HA-fructose and HA-BOR/HA-fructose assemblies ($G'_{1\text{Hz}} = 276$ and 332 Pa, respectively). The same observation can be made for the HA-PBA/HA-gluconamide network, for which the value of G' in the plateau region is 558 Pa. The dynamic rheological properties of the HA-PBA/HA-maltose (gluconamide) mixtures are in sharp contrast with those of the HA-BOR/HA-maltose (gluconamide) assemblies. Indeed, viscoelastic behaviors are observed for the two latter mixtures (Figure 2b and 2c). These results are rather unexpected, especially in the case of the HA-BOR/HA-maltose mixture as BOR is reported to have a higher binding affinity towards glycopyranosides than PBA. These results suggest that the mechanism of binding of PBA to the maltose derivative grafted on HA is different from that of PBA to natural maltose due to the ring-opened form of the glucose unit in the maltose derivative immobilized on the HA backbone. The rheological data obtained from the mixtures based on HA-glucose (i.e. HA containing glucose units locked in their pyranose form) support this assumption (Figure 2d). These assemblies display a viscous behavior ($G'' > G'$) in the frequency window covered which correlates with the low binding of PBA and BOR to natural glucose ($K_a \sim 5$ L/mol⁹ and ~ 20 L/mol^{17, 23}, respectively), which is mainly in the pyranose form (99.7 % in D₂O at neutral pH and 27 °C)²⁴ in aqueous solution.

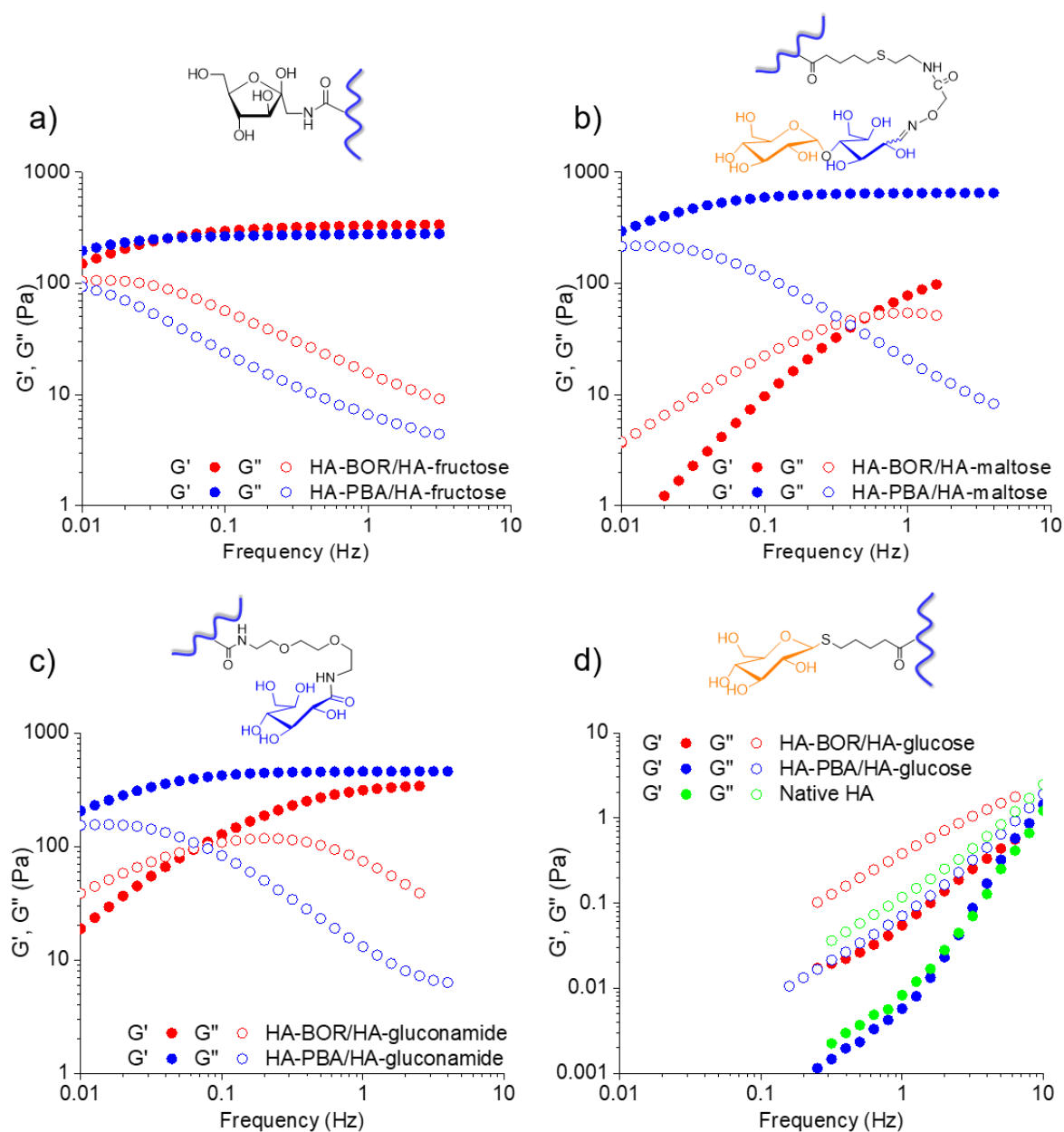


Figure 2. Frequency dependence of storage and loss moduli of networks based on HA-PBA (BOR)/HA-fructose (a), HA-PBA (BOR)/HA-maltose (b), HA-PBA (BOR)/HA-gluconamide (c) and HA-PBA (BOR)/HA-glucose (d); closed symbols: G' curves; open symbols: G'' curves.

2.3. Relationships between the macroscopic mechanical properties of the HA networks and the small molecule crosslinkers

On the basis of these observations, we investigated the relationships between the macroscopic mechanical properties and the small molecule crosslinkers by analyzing the thermodynamics and kinetics of boronic acid-saccharide (fructose, maltose and gluconamide) complexation (Table 1).

CHAPTER 2: Mechanistic insight into the properties of boronate-crosslinked HA hydrogels

Table 1. Binding constants and/or exchange rate constants of complexes based on APBA/free fructose (free maltose-COOH), APBA/HA-fructose (HA-maltose), ABOR/free fructose (free maltose-COOH), ABOR/HA-fructose (HA-maltose).

Entry	Boronic acid	Saccharide	K_a^a (M ⁻¹)	K_a^b ITC (M ⁻¹)	n^b (n saccharide : 1 boronic acid)	ΔH^b (kJ.mol ⁻¹)	ΔS^b (J.mol ⁻¹ .K ⁻¹)	k_{ex} (s ⁻¹)
1	APBA	Free D-fructose	201 ± 5	112 ± 16	1.3 ± 0.3	-11.2 ± 2.8	1.6	0.66 ± 0.07 ^c
2	APBA	HA-fructose	503 ± 18					-- ^d
3	ABOR	Free D-fructose	461 ± 73	484 ± 50	1.24 ± 0.1	-11.7 ± 1.2	12.1	0.18 ± 0.04 ^c
4	ABOR	HA-fructose	545 ± 28					-- ^d
5	APBA	Free maltose-COOH	-- ^e	2070 ± 146	0.46 ± 0.05	-17.7 ± 2.3	4.1	-- ^f
6	APBA	HA-maltose	768 ± 71					0.27 ^c
7	ABOR	Free maltose-COOH	-- ^g	305 ± 36	0.61 ± 0.3	-13.7 ± 6.6	1.5	184 ^h
8	ABOR	HA-maltose	-- ^g					191 ^h
9	APBA	Free gluconamide diamine-Boc	3220 ± 356	2340 ± 56	0.69 ± 0.01	-38.3 ± 0.7	-64	-- ^f
10	APBA	HA-gluconamide	1751 ± 221					0.20 ^c
11	ABOR	Free gluconamide diamine-Boc	995 ± 125	933 ± 29	0.88 ± 0.03	-29.2 ± 1.2	-41	-- ^f
12	ABOR	HA-gluconamide	477 ± 132					-- ^d

^aValues measured from at least two ¹H NMR experiments, assuming formation of a 1:1 complex; ^bmeasured from at least two ITC experiments; ^cmeasured using EXSY experiments; ^dnot determined because of superposition of diagonal and cross-peaks arising from the bound and unbound APBA (ABOR) species; ^enot determined because the concentration of molecules used was too low to apply equations related to 1:2 equilibria²⁵; ^fnot measured; ^gnot measured because of rapid exchange dynamics relative to NMR time-scale (extensive broadening of proton signals); ^hestimated from variable-temperature NMR experiments. Of note, despite the values of k_{ex} were measured for the major complexes of ABOR/maltose-COOH (HA-maltose) observed in the NMR spectra, the existence of other complexes cannot be excluded as small additional signals are also observed (Figure S22 and S23).

As the bound and unbound forms of APBA (ABOR) in the presence of fructose are distinguishable by ¹H NMR spectroscopy,^{18, 22} we used this technique to evaluate directly the affinity of APBA and ABOR for free D-fructose and grafted fructose (Figure S9-S12) as well as to measure the rate of exchange between the free and bound states (Figure S13 and S14). NMR analysis of ABOR/free fructose and ABOR/grafted fructose revealed nearly identical association constants of 461 L/mol and 545 L/mol, respectively (Table 1, entries 3 and 4). On the other hand, in the case of APBA, the grafting of fructose on HA resulted in a 2.5-fold increase in the binding constant (Table 1, entries 1 and 2). Moreover, the K_a value

for APBA/grafted fructose (503 L/mol) is relatively close to that measured for ABOR/grafted fructose. This is consistent with the fact that the G' values in the plateau region of HA-PBA/HA-fructose and HA-BOR/HA-fructose assemblies are similar, taking into account the fact that both assemblies differ only in the nature of the boronic acid moiety. Indeed, as the plateau modulus scales with the density number of elastically active chains, its value strongly depends on the crosslink density, which is closely related to the binding constant of the PBA (BOR)/saccharide complex. The binding constants for APBA/free fructose and ABOR/free fructose were also assessed by isothermal titration calorimetry (ITC), and were in the same order of magnitude as the values derived from ^1H NMR (Table 1, entries 1 and 3). Regarding the interaction between APBA (ABOR) and HA-fructose (or vice-versa, i.e. free fructose with HA-PBA (BOR)), ITC proved to be unsuitable for studying the boronic acid/fructose interaction as the thermodynamic parameters were affected by contributions from other effects related to the presence of the HA backbone. Two-dimensional NMR exchange (2D EXSY) experiments used to quantify molecular exchange dynamics revealed that the rates of chemical exchange between the bound and free states for APBA/free fructose and ABOR/free fructose are in the same order of magnitude (0.66 s^{-1} and 0.18 s^{-1} , respectively, see Table 1, entries 1 and 3). Such values correlate with the gel-like behavior of these assemblies. Indeed, the values are of the same order of magnitude as those previously reported in a study on bulk materials based on a diol-containing polymer cross-linked by telechelic diboronic ester crosslinkers.¹⁵ Highly elastic properties were obtained using a diboronic ester crosslinker with a transesterification rate of 0.016 s^{-1} , while a viscoelastic behavior was observed with a crosslinker possessing a transesterification rate of 3000 s^{-1} . It should be noted here that the values were determined from the free molecules. We cannot exclude slight variations due to the grafting of boronic acid/fructose moieties on the HA backbone. Indeed, looking at the frequency dependence of the dynamic moduli, a larger discrepancy between the G' and G'' values is observed for the HA-PBA/HA-fructose network than for HA-BOR/HA-fructose, indicating a high resistance to flow (Figure 2a). This also suggests that the crossover frequency where $G' = G''$ (ω_c), which can be considered as the inverse of the characteristic relaxation time of the network ($\tau = (\omega_c)^{-1}$),^{11, 26} is lower for the HA-PBA/HA-fructose assembly than for HA-BOR/HA-fructose. The rheological data thus indicate that the transesterification is a little slower for the HA-PBA/HA-fructose network. Taken together, these NMR studies led us to conclude that the HA-PBA/HA-fructose and HA-BOR/HA-fructose networks are nearly identical in their extent of cross-linking as well as in the dynamics of the interactions between the cross-linkers and the HA backbone.

With regard to the binding of APBA and ABOR to free maltose-COOH and grafted maltose (HA-maltose), NMR and ITC analysis (Figure S15-S20) showed strikingly high

affinity of APBA for free maltose-COOH and grafted maltose (Table 1, entries 5 and 6, Figure S17 and S19). In the case of the APBA/maltose-COOH system, analysis of the ITC data with a one set of site model gave a value of $K = 2070$ L/mol and a stoichiometry n (n saccharide:1 boronic acid) of 0.46. To confirm deviation from the 1:1 stoichiometry, we turned to the method of continuous variations (also referred as Job's method)²⁷ in conjunction with ¹H NMR spectroscopy. Figure 3a displays the Job plot obtained for the PBA/maltose-COOH pair. This shows a maximum at a molar fraction of ~ 0.4 , indicating a composite binding stoichiometry.²⁸ The binding constant of APBA/maltose-COOH derived from the one set of site model is thus only an approximate estimate. Unfortunately, our attempt to fit the experimental ITC data with a composite binding model (model of two sets of sites which requires more free parameters) was unsuccessful. In the case of APBA/HA-maltose, however, the Job plot indicated a stoichiometry of 1:1 (Figure 3b), which suggests that HA plays a role in the binding of APBA to the grafted maltose derivative. Assuming formation of a 1:1 complex, a binding constant of 768 L/mol was found for the APBA/grafted maltose pair from ¹H NMR analysis (Table 1, entry 6).

These relatively high values compared to the binding affinity of PBA towards natural maltose are probably connected with the structure of the modified maltose derivatives, consisting of a terminal α -D-glucopyranoside unit linked to a ring-opened glucose unit. Of note, the 1.5-fold higher binding constant value of APBA with HA-maltose compared to that of APBA with HA-fructose can partly explain the higher plateau value of G' of the HA-PBA/HA-maltose network compared with that of the HA-PBA/HA-fructose assembly (Figure 2a and 2b).

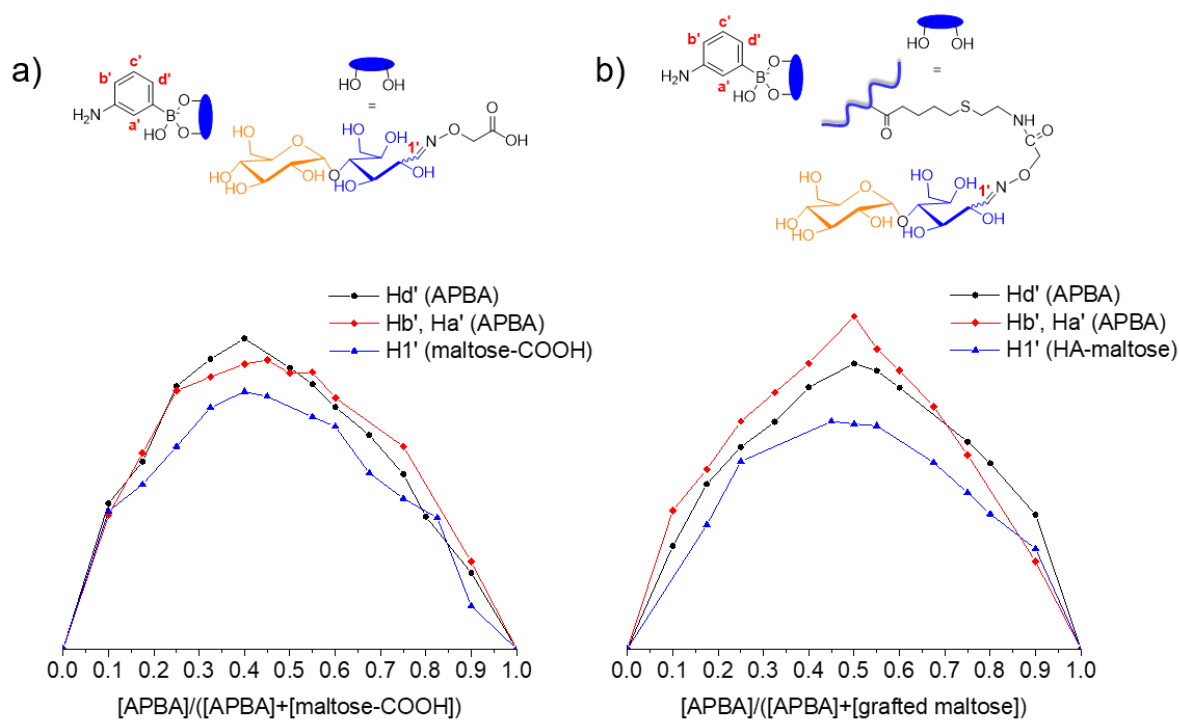


Figure 3. ^1H NMR Job plots for APBA and maltose-COOH (a), and for APBA and grafted maltose (HA-maltose) (b), showing a maximum at a molar ratio of 0.4 and 0.5, respectively.

In the case of ABOR/maltose-COOH complexation, ITC analysis also revealed significant deviation from 1:1 stoichiometry (Table 1, entry 7). Similar to APBA, this indicates the possibility that two ABOR molecules are bound to the maltose derivative.

^1H NMR experiments further showed that the rate of chemical exchange between the bound and free forms is slower for APBA/free maltose-COOH (HA-maltose) than for ABOR/free maltose-COOH (HA-maltose). Indeed, the bound and unbound forms of maltose could be clearly distinguished for APBA/free maltose-COOH as well as for APBA/HA-maltose (Figure S17 and S19). As seen from Table 1, the rate of chemical exchange for APBA/grafted maltose was found to be slightly lower than that for APBA/free fructose (0.27 s^{-1} and 0.66 s^{-1} , respectively, see entries 6 and 1 in Table 1, Figure S21). By contrast, extensive broadening of proton signals was observed in the spectra of ABOR/free maltose-COOH as well as of ABOR/grafted maltose (Figure S18 and S20). In the two latter cases, it was not possible to clearly observe significant chemical shift variations. This precluded easy determination of association constants from the ^1H NMR spectra and quantification of molecular exchange dynamics by 2D EXSY. The molecular exchange dynamics was examined by variable-temperature NMR spectroscopy. In NMR experiments, the exchange signals for ABOR/free maltose and ABOR/grafted maltose coalesced at $15\text{ }^\circ\text{C}$ (Figure S22 and S23), which allowed estimating the molecular exchange rate constant at the coalescence temperature.²⁹⁻³⁰ From these experiments, the extrapolated exchange rate

constant k_{ex} at 25 °C of ABOR/free maltose and ABOR/grafted maltose were found to be 184 and 191 s⁻¹, respectively.

The difference in molecular exchange dynamics between the complexes based on APBA and those based on ABOR may provide an explanation for the unexpected gel-like behavior of the HA-PBA/HA-maltose assembly compared to the viscoelastic behavior observed for HA-BOR/HA-maltose.

Interestingly, the results obtained from the analysis of the binding of APBA and ABOR to free gluconamide (Boc-1-amino-DOOA-gluconamide) and grafted gluconamide (HA-gluconamide) supported our assumption that the ring-opened form of the glucose unit in the maltose derivative is partly responsible for its strong interaction with APBA (Figure S24-S27). The interaction of APBA with free gluconamide produced a complex with a binding constant of nearly two orders of magnitude higher than that with free fructose (Table 1, entries 1 and 9, Figure S24). The Job plot for APBA and free gluconamide indicated the formation of a complex with a stoichiometry of 1:1 with a maximum at 0.5 (Figure S28). Although a decrease of the K value is observed once the gluconamide derivative is grafted on HA (Table 1, entry 10), it remains high compared to association constants reported for the binding of PBA to various natural mono- and disaccharides which do not exceed 400 L/mol.⁹ The interaction of ABOR with free gluconamide also resulted in a binding constant significantly higher than that with free fructose (Table 1, entries 3 and 11, Figure S25). Contrary to the maltose derivative, the bound and unbound forms of gluconamide are in a relatively slower exchange compared to the NMR time-scale at 25 °C. However, superposition of cross-peaks in the 2D EXSY spectrum precluded quantification of k_{ex} for ABOR/gluconamide.

Collectively, these results demonstrate the high binding capacity of PBA towards glucose units in the ring-opened form (i.e. the maltose and gluconamide derivatives), resulting in the formation of complexes with slow exchange dynamics. However, in view of the different binding constant and stoichiometry values found for the APBA/maltose-COOH and APBA/free gluconamide complexes, it can be reasonably assumed that the binding mode mechanism of PBA to the maltose and gluconamide derivatives is different. Moreover, another striking result is the high binding capacity of APBA towards fructose when grafted on HA, which results in the formation of a hydrogel network with dynamic rheological properties similar to the network based on BOR/fructose crosslinks.

2.4. Influence of the pH on the HA-PBA (BOR)/HA-saccharide hydrogel networks

Taking into account that the pK_a of boronic acid derivatives is one of the factors affecting the binding affinity between boronic acid and diol moieties, we investigated the effect of pH

on the viscoelastic properties of the networks based on HA-PBA (BOR)/HA-fructose, HA-PBA/HA-maltose, and HA-PBA/HA-gluconamide. As mentioned earlier, it is generally believed that the pH needs to be above the pK_a of the phenylboronic acid derivative to see meaningful binding.³¹ More precisely, it is commonly assumed that optimal pH for phenylboronate ester formation is about half-way between the pK_a of the phenylboronic acid and the pK_a of the diol.³¹ From the pK_a values of BOR and PBA (7.3¹⁶ and 8.8³¹, respectively), and of neutral saccharides (about 12 for glucose and fructose)³¹, the optimal pH for boronate ester crosslinking should be around 9.6 and 10.4 for the networks prepared from HA-BOR and HA-PBA, respectively. Regarding networks based on HA-PBA (BOR)/HA-fructose, dynamic rheological experiments indicated that the optimal pH is around 8 for both networks, which is lower than the calculated values (Figure 4a, 4b and 4c). In fact, there are no significant differences between the dynamic rheological properties of both networks at pH 7.4 and 8 by contrast with measurements at pH < 7.4. The differences observed below physiological pH may be related to the different pK_a values of BOR and PBA. However, different sensitivities to pH are also observed for networks based on HA-PBA/HA-fructose, HA-PBA/HA-maltose and HA-PBA/HA-gluconamide, in spite the similar pK_a value of the grafted sugar moieties (Figure 4a, 4c, 4d and S29). Interestingly, the networks prepared from HA modified with glucose-like molecules are less sensitive to pH below pH 7.4. Collectively, these results indicate that other factors specific to each boronic acid/diol complex (conformational changes, interactions such as binding by a third hydroxyl)³¹ can affect the binding as previously described for boronate complexes between small molecules.³¹

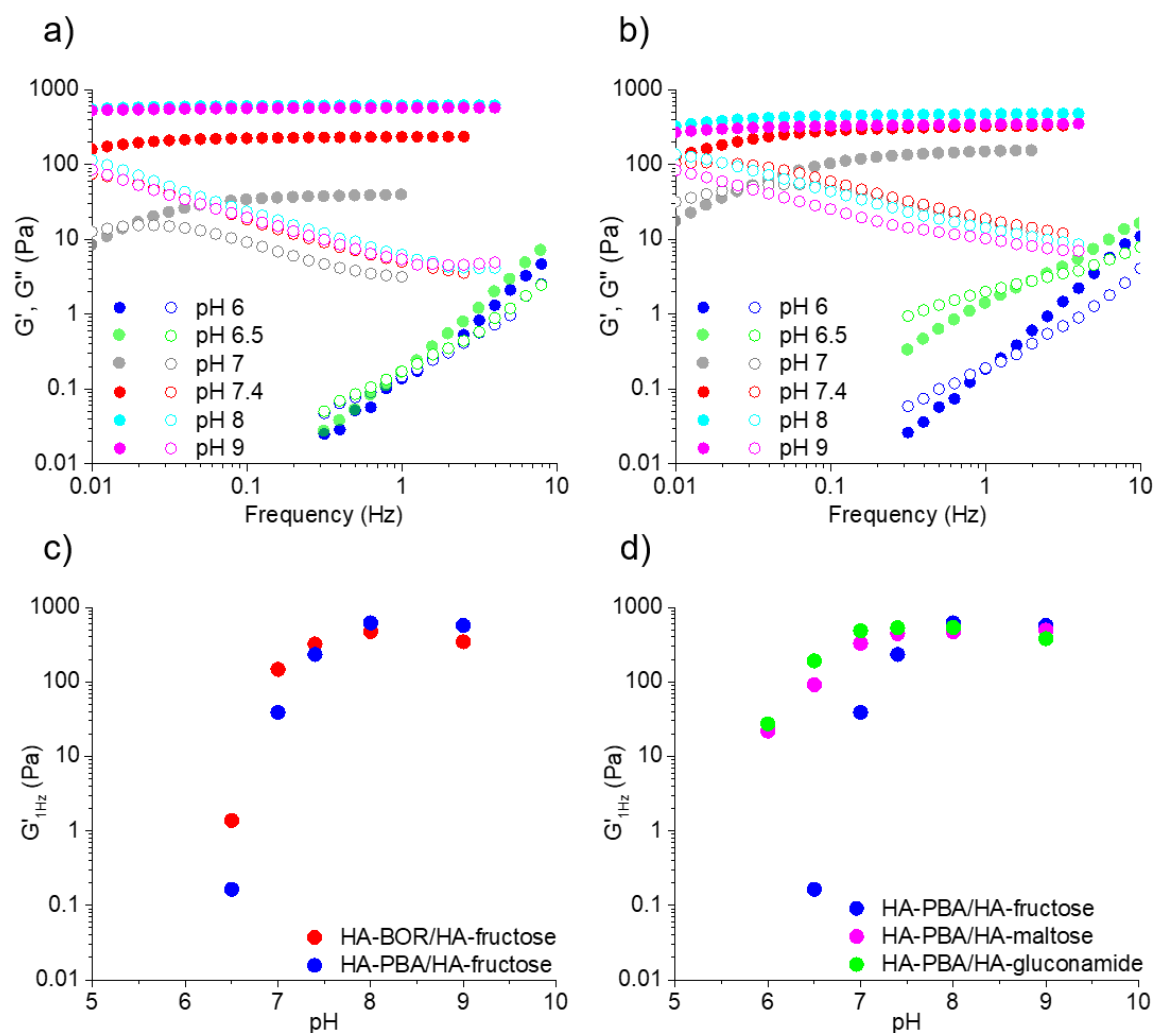


Figure 4. Dynamic rheological properties of the HA-PBA (BOR)/HA-saccharide networks by varying the pH of the medium from 6 to 9: frequency dependence of G' and G'' of HA-PBA/HA-fructose (a) and HA-BOR/HA-fructose (b); variation of G' at 1 Hz as a function of pH of HA-PBA (BOR)/HA-fructose (c) and of HA-PBA/HA-saccharide networks (d).

2.5. Determination of the structures of the boronic acid complexes with maltose and fructose grafted on HA

To gain more insight into the binding mode of PBA to the fructose, maltose and gluconamide derivatives which is connected with the unexpected macroscopic mechanical properties of the HA-PBA/HA-fructose (maltose) (gluconamide) networks compared to their counterparts based on HA-BOR, we studied the structures of the boronic acid complexes by NMR and molecular modeling. On the basis of the $^1J_{CC}$ coupling constants which provide information of the binding sites for the formed cyclic boronic esters, Norrild et al. previously assigned the structures of the different PBA/fructose complexes formed in neutral non-aqueous and alkaline aqueous solutions.³² From this study, the binding mode of APBA towards fructose grafted on HA could be readily determined from ^{13}C NMR based on the ^{13}C

chemical shift values reported for the fructose part of the complexes with PBA. Comparison of the ^{13}C NMR spectra of the 1:1 complexes formed between D-fructose and APBA in D_2O (pD 7.4 and pD 11-12) with the spectrum of APBA in the presence of HA-fructose ($[\text{PBA}]/[\text{fructose}] = 1$, pD 7.4) showed that APBA mainly binds the fructose moiety grafted on HA in a tricovalent fashion, similar to the APBA/D-fructose complex in alkaline conditions (Figure 5). This binding mode was evidenced by the upshift of the C6' signal of bound fructose (in the furanose form, from 62.8 to 65 ppm) observed for both the APBA/D-fructose complex (pD = 11-12, Figure 5c) and APBA/HA-fructose (pD = 7.4, Figure 5b), which is due to bond formation between the C6'-OH group and boron in addition to B-O bond formation between the C2'-OH and C3'-OH of fructose. Indeed, the upshift of C6' is not observed in the spectrum of APBA/D-fructose at pD 7.4 (Figure 5d), which remains similar to the spectrum of D-fructose alone (Figure 5e, C6 at 62.8 ppm), indicating complexation of APBA only with the C2'-OH and C3'-OH groups of D-fructose. This is a rather startling result which, however, fully supports the assumption that the HA backbone may contribute to the increased binding affinity of PBA for grafted fructose.

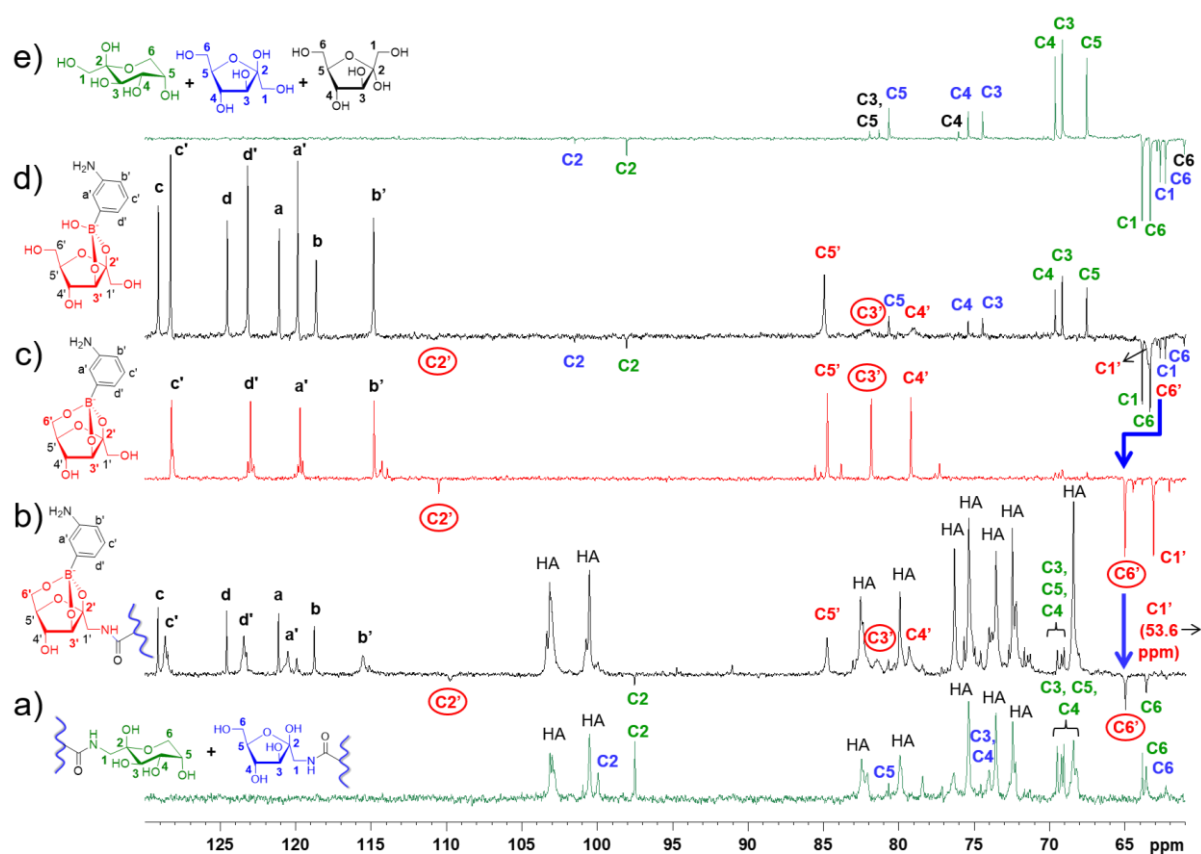


Figure 5. ^{13}C NMR spectrum of HA-fructose alone at pD 7.4 (a), and DEPTQ-135 NMR spectra of APBA/HA-fructose at pD 7.4 (b), APBA/D-fructose at pD 12 (c), APBA/D-fructose at pD 7.4 (d) and D-fructose alone at pD 7.4 (e). Of note, spectrum (a) shows that β -D-fructopyranose (highlighted in green) is the major tautomeric form observed for grafted fructose moieties (HA-fructose), followed by the β -D-fructofuranose form (highlighted in blue); these forms are also observed in the spectrum (e) of D-fructose, in addition to a small

fraction of the α -D-fructofuranose form (highlighted in black). In the spectra of APBA/HA-fructose and APBA/D-fructose (spectra (b) and (d), respectively), fructose is partially bound to APBA in the furanose form (highlighted in red), in addition to the unbound β -D-fructofuranose and/or β -D-fructopyranose forms.

The binding mode of ABOR towards free (grafted) fructose was also investigated by ^1H and ^{13}C NMR analysis at physiological pH. Surprisingly, the complexation between ABOR and fructose was found to involve the opening of the endocyclic B-O bond of ABOR. This was demonstrated by comparing the ^1H NMR spectra of ABOR alone in the open form (i.e. at pD 11-12)¹⁸ and in the closed form (at pD 7.4) as well as of ABOR in the presence of free D-fructose (Figure S30a) and grafted fructose (HA-fructose, Figure S30b) at pD 7.4. The upshift observed for the CH_2O group of ABOR in the presence of both free/grafted fructose similar to that of ABOR alone at alkaline pH indeed provided evidence of the opening of the oxaborole ring. Further 2-D INADEQUATE NMR experiments using ^{13}C labeled D-fructose revealed that ABOR forms a vicinal cyclic boronic ester with the *syn*-periplanar anomeric hydroxyl pair (C2–C3) of D-fructose (Table S1 and S2, Figure S31). The formation of this bidentate complex with fructose (mainly in the furanose form) was evidenced by a significant decrease in the $^1\text{J}_{\text{C}2-\text{C}3}$ value of the bound β -D-fructofuranose form. Indeed, exceptionally low values for $^1\text{J}_{\text{CC}}$ are measured for vicinal diols when the O-C-C-O fragment becomes incorporated in a five-membered ring, as is the case for vicinal cyclic boronic esters.³³ It is also worth noting that upon complexation with ABOR, the C2 and C3 carbon signals of β -D-fructofuranose experience the largest chemical shift changes, similar to those observed for complexation of APBA with fructose/grafted fructose at pD 7.4, whereas no chemical shift change is observed for the C6 carbon of β -D-fructofuranose (Table S1 and Figure 5). Collectively, these data demonstrate that complexation of ABOR with fructose leads to the formation of a monocyclic adduct instead of a spiro adduct due to the opening of the oxaborole ring.

In order to investigate the structure of the complex formed between APBA and maltose grafted on HA, we followed the same methodology described by Norrild et al.³², which was based on the measurement of $^1\text{J}_{\text{CC}}$ coupling constants of a ^{13}C labeled maltose derivative grafted on HA in the absence and in the presence of APBA. To elucidate the binding mode of APBA with grafted maltose, the chemical shifts and $^1\text{J}_{\text{CC}}$ coupling constants of grafted maltose were measured using the INADEQUATE technique, performed on an ultra-high field NMR spectrometer (950 MHz). Comparison of the INADEQUATE spectrum of the 1:1 complex formed between grafted maltose and APBA and the spectrum of grafted maltose alone in D_2O (pD 7.4) indicated an upshift of the C6 signal of the open glucose unit, whereas no change in the chemical shift was observed for all ^{13}C of the terminal glucopyranose unit (Table S3, Figure S32). Furthermore, no significant change in the values of $^1\text{J}_{\text{CC}}$ of grafted

maltose was observed in the presence of APBA (Table S4). Unfortunately, this analysis did not allow determination of the exact structure(s) of the complex(es) because of a poor resolution of the spectrum of the complex, in particular in the regions of the carbons of the open glucose unit (C2 and C3, Figure S32b). Therefore, it remains to be clarified whether other carbons also undergo chemical shift changes similar to C6, as a possible indication for the binding APBA to other hydroxyl groups of the open glucose unit. Nevertheless, to date, these partial data suggest the binding of APBA only towards the open glucose unit of grafted maltose. Besides the upshift of the C6 that indicates complexation of the C6-OH by APBA, this assumption is also supported by the fact that no variation in the values of chemical shift and $^1J_{CC}$ were noticed for the terminal glucopyranose unit. Previous studies on carbohydrate systems have, indeed, demonstrated that the O-C-C torsional angles in O-C-C-O fragments are the most important parameters determining the value of $^1J_{CC}$. This means that complexation of boronic acids with cyclic saccharides in their furanose or pyranose forms would be expected to affect $^1J_{CC}$ coupling constants due to (i) a decrease in the dihedral angles of bound vicinal diol groups (as observed for fructose and glucose)³²⁻³³ and/or (ii) changes in orientation of pyranose rings, including twist conformations (as observed for galactopyranose).³⁴ However, in the case of the open glucose unit of grafted maltose, it can be reasonably assumed that complexation of hydroxyl groups by APBA may have a minimal effect in the NMR coupling constants, as no significant changes in the torsional angles would be expected due to the flexible structure of this sugar.

To support the assumption that only the glucose unit which is in the open form is involved in the binding mode of grafted maltose with APBA, density functional theory (DFT) calculations were performed on the different possible complexes formed between APBA/grafted maltose, in order to determine which binding mode is the most stable. To simplify the molecules for the calculations, complexes were simulated using the PBA molecule and a model of the maltose derivative possessing a vinyl group replacing the C1 of its open glucose unit to avoid the problem connected with the stereochemistry of the HC=NO bond of the maltose moiety grafted on HA. The solvent model density (SMD)³⁵ method was used to simulate the aqueous environment of the complexes. The fact that the stoichiometry of ~ 2:1 measured for APBA/free maltose-COOH changes to 1:1 when maltose is grafted on HA (Figure 3 and Table 1, entry 5) suggests that the binding mode of PBA towards free/grafted maltose changes. It can be assumed that a trivalent complex is observed with the maltose derivative grafted on HA, similar to that observed for free/grafted fructose (Figure 5). Based on this assumption, only trivalent complexes formed between PBA and the open glucose unit of the grafted maltose derivative were taken into consideration for the calculations. Indeed, when simulating a possible complex of PBA bound to the open and

closed glucose units of the disaccharide model (including C5-OH, C6-OH and C6'-OH as binding sites), a free energy above 15 kcal/mol was obtained with respect to the energy of the most stable complex (data not shown). This indicates that this binding mode is not the most stable for PBA-grafted maltose, which fully supports the NMR observations. This result may be explained by the fact that the binding of PBA to the glucopyranose ring would require the formation of cycles with a large size, including at least a 8-membered ring (which is known to be less favorable than 5- or 6-membered cycles).

Based on this, we focused on studying the 4 possible bridged bicyclic compounds formed by a trivalent complexation between the open glucose unit of maltose and PBA (complexes **1-4**, Figure 6). Prior to DFT calculations, molecular dynamics (MD) studies were performed on each complex in order to reduce the number of conformers which include rotamers (see experimental section and Figure S33-S36). DFT calculations suggested that the four possible complexes may exist at room temperature, as there are only 2 kcal/mol of difference of free energy between the most stable and the less stable binding modes (Figure 6). Surprisingly, complex **3** (a 5- and 7-membered bridged bicyclic compound) was found to be as stable as complex **2** (a 5- and 6-membered bridged bicyclic compound). This unexpected result could be explained by an intramolecular hydrogen bond formed between the only free hydroxyl group of the open chain glucose and an oxygen atom in the phenylboronate ester, thus stabilizing the bicyclic compound. These results confirm that various binding modes may exist for PBA-grafted maltose, which correlates with the fact that their NMR spectrum may not be easily interpreted. However, taking into account the energies of the different conformers of each complex studied (meaning the Boltzmann distribution), we would expect that only complexes **2** and **3** would be more easily observed experimentally by NMR analysis. These results are in correlation with the partial observations obtained from the NMR studies of the ^{13}C labeled maltose grafted on HA, as the upshift of the C6 signal indicates complexation of the C6-OH similar to the most stable binding mode **3**.

When performing the same study using a gluconamide model (an open glucose with a vinyl group replacing the C1), we observed that among ten possible trivalent complexes, only five showed a significant population at room temperature, and four of them were the corresponding analogues of the PBA/maltose complexes (Figure S37). It should be noted that the values of ΔG between these five complexes are very low, which indicates that all these binding modes could be, hypothetically, observed in a typical INADEQUATE NMR spectrum of a ^{13}C labeled gluconamide grafted on HA in the presence of APBA (as performed for maltose), making this analysis of a greater complexity.

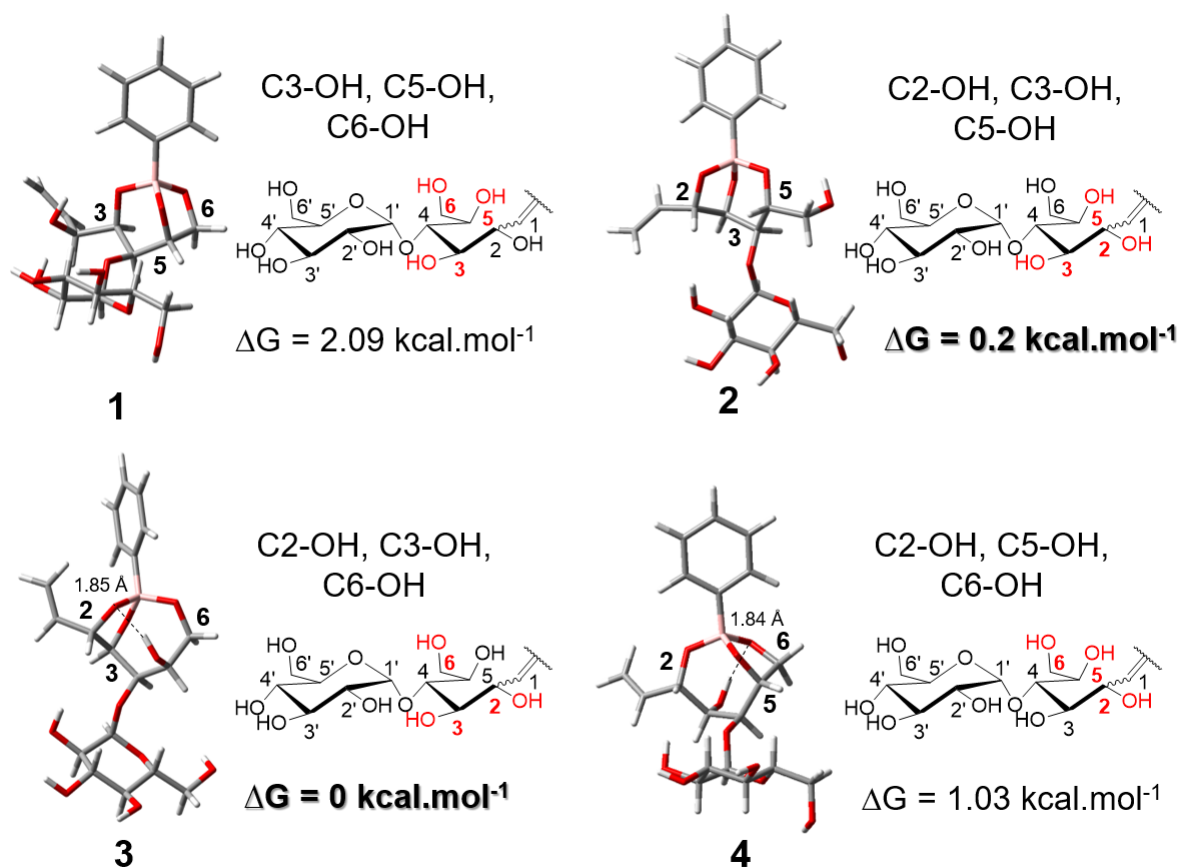


Figure 6. Optimized structures (M062X/6-311+G(d,p)/SMD) of most stable complexes between PBA and maltose derivative. Note: The indicated values of energy are relative ones, with the minima set at 0 kcal/mol for the respective lowest energy structures of complex 3.

With regard to the binding mode of BOR to the maltose derivative in HA-BOR/HA-maltose network, because of the steric hindrance caused by the HA chains, it can be reasonably assumed that only complexes with a stoichiometry of 1:1 are formed. Besides possible binding to the terminal glucopyranose unit as discussed above, BOR may also form complexes with the open glucose unit. In the latter case, considering the most stable structures of the complexes determined for PBA-grafted maltose, we would expect the formation of five structures as dicovalent complexes (Figure S38). It should be noted that in this case, no upfield shift of the CH_2O group was observed for BOR in the presence of HA-maltose in comparison to BOR alone (Figure S39). This indicates that BOR is mainly in the closed form.

A different situation was observed from the ^1H NMR analysis of complexes of BOR with free-grafted gluconamide. Although extensive broadening of proton signals was observed in the NMR spectra of the complexes, it was possible to distinguish both the closed and open forms of ABOR (Figure S40). Despite the fact that the open form of ABOR represents a very small fraction and that the flexible open chain glucose derivative can adopt various

conformations, the existence of a small proportion of monocyclic adduct due to the opening of the oxaborole ring, besides spiro adducts, cannot be excluded. Therefore, looking at the complexes of PBA/gluconamide, we would expect that the complexation between BOR and gluconamide would include at least nine possible binding modes in a dicovalent fashion involving the cyclic form of BOR (spiro adducts). Nevertheless, as discussed above, we cannot exclude that other binding modes would exist including the open form of BOR.

3. Discussion

In recent years, the desire to control rationally the properties of injectable hydrogels has promoted the emergence of new synthetic and natural polymer networks crosslinked via ester bond formation between boronic acid derivatives and glucose-like diols.^{8, 36-41} In this regard, Yesilyurt et al. designed boronate-ester crosslinked poly(ethylene glycol) (PEG) hydrogels using three different phenylboronic acid derivatives and a glucose unit in the ring-opened form, and showed that the location of the crossover frequency during dynamic rheology was sensitive to the pK_a of the PBA derivative used.⁴¹ In that work, the three hydrogels networks exhibited a viscoelastic behavior in the frequency window explored, with the crossover frequency (ω_c) correlating with the rank of pK_a values (7.8, 7.2, and 6.5-6.7). On the other hand, the results obtained by the same authors in another study on poly(acrylamide) networks assembled via complexation between the same APBA derivative as used in our work ($pK_a \sim 8.8$) and glucose in the ring-opened form did not confirm this trend, as a gel-like behavior ($G' > G''$ in the frequency window explored) was observed.³⁷ The latter results are however consistent with our findings, which highlights the anomalously high binding profile for glucose (in the ring-opened form)-APBA complexation. Our work additionally points out the fact that the pK_a of phenylboronic acid derivatives is not a reliable factor that determines rheological properties of boronate ester-crosslinked networks. This is clearly demonstrated by the comparative analysis of the networks based on HA-PBA and HA-BOR. When HA-maltose and HA-gluconamide are used as partners of HA-PBA and HA-BOR, a gel-like behavior was only observed for the assemblies based on HA-PBA, despite the lower pK_a of ABOR (~ 7.3) compared to APBA. On the other hand, with HA-fructose, gel-like properties were obtained for both HA-PBA and HA-BOR-based networks. The viscoelastic behavior observed for the assemblies based on HA-BOR/HA-maltose (gluconamide) is in full agreement with rheological data reported previously for synthetic polymer networks crosslinked via glucose (in the ring-opened form)-BOR complexation.^{36, 40} All these results led us to conduct mechanistic studies of the molecular contributions to the rheological dynamic properties of the hydrogel networks. Although the thermodynamics of small molecular crosslinkers are often a primary consideration in polymer network design,

dynamics also play a key role.^{14-15, 26} Therefore, we focused our efforts on analyzing the relative influence of dynamics and thermodynamics in the HA networks. The data given in Table 1 make us really believe that the dynamics of the boronate ester crosslinks are the primary determinants of the dynamic rheological behavior of the HA assemblies. Indeed, though similar binding constants were found for ABOR/HA-fructose and ABOR/HA-gluconamide, dynamic rheology revealed a gel-like behavior for HA-BOR/HA-fructose and viscoelastic properties for HA-BOR/HA-gluconamide. Similar observations were reported by Lin et al. in a study on hydrogels formed from BOR-containing poly(acrylamides) and three glycopolymers possessing an identical main chain but different pendent sugars.³⁸ Indeed, these authors found that the binding constants between BOR and the sugars did not show any significant impact on the dynamics of the polymer assemblies. Moreover, it can be noted that the difference in boronic ester exchange kinetics for ABOR/HA-maltose ($k_{ex} \sim 191 \text{ s}^{-1}$) and APBA/HA-maltose ($k_{ex} \sim 0.27 \text{ s}^{-1}$) agrees well with the different rheological behavior of HA-BOR/HA-maltose and HA-PBA/HA-maltose (viscoelastic vs gel-like character, respectively). Of note, the exchange rate between free ABOR and ABOR bound to HA-maltose is about 380-fold higher than the crossover frequency of the HA-BOR/HA-maltose network ($\omega_c \sim 0.5 \text{ Hz}$). Furthermore, although the exact value of ω_c for HA-PBA/HA-maltose is unknown, it is much lower than 0.01 s^{-1} , which also indicates that the transesterification rate for APBA/HA-maltose is more than two orders of magnitude higher than the crossover frequency ω_c . The fact that the dynamics of the “cause” (molecular crosslinkers) is several orders of magnitude faster than that of the “effect” (dynamic property of the assembly) is related to the multivalent character of the interactions in the HA assembly.

In order to elucidate the origin of the high-affinity binding properties of APBA/HA-maltose (gluconamide), we investigated the binding mode of APBA to maltose grafted on HA by ¹³C NMR and computational analyses. Together with the structural investigation of the APBA/HA-fructose complex by ¹³C NMR spectroscopy, these studies provide evidence of the formation of a trivalent complex for APBA/HA-maltose. All together, these results offer some insight into why differences in the thermodynamic and/or kinetic parameters in Table 1 are observed i) for complexation with APBA when a given saccharide derivative is free or grafted on HA as well as ii) for complexation of a given saccharide by APBA or ABOR.

First, from the analysis of the structure of the complexes of APBA with free and grafted fructose and the complexation thermodynamics, it can reasonably be inferred that the higher binding affinity of APBA for fructose grafted on HA than for free fructose is due to the formation of a trivalent complex. Regarding ABOR, no significant difference in the binding constants is observed between free and grafted fructose suggesting that ABOR binds free and grafted fructose in the same manner. Interestingly, careful analysis of ¹H and ¹³C NMR

spectra of ABOR alone and in the presence of free/grafted fructose revealed that complexation is accompanied by the breaking of the endocyclic B-O bond of ABOR resulting in the formation of a bidentate adduct similar to APBA/free fructose (Figure S31). It is speculated that an energetic advantage can be achieved by the opening of the oxaborole ring to relieve ring strain and thereby, to form a monocyclic adduct with the syn-1,2-diol of fructofuranose instead of a spiro adduct.

Regarding complexation of APBA with the maltose derivatives, a lower binding constant was found when maltose is grafted on HA compared to free maltose-COOH which is in contrast with the results obtained with fructose. These differences are related to the disaccharidic nature of maltose. Indeed, in the case of free maltose-COOH, it can be assumed that, similar to free fructose, bidentate complexes are formed but the presence of two glucose units allows possible binding of two PBA molecules as reflected by the stoichiometry of $\sim 2:1$ measured for APBA/free maltose-COOH. When maltose is grafted on HA, a trivalent complex with a 1:1 stoichiometry is formed. Because of this change in stoichiometry, the binding constants measured with free and grafted maltose cannot be really compared. With regard to ABOR/free maltose-COOH complexation, the binding of two ABOR molecules to the disaccharide as suggested by the stoichiometry of $\sim 2:1$ determined by ITC, is even more obvious taking into account of the capability of ABOR to form bidentate complexes with sugars locked in the pyranose form (glycopyranosides)¹⁸. This is particularly highlighted by the higher G' and G'' values observed for the HA-BOR/HA-glucose mixture in comparison to the HA-PBA/HA-glucose one (Figure 2d). These data suggest possible binding of one ABOR molecule to the terminal glucose unit in maltose-COOH and of another one to the glucose residue in the open-chain form as dicovalent adducts. Finally, the high binding affinities obtained for complexation of APBA with the free and grafted gluconamide derivatives also strongly suggest formation of trivalent adducts. Yet, on the basis of the different binding constant and stoichiometry values found for the APBA/maltose-COOH and APBA/free gluconamide complexes, it can be reasonably assumed that the binding mode mechanism of APBA to the maltose and gluconamide derivatives is different. Also worthy of note is the higher binding affinity of ABOR for the free gluconamide derivative compared the free maltose-COOH. Although the binding constant is reduced when gluconamide is grafted on HA, it remains of the same order of magnitude as that measured for ABOR/HA-fructose complexation. This raises the question of whether a monocyclic adduct or a spiro adduct is formed between ABOR and the free/grafted gluconamide derivative. According to NMR analysis, the existence of a small proportion of monocyclic adduct due to the opening of the oxaborole ring cannot be excluded.

From these observations, it is also possible to gain some understanding of the different dynamics observed between the networks based on HA-PBA and HA-BOR.

When looking at the geometry of the small molecular crosslinkers in the HA-PBA/HA-maltose and HA-BOR/HA-maltose networks, there are noticeable differences in that diester spiro adducts are formed in the latter case whereas bridged bicyclic compounds are obtained in the former case (Figure 6 and S38). The strained spiro-structure in the case of complexes based on BOR may promote B-O bond cleavage and thereby, complex dissociation. Nevertheless, as the neutral, trigonal planar boron atom is also constrained in the uncomplexed five-membered oxaborole ring, spiro adducts are rapidly re-formed to alleviate ring strain. It is indeed believed that the ring strain in the oxaborole heterocyclic ring is at the origin of the decrease in pK_a in comparison to PBA as the ring strain is relieved upon ionization.⁴²⁻⁴³ This phenomenon may result in rapid molecular exchange dynamics. This is in contrast to the complexes with PBA which consist of more stable bridged bicyclic compounds. In these systems, we believe that the formation of trivalent adducts is a major cause of the slow network dynamics. This is supported by a recent study showing fast relaxation dynamics for PEG networks crosslinked via boronate ester bonds between catechol and PBA moieties grafted on the PEG derivatives.⁴⁴ Catechols have special features in that their structure precludes formation of tridentate complexes on the one hand, and that they bind with boronic acids with much higher affinities than most carbohydrates, on the other.³¹ Based on this, we examined formation of networks by combining HA-PBA with HA modified with catecholamine (dopamine)⁴⁵ and interestingly, fast network relaxation was also observed in this case (Figure S41).

The assumption that the fast relaxation dynamics of HA-BOR/HA-maltose lies in the strained structures of free and bound BOR sheds light on why slow network dynamics is observed for the HA-BOR/HA-fructose. The original and previously unobserved binding mode between BOR and fructose, leading to the formation of a monocyclic adduct instead of a spiro adduct due to the opening of the oxaborole ring, may be the reason for the slow molecular exchange dynamics in the HA-BOR/HA-fructose networks. This phenomenon is more specifically observed with fructose, which may be due to the locally optimised geometry of the hydroxyl groups of its β -D-fructofuranose tautomeric form. This favors formation of a bidentate complex with the cis-1,2 diol which may be further stabilized by hydrogen bonding with the free hydroxyl groups of fructose and oxaborole.

Finally, although it is difficult to have a clear picture of the binding mode of BOR to gluconamide, we hypothesize that the formation of a monocyclic adduct at a small proportion with respect to “classical” spiro adducts may account for the slower dynamics observed for the HA-BOR/HA-gluconamide assemblies in comparison to the HA-BOR/HA-maltose ones.

One question remains with regard to the formation of a tricovalent APBA/fructose complex rather than a dicovalent one when fructose is grafted on HA. While it has been traditionally thought that boronate ester formation proceeded through the boronate anion exclusively,³¹ more recent studies showed that the kinetically preferred pathway to the boronate ester species is via trigonal boronic acid.⁴⁶⁻⁴⁷ In this latter case, the neutral diester formed by reaction of trigonal boronic acid and the diol-containing molecule reacts with a water molecule in a second step to produce the anionic tetrahedral diester adduct. (Figure S42).

On the basis of these data, it can be inferred that the environment created by HA makes the OH-6 group of fructose more efficient to react with the neutral diester intermediate than water. The high water-binding capacity of HA may provide some explanation for this. Indeed, it can be assumed that the water molecules organized near the polysaccharide chains- tightly bound and weakly bound water via formation of hydrogen bonds with HA-,⁴⁸⁻⁵¹ decreases ability of water to react with neutral boronate ester species. As a result, the formation of tricovalent complexes with fructose as well as with the maltose and gluconamide derivatives grafted on HA is favored. With this hypothesis, efficient boronate ester crosslinking via tricovalent complex formation should be also observed with other derivatives of highly hydrated polymers. In this regard, we previously reported efficient boronate ester crosslinking upon mixing PBA- and maltose-linked carboxymethylcellulose (CMC) derivatives.⁸ Similarly to HA-PBA/HA-maltose, the CMC-PBA/CMC-maltose mixture displayed a gel-like behavior in the frequency window explored.

4. Conclusion

In this study, we demonstrated the outstanding capability of 3-aminophenylboronic acid to bind fructose and open chain glucose derivatives grafted on hyaluronic acid, resulting in the formation of hydrogel networks with slow relaxation times and relatively high dynamic moduli. The correlation between the structure of the APBA/carbohydrate complexes and their thermodynamics and molecular exchange dynamics reveals the importance of the tricovalent binding mode for efficient boronate ester crosslinking in HA hydrogels. Notably, the previously unobserved tricovalent structure of complexes with APBA at neutral pH plays a key role in increasing the lifetime of the small molecular crosslinkers. Remarkably, we also found that complexation of 6-aminobenzoboroxole with fructose results in a monocyclic adduct instead of a spiro adduct as observed with other carbohydrates, leading to the formation of hydrogel networks that feature slow relaxation dynamics compared to the other assemblies formed by complexation of BOR and glucose-derivatives grafted on HA.

Furthermore, we also demonstrate that the polymer backbone on which the boronic acid and sugar moieties are grafted can also affect the structure of the boronate complexes. This is highlighted here in the case of the APBA/fructose complexation.

Understanding the factors that affect the binding mode between boronic acid and polyols moieties is important to the future design of boronic acid based hydrogels.

5. Experimental Section

Materials. Sodium hyaluronate (HA) possessing a weight average molar mass (M_w) of 100 kg/mol was supplied by Lifecore Biomedical (USA). The molar mass distribution and the weight-average molar mass of this sample were determined by size exclusion chromatography using a Waters GPC Alliance chromatograph (USA) equipped with a differential refractometer and a light scattering detector (MALLS) from Wyatt (USA); the solution was injected at a concentration of 1×10^{-3} g/mL in 0.1 M NaNO_3 , at a flow rate of 0.5 mL/min and at a column temperature of 30 °C. The dispersity (\mathcal{D}) of the sample is $M_w/M_n \approx 1.5$ -2. The overlap concentration C^* for this HA sample in buffer at 25 °C is around 3 g/L. This value was derived from the intrinsic viscosity assuming that $C^*[\eta]$ is about unity.⁵² HA samples with lower M_w (5 or 10 kg/mol), purchased from the same supplier, were used to synthesize HA derivatives for NMR studies (thermodynamics, kinetics and elucidation of the structure of boronic acid complexes). This low M_w HA sample was used to circumvent limitations due to the high viscosity of concentrated solutions of high M_w HA. 5-amino-2-(hydroxymethyl)phenylboronic acid hydrochloride (ABOR, 6-aminobenzoboroxole) and Boc-1-amino-3,6-dioxo-8-octanamine (Boc-DOOA) were purchased from Combi-Blocks and Iris Biotech, respectively. 1-Amino-1-deoxy-D-fructose hydrochloride (fructosamine) and D-gluconolactone were supplied by Carbosynth. 3-Aminophenylboronic acid hemisulfate salt (APBA), 4-(4,6-dimethoxy-1,3,5-triazin-2-yl)-4-methylmorpholinium chloride (DMTMM), D-maltose, 1-thio- β -D-glucose sodium salt(thiogluucose), 4-pentenoic anhydride, O-(carboxymethyl)hydroxylamine hemihydrochloride, cystamine dihydrochloride, *N,N'*-diisopropylcarbodiimide (DIC), 1-hydroxybenzotriazole (HOBT), tris(2-carboxyethyl)phosphine hydrochloride (TCEP), trifluoroacetic acid (TFA), picrylsulfonic acid solution (TNBS), 4-(2-hydroxyethyl)piperazine-1-ethanesulfonic acid (HEPES), phosphate buffered saline (PBS) and other chemicals were purchased from Sigma-Aldrich-Fluka and were used without further purification. A ^{13}C labeled maltose (maltose- $^{13}\text{C}_{12}$ monohydrate) was supplied by Cambridge Isotope Laboratoires and a ^{13}C labeled D-fructose was purchased from Carbosynth.

Methods.

NMR spectroscopy. ^1H and ^{13}C NMR spectra were recorded at 25 °C or 80 °C using a Bruker AVANCE III HD spectrometer operating at 400.13 MHz (^1H) and at 100.61 MHz (^{13}C). ^1H NMR spectra were recorded by applying a 90° tip angle for the excitation pulse, and a 10 s recycle delay for accurate integration of the proton signals. ^{13}C NMR spectra were recorded by applying a 90° tip angle for the excitation pulse and a 2 s recycle delay. Analyses using the HA derivative modified with ^{13}C labeled maltose were recorded on a Bruker AVANCE III HD operating at 950 MHz (^1H) and at 239 MHz (^{13}C). 2-D INADEQUATE experiments were performed using the pulse sequence inadphsp given by Bruker. For each experiment, 256 (or 64) transients were acquired for each of the 128 (or 512) increments in F1. The recycle delay was set to 3 s. The spectral width was set to 20161 Hz (number of data points = 8192). The data were processed with shifted sine bell weighting and zero filling to form a 8192 x 1024 matrix prior to Fourier transform. Deuterium oxide (D_2O) was obtained from Euriso-top (Saint-Aubin, France). Chemical shifts (δ in ppm) are given relative to external tetramethylsilane (TMS = 0 ppm) and calibration was performed using the signal of the residual protons of the solvent as a secondary reference. All NMR spectra were analyzed with Topspin 3.1 (or 3.5) software from Bruker AXS.

Computational analysis. Four possible trivalent PBA/maltose complexes (Figure 6), formed between the open glucose unit of the maltose derivative and PBA, have been studied: two bridged bicyclic compounds formed by 5- and 6-membered rings (complexes **1** and **2**) and two bridged bicyclic compounds formed by 5- and 7-membered rings (complexes **3** and **4**). For a better representation of the maltose derivative which is grafted to HA, C1 of the open glucose unit was replaced by a vinyl group. First, force field molecular dynamics (MD) simulations were carried out on the complexes for screening the different rotamers and rings conformations. The MD simulations were performed in the GROMACAS software, ver. 2018,⁵³ with all-atom Gromos 54a7 force field.⁵⁴ All the MD simulations were performed in an NPT (constant number of atoms, pressure, and temperature) ensemble with velocity-rescale temperature coupling⁵⁵ and Berendsen pressure coupling algorithms⁵⁶ with temperature and pressure coupling constants of 0.2 ps and 2 ps, respectively. Each complex was placed in a box with dimensions with $5 \times 5 \times 5 \text{ nm}^3$ where single point charge (SPC) water molecules⁵⁷ are filled. The structure is then relaxed with energy minimization followed by MD simulation with slow heating from 0 K to 300 K in 2 ns. The system was then equilibrated for 8 ns at 300 K. The production run was performed for 10 ns at 300 K. Distributions of selected dihedral angles were summarized in Figure S33-36 in the supporting information. From the above MD simulations, the feasible conformers and rotamers of the different complexes were selected

and submitted to DFT calculations using Gaussian 09 (rev. D.01)⁵⁸ with standard termination options. Optimizations were performed with M062X⁵⁹ at 6-311+G(d,p) level and with SMD³⁵ in water. The functional was chosen for its proven performance in estimations of the relative energies of sugar conformers⁶⁰⁻⁶¹ and B-O bond length.⁶² The SMD solvent simulation was chosen as it was shown to well reproduce the solvation effect.⁶⁰ For each DFT optimization, a frequency calculation was performed in order to verify that there is no negative frequency (i.e. confirm that it is a minimum) and to determine the absolute free energy of each rotamer at 298 K. For the complexes of PBA and an open glucose used to simulate the gluconamide derivative (with the C1 replaced by a vinyl group, Figure S37), ten different trivalent possibilities have been studied: three bridged bicyclic compounds formed by two 5-membered rings and four bridged bicyclic compounds formed by 5- and 6-membered rings, one bridged bicyclic compound formed by two 6-membered rings and two bridged bicyclic compounds formed by 5- and 7-membered rings. In this case, the DFT calculation was performed for all possible rotamers of each complex, using the same condition described for the PBA/maltose derivative complexes.

Syntheses.

Thiol-ene coupling reaction. This required the functionalization of HA with alkene groups, (pentenoate-modified HA, DS = 0.18), as previously described.¹⁹

HA-maltose. The HA-maltose derivative was synthesized as previously reported.⁸ In brief, this included a first step to prepare an unprotected carboxylic acid derivative of maltose (maltose-COOH) by reaction of D-maltose (0.5 g, 1.4 mmol) with *O*-(carboxymethyl)hydroxylamine (0.153 g, 1.4 mmol) in water at pH 4.8. Then, a maltose-disulfide derivative was obtained by reaction of maltose-COOH with cystamine dihydrochloride (0.157 g, 0.7 mmol) in dry DMF under nitrogen, using DIC (0.7 g, 5.57 mmol) and HOBT (0.38 g, 2.79 mmol). The synthesis of HA-maltose consisted in the reduction of the disulfide bond of maltose-disulfide (0.16 g, 1.69 mmol) with TCEP (0.062 g, 0.22 mmol), followed by the coupling reaction in ultrapure water of maltose-thiol with pentenoate-modified HA (0.25 g, 0.6 mmol), in the presence of the photoinitiator Irgacure 2959 (0.1 % w/v), at room temperature for ten minutes under UV light ($\lambda = 365$ nm, 20 mW/cm²). Successful grafting of maltose-thiol onto HA was confirmed by ¹H NMR spectroscopy, which also allowed determination of a DS of 0.1 (Figure S2a, Table 2). ¹H NMR (400 MHz, D₂O, 25 °C) of **maltose-disulfide (Figure S1b)**: δ_{H} (ppm) 7.54 and 6.89 (1H, H1), 5.33 (1H, H1'), 4.53 (2H, Ha), 3.95-3.40 (12H, H2-H6 and H2'-H6'), 2.60 (4H, Hb and Hc).

HA-glucose. The commercially available 1-thio- β -D-glucose (0.033 g, 0.15 mmol) was reacted with pentenoate-modified HA (0.1 g, 0.24 mmol) at room temperature for ten minutes under UV light in ultrapure water. ^1H NMR analysis of the product allowed determination of a DS of 0.15 of the HA-glucose derivative (Figure S2b, Table 2).

Table 2. Reaction conditions for the synthesis of HA-maltose and HA-glucose.

HA derivative	[SH]/[pentenoate]	DS ^a	Yield (%)
HA-maltose	1.6	0.1	88
HA-glucose	3.5	0.15	90

^aDS determined by ^1H NMR (10 % of accuracy).

Amine-acid coupling reaction.

HA-gluconamide. To a solution of Boc-DOOA (0.113 g, 0.45 mmol) in DMF (25 mL), a solution of D-glucono-1,5-lactone (0.081 g, 0.45 mmol) in DMF (20 mL) was added dropwise for ~ 3 h. After stirring overnight at room temperature, the solvent was removed under reduced pressure and the resulting transparent syrup was dried under vacuum (60 mbars, 40 °C) to give a Boc-DOOA-gluconamide derivative (0.178 g, 92 %). The removal of the Boc protecting group was performed by acid treatment of Boc-DOOA-gluconamide (0.055 g, 0.13 mmol) in TFA (0.6 mL, 7.77 mmol) for 5 min at room temperature. The reaction medium was neutralized by adding 1 M NaOH dropwise (\approx 5 mL) at ~ 0 °C, and the solvent was removed under reduced pressure. The complete deprotection of the amine group yielding 1-amino-DOOA-gluconamide derivative was confirmed by ^1H NMR analysis. The HA-gluconamide derivative was then prepared by amide coupling. The reaction consisted in adding DMTMM (0.207 g, 0.75 mmol) to a solution of HA (0.3 g, 0.75 mmol) at a concentration of 3 g/L in a water/DMF (3/2, v/v) mixture. After 15 min of stirring at room temperature, 1-amino-DOOA-gluconamide (0.056 g, 0.17 mmol) was added and the pH was adjusted to 6.5 using 0.5 M aqueous NaOH. After stirring for 65 h at room temperature, the HA-gluconamide conjugate was purified by ultrafiltration using deionized water and the product was recovered by freeze-drying (Table 3). The DS of HA-gluconamide was found to be 0.1 from ^{13}C NMR analysis (Figure S5). It was also estimated from the reaction kinetics performed by quantifying the free primary amine in the reaction medium as a function of time (Figure S7). ^1H NMR (400 MHz, D_2O , 25 °C) of **Boc-1-amino-DOOA-gluconamide (Figure S3b)**: δ_{H} (ppm) 4.35 (1H, H2), 4.15 (1H, H3), 3.88-3.72 (10H, H4-H6 and Hb-Hd), 3.65 (2H, He), 3.55 (2H, Ha), 3.32 (2H, Hf), 1.5 (9H, Hg).

HA-PBA, HA-BOR and HA-fructose. HA-PBA, HA-BOR and HA-fructose were synthesized by an amide coupling reaction from APBA, ABOR and fructosamine (containing free primary amine groups), respectively. To this end, APBA (0.022 g, 0.12 mmol) or ABOR (0.025 g,

0.135 mmol) or fructosamine (0.024 g, 0.112 mmol) was added to a water/DMF (3/2, v/v) mixture containing DMTMM (0.207 g, 0.75 mmol) and HA (0.3 g, 0.75 mmol) and the pH was adjusted to 6.5 using 0.5 M aqueous NaOH. After stirring for 24 h at room temperature, the different HA derivatives were purified by ultrafiltration using deionized water and the products were recovered by freeze-drying (Table 3). The DS of the HA derivatives were found to be 0.15 from ^1H and ^{13}C NMR analyses (Figure S4 and S6). The DS of HA-fructose was also estimated from the reaction kinetics using the TNBS method (Figure S7).

Table 3. Reaction conditions for the synthesis of HA-BOR, HA-PBA, HA-fructose and HA-gluconamide.

HA derivative	R-NH ₂ /HA molar ratio	DS	Coupling (%)	Yield (%)
HA-BOR	0.18	0.15 ^a	83	86
HA-PBA	0.16	0.15 ^a	100	98
HA-fructose	0.15	0.15 ^b	100	96
HA-gluconamide	0.22	0.1 ^{b,c}	50	73

^aDS by ^1H NMR (10 % of accuracy).

^bDS estimated from the reaction kinetics using TNBS.

^cDS by ^{13}C NMR (20 % of accuracy).

Preparation of HA-PBA (HA-BOR) and HA-saccharides mixtures. The different HA derivatives were solubilized in 0.01 M HEPES buffer containing 0.15 M NaCl pH 7.4. The dissolution time was at least 12 h at 4 °C. The solutions of HA-BOR or HA-PBA and of HA-saccharide (HA-fructose, HA-maltose, HA-glucose or HA-gluconamide) were mixed under vigorous stirring at room temperature, at a total polymer concentration of 15 g/L and with BOR or PBA/sugar molar ratio of 1. The mixtures were then allowed to rest at 4 °C overnight before rheological analysis.

Rheology. Oscillatory shear experiments were performed with a cone-plate rheometer (AR2000EX from TA Instruments). All the dynamic rheological data were checked as a function of strain amplitude to ensure that the measurements were performed in the linear viscoelastic region. The cone used for viscoelastic samples has a diameter of 2 cm and an angle of 4°, whereas viscous solutions were analyzed using a cone of 6 cm of diameter and an angle of 1°. To prevent water evaporation, the measuring system was surrounded with a low-viscosity silicon oil (50 mPa.s) carefully added to the edges of the cone.

Determination of K_a by ITC. Calorimetric titration experiments were carried out on a Microcal VP-ITC titration microcalorimeter (Northampton, U.S.A.). All titrations were performed using solutions of APBA (ABOR) and free saccharides (D-fructose, maltose-COOH and Boc-DOOA-gluconamide) solubilized in 0.01 M PBS, with pH adjusted to 7.4 (\pm 0.1) using a pH-meter, by carefully adding 1 M NaOH when necessary. The reaction cell ($V = 1.4478$ mL) contained a solution of “molecule 2” (Table 6). A series of 28 injections of 5 or

10 μL of a solution of “molecule 1” was made from a computer-controlled 300 μL microsyringe at an interval of 400 s into the solution contained in the reaction cell, while stirring at 300 rpm at 25°C. The raw experimental data were reported as the amount of heat produced after each injection of boronic acid as a function of time. The amount of heat produced per injection was calculated by integration of the area under individual peaks by the instrument software, after taking into account heat of dilution. The data were analyzed using the one set of site fitting model (Origin 7.0 software package). Table 4 summarizes the experimental conditions used for the ITC measurements.

Table 4. Experimental conditions of the calorimetric titrations.

Entry	Molecule 1 in syringe	[Molecule 1] (mM)	Molecule 2 in cell	[Molecule 2] (mM)
1	Free D-fructose	130	APBA	3.7
2	Free D-fructose	75	ABOR	2
3	APBA	15	Free maltose-COOH	0.5
4	ABOR	35	Free maltose-COOH	1
5	APBA	20	Free gluconamide-diamine-Boc	1
6	ABOR	35	Free gluconamide-diamine-Boc	1

6. References

- (1) Taylor, D. L.; in het Panhuis, M., Self-Healing Hydrogels. *Adv. Mater. (Weinheim, Ger.)* **2016**, *28*, 9060-9093.
- (2) Wang, H.; Heilshorn, S. C., Adaptable Hydrogel Networks with Reversible Linkages for Tissue Engineering. *Adv. Mater. (Weinheim, Ger.)* **2015**, *27*, 3717-3736.
- (3) Patenaude, M.; Smeets, N. M. B.; Hoare, T., Designing Injectable, Covalently Cross-Linked Hydrogels for Biomedical Applications. *Macromol. Rapid Commun.* **2014**, *35*, 598-617.
- (4) Sivashanmugam, A.; Arun Kumar, R.; Vishnu Priya, M.; Nair, S. V.; Jayakumar, R., An Overview of Injectable Polymeric Hydrogels for Tissue Engineering [Erratum to Document Cited in Ca164:027228]. *Eur. Polym. J.* **2016**, *75*, 538.
- (5) Yang, J.-A.; Yeom, J.; Hwang, B. W.; Hoffman, A. S.; Hahn, S. K., In Situ-Forming Injectable Hydrogels for Regenerative Medicine. *Prog. Polym. Sci.* **2014**, *39*, 1973-1986.
- (6) Loebel, C.; Rodell, C. B.; Chen, M. H.; Burdick, J. A., Shear-Thinning and Self-Healing Hydrogels as Injectable Therapeutics and for 3d-Printing. *Nat. Protoc.* **2017**, *12*, 1521-1541.
- (7) Jin, Y.; Yu, C.; Denman, R. J.; Zhang, W., Recent Advances in Dynamic Covalent Chemistry. *Chem. Soc. Rev.* **2013**, *42*, 6634-6654.
- (8) Tarus, D.; Hachet, E.; Messenger, L.; Catargi, B.; Ravaine, V.; Auzely-Velty, R., Readily Prepared Dynamic Hydrogels by Combining Phenyl Boronic Acid- and Maltose-Modified Anionic Polysaccharides at Neutral Ph. *Macromol. Rapid Commun.* **2014**, *35*, 2089-2095.
- (9) Springsteen, G.; Wang, B., A Detailed Examination of Boronic Acid-Diol Complexation. *Tetrahedron* **2002**, *58*, 5291-5300.

- (10) Charlot, A.; Auzely-Velty, R., Synthesis of Novel Supramolecular Assemblies Based on Hyaluronic Acid Derivatives Bearing Bivalent B-Cyclodextrin and Adamantane Moieties. *Macromolecules* **2007**, *40*, 1147-1158.
- (11) Charlot, A.; Auzely-Velty, R., Novel Hyaluronic Acid Based Supramolecular Assemblies Stabilized by Multivalent Specific Interactions: Rheological Behavior in Aqueous Solution. *Macromolecules (Washington, DC, U. S.)* **2007**, *40*, 9555-9563.
- (12) Chen, M. H.; Wang, L. L.; Chung, J. J.; Kim, Y.-H.; Atluri, P.; Burdick, J. A., Methods to Assess Shear-Thinning Hydrogels for Application as Injectable Biomaterials. *ACS Biomater. Sci. Eng.* **2017**, *3*, 3146-3160.
- (13) Rodell, C. B.; Kaminski, A. L.; Burdick, J. A., Rational Design of Network Properties in Guest-Host Assembled and Shear-Thinning Hyaluronic Acid Hydrogels. *Biomacromolecules* **2013**, *14*, 4125-4134.
- (14) Yount, W. C.; Loveless, D. M.; Craig, S. L., Strong Means Slow: Dynamic Contributions to the Bulk Mechanical Properties of Supramolecular Networks. *Angew. Chem., Int. Ed.* **2005**, *44*, 2746-2748.
- (15) Cromwell, O. R.; Chung, J.; Guan, Z., Malleable and Self-Healing Covalent Polymer Networks through Tunable Dynamic Boronic Ester Bonds. *J. Am. Chem. Soc.* **2015**, *137*, 6492-6495.
- (16) Adamczyk-Wozniak, A.; Borys, K. M.; Sporzynski, A., Recent Developments in the Chemistry and Biological Applications of Benzoxaboroles. *Chem. Rev. (Washington, DC, U. S.)* **2015**, *115*, 5224-5247.
- (17) Dowlut, M.; Hall, D. G., An Improved Class of Sugar-Binding Boronic Acids, Soluble and Capable of Complexing Glycosides in Neutral Water. *J. Am. Chem. Soc.* **2006**, *128*, 4226-4227.
- (18) Berube, M.; Dowlut, M.; Hall, D. G., Benzoboroxoles as Efficient Glycopyranoside-Binding Agents in Physiological Conditions: Structure and Selectivity of Complex Formation. *J. Org. Chem.* **2008**, *73*, 6471-6479.
- (19) Mergy, J.; Fournier, A.; Hachet, E.; Auzely-Velty, R., Modification of Polysaccharides Via Thiol-Ene Chemistry: A Versatile Route to Functional Biomaterials. *J. Polym. Sci., Part A Polym. Chem.* **2012**, *50*, 4019-4028, S4019/4011-S4019/4016.
- (20) D'Este, M.; Eglin, D.; Alini, M., A Systematic Analysis of Dmtmm Vs Edc/Nhs for Ligation of Amines to Hyaluronan in Water. *Carbohydr. Polym.* **2014**, *108*, 239-246.
- (21) Auzely-Velty, R.; Cristea, M.; Rinaudo, M., Galactosylated N-Vinylpyrrolidone-Maleic Acid Copolymers: Synthesis, Characterization, and Interaction with Lectins. *Biomacromolecules* **2002**, *3*, 998-1005.
- (22) Ellis, G. A.; Palte, M. J.; Raines, R. T., Boronate-Mediated Biologic Delivery. *J. Am. Chem. Soc.* **2012**, *134*, 3631-3634.
- (23) Mahalingam, A.; Geonnotti, A. R.; Balzarini, J.; Kiser, P. F., Activity and Safety of Synthetic Lectins Based on Benzoboroxole-Functionalized Polymers for Inhibition of Hiv Entry. *Mol. Pharmaceutics* **2011**, *8*, 2465-2475.
- (24) Angyal, S. J., The Composition of Reducing Sugars in Solution. *Adv. Carbohydr. Chem. Biochem.* **1984**, *42*, 15-68.
- (25) Thordarson, P., Determining Association Constants from Titration Experiments in Supramolecular Chemistry. *Chem. Soc. Rev.* **2011**, *40*, 1305-1323.
- (26) Yount Wayne, C.; Loveless David, M.; Craig Stephen, L., Small-Molecule Dynamics and Mechanisms Underlying the Macroscopic Mechanical Properties of Coordinatively Cross-Linked Polymer Networks. *J Am Chem Soc* **2005**, *127*, 14488-14496.

- (27) Huang, C. Y., Determination of Binding Stoichiometry by the Continuous Variation Method: The Job Plot. *Methods Enzymol.* **1982**, *87*, 509-525.
- (28) Ulatowski, F.; Dabrowa, K.; Balakier, T.; Jurczak, J., Recognizing the Limited Applicability of Job Plots in Studying Host-Guest Interactions in Supramolecular Chemistry. *J. Org. Chem.* **2016**, *81*, 1746-1756.
- (29) Sandstroem, J., *Dynamic Nmr Spectroscopy.* **1982**; p 226 pp.
- (30) Sutherland, I. O., Investigation of the Kinetics of Conformational Changes by Nuclear Magnetic Resonance Spectroscopy. *Annu. Rep. NMR (Nucl. Magn. Resonance) Spectrosc.* **1971**, *4*, 71-235.
- (31) Yan, J.; Springsteen, G.; Deeter, S.; Wang, B., The Relationship among Pka, Ph, and Binding Constants in the Interactions between Boronic Acids and Diols-It Is Not as Simple as It Appears. *Tetrahedron* **2004**, *60*, 11205-11209.
- (32) Norrild, J. C.; Eggert, H., Boronic Acids as Fructose Sensors. Structure Determination of the Complexes Involved Using ^1jcc Coupling Constants. *J. Chem. Soc., Perkin Trans. 2* **1996**, 2583-2588.
- (33) Norrild, J. C.; Eggert, H., Evidence for Mono- and Bidentate Boronate Complexes of Glucose in the Furanose Form. Application of ^1jcc -C Coupling Constants as a Structural Probe. *J. Am. Chem. Soc.* **1995**, *117*, 1479-1484.
- (34) Nicholls, M. P.; Paul, P. K. C., Structures of Carbohydrate-Boronic Acid Complexes Determined by Nmr and Molecular Modeling in Aqueous Alkaline Media. *Org. Biomol. Chem.* **2004**, *2*, 1434-1441.
- (35) Marenich, A. V.; Cramer, C. J.; Truhlar, D. G., Universal Solvation Model Based on Solute Electron Density and on a Continuum Model of the Solvent Defined by the Bulk Dielectric Constant and Atomic Surface Tensions. *J. Phys. Chem. B* **2009**, *113*, 6378-6396.
- (36) Chen, Y.; Wang, W.; Wu, D.; Nagao, M.; Hall, D. G.; Thundat, T.; Narain, R., Injectable Self-Healing Zwitterionic Hydrogels Based on Dynamic Benzoxaborole-Sugar Interactions with Tunable Mechanical Properties. *Biomacromolecules* **2018**, *19*, 596-605.
- (37) Dong, Y.; Wang, W.; Veisoh, O.; Appel, E. A.; Xue, K.; Webber, M. J.; Tang, B. C.; Yang, X.-W.; Weir, G. C.; Langer, R.; Anderson, D. G., Injectable and Glucose-Responsive Hydrogels Based on Boronic Acid-Glucose Complexation. *Langmuir* **2016**, *32*, 8743-8747.
- (38) Lin, M.; Sun, P.; Chen, G.; Jiang, M., The Glyco-Stereoisomerism Effect on Hydrogelation of Polymers Interacting Via Dynamic Covalent Bonds. *Chem Commun (Camb)* **2014**, *50*, 9779-9782.
- (39) Pettignano, A.; Grijalvo, S.; Haering, M.; Eritja, R.; Tanchoux, N.; Quignard, F.; Diaz Diaz, D., Boronic Acid-Modified Alginate Enables Direct Formation of Injectable, Self-Healing and Multistimuli-Responsive Hydrogels. *Chem. Commun. (Cambridge, U. K.)* **2017**, *53*, 3350-3353.
- (40) Wang, Y.; Li, L.; Kotsuchibashi, Y.; Vshyvenko, S.; Liu, Y.; Hall, D.; Zeng, H.; Narain, R., Self-Healing and Injectable Shear Thinning Hydrogels Based on Dynamic Oxaborole-Diol Covalent Cross-Linking. *ACS Biomater. Sci. Eng.* **2016**, *2*, 2315-2323.
- (41) Yesilyurt, V.; Webber, M. J.; Appel, E. A.; Godwin, C.; Langer, R.; Anderson, D. G., Injectable Self-Healing Glucose-Responsive Hydrogels with Ph-Regulated Mechanical Properties. *Adv. Mater. (Weinheim, Ger.)* **2016**, *28*, 86-91.

- (42) Liu, C. T.; Tomsho John, W.; Benkovic Stephen, J., The Unique Chemistry of Benzoxaboroles: Current and Emerging Applications in Biotechnology and Therapeutic Treatments. *Bioorg Med Chem* **2014**, *22*, 4462-4473.
- (43) Tomsho, J. W.; Pal, A.; Hall, D. G.; Benkovic, S. J., Ring Structure and Aromatic Substituent Effects on the Pka of the Benzoxaborole Pharmacophore. *ACS Med. Chem. Lett.* **2012**, *3*, 48-52.
- (44) Tang, S.; Ma, H.; Tu, H.-C.; Wang, H.-R.; Lin, P.-C.; Anseth, K. S., Adaptable Fast Relaxing Boronate-Based Hydrogels for Probing Cell-Matrix Interactions. *Adv. Sci. (Weinheim, Ger.)* **2018**, *5*, n/a.
- (45) Sato, T.; Aoyagi, T.; Ebara, M.; Auzely-Velty, R., Catechol-Modified Hyaluronic Acid: In Situ-Forming Hydrogels by Auto-Oxidation of Catechol or Photo-Oxidation Using Visible Light. *Polym. Bull. (Heidelberg, Ger.)* **2017**, *74*, 4069-4085.
- (46) Miyamoto, C.; Suzuki, K.; Iwatsuki, S.; Inamo, M.; Takagi, H. D.; Ishihara, K., Kinetic Evidence for High Reactivity of 3-Nitrophenylboronic Acid Compared to Its Conjugate Boronate Ion in Reactions with Ethylene and Propylene Glycols. *Inorg. Chem.* **2008**, *47*, 1417-1419.
- (47) Peters, J. A., Interactions between Boric Acid Derivatives and Saccharides in Aqueous Media: Structures and Stabilities of Resulting Esters. *Coord. Chem. Rev.* **2014**, *268*, 1-22.
- (48) Hatakeyama, H.; Hatakeyama, T., Interaction between Water and Hydrophilic Polymers. *Thermochim. Acta* **1998**, *308*, 3-22.
- (49) Haxaire, K.; Marechal, Y.; Milas, M.; Rinaudo, M., Hydration of Hyaluronan Polysaccharide Observed by Ir Spectrometry. II. Definition and Quantitative Analysis of Elementary Hydration Spectra and Water Uptake. *Biopolymers* **2003**, *72*, 149-161.
- (50) Joshi, H. N.; Topp, E. M., Hydration in Hyaluronic Acid and Its Esters Using Differential Scanning Calorimetry. *Int. J. Pharm.* **1992**, *80*, 213-225.
- (51) Servaty, R.; Schiller, J.; Binder, H.; Arnold, K., Hydration of Polymeric Components of Cartilage - an Infrared Spectroscopic Study on Hyaluronic Acid and Chondroitin Sulfate. *Int. J. Biol. Macromol.* **2001**, *28*, 121-127.
- (52) Macosko, C. W., *Rheology: Principles, Measurements, and Applications*; Ed.; VCH Publishers: Weinheim, Germany, **1994**.
- (53) Abraham, M. J.; Murtola, T.; Schulz, R.; Páll, S.; Smith, J. C.; Hess, B.; Lindahl, B. E., *SoftwareX* **2015**, *1*, 19-25.
- (54) Berendsen, H. J. C.; Postma, J. P.; van Gunsteren, W. F.; Hermans, J., *Intermolecular Forces*, ed. B. Pullman, Springer, Netherlands **1981**, 331-342.
- (55) Schmid, N.; Eichenberger, A. P.; Choutko, A.; Riniker, S.; Winger, M.; Mark, A. E.; Gunsteren, W. F., Definition and Testing of the Gromos Force-Field Versions 54a7 and 54b7. *Eur. Biophys. J.* **2011**, *40*, 843-856.
- (56) Bussi, G.; Donadio, D.; Parrinello, M., Canonical Sampling through Velocity Rescaling. *J. Chem. Phys.* **2007**, *126*, 014101/014101-014101/014107.
- (57) Berendsen, H. J. C.; Postma, J. P. M.; Van Gunsteren, W. F.; DiNola, A.; Haak, J. R., Molecular Dynamics with Coupling to an External Bath. *J. Chem. Phys.* **1984**, *81*, 3684-3690.
- (58) Frisch, M. J.; Trucks, G. W.; Schlegel, H. B.; Scuseria, G. E.; Robb, M. A.; Cheeseman, J. R.; Scalmani, G.; Barone, V.; Mennucci, B.; Petersson, G. A.; Nakatsuji, H.; Caricato, M.; Li, X.; Hratchian, H. P.; Izmaylov, A. F.; Bloino, J.; Zheng, G.; Sonnenberg, J. L.; Hada, M.; Ehara, M.; Toyota, K.; Fukuda, R.; Hasegawa, J.; Ishida, M.; Nakajima, T.;

- Honda, Y.; Kitao, O.; Nakai, H.; Vreven, T.; Montgomery, J., J. A.; Peralta, J. E.; Ogliaro, F.; Bearpark, M.; Heyd, J. J.; Brothers, E.; Kudin, K. N.; Staroverov, V. N.; Kobayashi, R.; Normand, J.; Raghavachari, K.; Rendell, A.; Burant, J. C.; Iyengar, S. S.; Tomasi, J.; Cossi, M.; Rega, N.; Millam, J. M.; Klene, M.; Knox, J. E.; Cross, J. B.; Bakken, V.; Adamo, C.; Jaramillo, J.; Gomperts, R.; Stratmann, R. E.; Yazyev, O.; Austin, A. J.; Cammi, R.; Pomelli, C.; Ochterski, J. W.; Martin, R. L.; Morokuma, K.; Zakrzewski, V. G.; Voth, G. A.; Salvador, P.; Dannenberg, J. J.; Dapprich, S.; Daniels, A. D.; Farkas, Ö.; Foresman, J. B.; Ortiz, J. V.; Cioslowski, J.; Fox, D. J., *Gaussian 09, Revision D.01*; Gaussian, Inc., Wallingford CT. **2009**.
- (59) Zhao, Y.; Truhlar, D. G., The M06 Suite of Density Functionals for Main Group Thermochemistry, Thermochemical Kinetics, Noncovalent Interactions, Excited States, and Transition Elements: Two New Functionals and Systematic Testing of Four M06-Class Functionals and 12 Other Functionals. *Theor. Chem. Acc.* **2008**, *120*, 215-241.
- (60) Del Vigo, E. A.; Marino, C.; Stortz, C. A., Exhaustive Rotamer Search of the 4c1 Conformation of A- and B-D-Galactopyranose. *Carbohydr. Res.* **2017**, *448*, 136-147.
- (61) Sameera, W. M. C.; Pantazis, D. A., A Hierarchy of Methods for the Energetically Accurate Modeling of Isomerism in Monosaccharides. *J. Chem. Theory Comput.* **2012**, *8*, 2630-2645.
- (62) Mierzwa, G.; Gordon, A. J.; Latajka, Z.; Berski, S., On the Multiple B-O Bonding Using the Topological Analysis of Electron Localisation Function (Elf). *Comput. Theor. Chem.* **2015**, *1053*, 130-141.

Supporting Information

Mechanistic Insight into the macroscopic mechanical properties of boronate-crosslinked hyaluronic acid hydrogels in relation to the structure of the small molecular crosslinkers

Table of Contents

91	1. Modification of hyaluronic acid with glucose or maltose moieties by thiol-ene photochemistry
92	2. ^1H NMR spectra of HA derivatives synthesized by thiol-ene photochemistry
93	3. Modification of hyaluronic acid with phenylboronic acid, benzoboroxole, fructose or gluconamide moieties by amide coupling reaction
94	4. ^1H NMR spectra of HA derivatives synthesized by amide coupling reaction
95	5. Determination of the degree of substitution (DS) of HA-fructose (HA-gluconamide) from the kinetics of the amide coupling reaction
98	6. Dynamic rheological behavior of the HA-PBA (BOR) conjugates alone
99	7. Methodology for K_a measurements by ^1H NMR spectroscopy
100	8. Determination of K_a by ^1H NMR for APBA (ABOR) and fructose (free fructose and HA-fructose)
103	9. Methodology for k_{ex} measurement by 2D EXSY (EXchange Spectroscopy)
104	10. Determination of k_{ex} by 2D EXSY for APBA (ABOR) and free fructose
106	11. Calorimetric titration of APBA (ABOR) with maltose-COOH
107	12. Determination of K_a by ^1H NMR for APBA (ABOR) and maltose derivatives (maltose-COOH and maltose grafted on HA)
110	13. Determination of k_{ex} by 2D EXSY for APBA and HA-maltose
111	14. Methodology for k_{ex} measurement by variable-temperature NMR spectroscopy
112	15. Determination of k_{ex} by variable-temperature NMR spectroscopy for ABOR/maltose-COOH or HA-maltose
114	16. Determination of K_a by ^1H NMR for APBA (ABOR) and gluconamide derivatives (free gluconamide and HA-gluconamide)
117	17. Determination of stoichiometry of complex by the Job plot method

CHAPTER 2: Mechanistic insight into the properties of boronate-crosslinked HA hydrogels

- 117 18. Job plot of the APBA/gluconamide complex
- 118 19. Influence of the pH on the HA-PBA/HA-maltose (gluconamide) hydrogel networks
- 119 20. Evidence of the opening of the endocyclic B-O bond of ABOR bound to free/grafted fructose by ^1H NMR spectroscopy
- 120 21. Determination of the structure of ABOR complexes with free/grafted fructose by the INADEQUATE NMR technique
- 122 22. Determination of the structure of the complex of APBA with a ^{13}C labeled maltose grafted on HA by the INADEQUATE NMR technique
- 125 23. Screening of rotamers of the PBA/maltose derivative complexes by classical molecular dynamics with all-atom GROMOS force field performed using GROMACS software
- 129 24. Cartesian coordinates (in Å), of the lower-energy conformers for the complexes of PBA/maltose optimized using M062X/6-311+G(d,p) including SMD in water
- 131 25. Lower-energy conformers for the complexes of PBA/gluconamide complexes obtained by DFT (M062X/6-311+(d,p) in water, SMD)
- 132 26. Cartesian coordinates (in Å), of the lower-energy conformers for the complexes of PBA/gluconamide optimized using M062X/6-311+G(d,p) including SMD in water
- 134 27. Possible structures of binding modes for BOR with the maltose derivative grafted on HA
- 135 28. Evidence of the cyclic structure of ABOR bound to free/grafted maltose by ^1H NMR spectroscopy
- 136 29. Evidence of the partial opening of the endocyclic B-O bond of ABOR bound to free/grafted gluconamide by ^1H NMR spectroscopy
- 137 30. Dynamic rheological analysis of HA-PBA/HA-catecholamine (dopamine) at pH 7.4
- 137 31. Mechanism of boronate ester formation
- 138 32. References

1. Modification of hyaluronic acid with glucose or maltose moieties by thiol-ene photochemistry

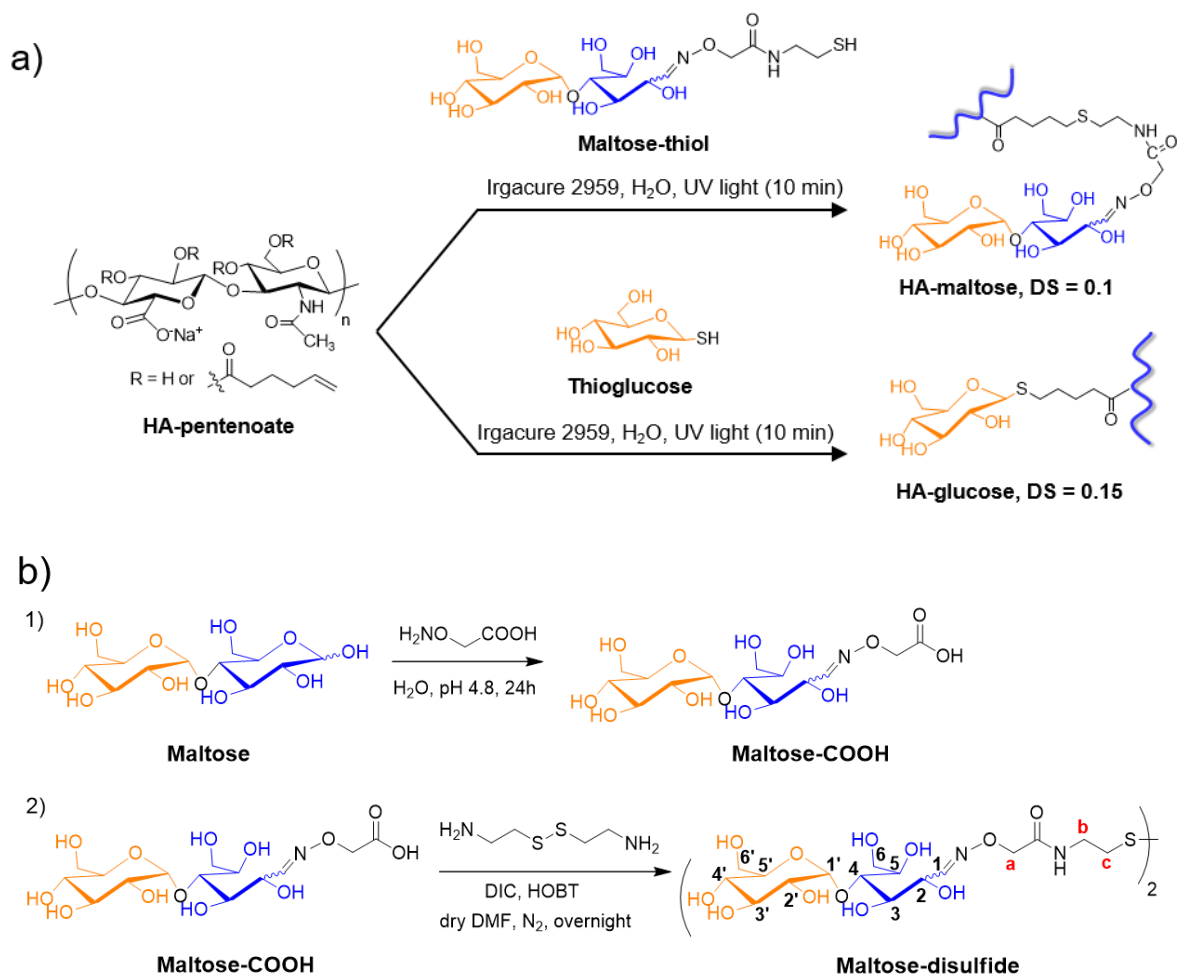


Figure S1. Synthetic scheme for the preparation of HA derivatives via thiol-ene coupling reaction (a), and synthesis of maltose-disulfide from a maltose-COOH derivative (b).

2. ^1H NMR spectra of HA derivatives synthesized by thiol-ene photochemistry

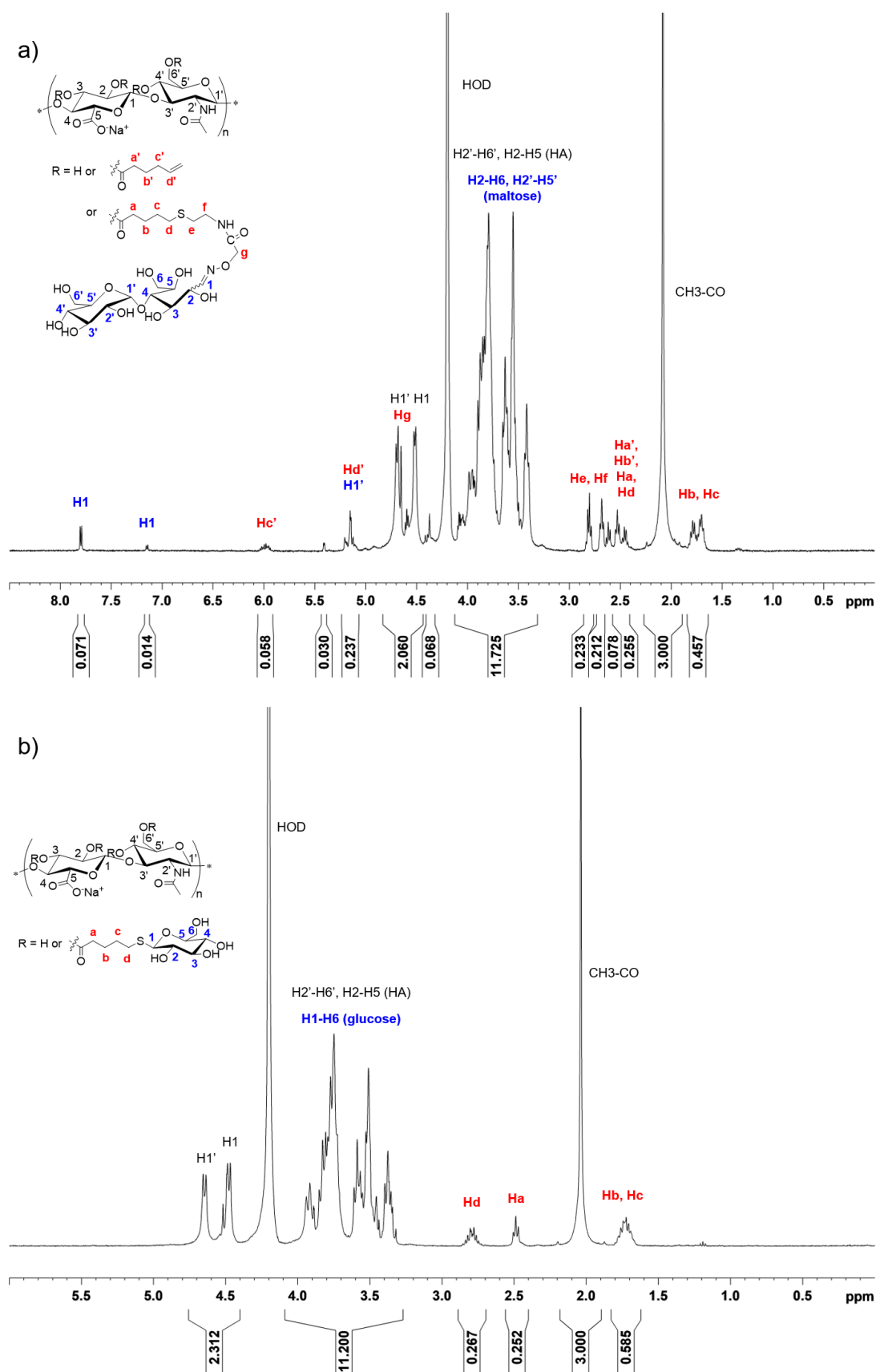


Figure S2. ^1H NMR spectra (400 MHz, D_2O , 6 $\text{mg}\cdot\text{mL}^{-1}$, 80 $^\circ\text{C}$) of HA-maltose (a) and HA-glucose (b).

3. Modification of hyaluronic acid with phenylboronic acid, benzoboroxole, fructose or gluconamide moieties by amide coupling reaction

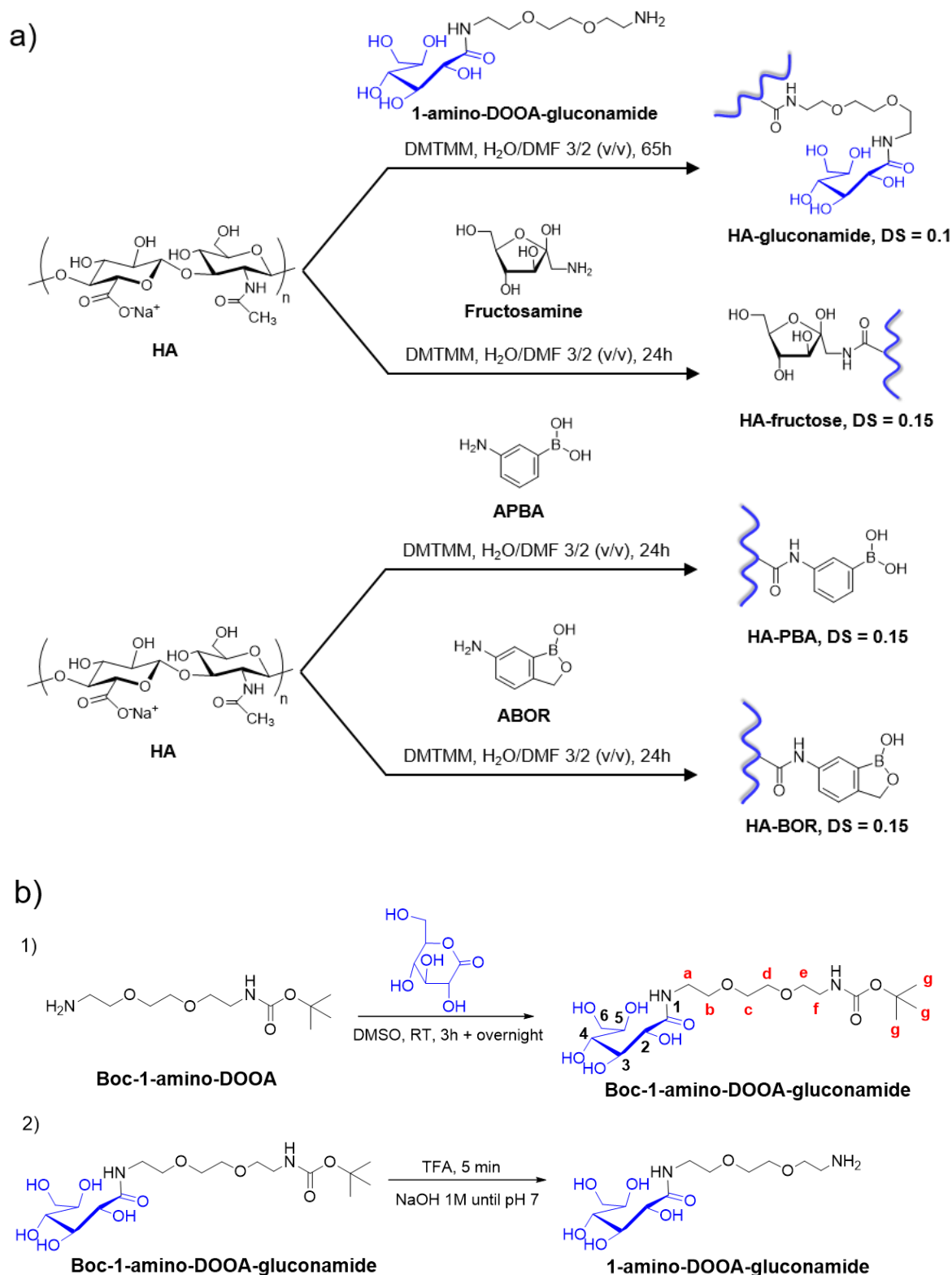


Figure S3. Synthetic scheme for the preparation of HA derivatives via amide coupling reaction (a), and synthesis of 1-amino-DOOA-gluconamide from a Boc-1-amino-DOOA-gluconamide derivative (b).

4. ^1H NMR spectra of HA derivatives synthesized by amide coupling reaction

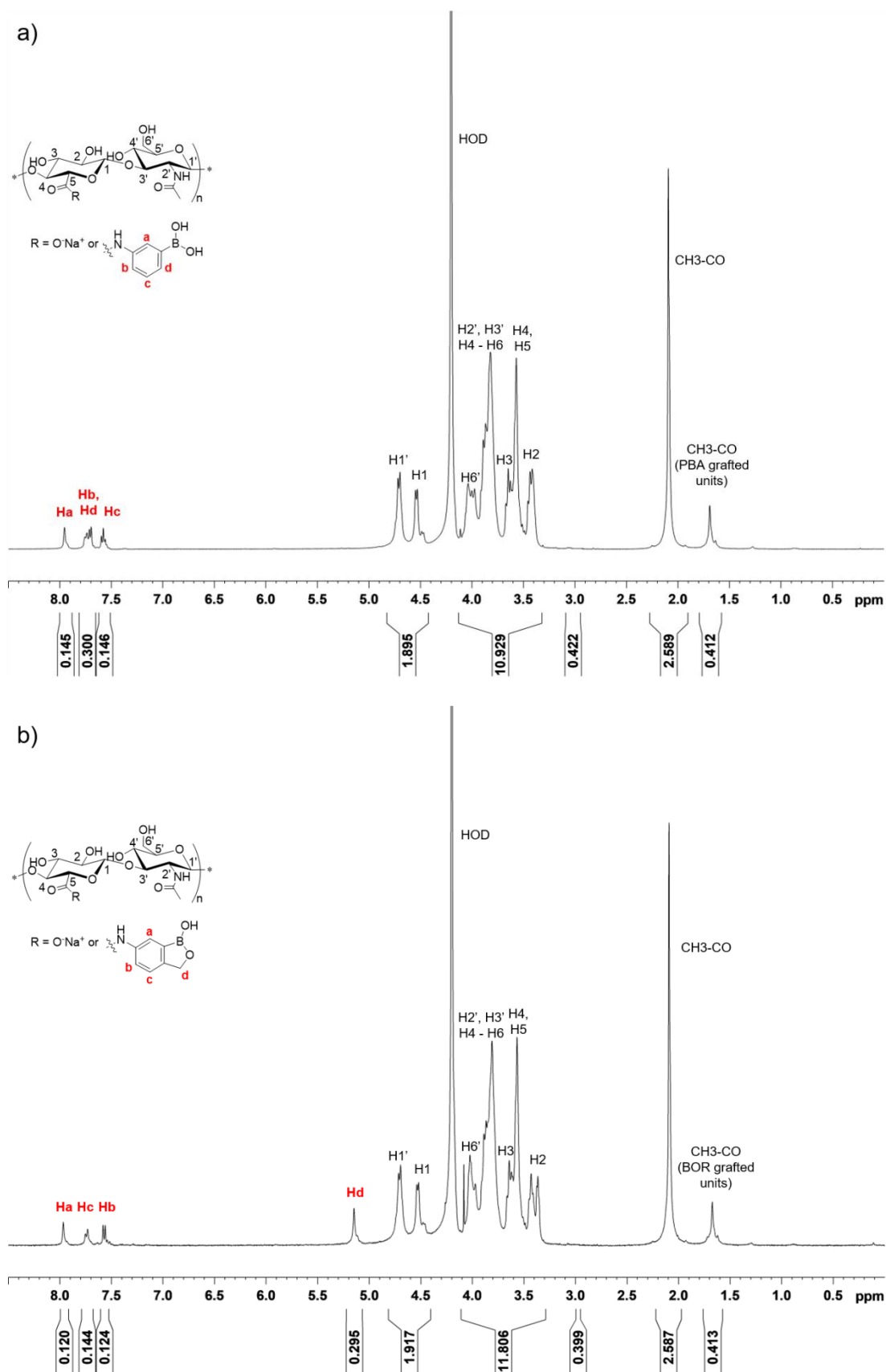


Figure S4. ^1H NMR spectra (400MHz, D_2O , 6 mg.mL $^{-1}$, 80 °C) of HA-PBA (a) and HA-BOR (b).

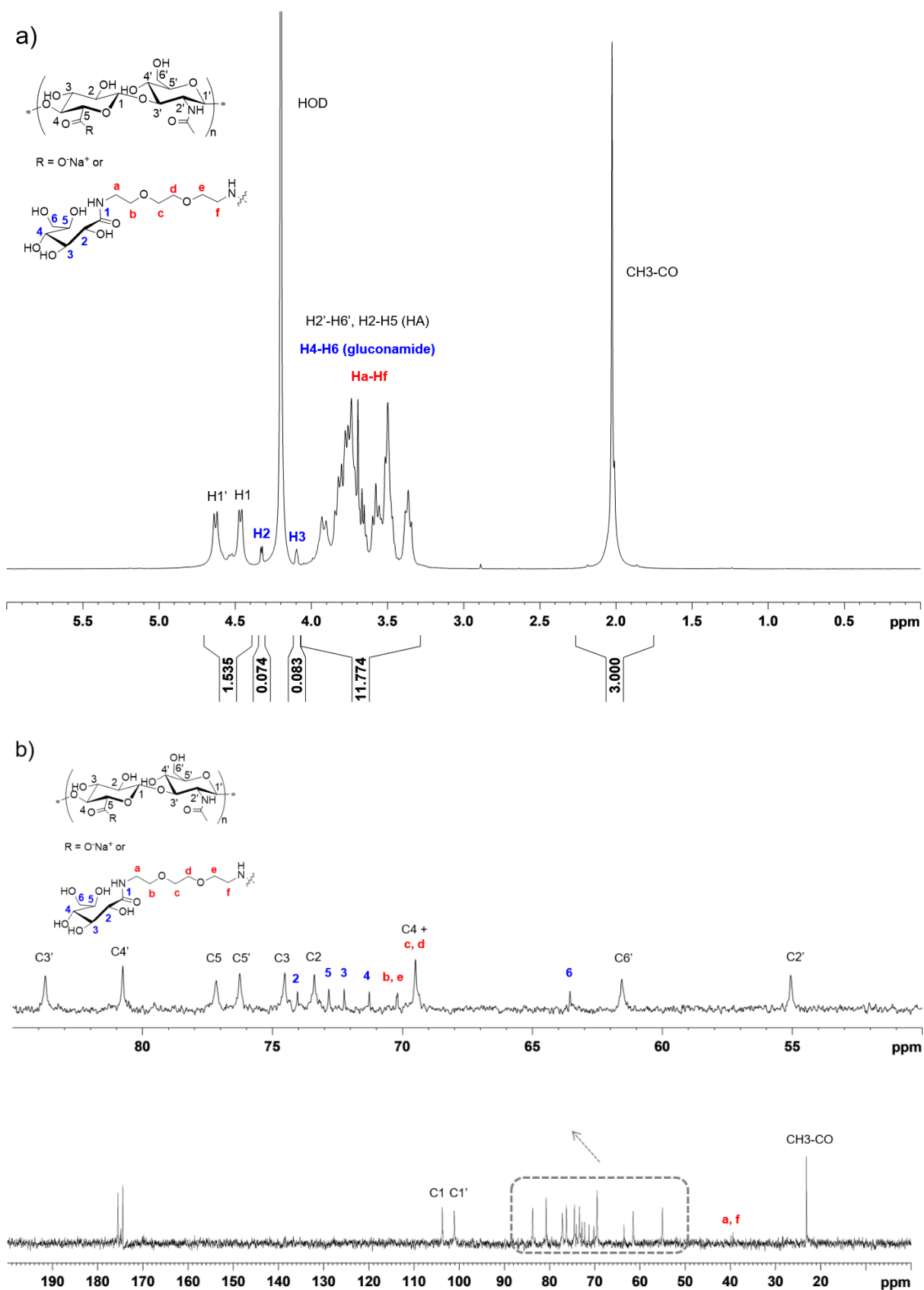


Figure S5. ¹H (a) and ¹³C (b) NMR spectra (400 or 100 MHz, D₂O, 6 mg·mL⁻¹, 80 °C) of HA-gluconamide.

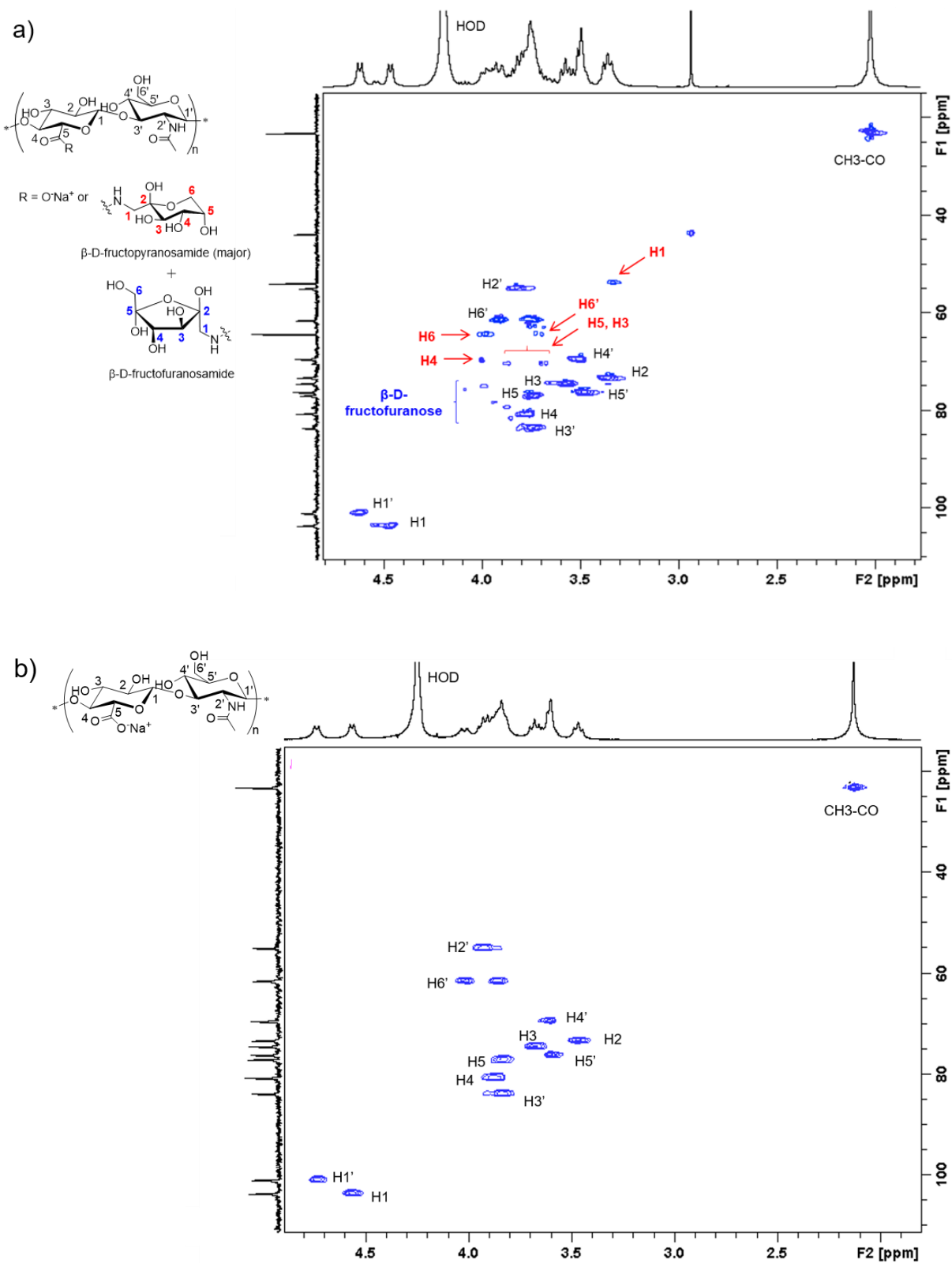
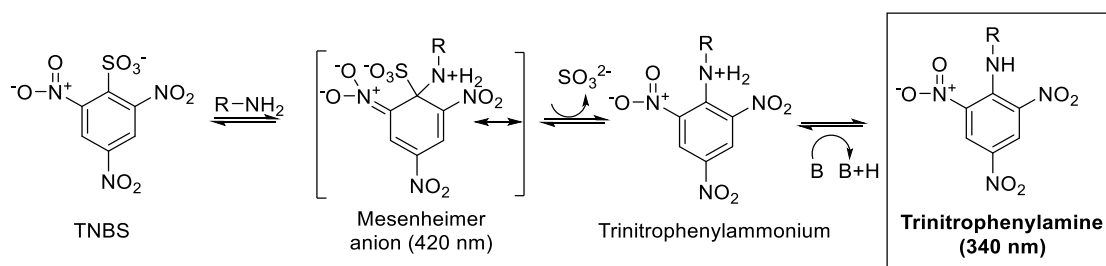


Figure S6. 2D HSQC NMR spectra (400 MHz, D_2O , 6 $mg \cdot mL^{-1}$, 80 $^{\circ}C$) of HA-fructose (a) compared to native HA (b). Of note, β -D-fructopyranose is the major tautomeric form observed for grafted fructose moieties, followed by the β -D-fructofuranose form.

5. Determination of the degree of substitution (DS) of HA-fructose (HA-gluconamide) from the kinetics of the amide coupling reaction

As the superposition of ^1H signals of HA and grafted fructose (or gluconamide) moieties precluded determination of the DS of HA-fructose (HA-gluconamide) by ^1H NMR, their DS were estimated from the kinetics of their syntheses, by quantifying the free primary amines in the reaction medium as a function of time. This was based on the reaction of fructosamine (or 1-amino-DOOA-gluconamide) with 2,4,6-Trinitrobenzene Sulfonic Acid (TNBS), which gives an orange-colored final product (trinitrophenylamine) that absorbs in the UV region, at around 340 nm (Scheme 1).¹



Scheme 1. Trinitrophenylation of primary amines with TNBS.

Procedure for the reaction kinetics by quantifying primary amines with TNBS

The methodology to quantify primary amines with TNBS was adapted from a procedure previously described.² Standard curves of primary amines (fructosamine or 1-amino-DOOA-gluconamide) were prepared by diluting 1 mg/mL stock solutions in 0.1 M sodium bicarbonate buffer pH 8.5 at known concentrations of amine (10 to 50 $\mu\text{g/mL}$). Various volumes of a fresh solution of 0.01 % TNBS (w/v) in the same buffer were added in each solution, in order to get a molar ratio of TNBS/amine of 1, and samples were incubated at 37 °C for 2 h. Then, the product of reaction between the amine and TNBS was analyzed by UV spectroscopy (from 580 to 280 nm) after addition of a small volume of 1 M HCl (150 μL) in the samples. The same procedure was used to quantify amines during the amide coupling reactions with HA, by taking small aliquots of the reaction medium as a function of time.

Procedure for determining the DS from the kinetics of amide coupling reactions

From the UV spectra recorded for fructosamine-TNB (1-amino-DOOA-gluconamide-TNB) derivatives, a standard curve was plotted with the maximal absorbance values (curves (a) in Figure S7). It is important to note that the wavelength of the maximal absorbance depends on the primary amines. This allowed us to determine the amount of unreacted primary amines during the amide coupling reaction with HA using an amine/HA molar ratio of 0.15 to 0.2. From the kinetic curves, we estimated approximately 100 % of conversion for HA-fructose and 65 % for HA-gluconamide within 24 h and 65 h, which gave values of DS of 0.15 and 0.1, respectively (curve (b) in Figure S7).

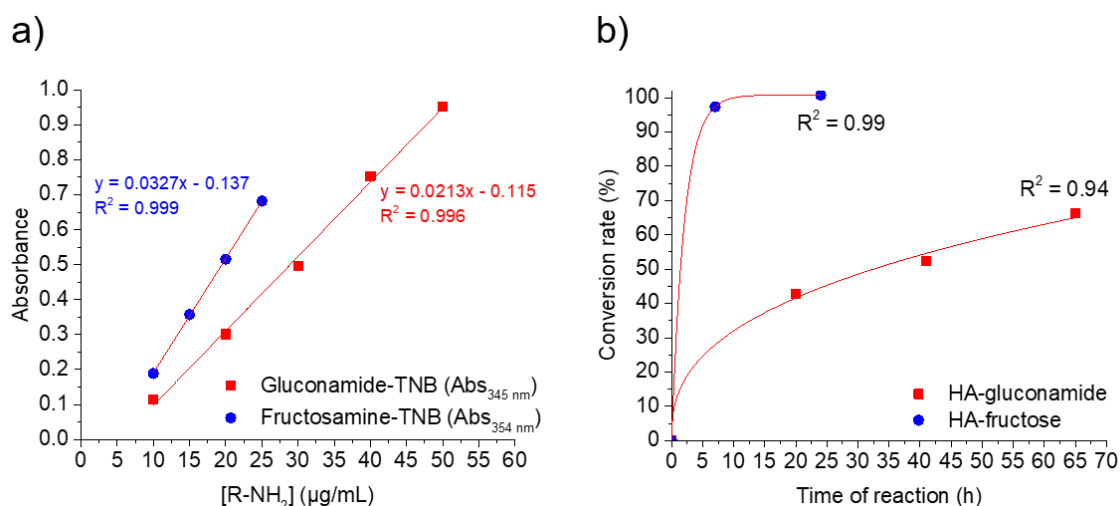


Figure S7. Reaction kinetics for the syntheses of HA-gluconamide and HA-fructose. Standard curves with the respective equations used to quantify the free amines (a), and kinetic curves plotted for the coupling reactions of fructosamine and gluconamide with HA (curve fitting by non-linear fit models using Origin 2015 software).

6. Dynamic rheological behavior of the HA-PBA (BOR) conjugates alone

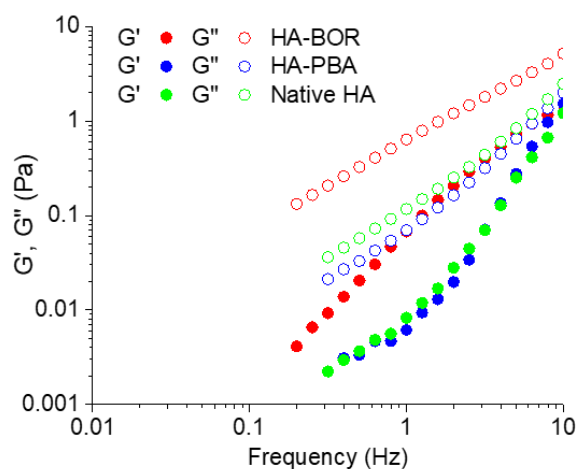


Figure S8. Frequency dependence of storage (G') and loss (G'') moduli of the HA-PBA and HA-BOR derivatives alone at pH 7.4, compared to native HA; closed symbols: G' curves; open symbols: G'' curves.

7. Methodology for K_a measurements by ^1H NMR spectroscopy

The procedure to determine the K_a values was adapted from previous studies using free boronic acids and saccharides.^{3,4} This method consisted in assuming that a boronic acid (B) and a saccharide (S) bind in one modality, BS:



$$K_a = \frac{[\text{BS}]}{[\text{B}][\text{S}]} \quad (1)$$

Where [B], [S] and [BS] are the molar concentrations of the free boronic acid, the free saccharide and the complex, respectively.

To calculate K_a , the [BS]/[B] ratio was determined by digital integration of the aryl protons of the boronic acid/saccharide complex and of the free boronic acid. This allowed calculation of [B], [BS] and [S], as follows:

$$[\text{B}] = \frac{[\text{B}]_0}{\frac{[\text{BS}]}{[\text{B}]} + 1} \quad (2)$$

Where $[\text{B}]_0$ is the initial concentration of boronic acid added in the NMR tube, and

$$[\text{BS}] = \frac{[\text{BS}]}{[\text{B}]} [\text{B}] \quad (3)$$

$$[\text{S}] = [\text{S}]_0 - [\text{BS}] \quad (4)$$

Where $[\text{S}]_0$ is the initial concentration of saccharide added in the NMR tube.

Procedure for the preparation of samples for NMR analysis

Stock solutions of APBA (ABOR) and free (grafted) saccharides were prepared by solubilization in distilled water. When necessary, the pH was carefully adjusted to 7.4 by adding 1 M NaOH, using a pH-meter, and water was added to get concentrations ranging from 4 to 60 mM. Then, the solutions were diluted with 0.02 M PBS pH 7.4 in order to obtain final concentrations of 2 to 30 mM APBA (ABOR) or saccharide in 0.01 M PBS at pH 7.4. The solutions of complexes were then prepared by mixing various volumes of a stock solution of APBA (ABOR) with a stock solution of a respective free (grafted) saccharide. This generated mixtures at pH 7.4 (± 0.1), with a APBA (ABOR)/saccharide molar ratio ranging from 0.3 to 1.5. Water was removed by freeze-drying and the samples were properly dissolved in D_2O prior to NMR analysis. Each value of K_a was determined from two experiments of titration using freshly prepared solutions. ^1H NMR titration was performed with at least 6 different concentrations at 25 °C.

Procedure for determining the chemical shifts of aryl protons of bound and free boronic acids

^1H NMR spectra of APBA and ABOR alone were first recorded (spectra (a) in Figure S9-S12, S17-S20 and S24-S27). Second, ^1H NMR spectra of APBA and ABOR in the presence of excess free saccharide (fructose or gluconamide derivative which is free in solution) to induce 100 % complex formation are acquired (spectra (b) in Figure S9-S10 and S24-S25). Comparison of spectra (a) and (b) allows the assignment of the aryl protons of bound and free boronic acids. This analysis was then used to interpret the spectra from the titrations with

sugars (fructose, maltose or gluconamide derivative which are free in solution or grafted on HA; spectra (c) in Figure S9-S10 and S24-S25 or spectra (b) in Figure S11-S12, S17-S20 and S26-S27).

8. Determination of K_a by ^1H NMR for APBA (ABOR) and fructose (free fructose and HA-fructose)

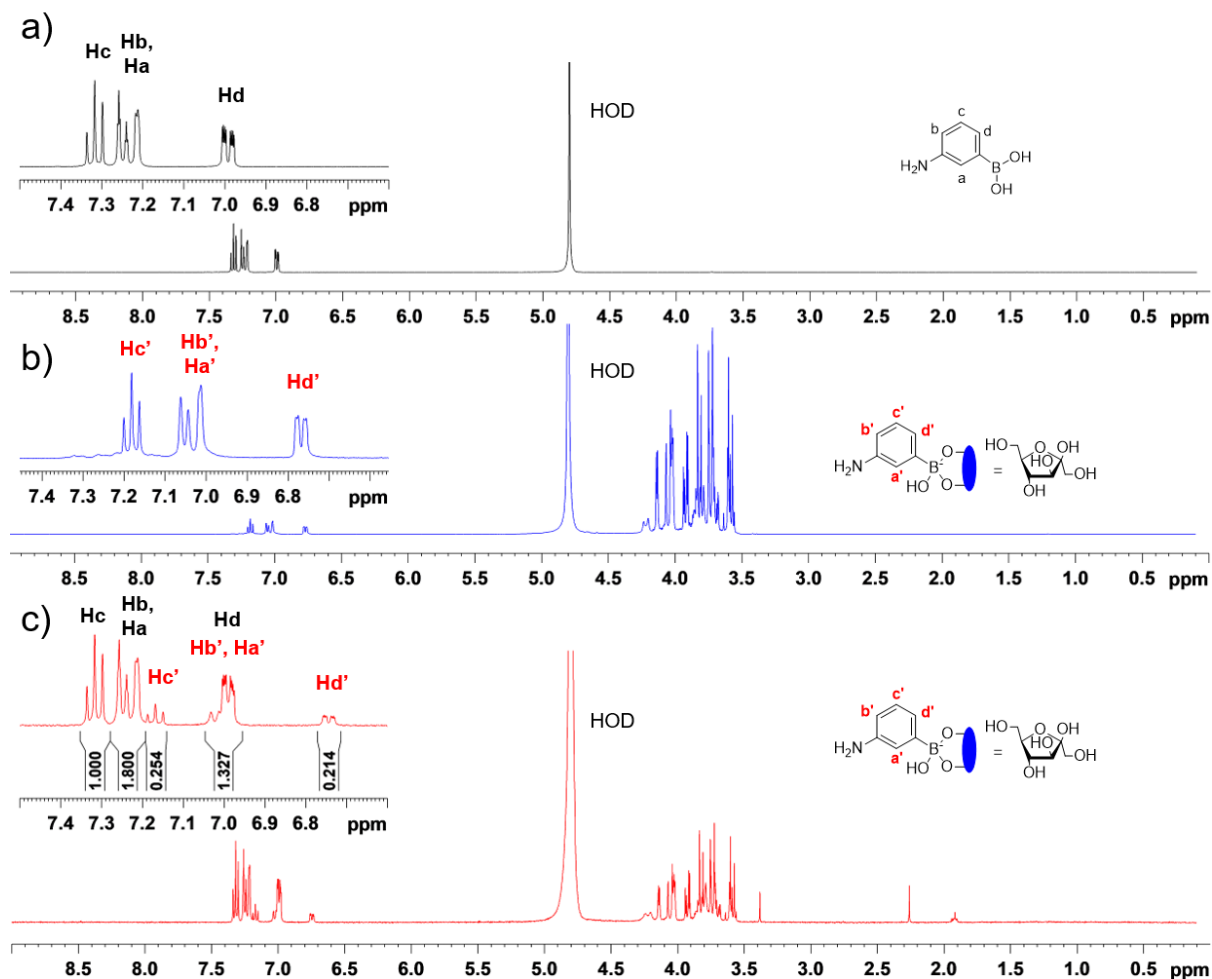


Figure S9. ^1H NMR spectra in 0.01 M deuterated PBS pH 7.4 at 25 °C of APBA alone (15 mM) (a), APBA (15 mM) in the presence of excess D-fructose (150 mM) (b), and APBA (15 mM) with D-fructose (15 mM) (c). The $[\text{BS}]/[\text{B}]$ ratio was calculated from the digital integration of Hc (free APBA) and Hd' (complexed APBA) signals.

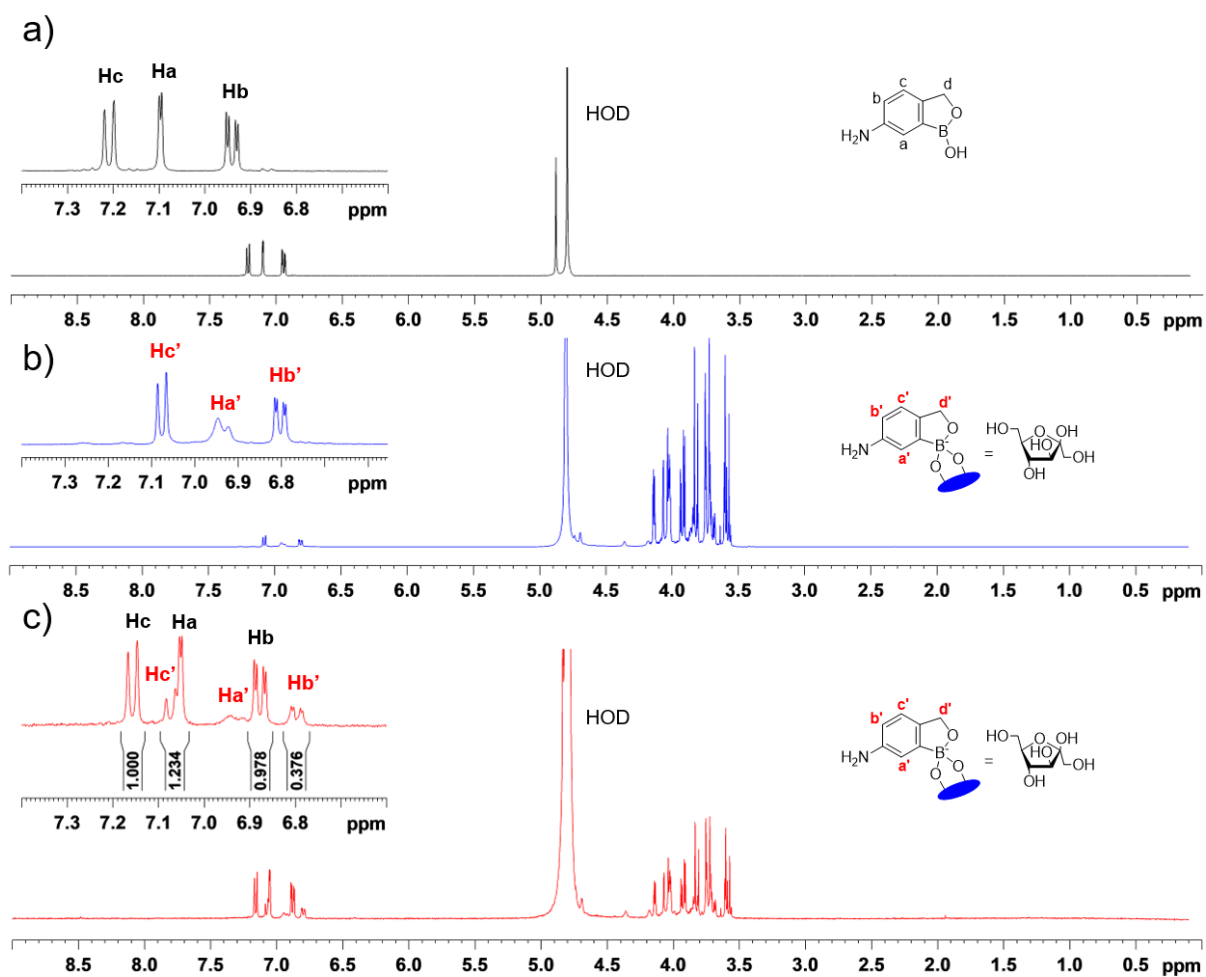


Figure S10. ^1H NMR spectra in 0.01 M deuterated PBS pH 7.4 at 25 °C of ABOR alone (15 mM) (a), ABOR (15mM) in the presence of excess D-fructose (150 mM) (b), and ABOR (15 mM) with D-fructose (15 mM) (c). The [BS]/[B] ratio was calculated from the digital integration of Hc (free ABOR) and Hb' (complexed ABOR) signals.

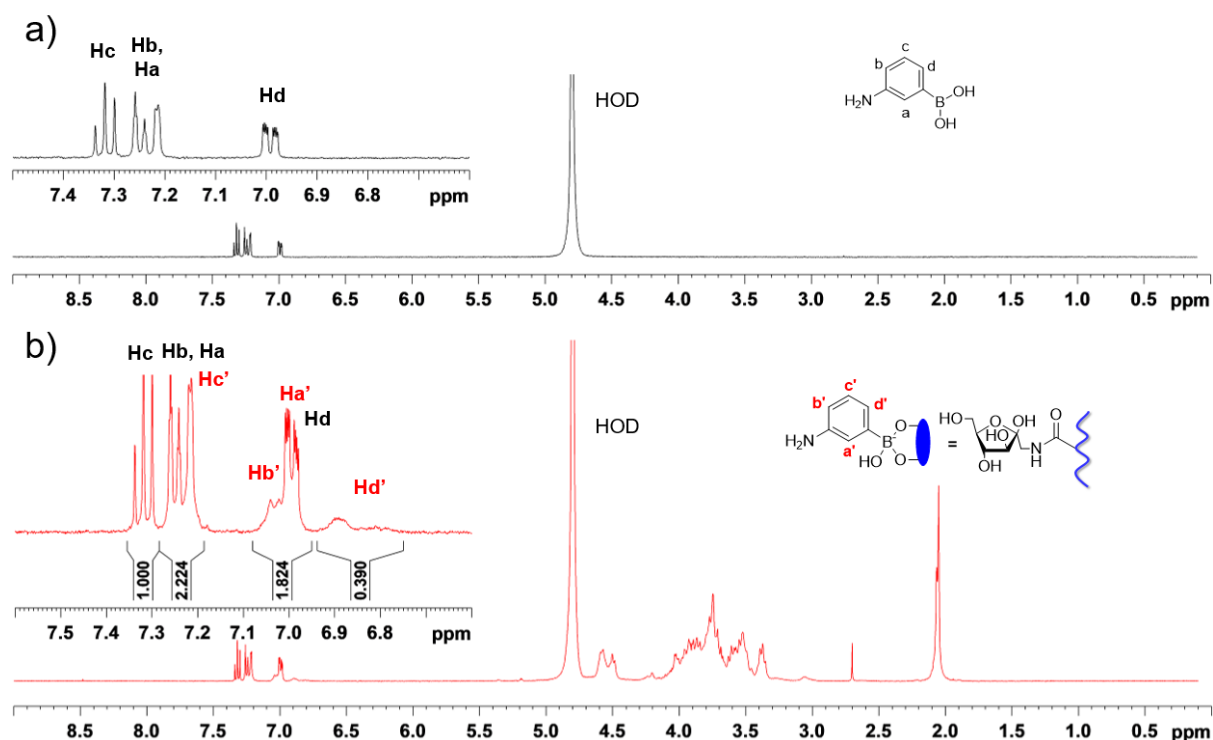


Figure S11. ^1H NMR spectra in 0.01 M deuterated PBS pH 7.4 at 25 °C of APBA alone (1 mM) (a) and APBA (1 mM) with D-fructose (1 mM of grafted fructose) (b). Similar to free D-fructose, the $[\text{BS}]/[\text{B}]$ ratio was calculated from the digital integration of Hc (free APBA) and Hd' (complexed APBA) signals.

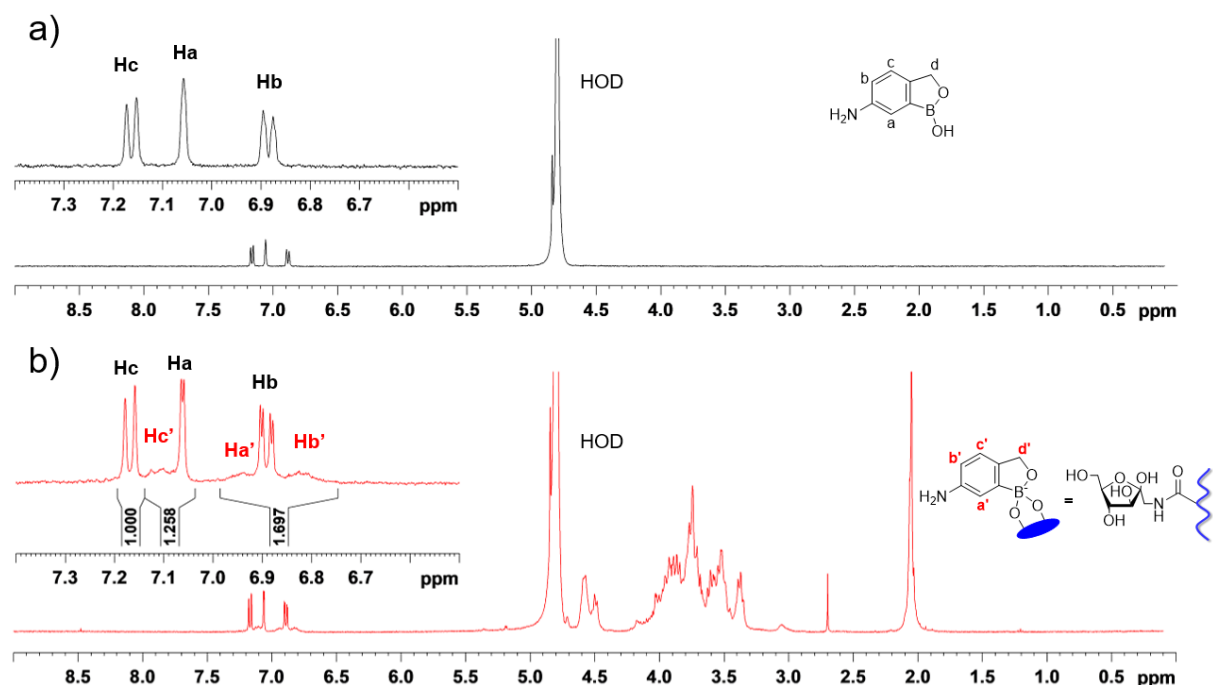


Figure S12. ^1H NMR spectra in 0.01 M deuterated PBS pH 7.4 at 25 °C of ABOR alone (1mM) (a) and ABOR (1mM) with HA-fructose (1 mM of grafted fructose) (b). Similar to free D-fructose, the $[\text{BS}]/[\text{B}]$ ratio was calculated from the digital integration of Hc (free ABOR) and Hb, Ha', Hb' (3H, free and complexed ABOR) signals.

9. Methodology for k_{ex} measurement by 2D EXSY (EXchange Spectroscopy)

The k_{ex} values for slow exchange systems were determined from EXSY experiments, set up with at least 3 different mixing times (τ_m) among 0.8, 1, 1.2 and 1.5 s.⁵ Solutions of APBA (ABOR) and saccharides were prepared as previously described for K_a measurements by ^1H NMR titration. From the 2D spectra of APBA (ABOR) in the presence of 0.6 molar equivalent of saccharide, the diagonal and cross-peaks for the bound and unbound aromatic resonances of APBA (ABOR) were carefully integrated, and the integration values were used to calculate k_{ex} by using the following equation⁶

$$\ln \frac{(r + 1)}{(r - 1)} = k_{ex} \tau_m \quad (5)$$

where τ_m is the mixing time and r is defined by the following equation

$$r = \frac{4\chi_c\chi_f (I_{HH} + I_{H'H'})}{(I_{HH'} + I_{H'H})} - (\chi_c - \chi_f)^2 \quad (6)$$

where χ_c and χ_f are the mole fraction of complexed and free APBA (ABOR), respectively, with $\chi_c = 0.4$ and $\chi_f = 0.6$. $I_{HH'}$ and $I_{H'H}$ are the intensities of the cross peaks between a ^1H signal of free and complexed APBA (ABOR), respectively, whereas I_{HH} and $I_{H'H'}$ are the intensities of the diagonal peaks.

10. Determination of k_{ex} by 2D EXSY for APBA (ABOR) and free fructose

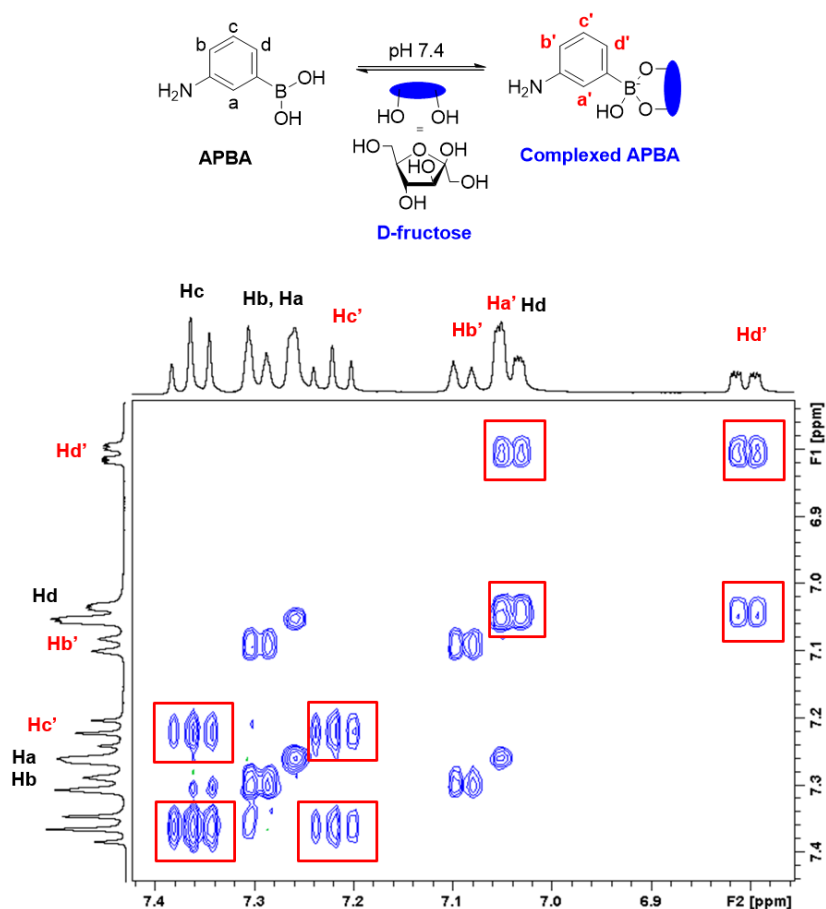


Figure S13. 2D EXSY spectra at 25 °C of APBA (18 mM) with D-fructose (12 mM) in 0.01 M deuterated PBS pH 7.4 ($\tau_m = 1.5$ s). k_{ex} was calculated from the digital integration of the diagonal peaks (Hcc, Hc'c' and Hdd, Hd'd') and of the cross peaks (Hcc', Hc'd' and Hdd', Hd'd) of APBA.

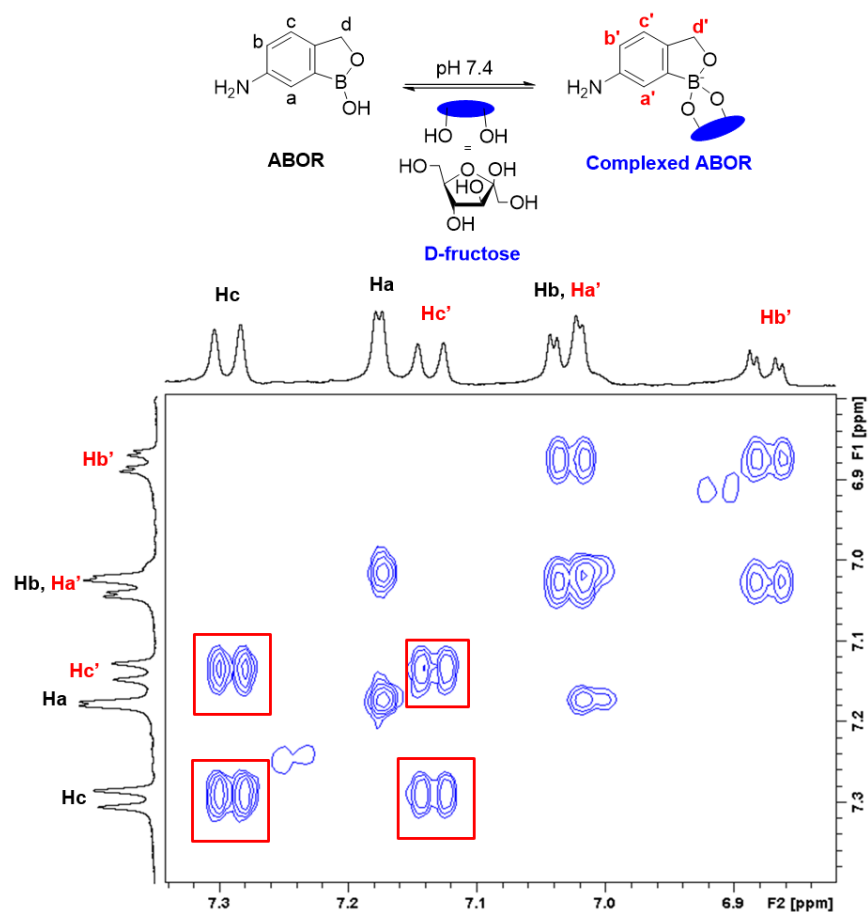


Figure S14. 2D EXSY spectra at 25 °C of ABOR (18 mM) with D-fructose (12 mM) in 0.01 M deuterated PBS pH 7.4 ($\tau_m = 1.5$ s). k_{ex} was calculated from the digital integration of the diagonal peaks (Hcc, Hc'c') and of the cross peaks (Hcc', Hc'c) of ABOR.

11. Calorimetric titration of APBA (ABOR) with maltose-COOH

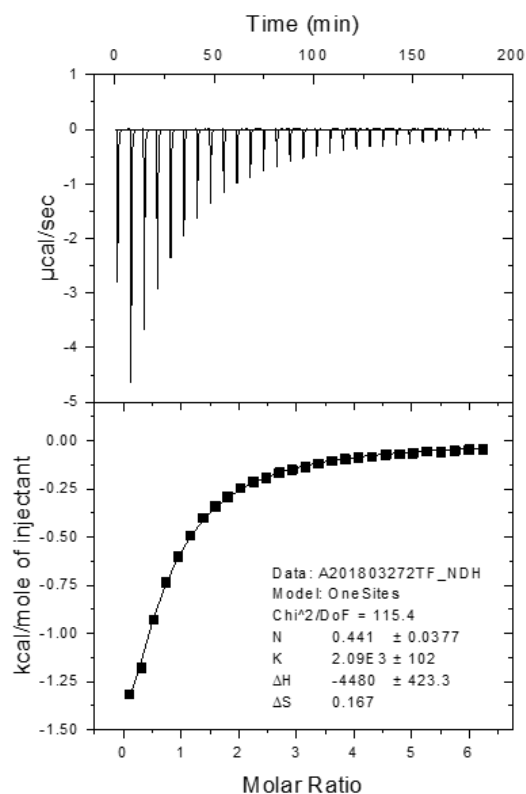


Figure S15. Calorimetric titration of maltose-COOH (0.5 mM) with APBA (15 mM) in 0.01 M PBS (pH 7.4, 25 °C).

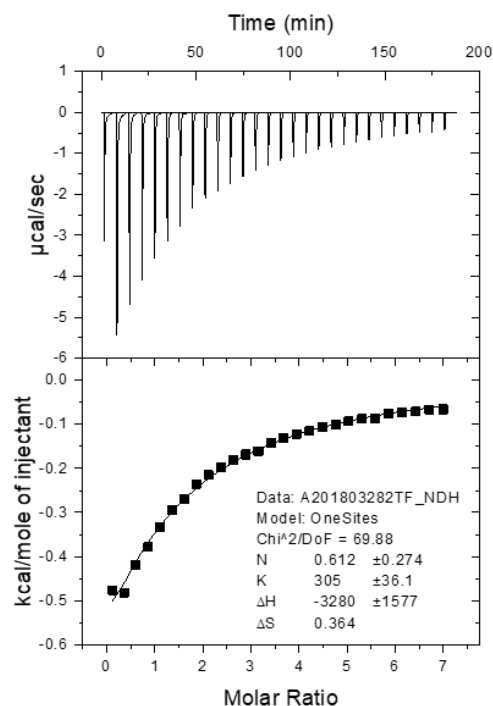


Figure S16. Calorimetric titration of maltose-COOH (1 mM) with ABOR (35 mM) in 0.01 M PBS (pH 7.4, 25 °C).

12. Determination of K_a by ^1H NMR for APBA (ABOR) and maltose derivatives (maltose-COOH and maltose grafted on HA)

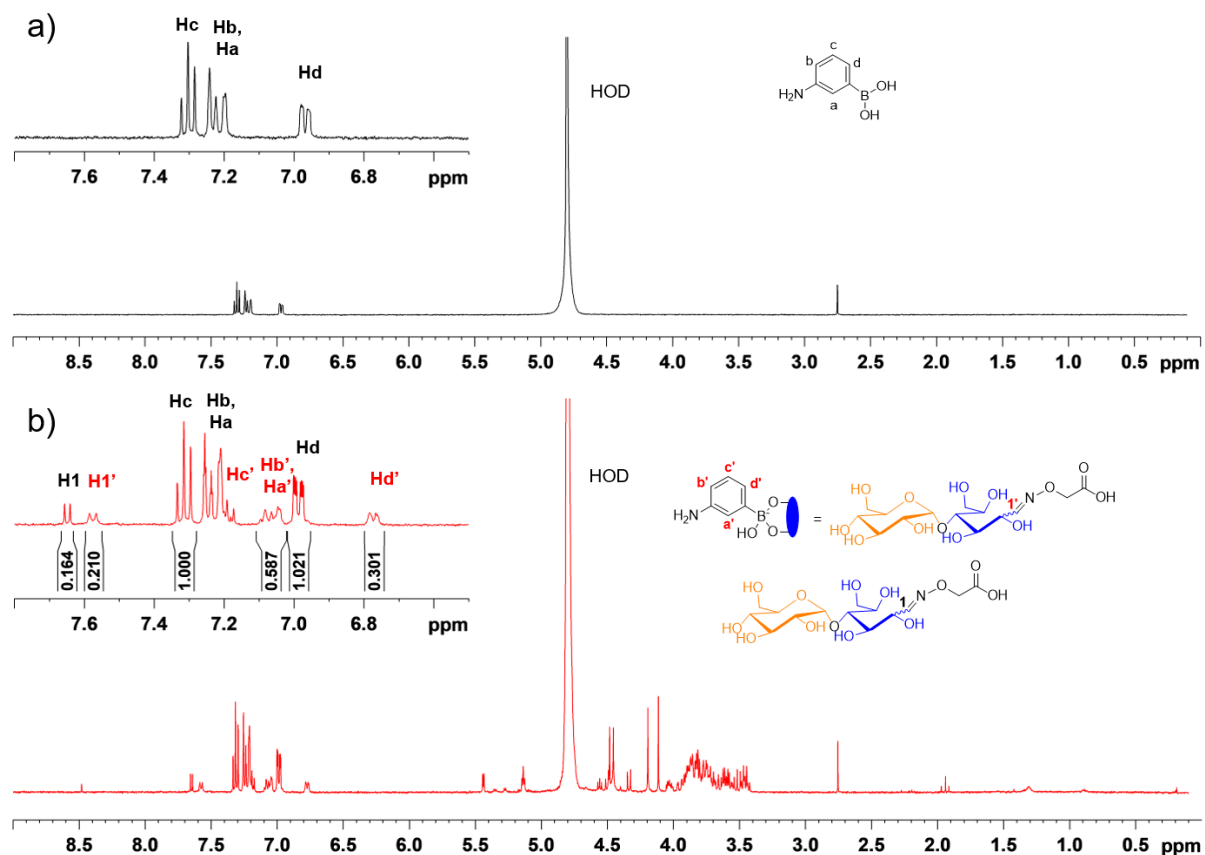


Figure S17. ^1H NMR spectra in 0.01 M deuterated PBS pH 7.4 at 25 °C of APBA alone (1 mM) (a) and APBA (1 mM) with maltose-COOH (1 mM) (b). Assuming a 2:1 stoichiometry for the APBA/maltose-COOH complex, K_a could not be determined because the concentration of molecules used was too low to apply equations related to 1:2 equilibria⁷ (H1 and H1' correspond to free and bound maltose-COOH, respectively).

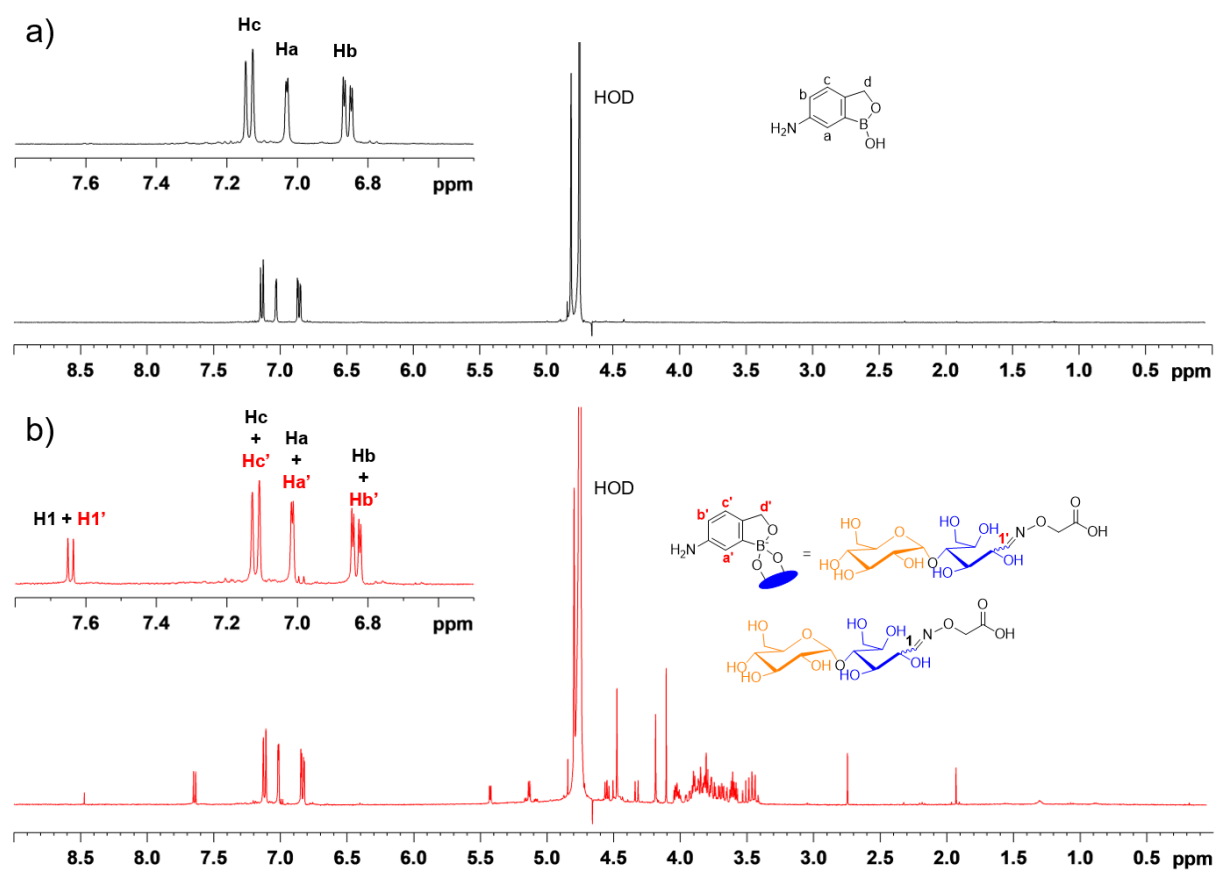


Figure S18. ^1H NMR spectra in 0.01 M deuterated PBS pH 7.4 at 25 °C of ABOR alone (1 mM) (a) and ABOR (1 mM) with maltose-COOH (1 mM) (b). K_a was not measured because of rapid exchange dynamics relative to NMR time-scale (mainly ^1H signals from free ABOR are observed at 25 °C; H1 and H1' correspond to free and bound maltose-COOH, respectively).

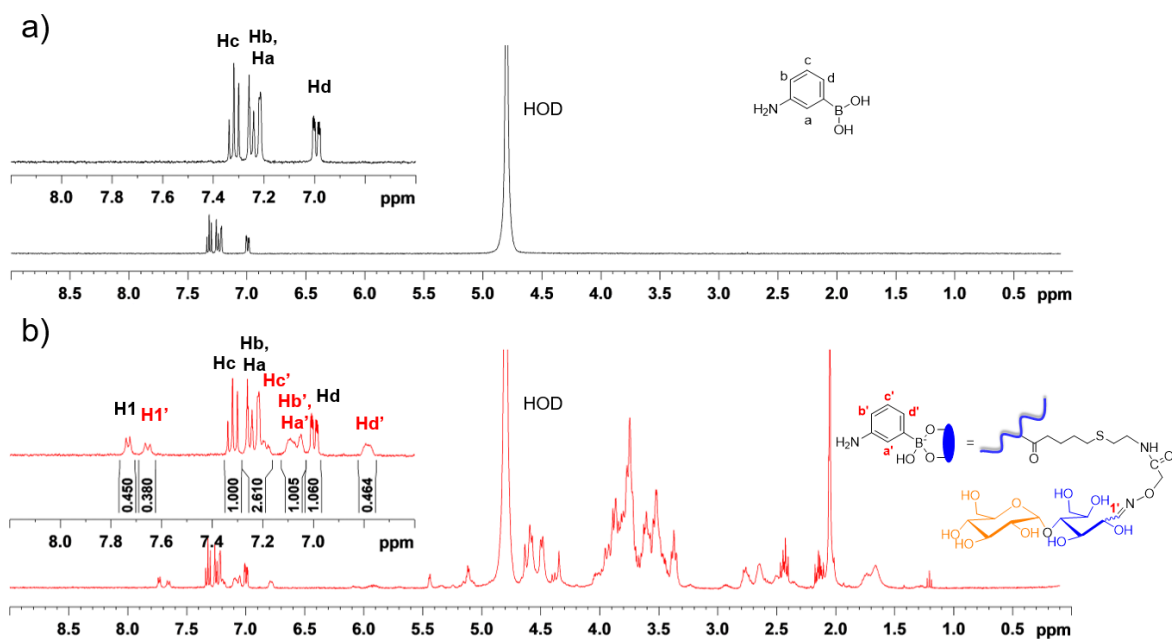


Figure S19. ^1H NMR spectra in 0.01 M deuterated PBS pH 7.4 at 25 °C of APBA alone (1 mM) (a) and APBA (1 mM) with HA-maltose (1 mM of grafted maltose) (b). Assuming a 1:1 stoichiometry of APBA/HA-maltose, the $[\text{BS}]/[\text{B}]$ ratio was calculated from the digital integration of Hc (free APBA) and Hd' (complexed APBA) signals (similar to the NMR spectrum of APBA/maltose-COOH, H1 and H1' correspond to free and bound HA-maltose, respectively).

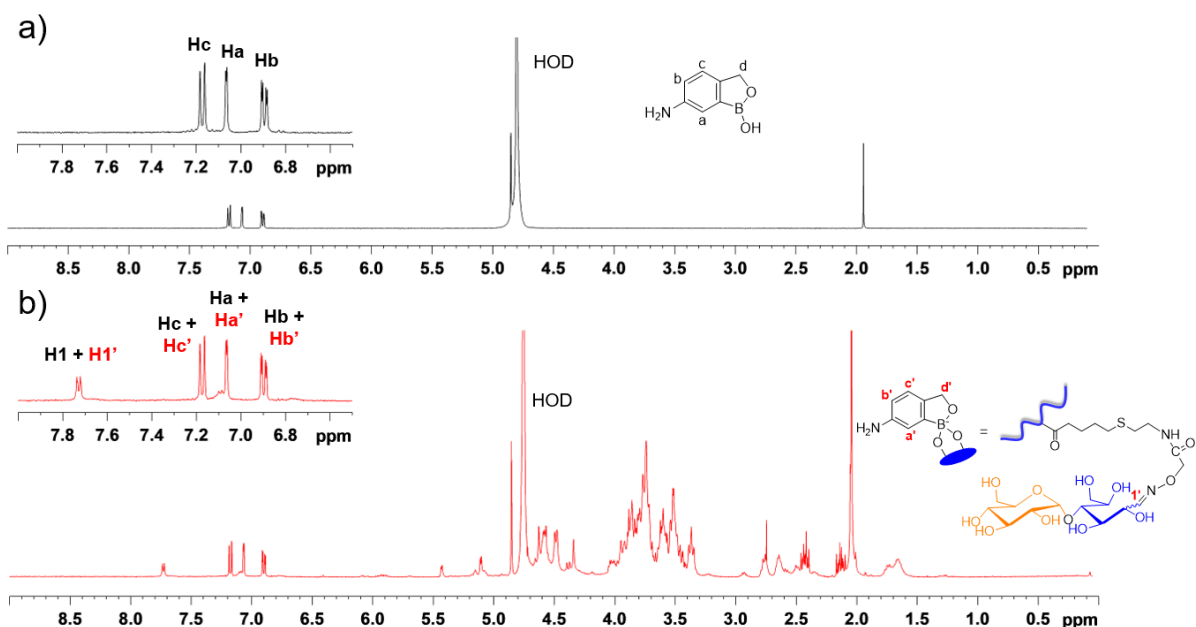


Figure S20. ^1H NMR spectra in 0.01 M deuterated PBS pH 7.4 at 25 °C of ABOR alone (1 mM) (a) and ABOR (1 mM) with HA-maltose (1 mM of grafted maltose) (b). Similar to maltose-COOH, K_a was not measured because of rapid exchange dynamics relative to NMR time-scale (mainly ^1H signals from free ABOR are observed at 25 °C; similar to the NMR spectrum of ABOR/maltose-COOH, H1 and H1' correspond to free and bound HA-maltose, respectively).

13. Determination of k_{ex} by 2D EXSY for APBA and HA-maltose

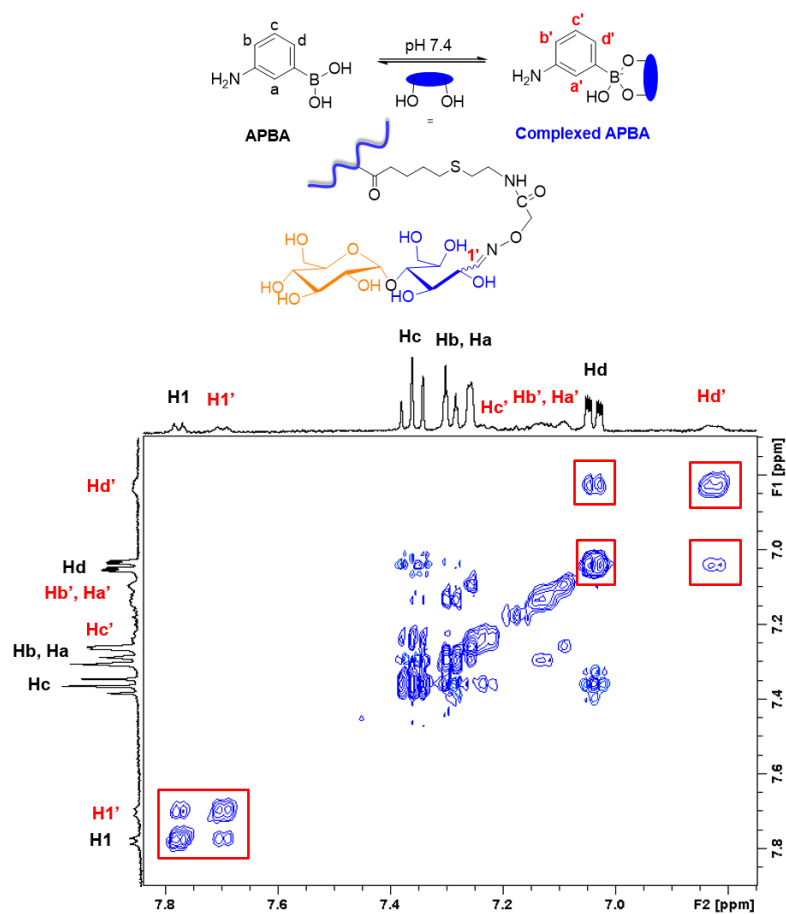


Figure S21. 2D EXSY spectra at 25 °C of APBA (1.2mM) with HA-maltose (0.8mM grafted maltose) in 0.01 M deuterated PBS pH 7.4 ($\tau_m = 1.5$ s). k_{ex} was calculated from the digital integration of the diagonal peaks (Hdd, Hd'd') and of the cross peaks (Hdd', Hd'd') of APBA, and of the diagonal peaks (H11, H1'1') and cross peaks (H11', H1'1') of grafted maltose.

14. Methodology for k_{ex} measurement by variable-temperature NMR spectroscopy

The molecular exchange rate constants at the coalescence temperature were estimated for ABOR in the presence of one molar equivalent of free or grafted maltose, using the following approximate expression^{6, 7}

$$k_c = \frac{\pi\Delta\nu}{\sqrt{2}} \quad (7)$$

where k_c is the molecular exchange rate constant at a coalescence temperature and $\Delta\nu$ is the chemical shift difference between the signal of free (Hb) and complexed (Hb') ABOR (and/or of free (H1) and complexed (H1') maltose) determined from the ¹H NMR spectra of the mixtures far below coalescence (1 °C). The extrapolated exchange rate constant k_{ex} at 25 °C was then obtained from the Eyring equation

$$k_{\text{ex}} = \left(\frac{k_b T}{h}\right) \exp\left(-\frac{\Delta G^\ddagger}{RT}\right) \quad (8)$$

where k_b is the Boltzmann constant, T is the absolute temperature, h is the Plank constant, ΔG^\ddagger is the free energy of activation for the molecular exchange and R is the gas constant.

15. Determination of k_{ex} by variable-temperature NMR spectroscopy for ABOR/maltose-COOH or HA-maltose

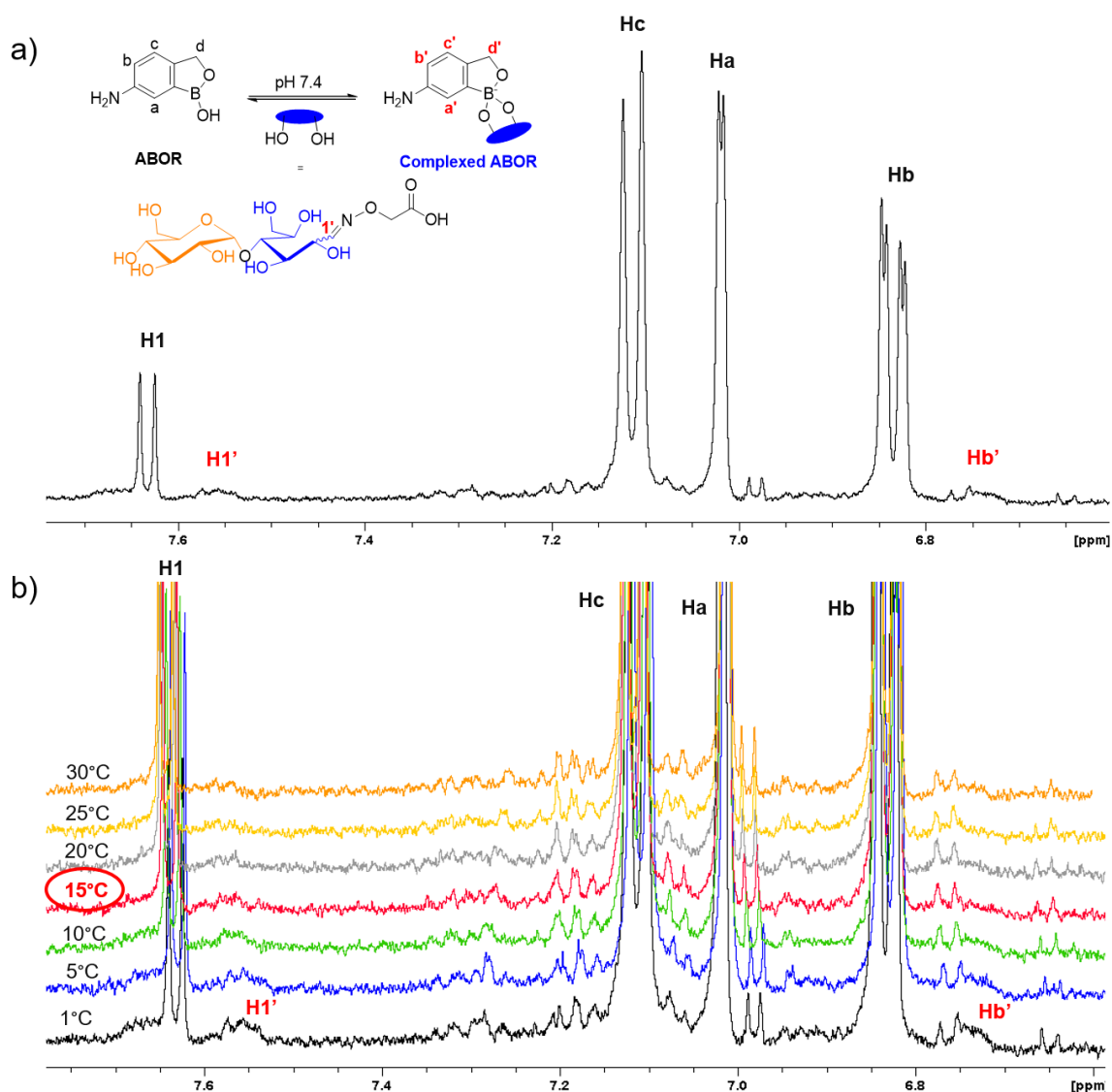


Figure S22. Variable-temperature ¹H NMR analysis of ABOR/maltose-COOH (at a molar ratio of 1/1), in 0.01 M deuterated PBS pH 7.4: ¹H NMR spectrum of the complex far below coalescence (1 °C) (a), and ¹H NMR spectra at different temperatures (b). k_{ex} was calculated following equations 7 and 8, using the chemical shifts of Hb and Hb' (free and complexed ABOR) and/or H1 and H1' (free and complexed maltose) at 1 °C. Of note, the existence of other complexes cannot be excluded as small additional signals are also observed in the NMR spectra.

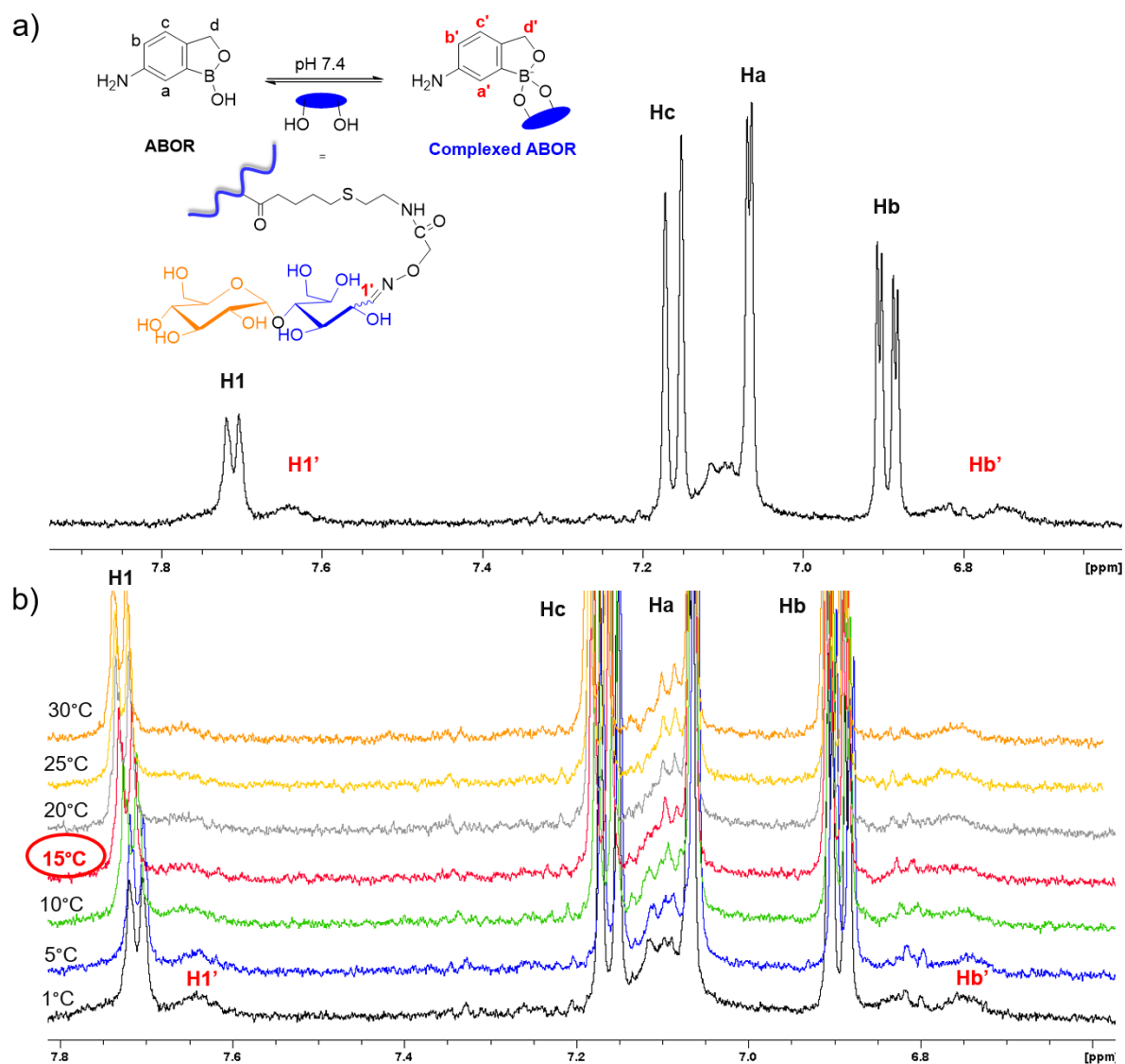


Figure S23. Variable-temperature ^1H NMR analysis of ABOR/HA-maltose (at a molar ratio of 1 ABOR/1 maltose), in 0.01 M deuterated PBS pH 7.4: ^1H NMR spectrum of the complex far below coalescence (1°C) (a), and ^1H NMR spectra at different temperatures (b). Similar to maltose-COOH, k_{ex} was calculated following equations 7 and 8, using the chemical shifts of Hb and Hb' (free and complexed ABOR) and/or H1 and H1' (free and complexed maltose) at 1°C . Of note, the existence of other complexes cannot be excluded as small additional signals are also observed in the NMR spectra.

16. Determination of K_a by ^1H NMR for APBA (ABOR) and gluconamide derivatives (free gluconamide and HA-gluconamide)

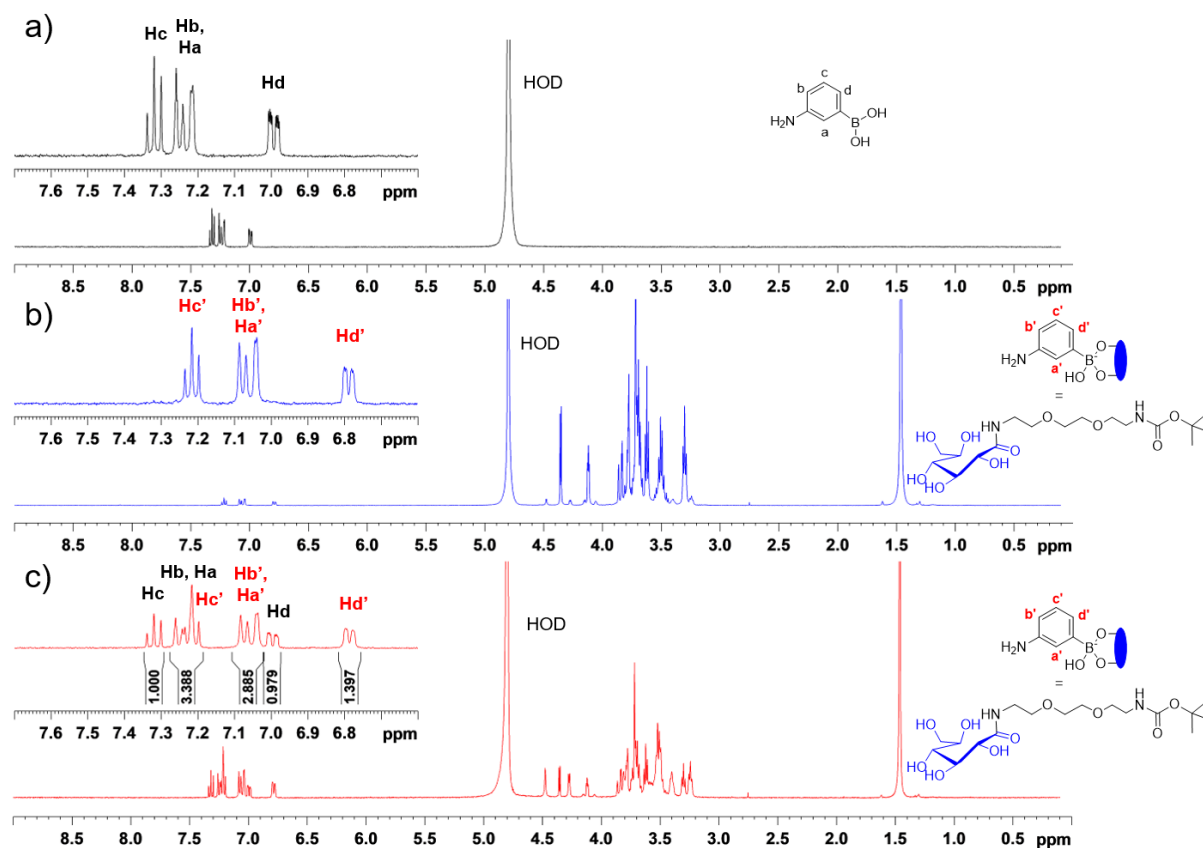


Figure S24. ^1H NMR spectra in 0.01 M deuterated PBS pH 7.4 at 25 °C of APBA alone (1 mM) (a), APBA (1 mM) in the presence of excess free gluconamide (10 mM) (b), and APBA (1 mM) with free gluconamide (1 mM) (c). The $[\text{BS}]/[\text{B}]$ ratio was calculated from the digital integration of Hc (free APBA) and Hd' (complexed APBA) signals.

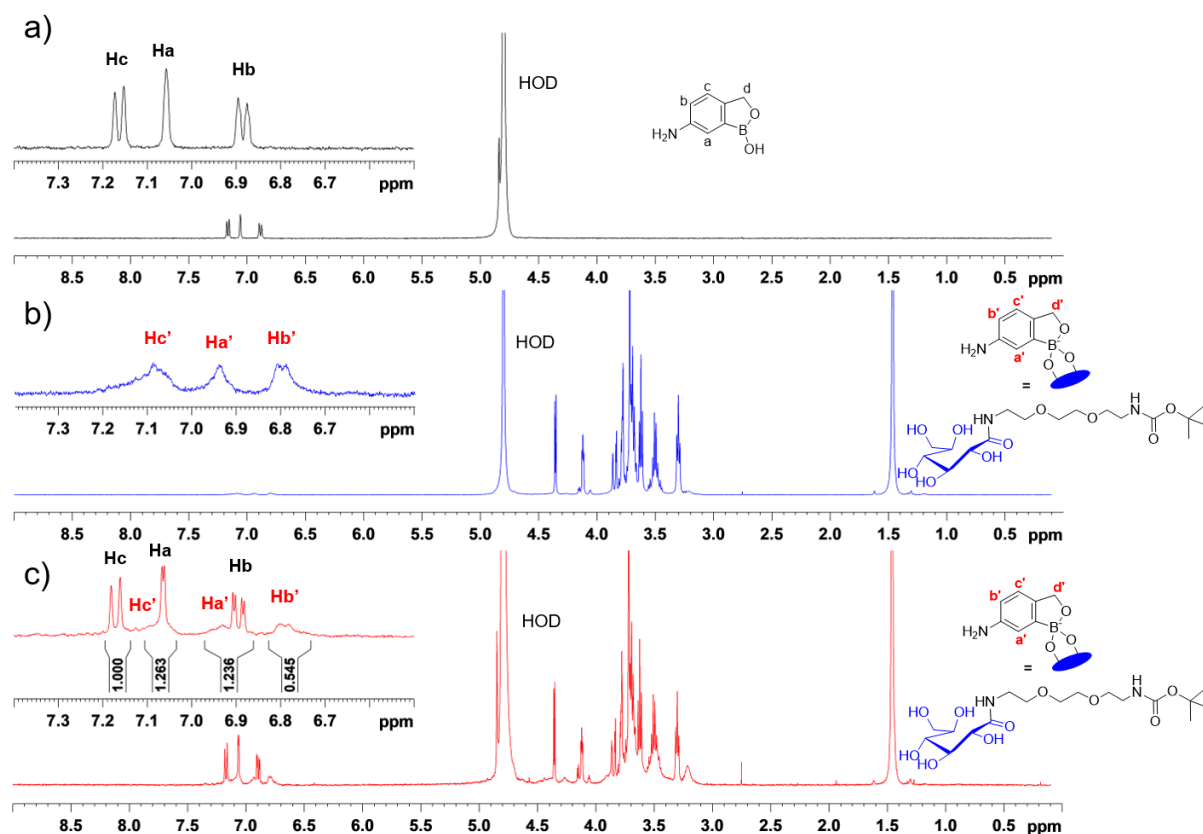


Figure S25. ^1H NMR spectra in 0.01 M deuterated PBS pH 7.4 at 25 °C of ABOR alone (1 mM) (a), ABOR (1 mM) in the presence of excess free gluconamide (10 mM) (b), and ABOR (1 mM) with free gluconamide (1 mM) (c). Compared to the maltose derivatives, the bound and unbound forms of gluconamide are in a slower exchange relative to the NMR time-scale, which allowed calculation of the $[\text{BS}]/[\text{B}]$ ratio from the digital integration of Hc (free ABOR) and Hb' (complexed ABOR) signals.

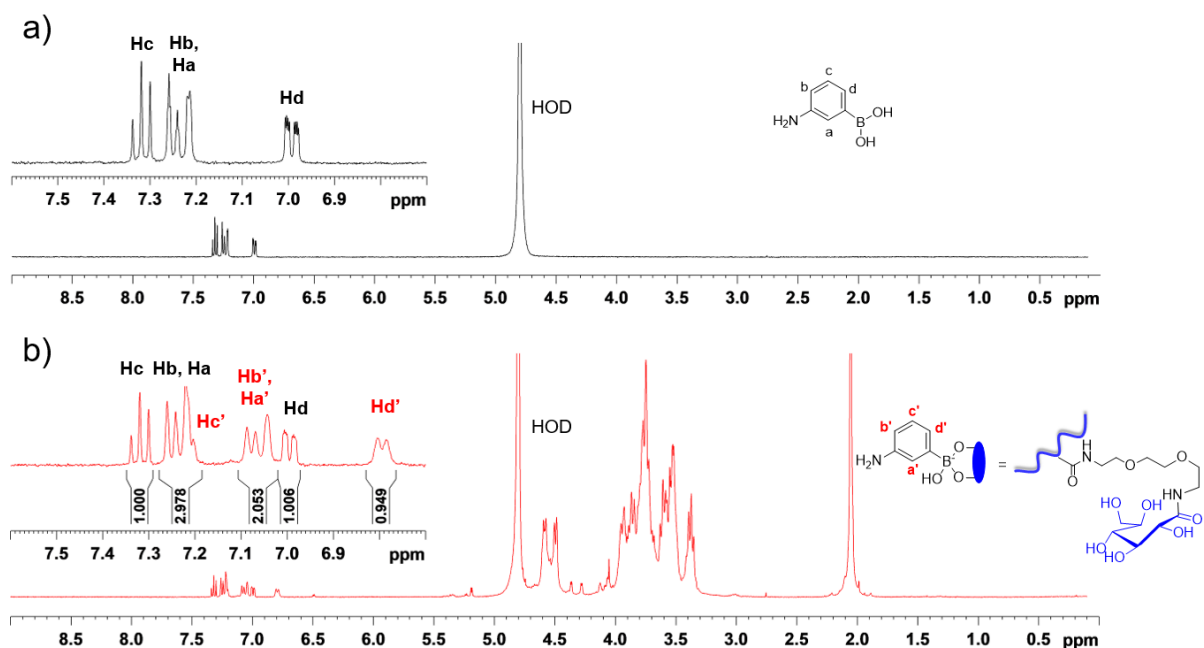


Figure S26. ¹H NMR spectra in 0.01 M deuterated PBS pH 7.4 at 25 °C of APBA alone (1 mM) (a) and APBA (1 mM) with HA-gluconamide (1 mM of grafted gluconamide) (b). Similar to the free gluconamide derivative, the [BS]/[B] ratio was calculated from the digital integration of Hc (free APBA) and Hd' (complexed APBA) signals.

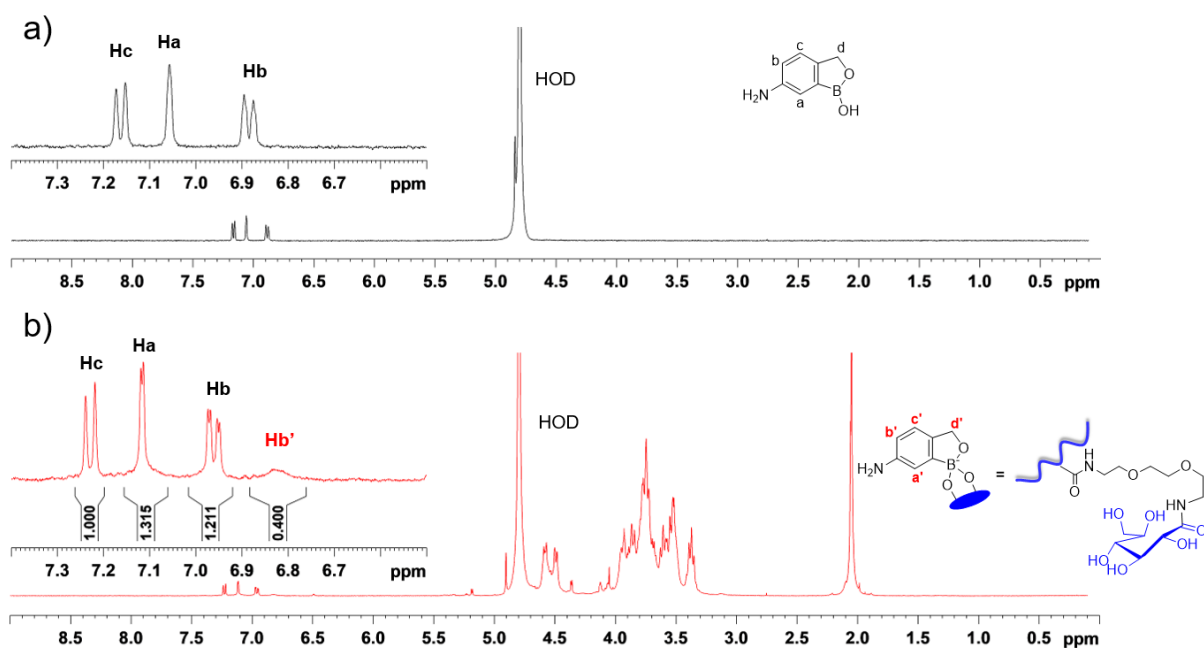


Figure S27. ¹H NMR spectra in 0.01 M deuterated PBS pH 7.4 at 25 °C of ABOR alone (1 mM) (a) and ABOR (1 mM) with HA-gluconamide (1 mM of grafted gluconamide) (b). Similar to free gluconamide, the [BS]/[B] ratio from the digital integration of Hc (free ABOR) and Hb' (complexed ABOR) signals.

17. Determination of stoichiometry of complex by the Job plot method

Similar to the procedure previously described to determine K_a from ^1H NMR spectra (section 3), solutions of the complexes of APBA with saccharides were obtained by mixing various volumes of a stock solution of APBA (2 mM) with a stock solution of saccharide (2 mM) prepared in 0.01 M PBS pH 7.4 (± 0.1). By varying the ratio r , which corresponds to $[\text{APBA}]/([\text{APBA}]+[\text{saccharide}])$, in the range 0.1-0.9, molar concentrations of complex were calculated from ^1H NMR spectra by digital integration of aryl protons of APBA/saccharide complexes and of free APBA. This allows determination of the stoichiometry of the complexes of APBA with sugars (free gluconamide, free maltose-COOH and HA-maltose) from Job plots obtained from the variation of [BS] (1:1 binding stoichiometry) or $[\text{B}_2\text{S} + \text{BS}]$ (2:1 binding stoichiometry) as a function of r (Figure S28).

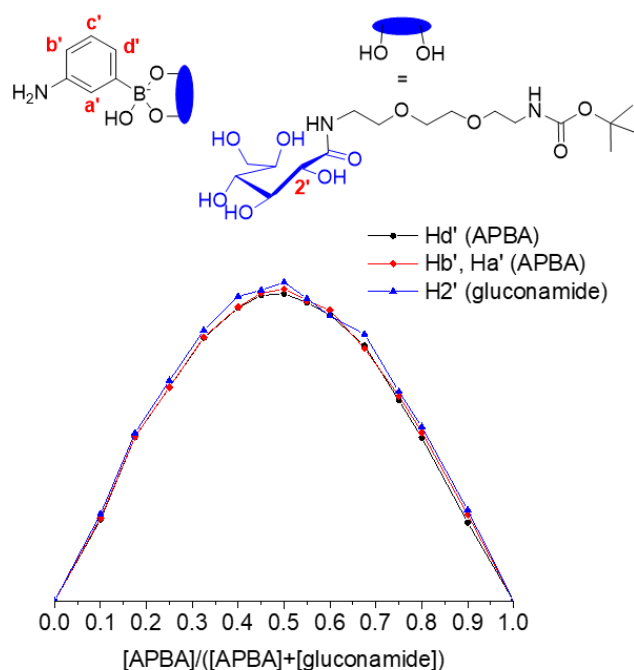
18. Job plot of the APBA/gluconamide complex

Figure S28. ^1H NMR Job plot for APBA and free gluconamide, showing a maximum at a molar ratio of 0.5.

19. Influence of the pH on the HA-PBA/HA-maltose (gluconamide) hydrogel networks

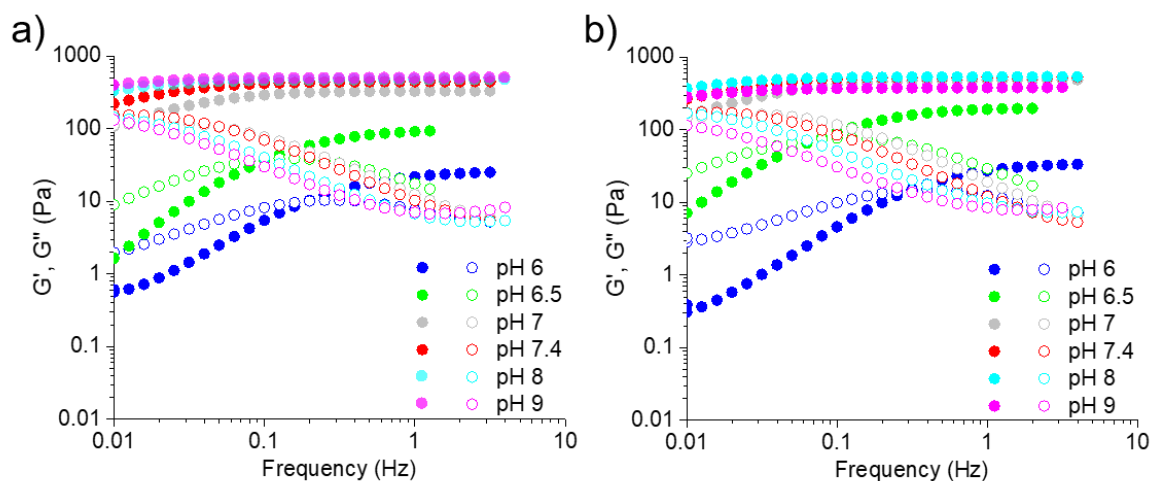


Figure S29. Frequency dependence of G' and G'' of the HA-PBA/HA-maltose (a) and HA-PBA/HA-gluconamide (b) networks by varying the pH of the medium from 6 to 9.

20. Evidence of the opening of the endocyclic B-O bond of ABOR bound to free/grafted fructose by ^1H NMR spectroscopy

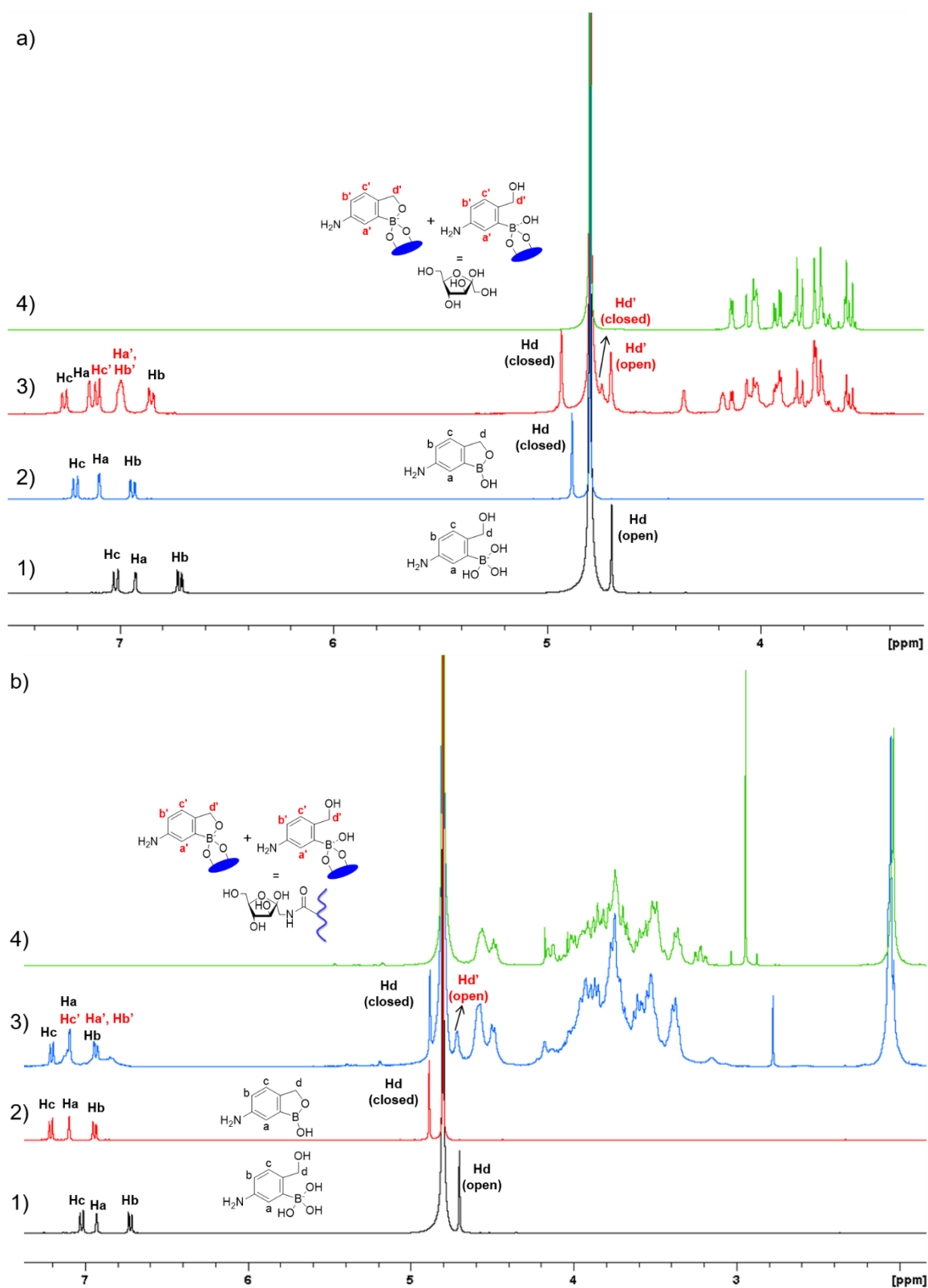


Figure S30. (a) ^1H NMR spectra of ABOR alone at pH 11-12 (1), at pH 7.4 (2), ABOR in the presence of D-fructose (3) at pH 7.4 and D-fructose alone (4). (b) ^1H NMR spectra of ABOR alone at pH 11-12 (1), at pH 7.4 (2), ABOR in the presence of HA-fructose (3) at pH 7.4 and HA-fructose alone (4) (ABOR/fructose molar ratio of 1:1).

21. Determination of the structure of ABOR complexes with free/grafted fructose by the INADEQUATE NMR technique**Table S1.** ^{13}C chemical shifts (ppm) for ^{13}C labeled D-fructose alone and complexed with ABOR at pD 7.4.

Compound	C1	C2	C3	C4	C5	C6
β -D-fructopyranose	63.8	98.1	67.5	69.6	69.2	63.4
β -D-fructofuranose	62.73	101.5	75.54	74.53	80.71	62.3
Complex β -D-fructofuranose/ABOR	64.6	111.6	83.9	77.6	85.6	62.4

Table S2. $^1\text{J}_{\text{CC}}$ coupling constants (Hz) for ^{13}C labeled D-fructose alone and complexed with ABOR at pD 7.4.

Compound	$^1\text{J}_{\text{C1-C2}}$	$^1\text{J}_{\text{C2-C3}}$	$^1\text{J}_{\text{C3-C4}}$	$^1\text{J}_{\text{C4-C5}}$	$^1\text{J}_{\text{C5-C6}}$
β -D-fructopyranose	49.9	49.3	46.4	40.2	38.2
β -D-fructofuranose	49.8	46.9	40.3	38.4	41.9
Complex β -D-fructofuranose/ABOR	52.9	38.1	36.5	40.1	40.7

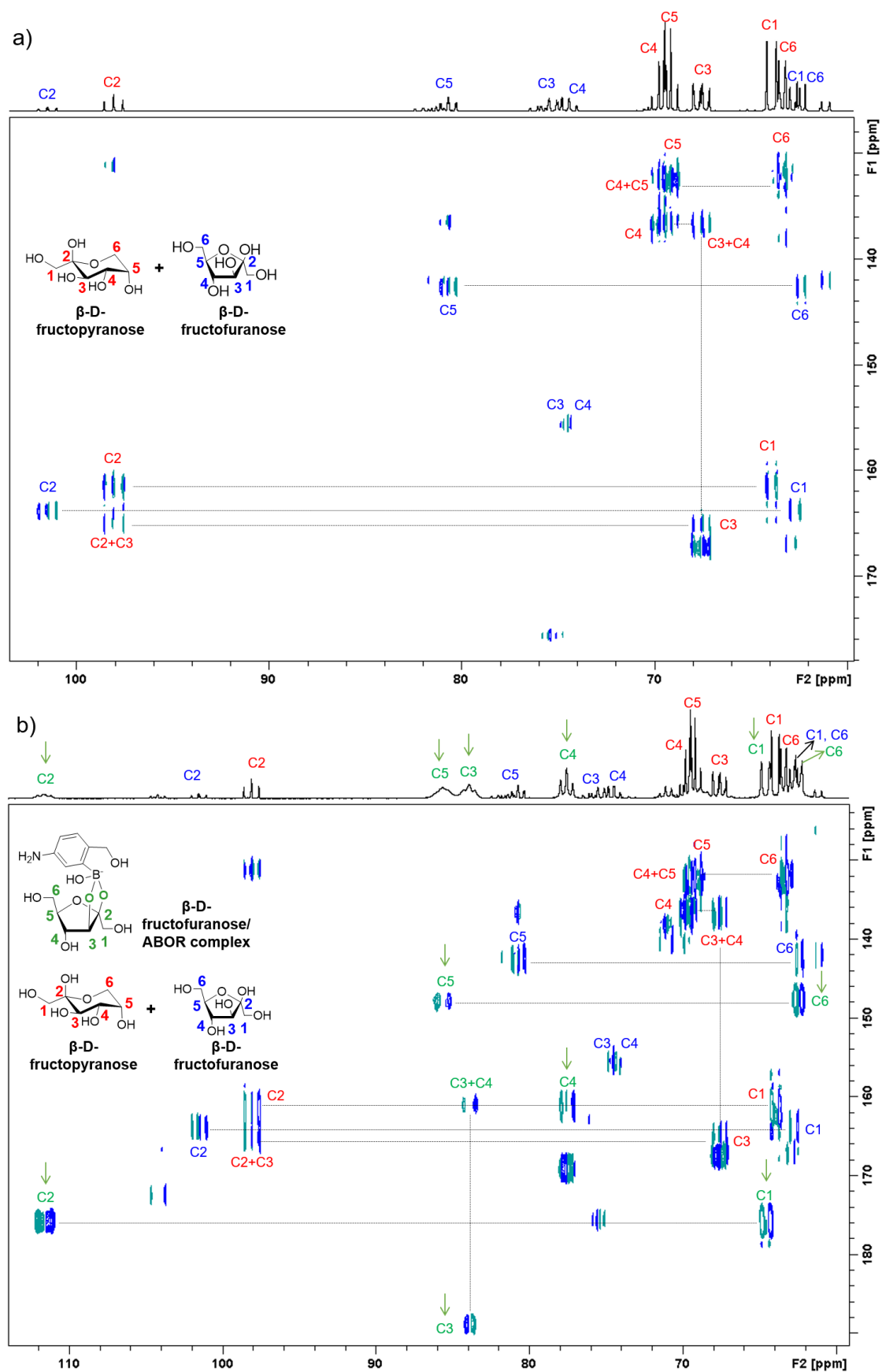


Figure S31. 2D INADEQUATE NMR spectra (400 MHz, D₂O, 298 K) of ¹³C labeled D-fructose (a) in the absence and (b) in the presence of ABOR at pD 7.4 (ABOR/fructose molar ratio of 1).

22. Determination of the structure of the complex of APBA with a ^{13}C labeled maltose grafted on HA by the INADEQUATE NMR technique

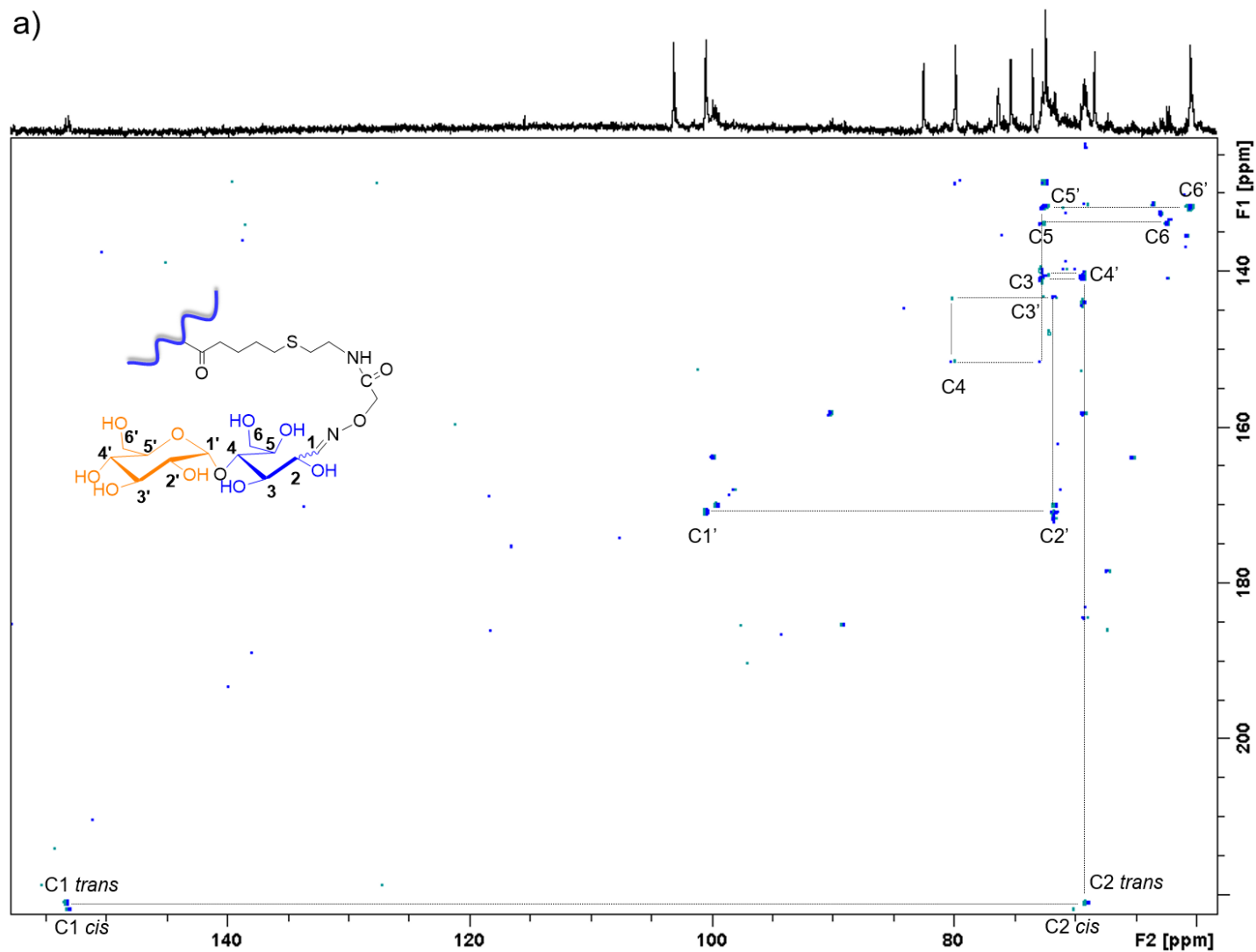
Table S3. ^{13}C chemical shifts (ppm) for the ^{13}C labeled maltose grafted on HA (HA-maltose) alone and complexed with APBA at pD 7.4 (C1-C6: open glucose; C1'-C6': terminal glucopyranose unit).

Compound	C1 <i>trans</i>	C1 <i>cis</i>	C2 <i>trans</i>	C2 <i>cis</i>	C3	C4	C5	C6
HA-maltose	153.2	153.1	69.1	70.1	72.6	80.0	72.7	62.3
APBA/HA-maltose	153.2	153.1	69.0	70.1 ^a	72.6 ^a	-	72.7	62.3 + 63.2
Compound	C1'	C2'	C3'	C4'	C5'	C6'		
HA-maltose	100.4	71.7	72.7	69.2	72.7	60.7		
APBA/HA-maltose	100.4	71.7	-	69.2	72.7	60.4		

^aDespite cross-signals of C2 and C3 are observed in the spectrum of the complex with APBA, its poor resolution precluded verification of the possible existence of additional C2 and C3 signals showing an upshift similar to C6.

Table S4. $^1\text{J}_{\text{CC}}$ coupling constants (Hz) for the ^{13}C labeled maltose grafted on HA (HA-maltose) alone and complexed with APBA at pD 7.4 (C1-C6: open glucose; C1'-C6': terminal glucopyranose unit).

Compound	$^1\text{J}_{\text{C1-C2}}$ <i>trans</i>	$^1\text{J}_{\text{C1-C2}}$ <i>cis</i>	$^1\text{J}_{\text{C2-C3}}$	$^1\text{J}_{\text{C3-C4}}$	$^1\text{J}_{\text{C4-C5}}$	$^1\text{J}_{\text{C5-C6}}$
HA-maltose	51.2	51.2	38.3	45.3	36.2	43.7
APBA/HA-maltose	50.3	50.6	38.2	-	35.2	39.8 + 45.1
Compound	$^1\text{J}_{\text{C1'-C2'}}$	$^1\text{J}_{\text{C2'-C3'}}$	$^1\text{J}_{\text{C3'-C4'}}$	$^1\text{J}_{\text{C4'-C5'}}$	$^1\text{J}_{\text{C5'-C6'}}$	
HA-maltose	46.2	43.4	38.1	34.0	48.0	
APBA/HA-maltose	46.4	45.8	-	35.0	44.6	



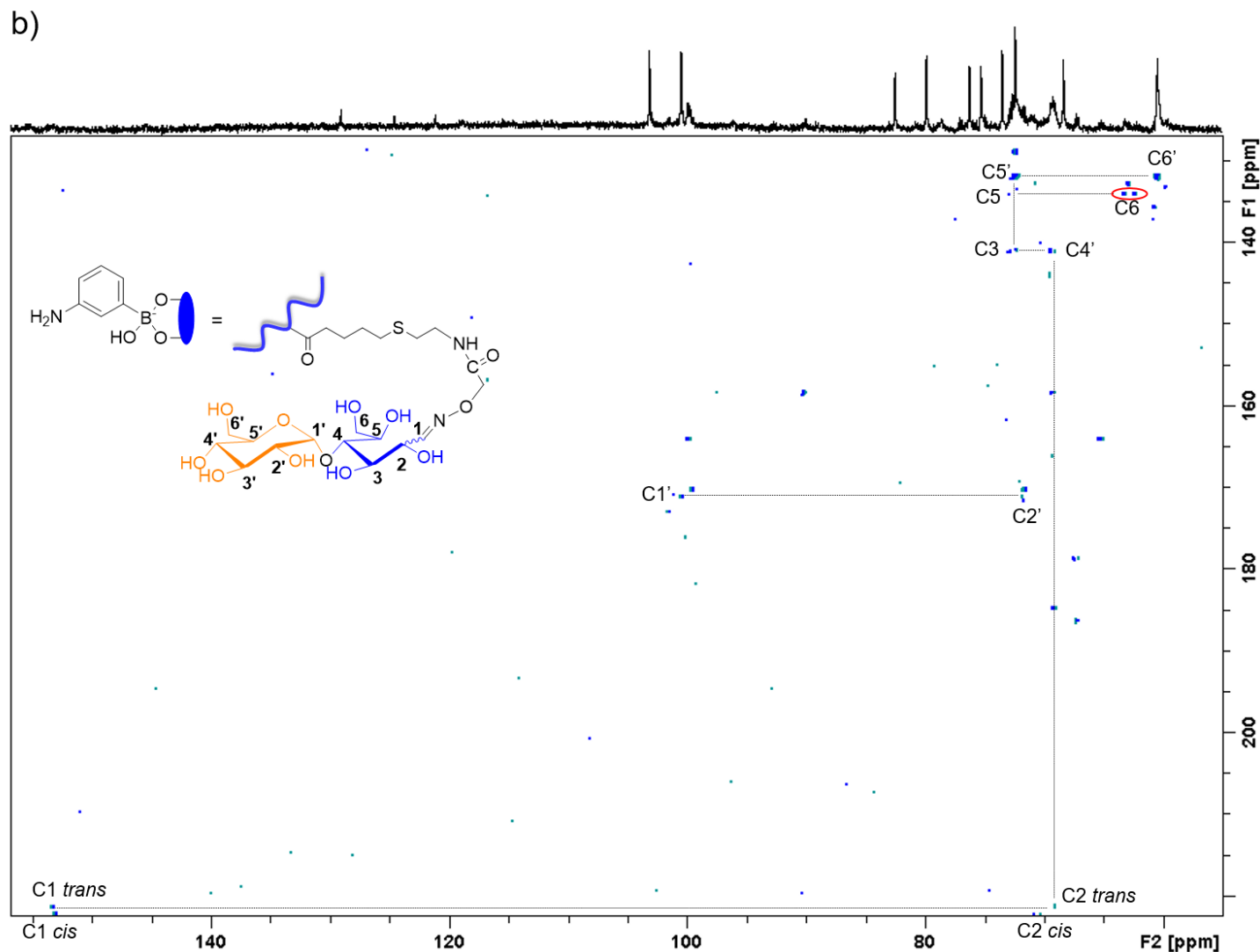


Figure S32. 2D INADEQUATE NMR spectra (950 MHz, D₂O, 298 K) of (a) HA-maltose alone (previous page) and of (b) the APBA/HA-maltose complex at pD 7.4 (APBA/grafted maltose molar ratio of 1). $^1J_{CC}$ coupling constants of the ^{13}C labeled maltose grafted on HA were measured from the cross-peaks of the spectra. The upshift of $^{13}\text{C6}$ (highlighted in red) suggests complexation of APBA towards the open glucose unit.

23. Screening of rotamers of the PBA/maltose derivative complexes by classical molecular dynamics with all-atom GROMOS force field performed using GROMACS software

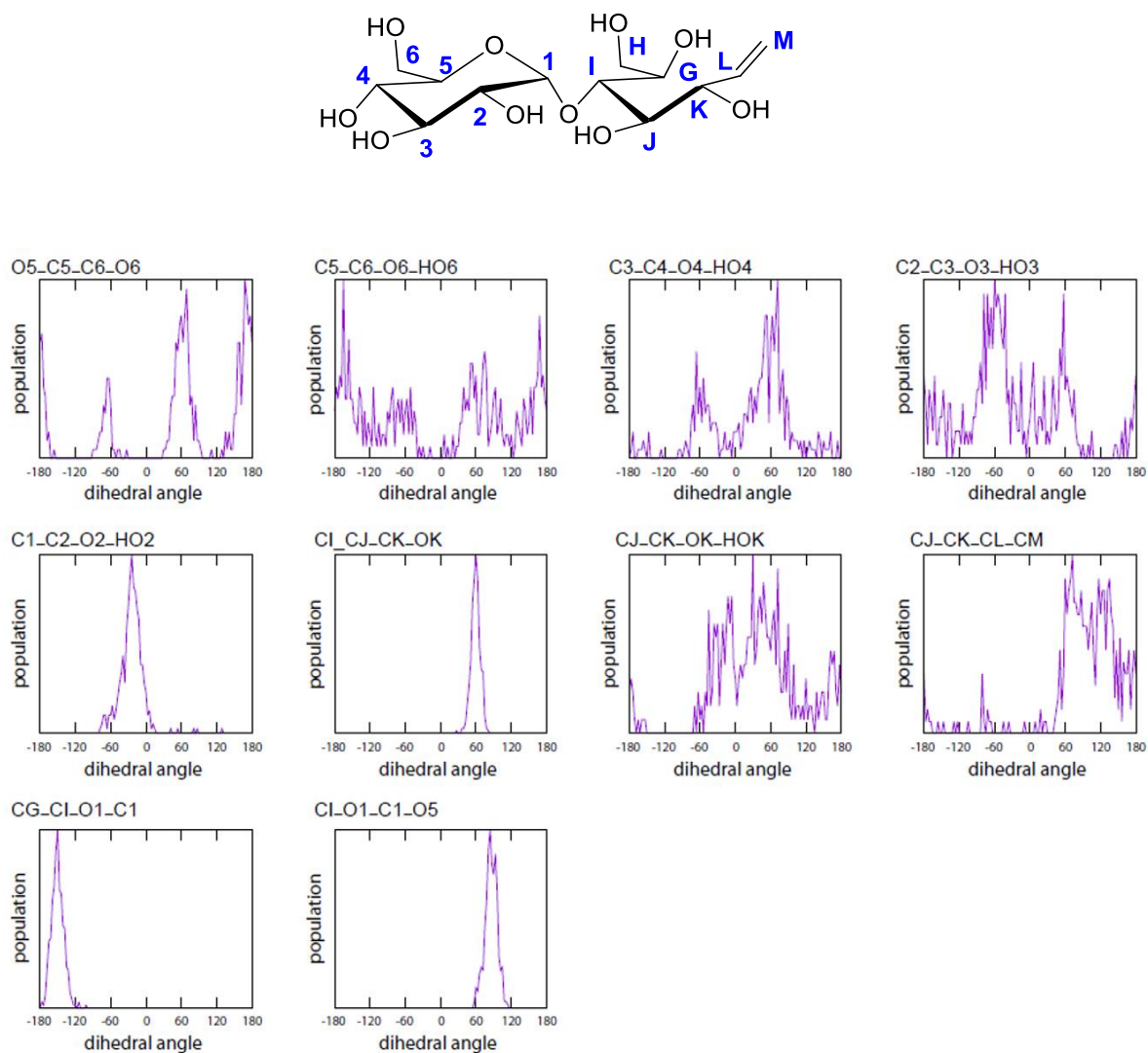


Figure S33. Distributions of selected dihedral angles of complex 1 calculated from MD trajectory.

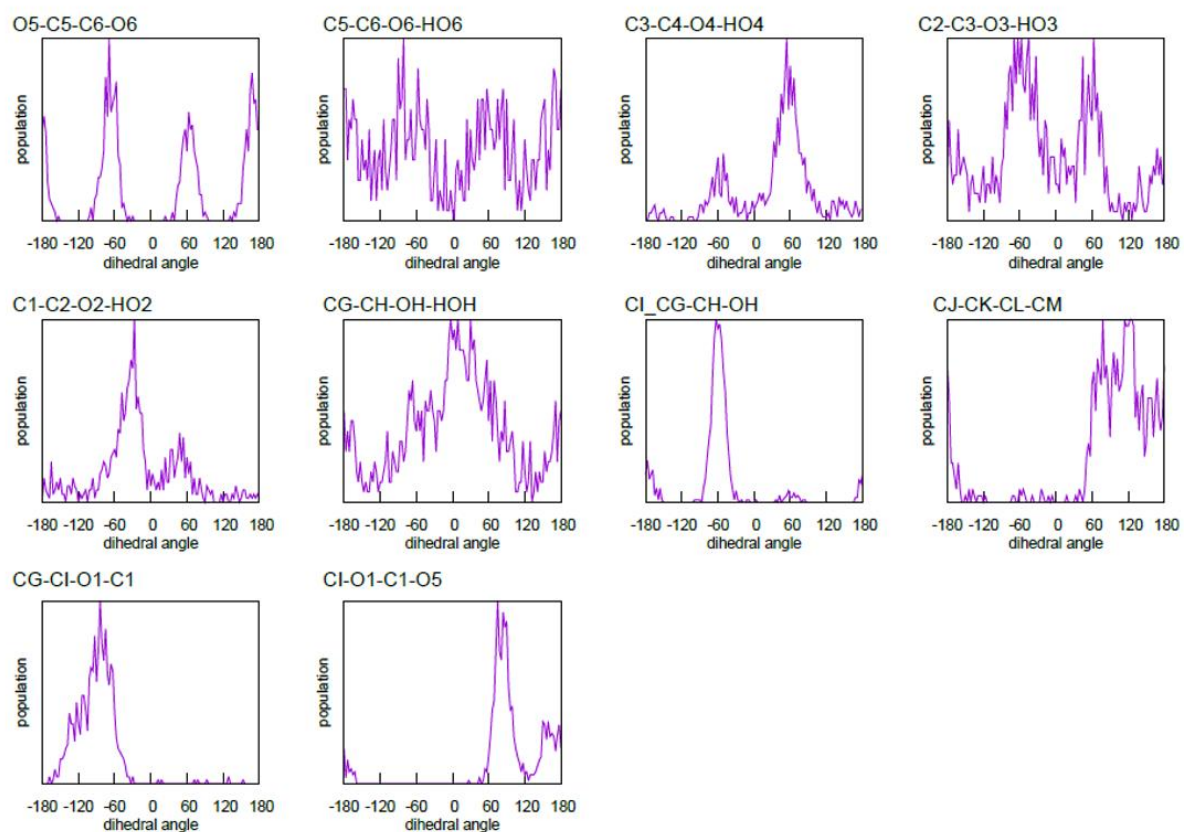


Figure S34. Distributions of selected dihedral angles of complex 2 calculated from MD trajectory.

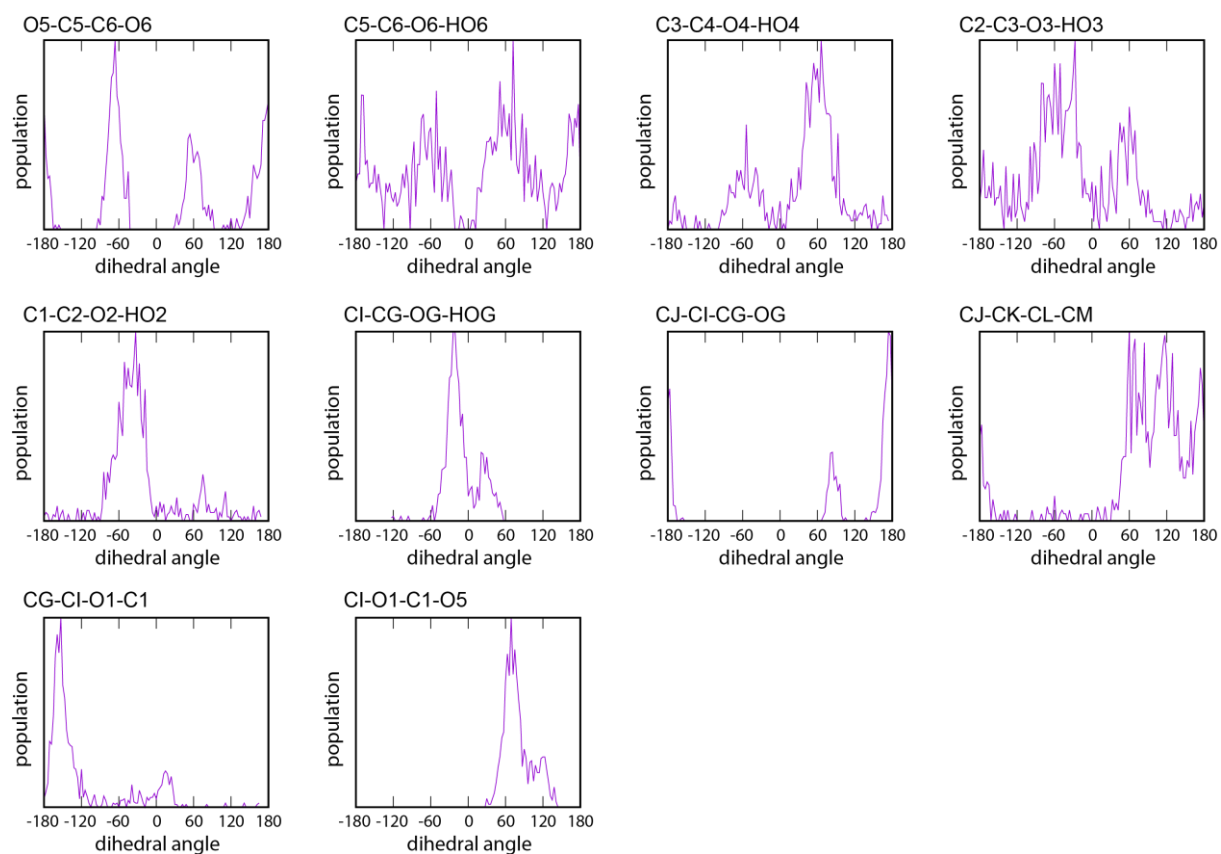


Figure S35. Distributions of selected dihedral angles of complex 3 calculated from MD trajectory.

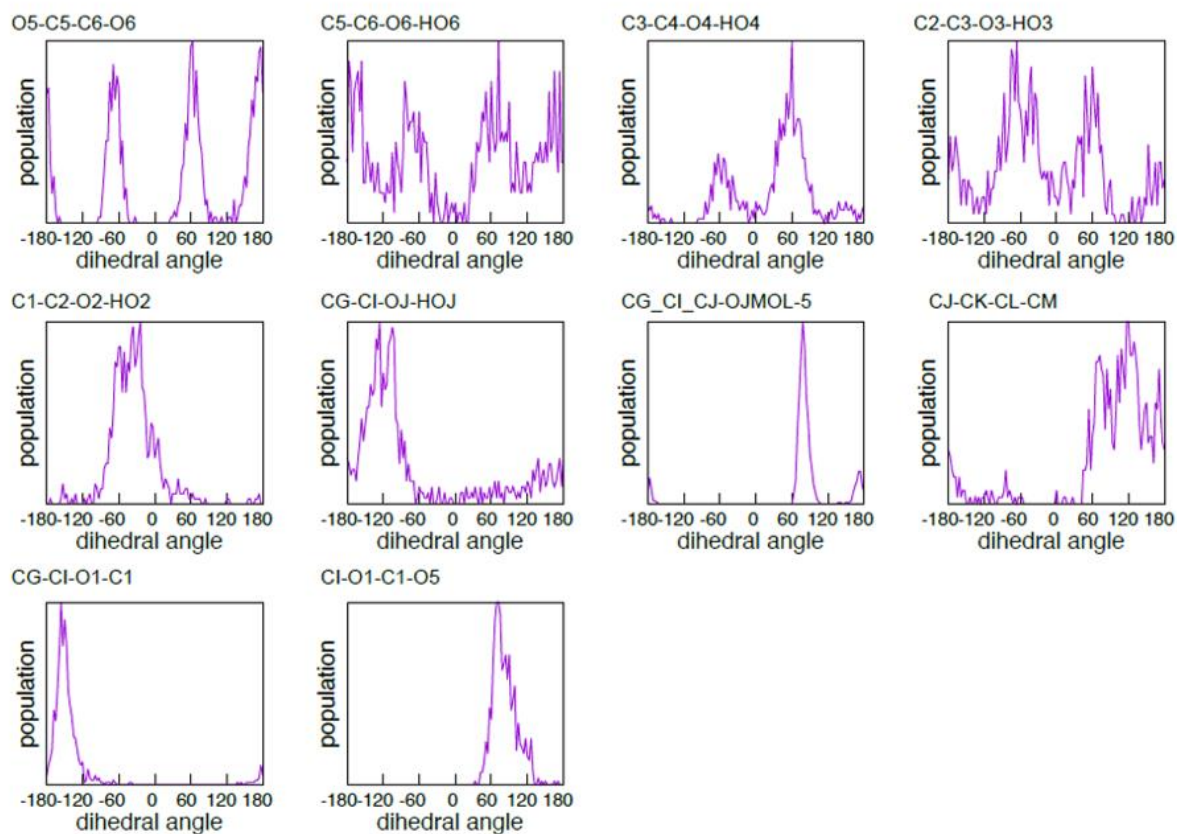


Figure S36. Distributions of selected dihedral angles of complex 4 calculated from MD trajectory.

24. Cartesian coordinates (in Å), of the lower-energy conformers for the complexes of PBA/maltose optimized using M062X/6-311+G(d,p) including SMD in water**Complex 1: C3-OH, C5-OH, C6-OH**

C 4.60569500 -1.20471100 2.37490000
H 4.83018400 -0.76343700 3.34017900
C 5.24722600 -2.37567000 1.97982900
H 5.97291600 -2.84841100 2.63232800
C 4.94988500 -2.93465900 0.73823800
H 5.44594300 -3.84617700 0.42202500
C 4.01740000 -2.32061700 -0.09528800
H 3.79850600 -2.76911000 -1.06078800
C 3.35924100 -1.14042000 0.27725000
C 3.67519400 -0.60006900 1.52997100
H 3.18462500 0.31270900 1.85494100
B 2.25974400 -0.48175800 -0.69321900
O 1.97129500 0.92224900 -0.27232700
O 0.97368800 -1.24098200 -0.70236000
O 2.64731100 -0.49426500 -2.13671300
C 1.46124100 -0.70523000 -2.89558300
H 1.33325500 0.07945800 -3.64876400
H 1.50699200 -1.67431600 -3.40340900
C 0.33580200 -0.70295800 -1.85181800
H -0.52059200 -1.31722000 -2.14014800
C -0.12379600 0.72288800 -1.52432800
H -0.62079800 1.17211100 -2.39164100
C 1.08107900 1.59447400 -1.13955600
H 1.59192400 1.85156000 -2.07697200
C 0.67511000 2.91256800 -0.45112100
C 1.75663700 3.94497600 -0.63425800
H 1.95472000 4.21424900 -1.66968300
C 2.45722700 4.50067200 0.34772200
H 2.27651800 4.24896400 1.38727100
H 3.23314300 5.22801700 0.13691700
O -1.03414700 0.68429900 -0.42539900
C -2.38790400 0.85229300 -0.71274400
H -2.52860100 1.58712500 -1.50983200
C -3.04461700 1.31826300 0.58456900
H -4.08859800 1.56423900 0.37330800
O -2.42603600 2.49525000 1.06687400
H -1.45621300 2.37264900 1.05131000
C -3.00283300 0.19721900 1.61665700
H -1.95993600 -0.01001300 1.88849000
O -3.74269200 0.54337000 2.77996900
H -3.32192200 1.31225800 3.18292500
C -3.62290500 -1.06166000 1.03573200
H -4.68226900 -0.86756300 0.82665500
O -3.49167800 -2.15969800 1.92535800
H -3.89984100 -1.91070700 2.76338800
C -2.91320800 -1.43503400 -0.26414000
H -1.86314400 -1.66662700 -0.04577300
O -2.98664700 -0.33962600 -1.18268900
C -3.52731400 -2.62959000 -0.96457100
H -3.46663200 -3.50149800 -0.31343300
H -2.95413300 -2.83489300 -1.87436900
O -4.90118700 -2.43700900 -1.27364700
H -4.96920100 -1.68384000 -1.87210800
O 0.38782700 2.69077000 0.92331800
H 0.97506500 1.97160800 1.20420200

H -0.24745900 3.27638700 -0.91876700

Complex 2: C2-OH, C3-OH, C5-OH

C -6.33868000 -1.75770900 -0.32336100
H -6.76986200 -2.72441800 -0.56091700
C -7.16675200 -0.69676600 0.03221400
H -8.24188800 -0.83221300 0.07157500
C -6.60208800 0.54092700 0.33724000
H -7.23909800 1.37378800 0.61535100
C -5.22050400 0.70580400 0.28039800
H -4.79427300 1.67844400 0.51443600
C -4.36438900 -0.34578500 -0.07694100
C -4.95578700 -1.57855100 -0.37489500
H -4.32814300 -2.41875100 -0.65569700
B -2.77820200 -0.08718900 -0.12041800
O -2.22237200 0.29118500 1.21570100
O -2.41044600 1.10044500 -0.95994900
O -2.05220700 -1.28770500 -0.60681600
C -0.02530500 -2.47844900 -0.90338100
H 1.06303400 -2.39893900 -0.93018400
H -0.36820800 -2.92811100 -1.84147200
O -0.36074100 -3.32137800 0.19385700
H -1.31523400 -3.23617800 0.31908300
C -0.65644800 -1.10432600 -0.75525200
H -0.44010300 -0.52946000 -1.66743800
C -0.05975100 -0.32670400 0.42838100
H 0.07290000 -0.99902800 1.28288600
C -0.96709500 0.83225600 0.85135700
H -0.51351000 1.38010800 1.68272100
C -1.30114300 1.74958200 -0.34646000
H -0.45577500 1.80355100 -1.04367900
C -1.66518500 3.13488200 0.09904000
H -2.54036200 3.20805800 0.74396900
C -0.97351900 4.22026500 -0.23282700
H -0.10367600 4.15361000 -0.88161500
H -1.24885100 5.20497400 0.12902400
O 1.20977300 0.17848100 0.00909300
C 2.17975100 0.27168200 1.01713000
H 1.71075700 0.37911000 1.99753600
C 3.05300400 1.48758700 0.71000200
H 3.72628300 1.64744900 1.55569300
O 2.26130200 2.65663900 0.59474900
H 1.56448600 2.47811400 -0.05348700
C 3.88555300 1.24389600 -0.54222500
H 3.22212200 1.16173000 -1.41313800
O 4.82392400 2.29005600 -0.74949900
H 4.33648500 3.10140200 -0.93542300
C 4.66720400 -0.04957900 -0.39225800
H 5.37417900 0.05801100 0.43953500
O 5.36082800 -0.37138400 -1.58735900
H 5.92860000 0.37700400 -1.80780100
C 3.70505300 -1.19611300 -0.09724000
H 3.02507100 -1.31336900 -0.94923200
O 2.95561000 -0.90496400 1.08806000
C 4.39833000 -2.52140800 0.14399600

CHAPTER 2: Mechanistic insight into the properties of boronate-crosslinked HA hydrogels

H 4.94818000 -2.81035900 -0.75151600
H 3.63729900 -3.28207500 0.34546700
O 5.33802600 -2.45993000 1.20812200
H 4.85752200 -2.25702600 2.01924500

H -5.41009600 -2.05570700 -1.39688000
H -5.38887900 -2.58979800 0.29944900
O -3.87526600 -3.33602800 -0.82693800
H -3.30647000 -3.05244100 -1.55285100

Complex 3: C2-OH, C3-OH, C6-OH

C 6.52328900 -0.54778500 0.96422600
H 7.14543400 -0.77270200 1.82424000
C 7.10931300 -0.11567400 -0.22476400
H 8.18546800 -0.00219800 -0.29498700
C 6.29828000 0.16973200 -1.32005700
H 6.74365200 0.50721000 -2.25015200
C 4.91382600 0.02758100 -1.22089600
H 4.29846700 0.26843000 -2.08276400
C 4.29998900 -0.40658700 -0.04028700
C 5.14001100 -0.69204600 1.04661900
H 4.70376000 -1.03054500 1.98316600
B 2.69551400 -0.53902400 0.10694700
O 1.97429800 -0.19574200 -1.14095500
O 2.14306800 0.46333500 1.10927300
O 2.37520800 -1.90065200 0.58256400
C 1.10904600 -2.45772700 0.28768400
H 1.00957600 -3.35808000 0.89990200
H 1.04981500 -2.76298700 -0.76486100
C -0.08775600 -1.55250700 0.59471500
H -0.98072400 -2.18568800 0.57927000
O -0.00766100 -1.02310600 1.91163400
H 0.83887400 -0.54131600 1.96043300
C -0.33272100 -0.48310700 -0.47776900
H -0.54634900 -1.03052700 -1.40309600
C 0.80196500 0.50278200 -0.77698000
H 0.47371300 1.14705400 -1.59931200
C 1.23823100 1.32680500 0.45002600
H 0.37863400 1.53501800 1.09877200
C 1.85322600 2.63489200 0.03511500
H 1.15783000 3.33690200 -0.42294900
C 3.13372600 2.95961500 0.17970500
H 3.84156200 2.27561900 0.63692500
H 3.50773200 3.92173800 -0.15310100
O -1.48690100 0.27228200 -0.09826400
C -2.42006900 0.48319600 -1.11897200
H -1.91963700 0.64678600 -2.07677800
C -3.24902600 1.70304600 -0.72585800
H -3.89890800 1.95997800 -1.56556100
O -2.41140100 2.82274600 -0.49791800
H -1.71484100 2.54511500 0.11431600
C -4.11284200 1.38782900 0.49074000
H -3.46778100 1.21721300 1.36228600
O -5.02168300 2.44437300 0.76462600
H -4.51400900 3.21681100 1.04070300
C -4.93540200 0.13313700 0.24028300
H -5.63988900 0.32768000 -0.57995100
O -5.63748700 -0.25842500 1.40896800
H -6.14872000 0.50153300 1.71322400
C -4.01087700 -1.01402100 -0.15312900
H -3.33192300 -1.23639300 0.67888800
O -3.24909800 -0.64363400 -1.30719700
C -4.76695300 -2.26829000 -0.53530300

Complex 4: C2-OH, C5-OH, C6-OH

C 5.66247700 -0.84945700 2.03176200
H 6.18931600 -0.34198700 2.83311400
C 6.07018400 -2.11692200 1.62671300
H 6.91247100 -2.60114600 2.10834500
C 5.38598800 -2.75916200 0.59488200
H 5.69767000 -3.74647200 0.27098400
C 4.30565600 -2.12973000 -0.01795200
H 3.78432300 -2.64321700 -0.82277700
C 3.87223700 -0.85329000 0.37086800
C 4.57738300 -0.23147500 1.40777200
H 4.27661600 0.75855000 1.73666900
B 2.58726500 -0.19083300 -0.35830200
O 1.32162900 -0.87634800 0.02469200
O 2.63960500 -0.38866200 -1.85974000
O 2.53918900 1.25332500 -0.06624900
C 1.51921600 -1.16660000 -2.25463000
H 1.78611100 -2.22834000 -2.30481600
H 1.15536800 -0.84605400 -3.23454400
C 0.50782400 -0.94089500 -1.13430700
H -0.19627200 -1.77329500 -1.04522100
C -0.31634600 0.33309300 -1.31651900
H -0.85915500 0.25296000 -2.26569500
C 0.44400600 1.67330900 -1.30558000
H -0.33106700 2.44617000 -1.32364400
O 1.22075000 1.86056800 -2.47672900
H 1.96362400 1.22889400 -2.41712900
C 1.29354000 1.90466400 -0.03079200
H 0.69548600 1.53460700 0.81498700
C 1.48132300 3.38348900 0.16839200
H 0.55357600 3.93919300 0.29280100
C 2.64550300 4.02326000 0.19591700
H 3.58694100 3.49812600 0.07864500
H 2.68530700 5.09694800 0.34301500
O -1.25711000 0.37948900 -0.23478000
C -2.53763000 0.83516700 -0.57293300
H -2.48709300 1.60943300 -1.34282900
C -3.17039100 1.38262300 0.70387200
H -4.12494800 1.84649500 0.44404500
O -2.36135000 2.39913600 1.26762000
H -1.46577600 2.04223000 1.35303300
C -3.42203400 0.24907200 1.69043100
H -2.46304400 -0.17766400 2.01105300
O -4.14858200 0.70363200 2.82337600
H -3.59334000 1.32753600 3.30594000
C -4.24801600 -0.83548900 1.02164300
H -5.23006500 -0.41939000 0.76413200
O -4.39905700 -1.96255600 1.87018500
H -4.78421500 -1.65591000 2.70007200
C -3.54963000 -1.31005900 -0.25049300
H -2.59111100 -1.77014500 0.01866500
O -3.32655900 -0.19771900 -1.12457300
C -4.35999100 -2.31951900 -1.03793400

H -4.53319800 -3.20267400 -0.42332200
 H -3.78649000 -2.61612700 -1.92151100

O -5.63485600 -1.81878200 -1.41662400
 H -5.49444600 -1.05369000 -1.98660100

25. Lower-energy conformers for the complexes of PBA/gluconamide complexes obtained by DFT (M062X/6-311+(d,p) in water, SMD)

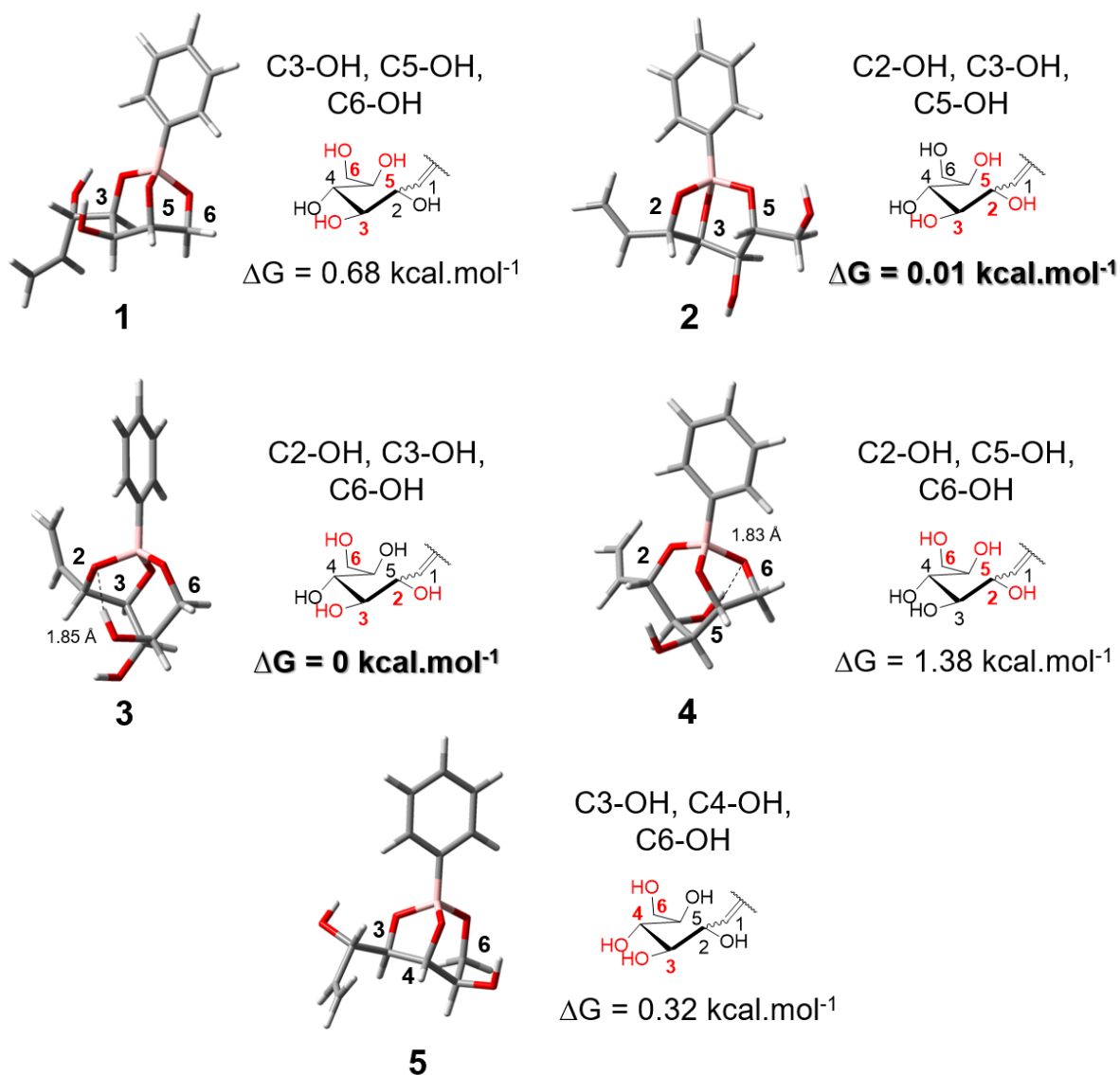


Figure S37. Optimized structures (M062X/6-311+G(d,p)/SMD) of most stable complexes between PBA and gluconamide. Note: The indicated values of energy are relative ones, with the minima set at 0 kcal/mol for the respective lowest energy structures of complex **3**.

26. Cartesian coordinates (in Å), of the lower-energy conformers for the complexes of PBA/gluconamide optimized using M062X/6-311+G(d,p) including SMD in water**Complex 1: C3-OH, C5-OH, C6-OH**

C -4.62773500 0.25065000 0.09578100
H -5.47028100 0.93311500 0.06276800
C -4.84376400 -1.11229100 0.29451500
H -5.85144500 -1.49405300 0.41574300
C -3.75558000 -1.97945300 0.33452500
H -3.91562900 -3.04131300 0.48861800
C -2.46099700 -1.48273400 0.17871500
H -1.62493400 -2.17451000 0.21303800
C -2.21643100 -0.11911400 -0.02188300
C -3.33003800 0.73248500 -0.05929100
H -3.17790200 1.79760400 -0.21534300
B -0.73767700 0.48963900 -0.19385300
O 0.28577200 -0.59090300 -0.14175700
O -0.40298100 1.50055200 0.85749100
O -0.56727900 1.27981400 -1.45445300
C 0.31867600 2.35635500 -1.16783200
H 1.17380400 2.35580500 -1.85219700
H -0.20722800 3.31186900 -1.26566200
C 0.74073800 2.12897700 0.28791600
H 0.97025600 3.05537200 0.81856300
C 1.91163500 1.14631800 0.42065600
C 1.60328300 -0.12687900 -0.38287800
H 1.71683900 0.11906900 -1.44952000
C 2.55114800 -1.28512500 -0.07354800
C 3.96595000 -0.96959000 -0.45109200
H 4.14507800 -0.78348700 -1.50880100
C 4.95758500 -0.89414500 0.42934100
H 4.78555500 -1.08160800 1.48544700
H 5.96747700 -0.64024600 0.12624600
H 2.49394900 -1.51597300 0.99525300
O 2.13065600 -2.42702600 -0.82775400
H 1.16524700 -2.44464700 -0.76478500
H 2.83403500 1.59600500 0.04688000
O 2.12150600 0.86807600 1.80330400
H 1.25534600 0.64198900 2.16881600

Complex 2: C2-OH, C3-OH, C5-OH

C -4.58520100 -0.87981700 0.13433400
C -3.68933700 -1.89218400 -0.19788800
C -2.31749400 -1.63684600 -0.20558800
C -1.80359200 -0.37419300 0.11261200
C -2.72755400 0.62779500 0.44391600
C -4.09916500 0.38592400 0.45852900
B -0.23301400 -0.03104400 0.07527000
O 0.22141200 0.74698300 1.26773900
O 0.12943300 0.88973500 -1.05510000
C 1.47005300 1.24069400 0.82043900
C 1.14773700 1.76145600 -0.60164000
C 0.71207700 3.19919400 -0.56765100
C -0.51557500 3.63407600 -0.83269400
O 0.58190300 -1.26814300 -0.01799400
C 2.45685000 0.06566600 0.79406500
C 1.96931200 -1.02531600 -0.16659300

C 2.69786000 -2.33414400 0.06738400
O 2.27352800 -3.32761700 -0.86105400
H -5.65195000 -1.07414100 0.14183300
H -4.05899100 -2.88012300 -0.45107300
H -1.63563900 -2.44081400 -0.46562900
H -2.36434000 1.62057600 0.69729900
H -4.78933300 1.18083500 0.72021600
H 1.84612000 2.02670200 1.48198400
H 2.03695100 1.67864500 -1.24032300
H 1.49229500 3.90477200 -0.28730100
H -1.30668000 2.94992000 -1.12060700
H -0.75920800 4.68941300 -0.77730100
H 2.17896400 -0.68432800 -1.19178400
H 2.50978400 -2.67169700 1.09379200
H 3.77184200 -2.20488700 -0.07179000
H 1.30912400 -3.34859300 -0.82337000
O 3.75008800 0.46746500 0.35717500
H 4.12662300 1.05140000 1.02572300
H 2.51276100 -0.34367700 1.81050800

Complex 3: C2-OH, C3-OH, C6-OH

C -3.92674300 -0.88617200 -0.97257200
C -4.62097600 -0.33343600 0.10269900
C -3.90870700 0.17465900 1.18561100
C -2.51400600 0.13179200 1.18704400
C -1.79213000 -0.41992900 0.12231800
C -2.53436100 -0.92876200 -0.95399200
B -0.17566800 -0.45544500 0.08856200
O 0.44000600 0.18253100 1.27432800
O 0.37937000 0.35998900 -1.07022800
O 0.26154300 -1.85597000 -0.08278400
C 1.53438600 -2.23796400 0.40074200
C 2.69285400 -1.32170400 -0.00059000
O 2.69273500 -1.06268500 -1.40205200
C 2.80715500 -0.02679900 0.81855800
C 1.57967300 0.89645700 0.83668000
C 1.15686900 1.41948800 -0.55014900
C 0.40173700 2.71527100 -0.43060400
C -0.88088900 2.88777800 -0.73224600
O 3.96221100 0.69947900 0.40701600
H -4.47193700 -1.28227300 -1.82286600
H -5.70470300 -0.29924900 0.09498900
H -4.43908900 0.60780900 2.02722900
H -1.97721900 0.54407500 2.03635500
H -2.01286000 -1.36374100 -1.80298500
H 1.74189500 -3.23086600 -0.00774500
H 1.53090200 -2.32278800 1.49492500
H 3.61536200 -1.87500600 0.19960100
H 1.81850800 -0.67858100 -1.60451800
H 2.98725400 -0.32939800 1.85431700
H 1.79447100 1.71816100 1.52595800
H 2.02982300 1.58823000 -1.19288100
H 0.99132100 3.55074000 -0.05688500
H -1.48852500 2.07178200 -1.10980100
H -1.35733700 3.85463500 -0.61066700

CHAPTER 2: Mechanistic insight into the properties of boronate-crosslinked HA hydrogels

H 3.96436700 0.71286700 -0.55906100

Complex 4: C2-OH, C5-OH, C6-OH

C 3.91651000 1.38780900 0.47630300
C 4.75505100 0.30622500 0.22361200
C 4.19929800 -0.92238300 -0.13279900
C 2.81712000 -1.05520400 -0.23243100
C 1.94807500 0.01770300 0.01824900
C 2.53208300 1.23845900 0.37375700
B 0.34972100 -0.21684500 -0.09808400
O -0.14066500 -1.15787000 0.94797200
O -0.01106200 -0.92284000 -1.39116900
O -0.34796300 1.07757000 -0.05219400
C -0.59948500 -2.17548400 -1.07390000
C -1.12509700 -1.98408300 0.34342300
C -2.49848800 -1.31680500 0.42566300
C -2.62173200 0.10331700 -0.16888600
O -2.52515300 0.10183900 -1.58522100
C -1.66197700 1.15224600 0.44442400
C -2.22197800 2.52913800 0.20544500
C -1.60394700 3.51351100 -0.43823800
O -2.90863400 -1.27215300 1.79278200
H 4.33984000 2.34760000 0.75318700
H 5.83097000 0.41786300 0.30113600
H 4.84500500 -1.77062000 -0.33440100
H 2.39958000 -2.01892200 -0.51569400
H 1.89492400 2.09434800 0.57485200
H 0.15601000 -2.96949900 -1.08629800
H -1.38471800 -2.42433100 -1.79297400
H -1.18847900 -2.93354300 0.88279400
H -3.22513500 -1.94983900 -0.09198600
H -3.64000600 0.42039000 0.07178300
H -1.59104100 -0.09268000 -1.79610000
H -1.66684800 0.99049600 1.53319600
H -3.21918900 2.68828000 0.61089200
H -0.60808900 3.38640200 -0.84820700
H -2.08055000 4.47907800 -0.56813500
H -2.15564000 -0.95984800 2.31128000

Complex 5: C3-OH, C4-OH, C6-OH

O 0.26037500 0.58513800 1.02628500
C 0.66268500 2.48369600 -1.07405300
H 1.03964100 2.03866200 -2.00370400
H 0.57002900 3.56139300 -1.23161200
C 1.63736600 -0.22464100 -0.64703900
H 2.32661500 0.10006000 -1.43691700
C 1.57526300 0.77303200 0.51820600
H 2.31664500 0.57252700 1.29610400
C 1.67657200 2.22623800 0.04192100
H 2.68330400 2.44456200 -0.32133100
O -0.61949800 1.95838700 -0.76096200
O 0.30774300 -0.26199000 -1.14353700
B -0.55042700 0.57762000 -0.23345900
C -2.01423500 -0.04835300 -0.01583700
C -3.18477100 0.71844200 -0.05190500
C -2.15214400 -1.41859400 0.24803100
C -4.43940500 0.14800000 0.16438000
H -3.11887000 1.78309400 -0.25413600
C -3.39847300 -2.00125000 0.46535800
H -1.26258200 -2.04428400 0.27770300
C -4.54943600 -1.21545700 0.42356400
H -5.33051300 0.76596300 0.13179500
H -3.47580500 -3.06469000 0.66496400
H -5.52283600 -1.66361000 0.59021100
C 2.03207200 -1.62999400 -0.17084500
H 1.50182200 -1.84064600 0.76697700
O 1.64216400 -2.57994800 -1.16303500
H 0.76766000 -2.29241500 -1.46393300
C 3.50952600 -1.74479100 0.03945200
C 4.07734400 -1.87214000 1.23363400
H 4.11718500 -1.69088500 -0.86234800
H 5.15498100 -1.91600500 1.34713100
H 3.47820800 -1.93043700 2.13800700
O 1.44446700 3.09124500 1.15451200
H 0.63045700 2.78081900 1.57307300

27. Possible structures of binding modes for BOR with the maltose derivative grafted on HA

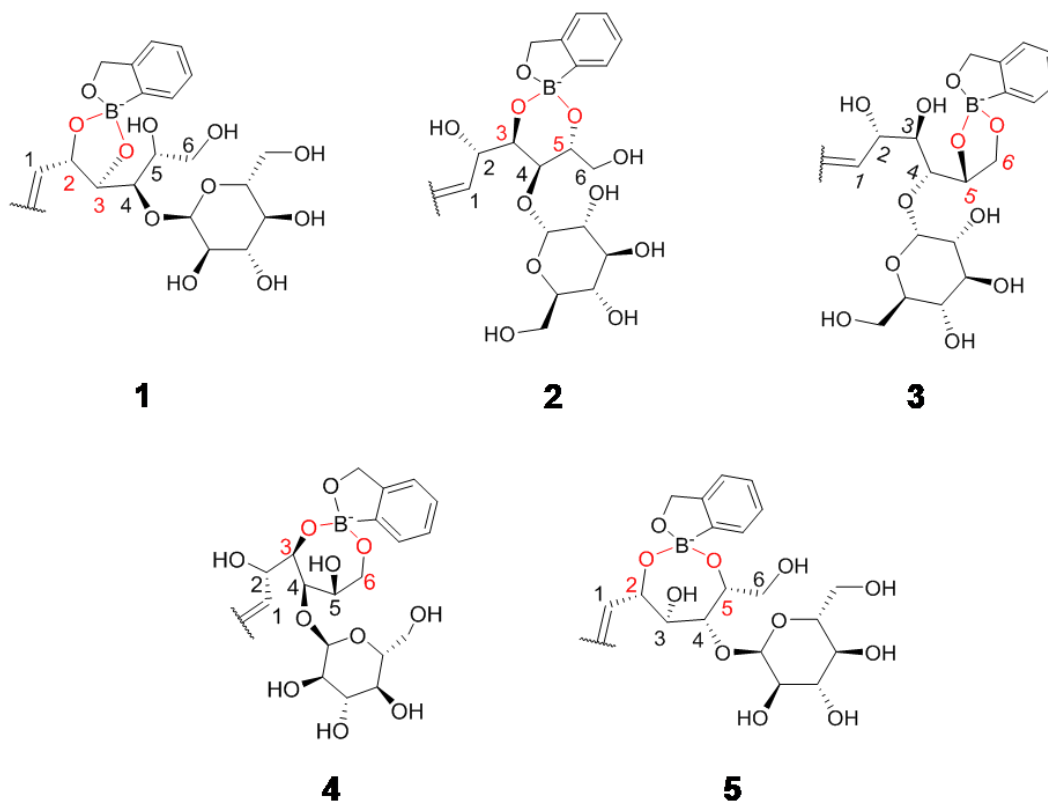


Figure S38. Possible binding modes of BOR with grafted maltose. These structures illustrate possible complexes based on the most favorable complexes found for PBA/maltose from DFT calculations, without considering possible complexation of OH groups from the glycopyranoside unit.

28. Evidence of the cyclic structure of ABOR bound to free/grafted maltose by ^1H NMR spectroscopy

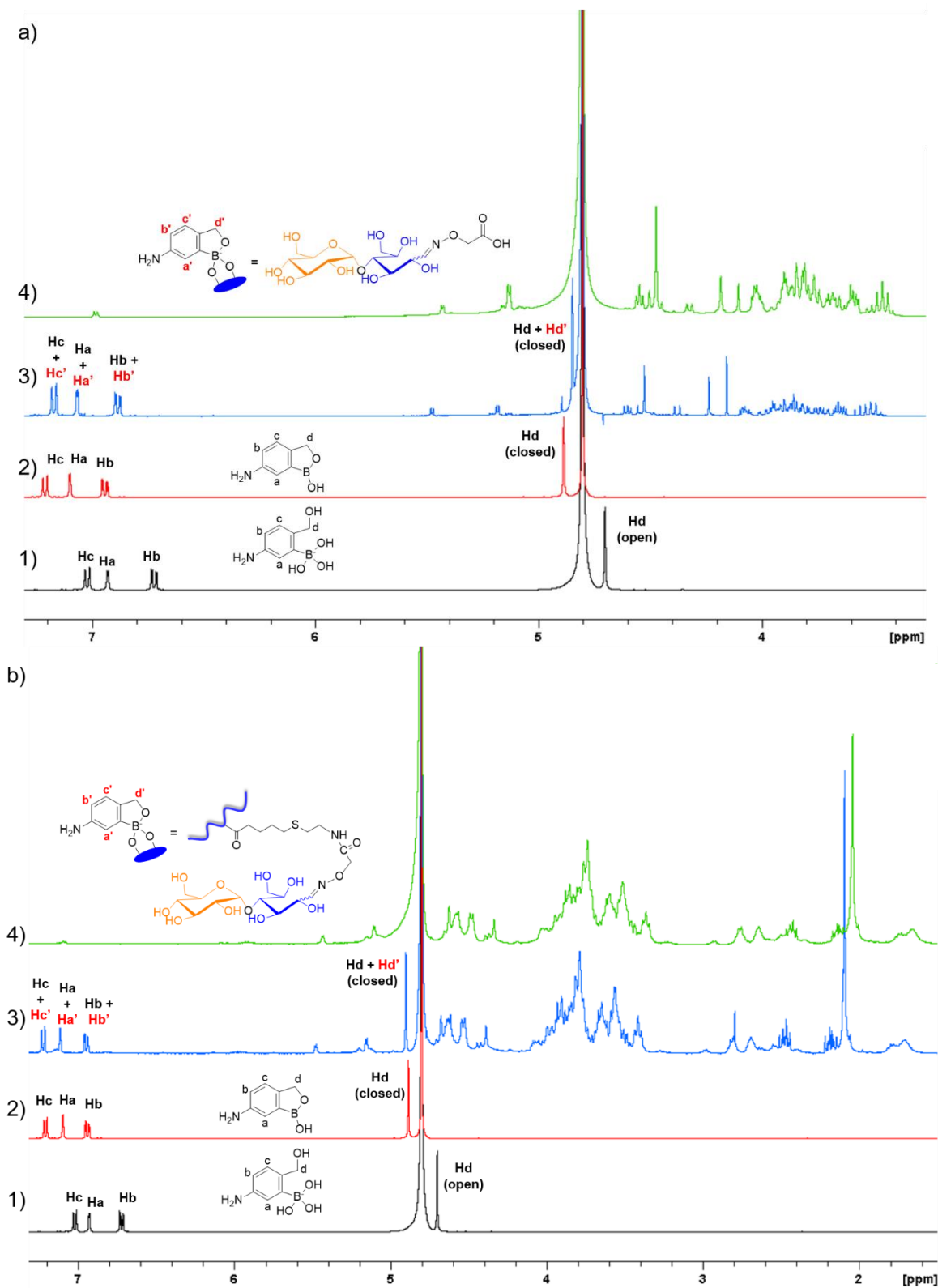


Figure S39. (a) ^1H NMR spectra of ABOR alone at pD 11-12 (1), at pD 7.4 (2), ABOR in the presence of maltose-COOH (3) at pD 7.4 and maltose-COOH alone (4). (b) ^1H NMR spectra of ABOR alone at pD 11-12 (1), at pD 7.4 (2), ABOR in the presence of HA-maltose (3) at pD 7.4 and HA-maltose alone (4) (ABOR/maltose molar ratio of 1:1).

29. Evidence of the partial opening of the endocyclic B-O bond of ABOR bound to free/granted gluconamide by ^1H NMR spectroscopy

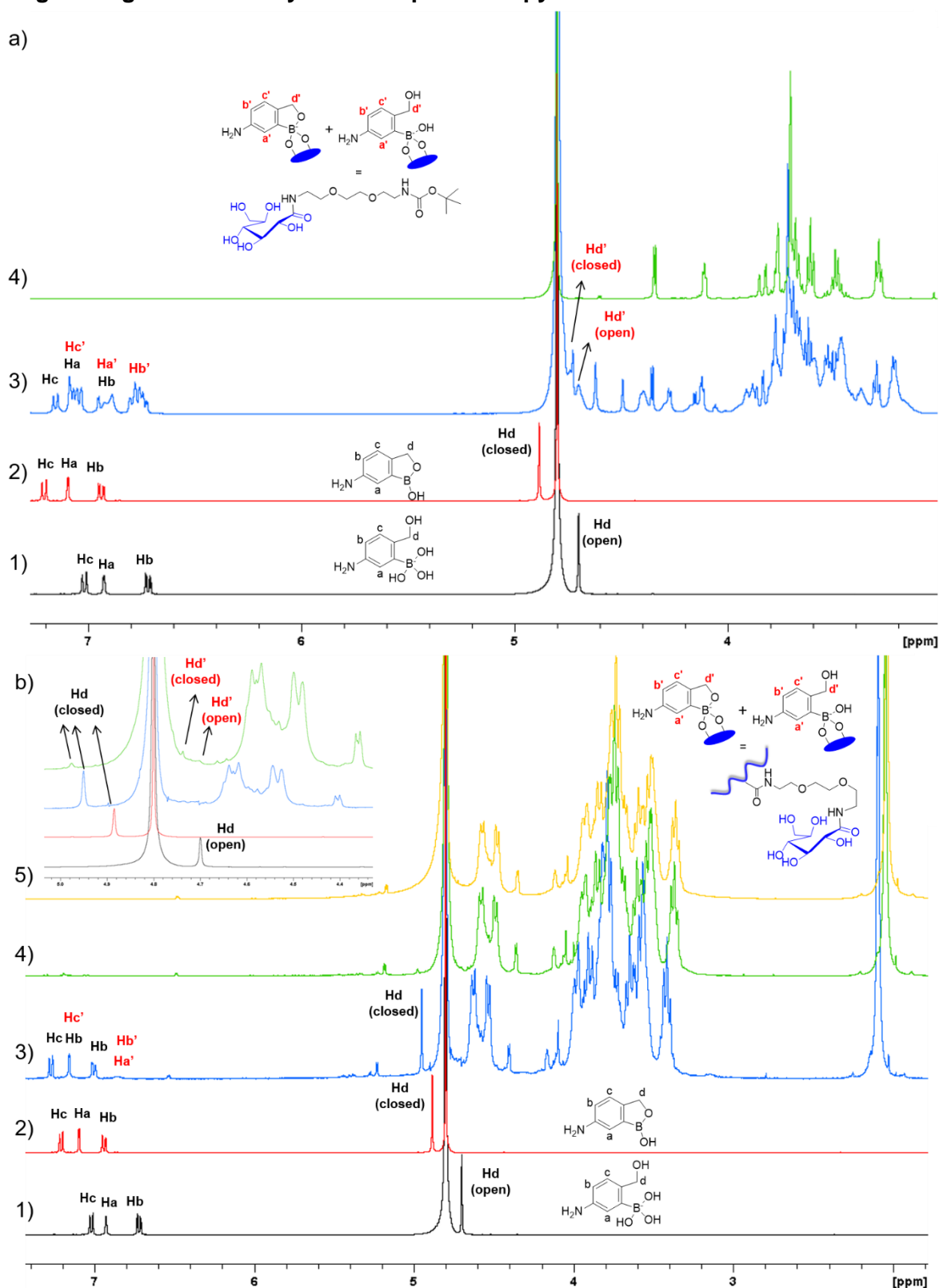


Figure S40. (a) ^1H NMR spectra of ABOR alone at pD 11-12 (1), at pD 7.4 (2), ABOR in the presence of free gluconamide (3) at pD 7.4 and free gluconamide alone (4). (b) ^1H NMR spectra of ABOR alone at pD 11-12 (1), at pD 7.4 (2), ABOR in the presence of HA-gluconamide (3 and 4, ABOR/gluconamide molar ratios of 1:1 and 1:10, respectively) at pD 7.4 and HA-gluconamide alone (5).

30. Dynamic rheological analysis of HA-PBA/HA-catecholamine (dopamine) at pH 7.4

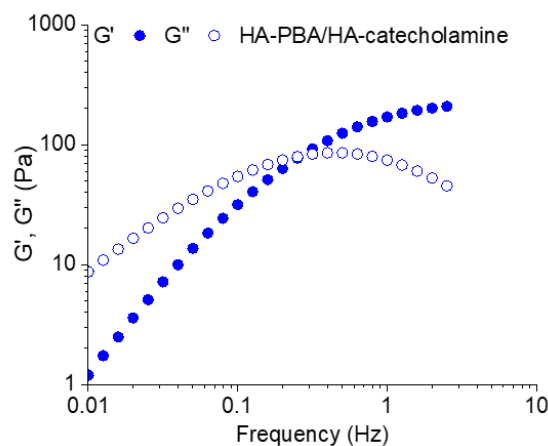


Figure S41. Frequency dependence of G' and G'' showing the fast network relaxation of a mixture of HA-PBA with a HA-catecholamine conjugate.

31. Mechanism of boronate ester formation

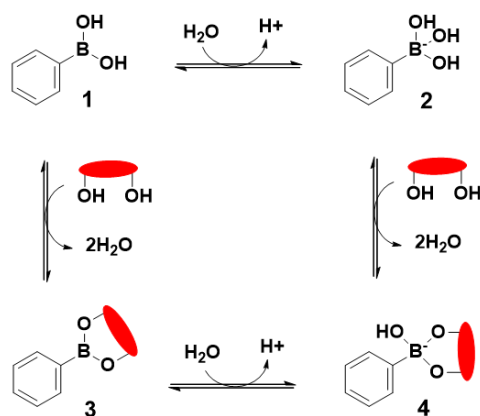


Figure S42. Equilibria between phenylboronic acid and diol-containing molecules in aqueous solution.⁸ It is traditionally believed that boronate esters are mainly formed via the boronate anion (2). Recent studies, however, have shown that the kinetically preferred pathway to the boronate ester species is via the trigonal boronic acid (1).^{9,10} This includes formation of a neutral diester (3) by reaction of 1 and the diol-containing molecule, which reacts with a water molecule in a second step to produce the anionic tetrahedral diester adduct (4).

32. References

- (1) Cayot, P.; Tainturier, G. The Quantification of Protein Amino Groups by the Trinitrobenzenesulfonic Acid Method: A Reexamination. *Anal. Biochem.* **1997**, *249* (2), 184–200.
- (2) Hermanson, G. Bioconjugate Techniques - 3rd Edition. In *Bioconjugate Techniques*; Academic Press: San Diego, California, 1996; pp 112–113.
- (3) Ellis, G. A.; Palte, M. J.; Raines, R. T. Boronate-Mediated Biologic Delivery. *J. Am. Chem. Soc.* **2012**, *134* (8), 3631–3634.
- (4) Dowlut, M.; Hall, D. G. An Improved Class of Sugar-Binding Boronic Acids, Soluble and Capable of Complexing Glycosides in Neutral Water. *J. Am. Chem. Soc.* **2006**, *128* (13), 4226–4227.
- (5) Cromwell, O. R.; Chung, J.; Guan, Z. Malleable and Self-Healing Covalent Polymer Networks through Tunable Dynamic Boronic Ester Bonds. *J. Am. Chem. Soc.* **2015**, *137* (20), 6492–6495.
- (6) Inoue, Y.; Miyauchi, M.; Nakajima, H.; Takashima, Y.; Yamaguchi, H.; Harada, A. Self-Threading and Dethreading Dynamics of Poly(Ethylene Glycol)-Substituted Cyclodextrins with Different Chain Lengths. *Macromolecules* **2007**, *40* (9), 3256–3262.
- (7) Thordarson, P. Determining Association Constants from Titration Experiments in Supramolecular Chemistry. *Chem Soc Rev* **2011**, *40* (3), 1305–1323.
- (8) Springsteen, G.; Wang, B. A Detailed Examination of Boronic Acid–Diol Complexation. *Tetrahedron* **2002**, *58* (26), 5291–5300.
- (9) Miyamoto, C.; Suzuki, K.; Iwatsuki, S.; Inamo, M.; Takagi, H. D.; Ishihara, K. Kinetic Evidence for High Reactivity of 3-Nitrophenylboronic Acid Compared to Its Conjugate Boronate Ion in Reactions with Ethylene and Propylene Glycols. *Inorg. Chem.* **2008**, *47* (5), 1417–1419.
- (10) Peters, J. A. Interactions between Boric Acid Derivatives and Saccharides in Aqueous Media: Structures and Stabilities of Resulting Esters. *Coord. Chem. Rev.* **2014**, *268*, 1–22.

CHAPTER 3

Self-crosslinking smart hydrogels through multivalent interactions between benzoboroxole derivatives and diols from hyaluronic acid

T. Figueiredo, J. Jing, C. Harris, Y. Ogawa, V. Cosenza, I. Jeacomine, J.-G. Boiteau, T. Gerfaud, J. Olsson, R. Auzély-Velty

Self-crosslinking smart hydrogels through multivalent interactions between benzoboroxole derivatives and diols from hyaluronic acid

1. Introduction

Boronic acid-containing macromolecules have gained increasing attention in recent years due to their potential as recognition element in carbohydrate-responsive platforms and sensors, and as building block for the construction of dynamic polymeric assemblies.^{1,2} Among polymeric assemblies, hydrogels crosslinked through boronate–diol complexes have emerged as promising injectable materials for drug delivery and tissue engineering mainly because of their self-healing ability.^{3–6} This property is related to the dynamic covalent nature of these bonds allowing hydrogels to reconfigure their covalent structure, and thereby to self-repair without any external stimuli after rupture.^{7–9} In these hydrogels, the formation of boronate ester crosslinks depends on the binding affinity (K_a) of the boronic acid derivative for a given diol or polyol, which is influenced by the pH of the medium and the pK_a of the small molecular partners.^{10,11} Boronate ester formation is indeed expected to be favored at a pH value half-way between the pK_a of the phenylboronic acid and the pK_a of the diol.¹² As most of arylboronic acids used to fabricate hydrogels have a pK_a in the range of 8–9, such as phenylboronic acid (PBA, pK_a 8.8¹³), pH values above physiological pH are often required to trigger gel formation by shifting the equilibrium towards the boronate ester. One method of synthetic manipulation used to improve formation of boronate crosslinks at neutral pH is to modify the PBA moiety by adding electron-withdrawing groups on the phenyl ring (i.e. fluorine, nitro) that reduce its pK_a .^{14–16} Such an approach was successfully applied by Yesilyurt *et al.* to enhance the dynamic mechanical properties of poly(ethylene glycol) (PEG)-based self-healing networks at physiological pH.³ Indeed, using a four-arm PEG derivative modified with 4-carboxy-3-fluorophenylboronic acid instead of 4-carboxyphenylboronic acid for network formation with a four-arm PEG derivative containing glucose-like moieties, the authors obtained assemblies with increased dynamic moduli and a lower relaxation time.

Besides, the position of the substituents on the aromatic ring was also demonstrated to have strong effect on boronic acid/diol complexation. In the case of 2-acrylamidophenylboronic acid (2-APBA), the participation of the amido group at the ortho-position relative to the boronic acid through an intramolecular B–O-coordinated interaction was thus found to induce boron changes from the trigonal planar form to the anionic tetrahedral form, favoring binding with glucose.¹⁷ By using this 2-APBA monomer to prepare

boronic acid-containing copolymers, Deng *et al.* showed the ability to obtain hydrogels at neutral and acidic pH via boronate ester formation with diol-containing polymers.¹⁸

As one of the *ortho*-substituted arylboronic acids, *o*-hydroxymethylphenylboronic acid (benzoboroxole, BOR, Figure 1) stands out not only for its efficient carbohydrate-binding capability at physiological pH but also for its ability to complex sugars locked in their pyranose form (i.e. glycopyranosides).^{19–21} Compared to PBA, BOR has a lower pK_a (7.3) due to its strained five-membered oxaborole ring,^{22,23} which is a contributing factor explaining its exceptional carbohydrate-binding behavior. This property was successfully used to prepare self-healing hydrogel networks at physiological pH by combining synthetic copolymers containing benzoboroxole moieties and various saccharide derivatives (glucose in the open-chain form, lactose with the glucose unit in the ring opened form, and mannopyranoside).^{4,5,24–26} Nevertheless, despite the capability of BOR to bind glycopyranosides, to date, there have been no published studies investigating formation of reversible hydrogels from benzoboroxole-modified polysaccharides via direct complexation between BOR and saccharide units in the biopolymer chain. While offering economy of raw materials and a simpler methodology for gel synthesis, such an approach may also benefit from the unique properties of natural polysaccharides such as biocompatibility and biodegradability. It should be noted that recently, a self-crosslinking polysaccharide gel was obtained under basic aqueous conditions from alginate functionalized with 3-aminophenylboronic acid moieties that can reversibly bind the vicinal diols of the alginate pyranose rings.²⁷ However, the synthesis of self-crosslinking hydrogels from one single polysaccharide component has never been demonstrated at neutral pH.

The present work establishes for the first time the feasibility of self-crosslinking hyaluronic acid hydrogel formation at physiological pH by taking advantage of the glycopyranoside-binding capability of benzoboroxole. Inspired by previous studies showing significant effects of substituents introduced on PBA as well as of their position on its diol-binding capability at neutral pH, we selected several aminobenzoboroxole derivatives as potential HA saccharide-binding sites in which both the position of the amine group and the structure of the oxaborole ring were varied. These consist of 4-, 5-, 6- and 7-aminobenzoboroxole and their counterpart (i.e. 4-, 5-, 6- and 7-amino-3,3-*gem*-dimethylbenzoboroxole) in which the 5-membered heterocycle is substituted at the 3 position by bulky methyl groups. Moreover, besides these eight derivatives, two additional compounds (6-aminobenzoboroxole and 6-amino-3,3-*gem*-dimethylbenzoboroxole) with a fluorine substituent in the *ortho*-position to the boron were also investigated to address the question of the role of the phenyl ring substitution by an electron-withdrawing group in the binding of BOR to HA. Of note, despite many studies on the structure-property relationships

of the BOR molecule related to its great potential for drug development and saccharide sensing,^{22,23} the effect of structural BOR modification on the bulk mechanical properties of hydrogels has not previously been investigated.

Very interestingly, among all the HA-BOR conjugates studied, those prepared from 7-amino-3,3-*gem*-dimethylbenzoboroxole (DM7ABOR) and fluoro-substituted 6-amino-3,3-*gem*-dimethylbenzoboroxole (DMF6ABOR) showed unprecedented self-crosslinking properties, leading to the formation of self-healing hydrogels with extremely slow dynamics (Figure 1). Following the identification of this special class of HA derivatives, we further investigated the mechanism of reversible covalent complexation of the grafted BOR moieties with HA in more detailed by combining dynamic rheological measurements in various environmental conditions and molecular dynamics studies. These revealed original properties for the HA-DM7ABOR and HA-DMF6ABOR hydrogels, ranging from self-healing capability to stimuli-responsive behaviors triggered by pH and addition of glucose. These unique features open the door to many innovative applications in the biomedical field.

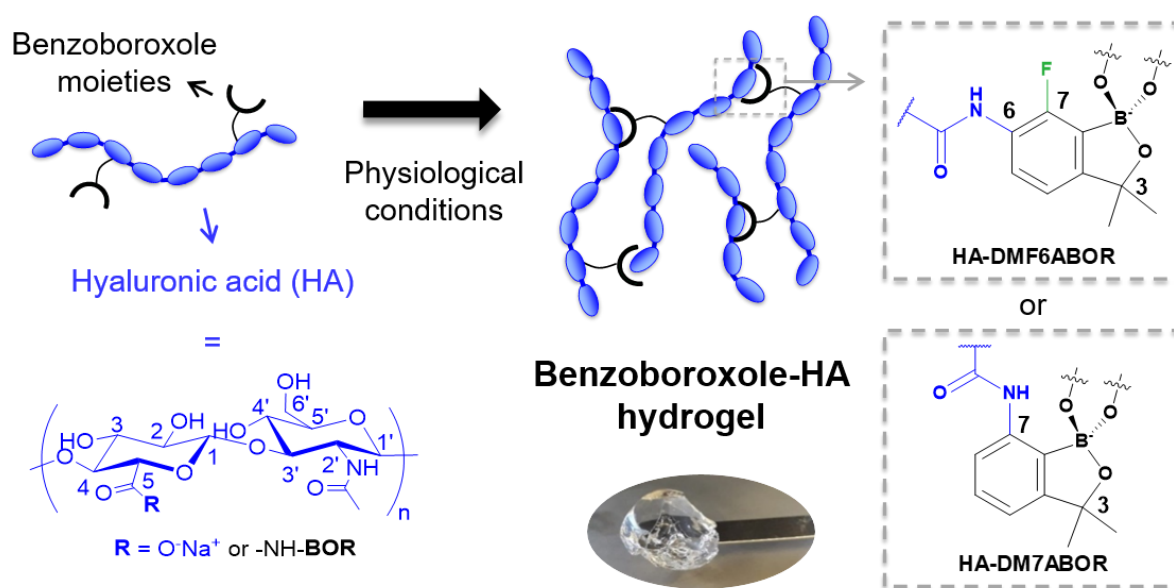


Figure 1. Self-healing HA hydrogels obtained from single BOR-modified HA components able to self-assemble via dynamic benzoboroxole-HA linkages.

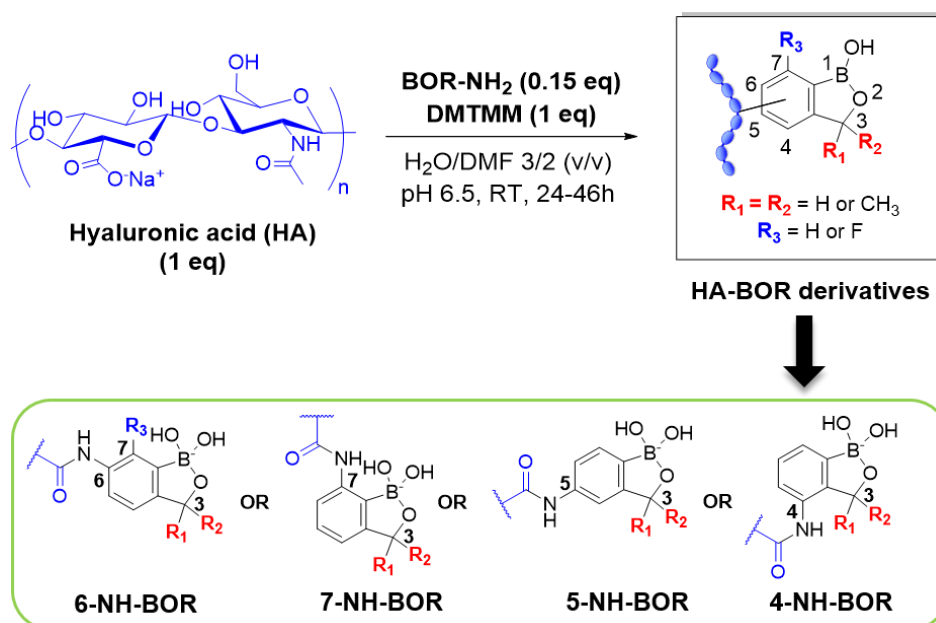
2. Results

2.1. Synthesis of benzoboroxole-modified HA and behavior in aqueous solution at neutral pH

The synthesis of the different benzoboroxole-modified HA required first that of aminobenzoboroxole derivatives. These custom-made products, except 6-aminobenzoboroxole (6ABOR) which is commercially available, were synthesized in four- to

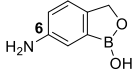
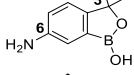
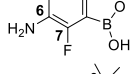
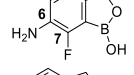
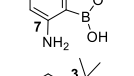
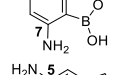
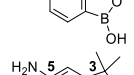
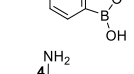
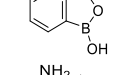
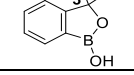
seven-steps, as described in the Supporting Information, and were isolated with yields comprised between 41-86 %. To properly investigate the self-crosslinking properties of the different HA-BOR conjugates, all HA derivatives were synthesized from the same HA sample, possessing a weight average molar mass (M_w) of 100 kg/mol (referred to as HA100), and with a similar degree of substitution (DS, average number of substituting group per repeating disaccharide unit). The HA-BOR conjugates were prepared by an amide coupling reaction in aqueous solution between BOR derivatives containing a primary amine group in position 4, 5, 6 or 7 on the aromatic ring (Table 1), and HA, using 4-(4,6-dimethoxy-1,3,5-triazin-2-yl)-4-methylmorpholinium chloride (DMTMM) as a coupling agent (Scheme 1).²⁸ The DS of the HA conjugates was controlled by the amount of BOR derivative and DMTMM. Herein, we used BOR derivative/HA and DMTMM/HA molar ratios of 0.15 and 1, respectively, to obtain DS values in the range of 0.1-0.15. The resulting HA conjugates were isolated in 95-98 % yields after purification by a diafiltration process using deionized water and freeze-drying. Successful grafting of BOR moieties on HA was confirmed by ¹H NMR spectroscopy, which also allowed determination of the DS (Table 1, Figures S1-S9).

Table 1 shows that the reactivity of the BOR compounds depends on the position of the amine group on the aromatic ring as well as on the fluorine substitution. The 6ABOR and DM6ABOR derivatives with the amine group in *meta*-position were thus found to be more reactive towards the carboxyl group of HA compared to the other ones, including the fluoro-substituted derivatives F6ABOR and DMF6ABOR. Of note, no grafting on HA was observed when using DM4ABOR (Table 1, entry 10), which can be ascribed to steric hindrance of the methyl substituents adjacent to the amine group.



Scheme 1. Schematic synthesis of the HA-BOR derivatives by an amide coupling reaction in aqueous conditions.

Table 1. Summary of the HA-BOR conjugates synthesized from a HA M_w of 100 kg/mol.

Entry	Derivative	Structure	Time of reaction (h)	DS ^a	Coupling yield ^a (%)
1	6ABOR		24	0.15	99
2	DM6ABOR		24	0.15	99
3	F6ABOR		24	0.1	67
4	DMF6ABOR		46	0.1	67
5	7ABOR		44	0.1	67
6	DM7ABOR		44	0.1	67
7	5ABOR		24	0.1	67
8	DM5ABOR		24	0.1	67
9	4ABOR		41	0.1	67
10	DM4ABOR		30	No coupling	

^aDetermined by ¹H NMR spectroscopy at 80 °C in D₂O.

To test gel formation via complexation of BOR moieties with HA saccharide units, all HA-BOR conjugates were simply solubilized in aqueous solution at physiological pH (0.01 M HEPES, 0.15 M NaCl), at a total polymer concentration ($C_p = 15$ g/L) higher than the overlap concentration of initial HA ($C^* \approx 3$ g/L). After stirring overnight at 4 °C, visual observations by inverting the vials of the different samples suggested formation of transparent hydrogels for HA-DMF6ABOR and HA-DM7ABOR. Dynamic rheological analyses confirmed the gel-like behavior ($G' > G''$ in the frequency window explored) for these two derivatives (Figures 2a and 2b). Furthermore, with the exception of HA-6ABOR, giving rise to a viscous solution like initial HA, all the other HA derivatives exhibited a viscoelastic behavior (crossover of G' and G'' seen within the tested frequencies). These results thus revealed formation of new interactions between HA chains that strongly depend on the structure of the BOR derivatives grafted on HA. Some of the striking examples include the 6ABOR and the 7ABOR derivatives linked to HA, which confer to the polysaccharide very different dynamic rheological properties upon introduction of a *gem*-dimethyl group in the oxaborole ring and/or a fluorine atom in the phenyl ring. The fact that slight modifications in the BOR molecule

induce dramatical changes in the macroscopic mechanical behavior led us to rule out the idea that interactions between HA chains are mediated by hydrophobic interactions between BOR moieties. Furthermore, ^1H NMR spectra of the HA-BOR derivatives provided some evidence of selective interaction between the grafted BOR moieties and HA saccharides. In the spectra of most HA-BOR derivatives (Figure S3-S7), the proton signals in the aromatic region exhibited splitting, suggesting the presence of free and complexed BOR species which are in slow exchange on the NMR timescale. It can be noted that similar observations were previously made for complexation of commercial free 6ABOR with D-fructose (*cf. chapter 2*),^{19,23} while only peak broadening in the aromatic region was observed for complexes involving small glycopyranosides.²⁰

Interestingly, the comparison of the variation of the loss factor, $\tan \delta$ (defined as G''/G'), with frequency for the different HA derivatives revealed a common feature in the HA modified with 5-, 6- and 7ABOR (Figure 2d). Whatever the family, the HA-DMABOR derivative shows systematically lower loss factor values than its HA-ABOR counterpart. This trend correlates with the lower crossover frequency where $G' = G''$ (i.e. ω_c which can be considered as the inverse of the characteristic relaxation time of the network), for HA-DMABOR in comparison to its HA-ABOR counterpart (Figure 2a, b and c). These data thus indicate that the *gem*-dimethyl group in the oxaborole ring plays a key role in the binding to HA, resulting macroscopically in a decrease of the network dynamics and in most cases, an increase of the G' and G'' moduli. In this regard, an increase of pK_a to 8.3 was reported for 3,3-*gem*-dimethyl benzoxaborole (DMBOR) in comparison to BOR ($pK_a = 7.3$).²⁹ This was attributed to steric bulk caused by the *gem*-dimethyl group at the 3-position in the oxaborole ring, which likely increases the bond angle around boron, alleviating the bond distortion and disfavoring ionization. The results obtained in the present work, indicating that the DMABOR moieties are more tightly bound to HA than their ABOR counterparts, are not consistent with the general belief that boronic acids with lower pK_a values show greater binding affinities for diols, as had already been pointed out previously.¹²

It is also worth noting from Figure 2d that HA-DMF6ABOR and HA-DM7ABOR stands out by displaying loss factor values lower than 1, indicating that the samples behave more like a soft elastic solid. On the basis of these results, these two derivatives were selected for more extensive physico-chemical studies with respect to their potential applications as injectable biomaterials.

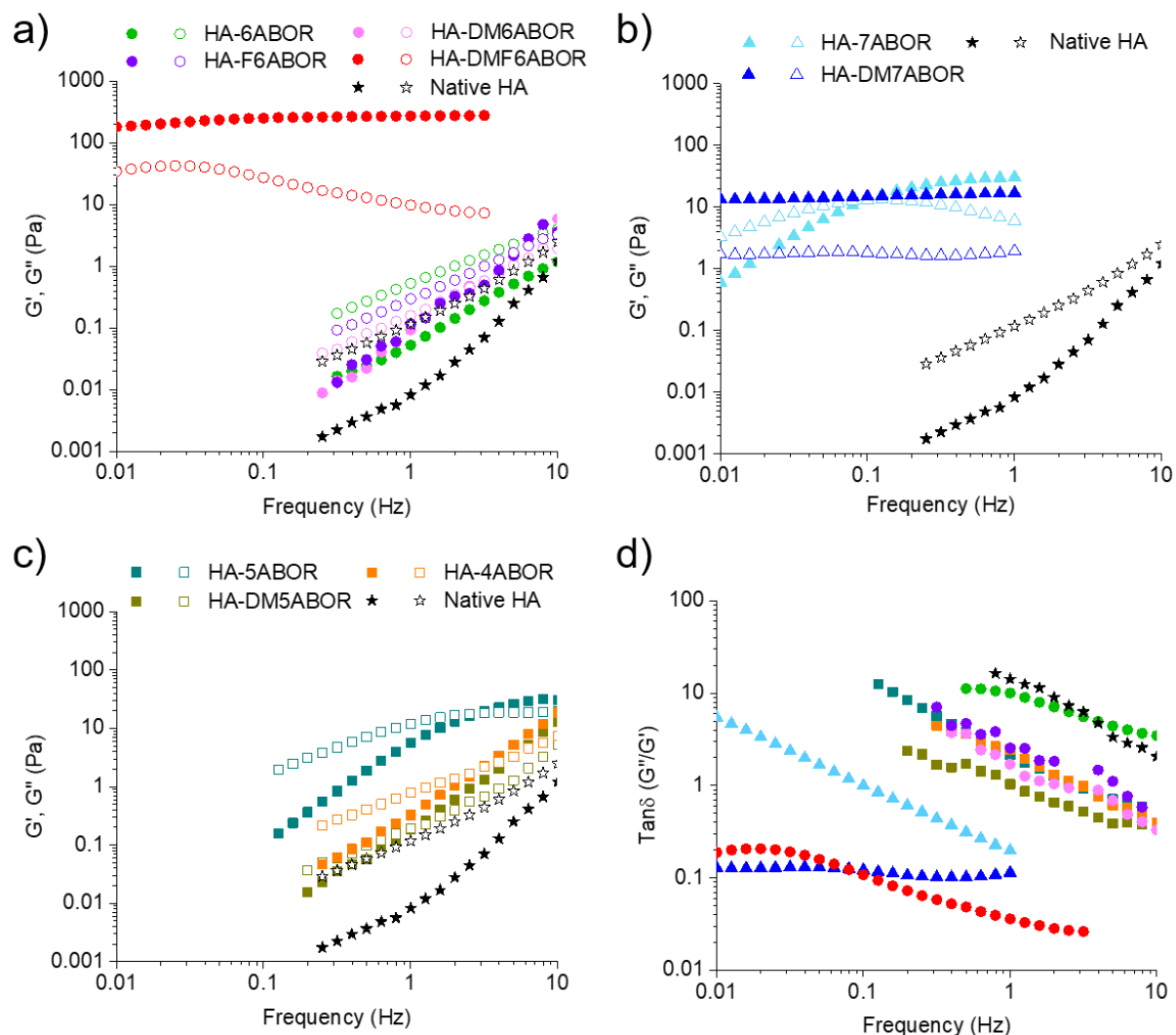


Figure 2. Dynamic rheological analysis of the HA-BOR conjugates prepared from HA100. Frequency dependence of the storage modulus (G' , filled symbols) and loss modulus (G'' , empty symbols) for the formulations based on HA modified with 6-amino-BOR derivatives (a), 7-amino-BOR derivatives (b) and 5- (or 4)-amino-BOR derivatives (c). Frequency dependence of $\tan \delta$ (G''/G') for all HA formulations (d; samples are referred to the same symbols used in Figures a-c).

2.2. Effect of molar mass and environmental parameters on the dynamic mechanical properties of HA-DMF6ABOR and HA-DM7ABOR conjugates

Assuming that tailoring the molar mass of HA can modulate the degree of interactions between HA chains via BOR complexation, we prepared new HA-DMF6ABOR and HA-DM7ABOR conjugates using an initial HA sample possessing a weight-average molar mass (M_w) of 360 kg/mol (referred to as HA360), while keeping the same DS (i.e. 0.1, see Table S1 and Figure S10 and S11). Figure 3 compares the rheological properties of aqueous formulations at physiological pH of HA-DMF6ABOR and HA-DM7ABOR prepared from HA100 and HA360. As expected, the two higher M_w HA derivatives (HA360-DMF6ABOR and

HA360-DM7ABOR) exhibited a hydrogel behavior with higher values of G' in the plateau region (371 ± 44 Pa and 160 ± 57 Pa, respectively) than HA100-DMF6ABOR and HA100-DM7ABOR. This increase of G' was more pronounced for the HA360-DM7ABOR hydrogel, which showed more than a 10-fold enhancement in the storage modulus compared to the HA100-DM7ABOR system.

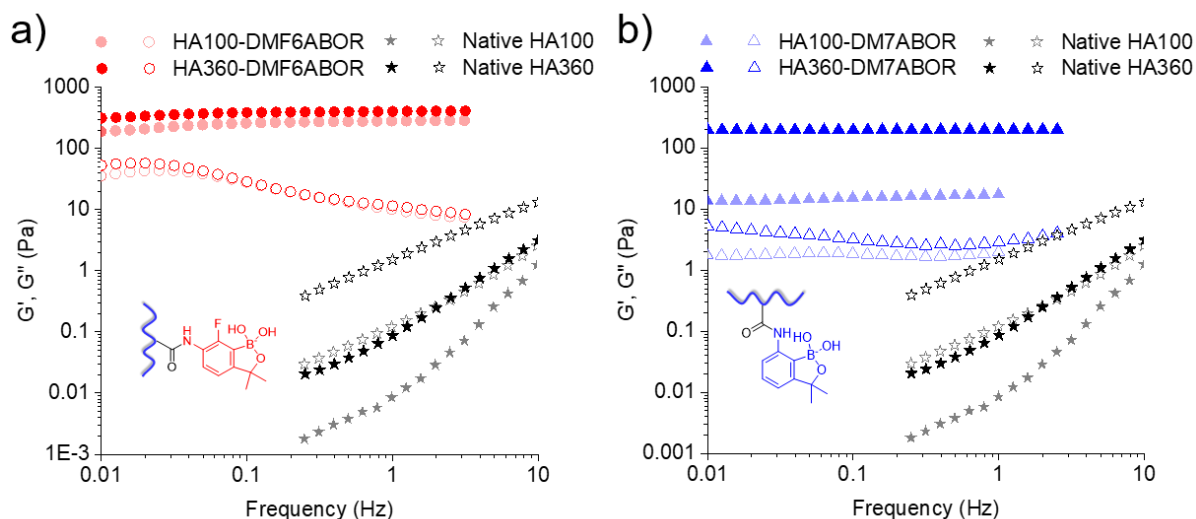


Figure 3. Effect of multivalent interaction using a HA of higher molar mass in the rheological properties of HA hydrogels at physiological pH. Frequency dependence of G' (filled symbols) and G'' (empty symbols) for the formulations based on HA-DMF6ABOR (a) and HA-DM7ABOR (b) conjugates prepared from HA100 and HA360.

Interestingly, comparison of the ^1H NMR spectra of the HA360-DMF6ABOR and HA360-DM7ABOR conjugates and of their HA100-DMF6ABOR and HA100-DM7ABOR counterparts showed an increase of the intensity of the proton signals assigned to the bound DMF6ABOR and DM7ABOR species (Figure S5, S6, S10 and S11). This increase appeared to be more pronounced for the HA-DM7ABOR derivatives.

Next, we investigated the dependence of gel strength on pH and on addition of competitive polyols. Rheological analysis of formulations based on HA360-DMF6ABOR (DM7ABOR) conjugates at pH ranging from 4.0 to 7.4 revealed network disassembly at pH around 6.5 in both cases (Figure 4). This is the likely consequence of the decrease of the DMF6ABOR (DM7ABOR)/HA saccharide affinity at lower pH values, taking into account that the affinity between boronic acids and diol-containing molecules is pH-dependent as previously mentioned.

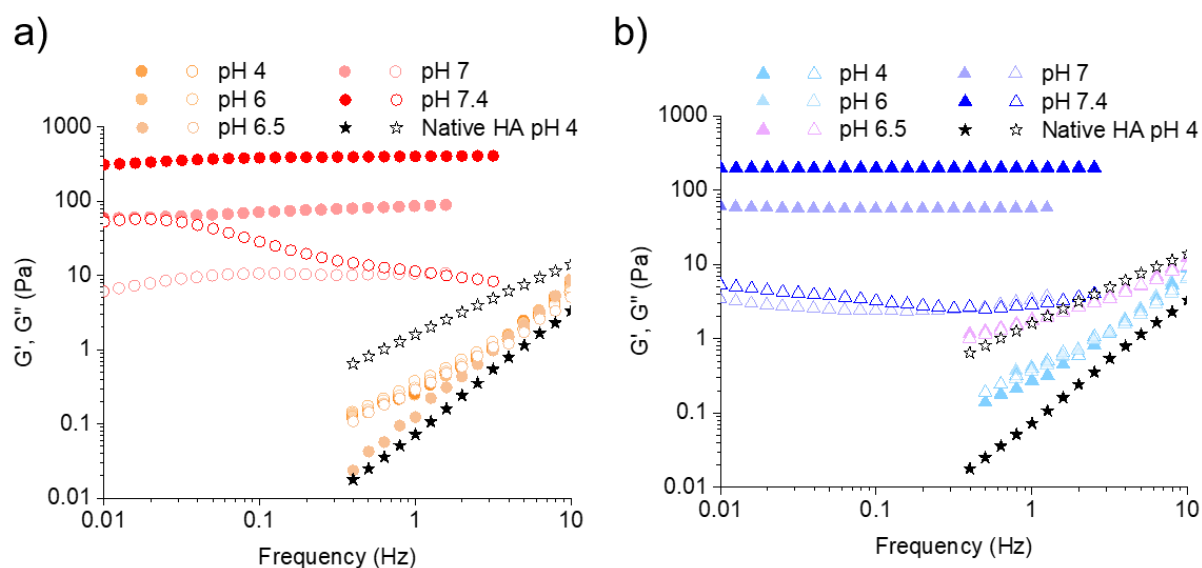
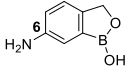
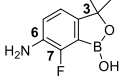
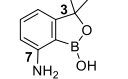


Figure 4. Frequency dependence of G' (filled symbols) and G'' (empty symbols) for the HA360-DMF6ABOR (a) and HA360-DM7ABOR (b) formulations at a pH range of 4.0-7.4.

To gain insight into the binding affinity of DMF6ABOR and DM7ABOR for the HA saccharide units, we performed competition experiments using fructose for which benzoboroxole has the highest affinity compared to D-glucose and hexopyranosides at neutral pH.²⁰ Prior to these experiments, we determined the binding constants (K_a) of the free 6ABOR/D-fructose, free DMF6ABOR/D-fructose, and free DM7ABOR/D-fructose complexes using isothermal titration calorimetry (ITC) and/or ^1H NMR spectroscopy for a better understanding of the results (Figure S12-S17).

As the bound and unbound forms of 6ABOR (DM7ABOR) in the presence of fructose are clearly distinguishable by ^1H NMR spectroscopy (Figure S12 and S16), allowing calculation of their proportion by integration of selected peaks and thereby, estimation of K_a , we also used this technique to evaluate directly the affinity of 6ABOR and DM7ABOR for D-fructose. As shown in Table 2, the K_a values derived from NMR were found to be in relatively good agreement with those measured by ITC. Table 2 also shows higher binding affinity of DMF6ABOR for D-fructose in comparison to 6ABOR and DM7ABOR, displaying similar binding constants.

Table 2. Binding constants of free DMF6ABOR (DM7ABOR) (6ABOR) with D-fructose.

Entry	Derivative	Structure	K_a^a (M^{-1})	K_a^b ITC (M^{-1})	n^b (n saccharide : 1 boronic acid)	ΔH^b ($kJ.mol^{-1}$)	ΔS^b ($J.mol^{-1}.K^{-1}$)
1	6ABOR		461 ± 73	484 ± 50	1.24 ± 0.1	-11.7 ± 2	12.1
2	DMF6ABOR		- ^c	1004 ± 58	0.85 ± 0.05	-19.1 ± 1.2	-6.5
3	DM7ABOR		778 ± 41	513 ± 64	1.2 ± 0.15	-19 ± 2.8	-11.95

^aMeasured from at least two 1H NMR experiments; ^bmeasured from at least two ITC experiments; ^cnot measured because 1H signals of bound and unbound forms of DMF6ABOR were not sufficiently separated to be properly integrated.

Oscillatory shear measurements of HA360-DMF6ABOR and HA360-DM7ABOR after addition of 1 molar equivalent of D-fructose with respect to the grafted DMF6ABOR (DM7ABOR) moieties showed different behaviors (Figure 5a, b and c). Indeed, complete network disassembly is obtained for HA360-DM7ABOR, while a 3-fold decrease of G' in the plateau region is observed for HA360-DMF6ABOR. The fact that the addition of only 1 molar equivalent of D-fructose is enough to compete with most of the benzoboroxole-HA crosslinks in the two networks demonstrates that the interaction of the BOR derivatives with HA is relatively weak and that hydrogel formation relies on multivalent binding effect.³⁰ From this experiment, which indicates a lower sensitivity of the HA360-DMF6ABOR to competitive D-fructose despite the higher K_a value of DMF6ABOR/fructose than DM7ABOR/fructose, it can be also concluded that DMF6ABOR has higher affinity for HA saccharide units than DM7ABOR. This is also supported by the higher G' value measured for the HA360-DMF6ABOR alone than for HA360-DM7ABOR. Indeed, as the plateau modulus scales with the density number of elastically active chains, its value strongly depends on the crosslink density, which is closely related to the binding constant of the BOR/HA saccharide complex. Regarding DMF6ABOR/HA complexation, attempts to quantify this interaction by the determination of K_a using NMR spectroscopy failed. Although hydrogel formation from HA-DMF6ABOR conjugates provide macroscopic evidences of the formation of crosslinks between HA and grafted DMF6ABOR moieties, only the unbound form of free DMF6ABOR could be observed in the 1H NMR spectra in the presence of native HA, precluding K_a measurement (Figure S18). This result makes us believe that the formation of complexes with HA only occurs in the polysaccharide-modified system, because HA presents multiple copies of DMF6ABOR as receptors of HA saccharides, allowing for multivalent complexation. Furthermore, the well-defined spatial disposition of HA saccharide ligands, as components of the repeating unit of the polysaccharide, is likely an important contributing factor to the multivalent effects, and thereby to the strong enhancement of the binding affinity.

With this in mind, we examined the sensitivity of the two networks to the addition of native HA360 at the same molar concentration of HA disaccharide in the HA-BOR conjugates (i.e. 14 mM). As can be seen from Figure 5a, b and c, the native HA sample was able to compete with HA-DMF6ABOR and HA-DM7ABOR by complexation with the grafted BOR moieties. The addition of HA360 resulted in 4.5-fold and 6-fold decreases in the G' plateau values, for the HA-DMF6ABOR and HA-DM7ABOR networks, respectively. Again, a higher resistance to network disruption is observed for HA-DMF6ABOR. These results raised the question of the effect of the HA molar mass on the efficiency to disrupt the networks. Although it is a rather hard question to answer taking into account that native HA can also acts as a crosslinker, we examined the viscoelastic response of HA-DMF6ABOR to the addition of HA100 and HA20 in comparison to HA360, keeping the same concentration for all the native HA samples (i.e. 14 mM). Similar to HA360, the addition of HA100 resulted in a 3-fold decrease in the elastic modulus of the initial gel, whereas a 2-fold decrease was observed when adding HA20 (Figure 5d). Even if HA with higher M_w contribute to the viscoelasticity of the systems, these results indicate that native HA360 and HA100 are more efficient to compete with HA-DMF6ABOR than HA20. This can be ascribed to cooperative effects promoted by high M_w HA.

Finally, besides fructose and native HA, we also investigated the sensitivity of HA360-DMF6ABOR (DM7ABOR) to D-glucose (Figure 5a, b and c). As seen from Figure 5b, almost complete gel disassembly was observed upon addition of 1 or 3 mol. equivalent(s) of D-glucose (with respect to the grafted DM7ABOR moieties) to the HA-DM7ABOR network. This result is in agreement with the weaker interaction of DM7ABOR moieties with HA, as previously indicated by the competition study using D-fructose. On the other hand, as the DMF6ABOR derivative has a higher affinity for HA saccharides, a gel-like behavior was still observed for HA-DMF6ABOR in the presence of glucose (1 or 3 equiv. of glucose/DMF6ABOR moiety). Surprisingly, a slight increase of the plateau modulus is noticed for the HA-DMF6ABOR self-assembly in the presence of D-glucose (Figure 5c). Visual observations of this polymer network upon addition of D-glucose revealed formation of small gel fragments that remained bound together, indicating partial disruption of the macroscopic assembly due to the competitive interaction of DMF6ABOR moieties with glucose. As the multivalent interactions between the DMF6ABOR groups and HA saccharides lead to tightly bound junction zones, only loosely bound junction zones may be disrupted by addition of glucose, which changes the structure of the gel network and thereby, the bulk mechanical properties.

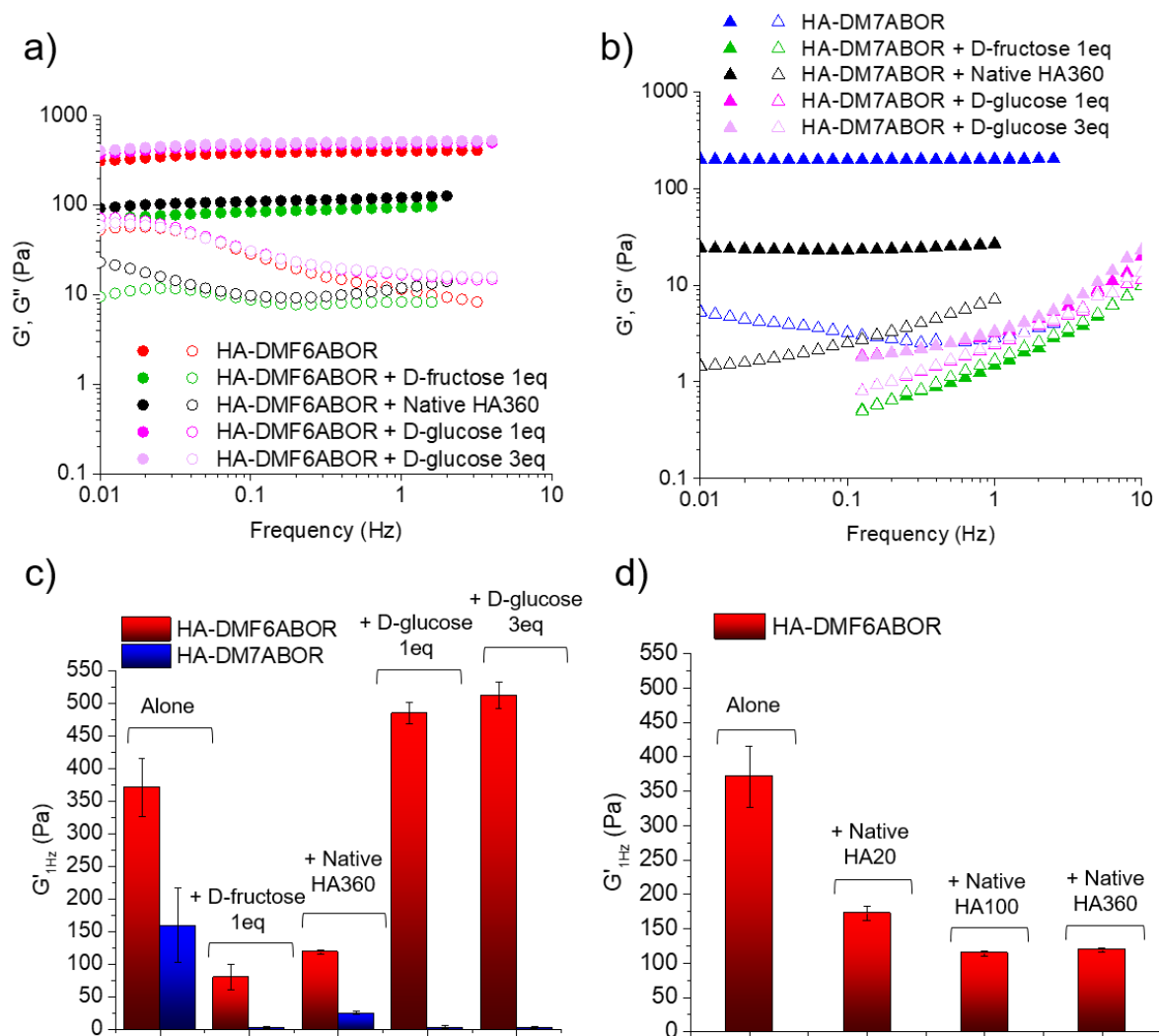


Figure 5. Dynamic rheological behavior from competitive studies of the (a) HA360-DMF6ABOR and (b) HA360-DM7ABOR networks in presence of: free D-fructose (1 molar equivalent) or D-glucose (1 or 3 molar equivalent) or native HA360 (molar concentration of HA disaccharide of 14 mM). (c) Variation of G' (average values from at least two identical experiments) at a frequency of 1 Hz for the HA networks studied. (d) Variation of G' of the HA360-DMF6ABOR network in presence of native HA samples with different molar masses (HA20, HA100 or HA360).

Considering the different strengths of interaction of grafted DMF6ABOR (DM7ABOR) moieties with HA, we investigated the resistance of the HA360-DMF6ABOR (DM7ABOR) hydrogels to failure, as well as their recovery by oscillatory shear experiments. Strain-dependent oscillatory rheology of the HA360-DMF6ABOR (DM7ABOR) networks displayed a broad linear viscoelastic region with network failure at high strains (approximately 400 % for HA360-DMF6ABOR and 600 % for HA360-DM7ABOR, Figure 6a and 6b). The networks were then found to self-heal immediately after removal of the applied strain, showing a recovery of most of their rheological properties (Figure 6a and 6b). Step-strain measurements were then performed to test the recovery of the benzoboroxole-HA properties

following network rupture at high strains (a critical parameter for injectability). A high magnitude strain (300 % for the two hydrogels, corresponding to a drop of approximately 50 % in G') was applied to break the hydrogel structure, followed by a low magnitude strain (5 %) to monitor the rate and extent of recovery of bulk properties (Figure 6c). After a series of four cycles of breaking and reforming, both hydrogels were able to retain a large percentage of their initial G' values within a 3 min recovery period (Figure 6c). However, it is important to note that the two HA networks behave differently. The HA360-DMF6ABOR gel was able to recover 82 % of its initial elastic modulus, which was found to be independent of the HA molar mass, as a similar trend was observed for the HA100-DMF6ABOR hydrogel (Figure S19). On the other hand, the HA360-DM7ABOR hydrogel showed a recovery of 92 % of its initial G' , indicating a better ability of this system to self-heal. The different affinities of DMF6ABOR and DM7ABOR for HA may provide some explanations for the divergent self-healing properties of these systems. The higher interaction of the former with HA saccharides leads to more strongly crosslinked HA chains. In particular, we cannot exclude formation of strongly bound double chains³¹ or loops³² promoted by the fact that the complementary motifs (DMF6ABOR and HA diols) belong to the same polymer chain. Thus, it can be assumed that some chains have dramatically reduced mobility and remain resilient over a large range of strain,³³ preventing complete gel disruption at failure. As a result, the mechanical properties are not fully recovered because of a lower number of elastically active crosslinks in comparison to the initial hydrogel network (Figure 6d). On the other hand, the weaker interaction of DM7ABOR moieties with HA may lead to complete breaking of crosslinks and gel disintegration at failure. This would allow nearly complete hydrogel restructuring, and a better recovery of the rheological properties.

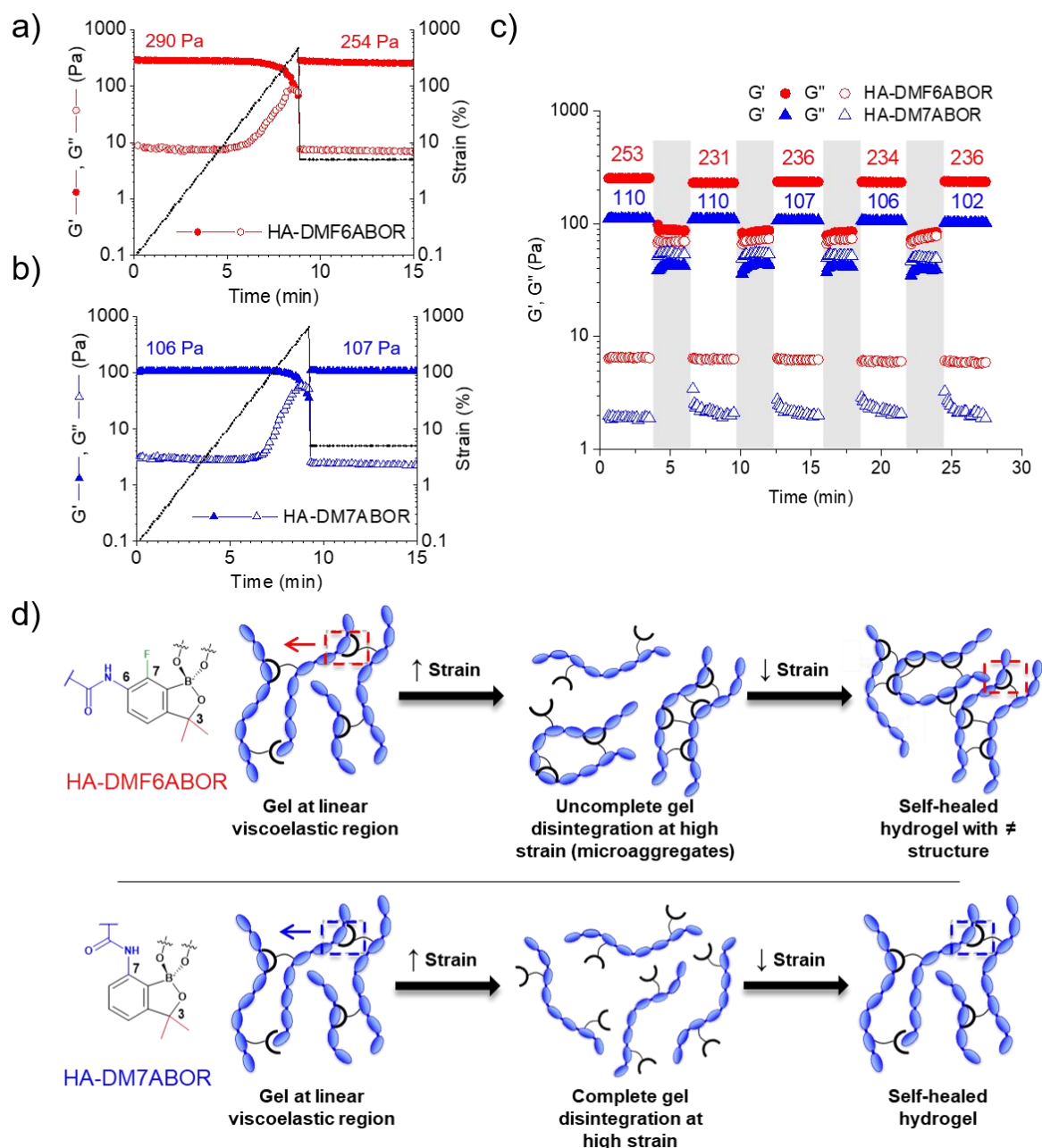


Figure 6. Self-healing of hydrogels after failure. Variation of G' and G'' for HA360-DMF6BOR (a) and HA360-DM7ABOR (b) when increasing strain, followed by the linear recovery of their moduli when strain was reduced. The gels fractured at a strain of, approximately, 400 % (a) and 600 % (b), and immediately recovered their moduli when strain was reduced to 5 %. (c) Four cycles of recovery from strain-induced breakdowns at physiological pH: a strain above the linear viscoelastic region (shaded regions, 300 % of strain) was applied for 2 min, followed by linear recovery measurements during 3 min (unshaded regions, 5 % of strain). (d) Scheme illustrating different macromolecular rearrangements proposed for the two HA hydrogels.

Collectively, these results highlight the key role played by multivalent interactions in the gelation process of HA-DMF6ABOR and HA-DM7ABOR. The multiple copies of DMF6ABOR (DM7ABOR) receptors and of saccharide ligands displayed by the two HA derivatives

promote the formation of multiple crosslinks. Such regions of interchain binding are called junction zones, which contribute to the formation of hydrogels with extremely slow dynamics. Of note, the peculiar response of the HA-DMF6ABOR to glucose and to high strains strongly suggests the presence of junction zones of different stability. The random incorporation of BOR moieties in the HA backbone, yielding a diverse library of spatial arrangement between the grafted BOR moieties, may provide some explanation for this. Also, noteworthy is the remarkable glucose-sensitivity of the HA-DM7ABOR network, which paves the way for the development of injectable glucose-responsive hydrogels as insulin delivery systems. The outstanding properties of HA-DM7ABOR take advantage of both the multivalent effect for gel formation and the weaker binding affinity of DM7ABOR for HA compared to DMF6ABOR allowing for efficient response to glucose. All together, these data raise questions about the special capability of DMF6ABOR and DM7ABOR to bind HA sugar units resulting in hydrogel network formation.

3. Discussion about the outstanding capability of DMF6ABOR and DM7ABOR to bind HA sugar units

Regarding HA diols involved in the complexation, the structure of the polysaccharide, consisting of two repeating disaccharide units of D-glucuronic acid (D-Glc) and *N*-acetyl-D-glucosamine (D-GlcNAc, Figure 1), provides limited options for possible diol binding sites. Indeed, it has been reported that for glucopyranosides, the only significant binding site for benzoboroxole is the C-4/C-6 diol as all vicinal diols in this system are of a *trans* relationship.²⁰ Therefore, it can be assumed that the C-4/C-6 diol of the D-GlcNAc unit is the most probable site of complexation for the BOR derivatives, compared to the C-2/C-3 diol pair of the D-Glc unit. With regard to the special capability of DMF6ABOR and DM7ABOR to complex HA diols under physiological conditions, several possible factors could explain this. It is generally believed that the pK_a of boronic acid is an important factor affecting carbohydrate recognition although there are exceptions in this trend.¹² To assess the role of Lewis acidity, we measured the pK_a of DMF6ABOR and DM7ABOR using a ¹¹B NMR titration, resulting in pK_a values of 6.3 and 7.7, respectively (Figure S20). Compared to standard benzoboroxole (pK_a 7.3²⁹) as well as 6-aminobenzoboroxole (pK_a 6.7, Figure S20), DMF6ABOR is more acidic because of an expected electron-withdrawing effect of fluorine, whereas DM7ABOR has a higher pK_a . These results indicate that other factors related to the structure of DMF6ABOR and DM7ABOR are of central importance in HA diol complexation. In addition to the presence of a *gem*-dimethyl group at the 3-position in the oxaborole, these two BOR derivatives have as a common feature the presence of a hydrogen bond donating substituent *ortho* to the boron center. It is therefore conceivable that these *ortho*-substituents

provide additional stabilization of the benzoboroxole-HA complexes by hydrogen bonding with some hydroxyl groups of HA.

The *gem*-dimethyl group in the oxaborole ring also plays a key role in the binding to HA. As previously discussed, the presence of this group results macroscopically in a decrease of the network dynamics and in most cases, in an increase of the dynamic moduli. The stabilization of boronate ester crosslinks may be related to increased steric bulk caused by these substituents in the oxaborole ring, called *gem*-dimethyl effect.²⁹ Accordingly, the substitution of the BOR heterocycle by bulky methyl groups would allow a widening of the angle between the two bonds of the substituted carbon (C_{Ph} -C3-O, Figure S21). This would lead to a corresponding decrease in the angles enclosed by the bonds of the cycle that form part of the complex (C3-O-B and O-B- C_{Ph}). This effect would therefore alleviate the bond distortion around boron and release ring strain, contributing to stabilize the geometry of the spiro adducts formed between BOR derivatives and HA diols.^{34,35} The *gem*-dimethyl group thus likely acts in synergy with the *ortho*-substituent to enable formation of hydrogel networks exhibiting extremely slow dynamics. Given the dynamic nature of boronate ester bonds, the fact the G' and G'' moduli are nearly independent of the frequency is rather unexpected. Several studies performed on reversibly crosslinked networks demonstrated that the lifetime of the associative group in junction points is the primary determinant of the dynamic rheological properties of the network.^{32,36-39} Even if we had not been able to assess the dissociation rate of the substituted BOR-based crosslinker, it can be reasonably assumed that the remarkably slow dynamics of the HA-DMF6ABOR and HA-DM7ABOR is mainly due to the formation of junction zones made of multiple crosslinks.

Analysis of the DMF6ABOR (DM7ABOR) binding modes to HA by force field simulations confirmed proposed C-4/C-6 diol of the D-Glc unit of HA as binding site for the BOR derivatives and provided some rationale for the possible roles of the *ortho*-substituents in stabilization of the complexes. MD studies were made using a DMF6ABOR model containing a *tert*-butyl group coupled to its amide moiety to simulate the steric effect of the HA chain (Figure 5 and S21). Initially, simulations were performed on a HA tetrasaccharide to confirm the involvement of the C-4/C-6 diol of the D-GlcNAc unit in the binding of the BOR moieties. Comparison between the binding models of DMF6ABOR to the C-4/C-6 diol of D-GlcNAc and, alternatively, to the C-2/C-3 diol pair of D-Glc showed that, the first model provides a more favorable conformation of the benzoboroxole-HA complex as the ring conformation of D-GlcNAc remains in a normal chair conformation thanks to the flexibility of the HA hydroxymethyl group (C-6, Figure 7a). By contrast, the second model involves an unfavorable conformation of HA, as this requires a large deformation of the D-Glc ring unit of HA to form a complex with DMF6ABOR (Figure 7b).

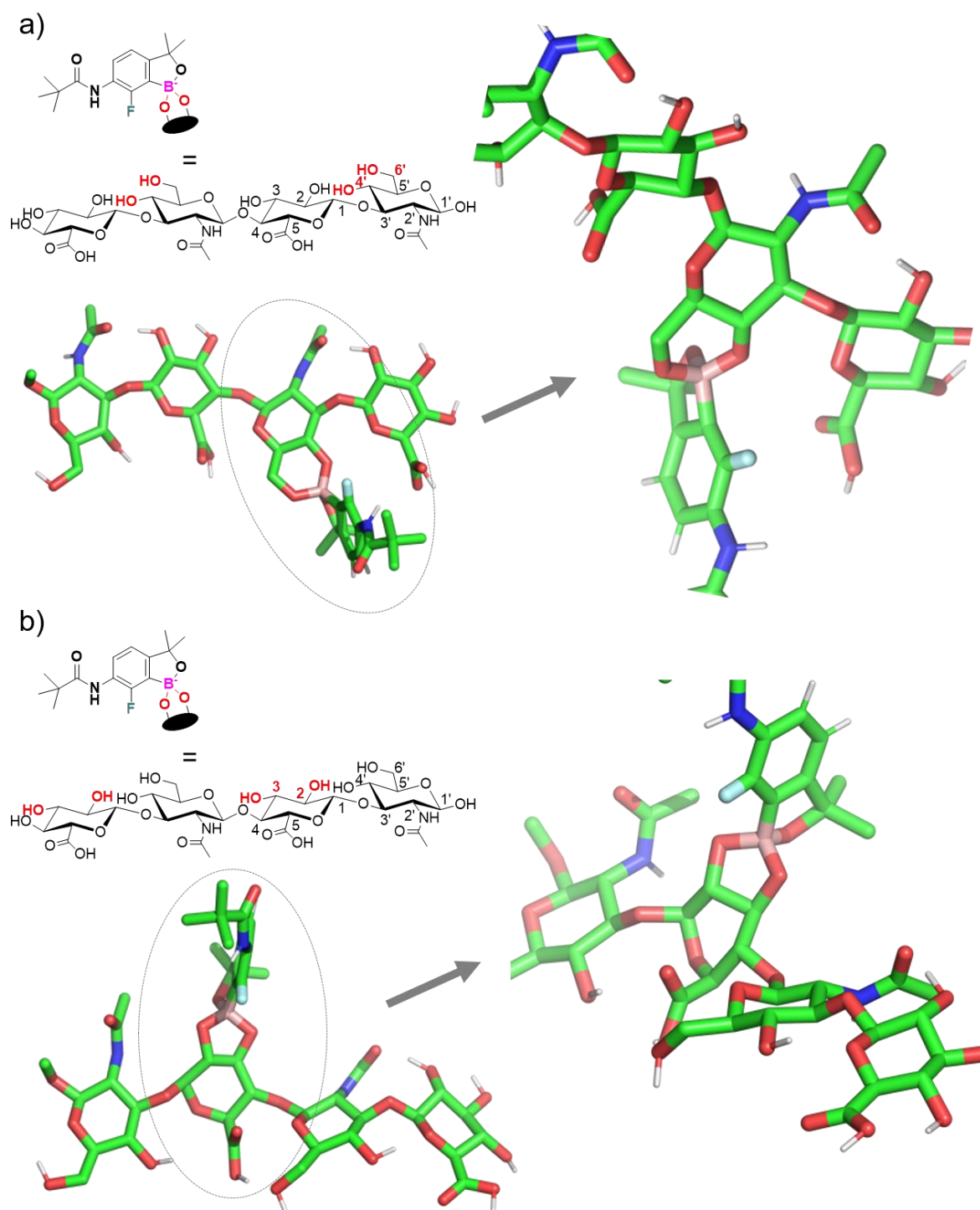


Figure 7. Force field energy minimized structures of two possible complexes for DMF6ABOR and HA (tetrasaccharide HA): (a) DMF6ABOR bound to the C-4/C-6 diol of the D-GlcNAc unit, and (b) DMF6ABOR bound to the C-2/C-3 diol pair of D-Glc. For the simulations, the complexes were first solubilized in spc water and energy minimized (GROMACS, Gromos54a7 ff).

Then, we investigated the structure of the complex formed with DMF6ABOR to prove the essential role of fluorine in the stabilization of the complexes through additional hydrogen

bonds. In order to investigate the possibility of intramolecular hydrogen bonding, we used a model of DMF6ABOR complexed with a HA chain made of 11 saccharides (i.e. 5 D-GlcNac and 6 D-Glc units). However, no direct intramolecular interaction was observed between the hydroxyl groups of HA and fluorine, even when the DMF6ABOR molecule was in a compacted form. These results led us to conclude that intramolecular hydrogen bonding is not a driving force for hydrogel formation (Figure S22). These data together with the high interaction previously demonstrated for DMF6ABOR moieties and HA saccharides make us believe that the formation of tightly bound junction zones in the HA-DMF6ABOR hydrogel is related to multiple intermolecular hydrogen bonding between several DMF6ABOR moieties grafted on HA and a second polysaccharide chain. This indication supports our assumption of the formation of strongly bound HA double chains in the hydrogel network, promoted by the well-defined spatial disposition of D-GlcNac ligands, as components of the repeating unit of HA. Further studies by force field simulations are on the way to investigate the formation of bound junction zones in the HA-DMF6ABOR (DM7ABOR) networks, with formation of additional intermolecular hydrogen bonding between a HA chain grafted with DMF6ABOR (DM7ABOR) moieties and a second HA chain.

4. Conclusion

In summary, we report a new class of self-crosslinking smart hyaluronic acid hydrogels based on the multivalent complexation between custom-made benzoboroxole derivatives and the C-4/C-6 diol of the HA D-GlcNac unit. These novel pH- and carbohydrate-responsive hydrogels were prepared from a single component, hyaluronic acid modified with DMF6ABOR or DM7ABOR. The HA-DMF6ABOR and HA-DM7ABOR conjugates are the first example of polysaccharide derivatives showing self-crosslinking properties via boronate ester bond formation at physiological pH. The molecular origin of gelation behavior of these two HA derivatives lies in the unique structures of the grafted DMF6ABOR and DM7ABOR moieties. Indeed, the *gem*-dimethyl group in their heterocycle and the *ortho*-substituent in their phenyl ring play a key role in their selective binding to the C-4/C-6 diol of the HA D-GlcNac unit, resulting in complexes that are further stabilized via hydrogen bonding with hydroxyl groups of HA. On the other hand, the presence of multiple copies of DMF6ABOR (DM7ABOR) receptors and of diol ligands in the HA derivatives is also an important factor contributing to the gelation mechanism by overcoming the weak binding affinity of the single BOR derivatives towards the HA diol. Because of the dynamic nature of the boronate ester crosslinks, these hydrogel networks show self-healing capability. This feature, combined with the unique biological properties of HA, a polysaccharide which is ubiquitous in the body, makes these new HA-based hydrogels promising candidates as injectable scaffolds for

tissue engineering and cell therapy. Continued investigation of hyaluronic acid as well as other biocompatible polysaccharides modified with such benzoboroxole derivatives will open doors to address the challenge of injectable hydrogels and expand the application space for these materials such as in glucose-sensing and insulin-delivery as well as benzoboroxole-based lectin mimics to prevent viral infections.

5. Experimental section

Materials. Sodium hyaluronate (HA) possessing a weight average molar mass (M_w) of 100 and 360 kg/mol were respectively supplied by Lifecore Biomedical (USA) and donated by Galderma-Nestlé Skin Health. The molar mass distribution and the weight-average molar mass of these samples were determined by size exclusion chromatography using a Waters GPC Alliance chromatograph (USA) equipped with a differential refractometer and a light scattering detector (MALLS) from Wyatt (USA); the solutions were injected at a concentration of 1×10^{-3} g.mL⁻¹ in 0.1 M NaNO₃, at a flow rate of 0.5 mL/min and at a column temperature of 30 °C. The polydispersity index (PDI) of the samples are $M_w/M_n \approx 1.5-2$. The overlap concentrations C^* for these HA samples in buffer at 25 °C are around 3 and 1 g/L. These values were derived from the intrinsic viscosity assuming that $C^*[\eta]$ is about unity.⁴⁰ A HA sample with a lower M_w of 20 kg/mol (used in the competitive rheological studies) was supplied by Lifecore Biomedical (USA). 5-amino-2-hydroxymethylphenylboronic acid (6-aminobenzoboroxole, 6ABOR) was purchased from Combi-Blocks. 4-(4,6-dimethoxy-1,3,5-triazin-2-yl)-4-methylmorpholinium chloride (DMTMM), 4-(2-hydroxyethyl)piperazine-1-ethanesulfonic acid (HEPES), phosphate buffered saline (PBS) and other chemicals were purchased from Sigma-Aldrich-Fluka and were used without further purification.

Methods.

NMR spectroscopy. ¹H, ¹³C and ¹¹B NMR spectra were recorded at 25 °C or 80 °C using a Bruker AVANCE III HD spectrometer operating at 400.13 MHz (¹H), 100.61 MHz (¹³C) and 128.38 MHz (¹¹B). ¹H NMR spectra were recorded by applying a 90° tip angle for the excitation pulse, and a 10 s recycle delay for accurate integration of the proton signals. ¹³C NMR spectra were recorded by applying a 90° tip angle for the excitation pulse and a 2 s recycle delay. Deuterium oxide (D₂O) was obtained from Euriso-top (Saint-Aubin, France). Chemical shifts (δ in ppm) are given relative to external tetramethylsilane (TMS = 0 ppm) and calibration was performed using the signal of the residual protons of the solvent as a secondary reference. All NMR spectra were analyzed with Topspin 3.1 software from Bruker AXS.

Computational methods. First, two possible complexes of DMF6ABOR with HA saccharides (using a HA tetrasaccharide) were studied, with the BOR derivative bound to (i) the C-4/C-6 diol of the D-GlcNAc unit or (ii) the C-2/C-3 diol pair of the D-Glc unit (Figure 7). For a better representation of the DMF6ABOR derivative which is grafted to HA, a DMF6ABOR model containing a *tert*-butyl group coupled to its amide moiety was used to simulate the steric effect of the HA chain. Force field molecular dynamics (MD) simulations were carried out on the complexes. The MD simulations were performed in the GROMACS software, ver. 2018⁴¹ with all-atom Gromos 54a7 force field.⁴² All the MD simulations were performed in an NPT (constant number of atoms, pressure, and temperature) ensemble with velocity-rescale temperature coupling⁴³ and Berendsen pressure coupling algorithms⁴⁴ with temperature and pressure coupling constants of 0.2 ps and 2 ps, respectively. Each complex was placed in a box with dimensions with 8×8×8 nm³ where single point charge (SPC) water molecules⁴⁵ are filled. The structure is then relaxed with energy minimization followed by MD simulation with slow heating from 0 K to 300 K in 2 ns. The system was then equilibrated for 8 ns at 300 K. The production run was performed for 20 ns at 300 K. Further simulations to investigate the possibility of intramolecular hydrogen bonding using a model of DMF6ABOR complexed with a HA chain made of 11 saccharides (i.e. 5 D-GlcNAc and 6 D-Glc units) were performed under the same conditions.

Determination of the pK_a of DMF6ABOR, DM7ABOR and 6ABOR by ¹¹B NMR spectroscopy. ¹¹B NMR chemical shifts of the aminobenzoboroxole compounds were determined with increasing pH (10 % D₂O in H₂O, 16 mM in 0.01 M phosphate buffer). Chemical shifts (δ in ppm) for each ¹¹B spectrum were given relative to external Et₂O-BF₃ in deuterated chloroform as zero. The values of pK_a were determined from the curve fitting of the variation of δ (in ppm) with the pH using the Boltzmann equation (Figure S20).

Synthesis of HA-benzoboroxole derivatives. All HA-BOR conjugates were synthesized by an amide coupling reaction in aqueous conditions. This consisted in adding DMTMM (0.207 g, 0.75 mmol) in a reaction medium containing HA (0.3 g, 0.75 mmol) previously solubilized in water/DMF (3/2, v/v) at a concentration of 3 g/L or 2 g/L respectively for HA samples with a M_w of 100 and 360 kg/mol. The medium was kept under stirring at room temperature for 15 min followed by addition of each aminobenzoboroxole compound (BOR-NH₂) at an amine/HA molar ratio of 0.15. The medium pH was adjusted to 6.5 using 0.5 M NaOH and the reaction was kept under stirring at room temperature for 24-46 h, depending on the BOR-NH₂ derivative. The reaction medium was then purified by ultrafiltration against water and the product was recovered by freeze-drying in 95-98 % yields. All HA-BOR conjugates were

synthesized with a DS of 0.1-0.15, as determined by ^1H NMR spectroscopy (Figure S1-S11, Table 1).

Preparation of formulations based on HA-BOR conjugates. Formulations of HA-BOR derivatives were prepared by simply solubilizing their lyophilized powder recovered from their syntheses in 0.01 M HEPES buffer containing 0.15 M NaCl pH 7.4. Salt was added in order to screen the long range electrostatic repulsions between negatively charged chains. The dissolution time was at least 12 h at 4 °C under stirring. All formulations contained a total polymer concentration of 15 g/L. To study the rheological properties of HA hydrogels as a function of pH, the same buffer was prepared at pH values adjusted to 4, 6, 6.5 and 7. Competition studies were performed by preparing HA hydrogels in the same buffer at pH 7.4, as described above, but at a higher concentration of HA. Then, diol-containing molecules solubilized in the same buffer were added in the gel formulations at room temperature under vortex stirring, in order to obtain a total polymer concentration of 15 g/L. All mixtures were kept under stirring at 4 °C overnight before rheological analysis.

Rheology. Oscillatory experiments were performed with a cone-plate rheometer (AR2000EX from TA Instruments). All the dynamic rheological data were checked as a function of strain amplitude to ensure that the measurements were performed in the linear viscoelastic region. The cone used for viscoelastic samples has a diameter of 2 cm and an angle of 4°, whereas viscous solutions were analyzed using a cone of 6 cm of diameter and an angle of 1°. To prevent water evaporation, the measuring system was surrounded with a low-viscosity silicon oil (50 mPa.s) carefully added to the edges of the cone.

Determination of K_a by ITC. Calorimetric titration experiments were carried out on a Microcal VP-ITC titration microcalorimeter (Northampton, U.S.A.). All titrations were made using solutions of free DMF6ABOR or DM7ABOR (free BOR-NH₂ compounds) and free D-fructose prepared in 0.01 M PBS with pH adjusted to 7.4 (\pm 0.1) using a pH-meter by carefully adding 1 M NaOH when necessary. The reaction cell ($V = 1.4478$ mL) contained a solution of a BOR derivative (Table 3). A series of 28 injections of 5 or 10 μL of a solution of D-fructose was made from a computer-controlled 300 μL microsyringe at an interval of 400 s into the solution contained in the reaction cell, while stirring at 300 rpm at 25°C. The raw experimental data were reported as the amount of heat produced after each injection of BOR derivative as a function of time. The amount of heat produced per injection was calculated by integration of the area under individual peaks by the instrument software, after taking into account heat of dilution. The data were analyzed utilizing the one set of site fitting model (Origin 7.0 software package). Table 3 summarizes the experimental conditions used.

Table 3. Experimental conditions of the calorimetric titrations.

Entry	D-fructose in syringe	[D-fructose] (mM)	Free BOR-NH ₂ in cell	[BOR-NH ₂] (mM)
1	D-fructose	75	6ABOR	2
2	D-fructose	37.5	DMF6ABOR	1
3	D-fructose	56	DM7ABOR	1.5

6. References

- (1) Bull, S. D.; Davidson, M. G.; van den Elsen, J. M. H.; Fossey, J. S.; Jenkins, A. T. A.; Jiang, Y.-B.; Kubo, Y.; Marken, F.; Sakurai, K.; Zhao, J.; et al. Exploiting the Reversible Covalent Bonding of Boronic Acids: Recognition, Sensing, and Assembly. *Acc. Chem. Res.* **2013**, *46* (2), 312–326.
- (2) Cambre, J. N.; Sumerlin, B. S. Biomedical Applications of Boronic Acid Polymers. *Polymer* **2011**, *52* (21), 4631–4643.
- (3) Yesilyurt, V.; Webber, M. J.; Appel, E. A.; Godwin, C.; Langer, R.; Anderson, D. G. Injectable Self-Healing Glucose-Responsive Hydrogels with PH-Regulated Mechanical Properties. *Adv. Mater.* **2016**, *28* (1), 86–91.
- (4) Chen, Y.; Wang, W.; Wu, D.; Nagao, M.; Hall, D. G.; Thundat, T.; Narain, R. Injectable Self-Healing Zwitterionic Hydrogels Based on Dynamic Benzoxaborole–Sugar Interactions with Tunable Mechanical Properties. *Biomacromolecules* **2018**, *19* (2), 596–605.
- (5) Chen, Y.; Diaz-Dussan, D.; Wu, D.; Wang, W.; Peng, Y.-Y.; Asha, A. B.; Hall, D. G.; Ishihara, K.; Narain, R. Bioinspired Self-Healing Hydrogel Based on Benzoxaborole–Catechol Dynamic Covalent Chemistry for 3D Cell Encapsulation. *ACS Macro Lett.* **2018**, *7* (8), 904–908.
- (6) Wang, Y.; Li, L.; Kotsuchibashi, Y.; Vshyvenko, S.; Liu, Y.; Hall, D.; Zeng, H.; Narain, R. Self-Healing and Injectable Shear Thinning Hydrogels Based on Dynamic Oxaborole–Diol Covalent Cross-Linking. *ACS Biomater. Sci. Eng.* **2016**, *2* (12), 2315–2323.
- (7) Wei, Z.; Yang, J. H.; Zhou, J.; Xu, F.; Zrínyi, M.; Dussault, P. H.; Osada, Y.; Chen, Y. M. Self-Healing Gels Based on Constitutional Dynamic Chemistry and Their Potential Applications. *Chem Soc Rev* **2014**, *43* (23), 8114–8131.
- (8) Wang, Y.; Adokoh, C. K.; Narain, R. Recent Development and Biomedical Applications of Self-Healing Hydrogels. *Expert Opin. Drug Deliv.* **2018**, *15* (1), 77–91.
- (9) Taylor, D. L.; in het Panhuis, M. Self-Healing Hydrogels. *Adv. Mater.* **2016**, *28* (41), 9060–9093.
- (10) Hall, D. G. *Boronic Acids: Preparation and Applications in Organic Synthesis, Medicine and Materials*; Vol. 2.
- (11) Brooks, W. L. A.; Sumerlin, B. S. Synthesis and Applications of Boronic Acid-Containing Polymers: From Materials to Medicine. *Chem. Rev.* **2016**, *116* (3), 1375–1397.
- (12) Yan, J.; Springsteen, G.; Deeter, S.; Wang, B. The Relationship among PK_a, PH, and Binding Constants in the Interactions between Boronic Acids and Diols—It Is Not as Simple as It Appears. *Tetrahedron* **2004**, *60* (49), 11205–11209.
- (13) Springsteen, G.; Wang, B. A Detailed Examination of Boronic Acid–Diol Complexation. *Tetrahedron* **2002**, *58* (26), 5291–5300.

- (14) Li, D.; Chen, Y.; Liu, Z. Boronate Affinity Materials for Separation and Molecular Recognition: Structure, Properties and Applications. *Chem. Soc. Rev.* **2015**, *44* (22), 8097–8123.
- (15) Mulla, H. R.; Agard, N. J.; Basu, A. 3-Methoxycarbonyl-5-Nitrophenyl Boronic Acid: High Affinity Diol Recognition at Neutral PH. *Bioorg. Med. Chem. Lett.* **2004**, *14* (1), 25–27.
- (16) Zhang, C.; Losego, M. D.; Braun, P. V. Hydrogel-Based Glucose Sensors: Effects of Phenylboronic Acid Chemical Structure on Response. *Chem. Mater.* **2013**, *25* (15), 3239–3250.
- (17) Yang, X.; Lee, M.-C.; Sartain, F.; Pan, X.; Lowe, C. R. Designed Boronate Ligands for Glucose-Selective Holographic Sensors. *Chem. – Eur. J.* **2006**, *12* (33), 8491–8497.
- (18) Deng, C. C.; Brooks, W. L. A.; Abboud, K. A.; Sumerlin, B. S. Boronic Acid-Based Hydrogels Undergo Self-Healing at Neutral and Acidic PH. *ACS Macro Lett.* **2015**, *4* (2), 220–224.
- (19) Dowlut, M.; Hall, D. G. An Improved Class of Sugar-Binding Boronic Acids, Soluble and Capable of Complexing Glycosides in Neutral Water. *J. Am. Chem. Soc.* **2006**, *128* (13), 4226–4227.
- (20) Bérubé, M.; Dowlut, M.; Hall, D. G. Benzoboroxoles as Efficient Glycopyranoside-Binding Agents in Physiological Conditions: Structure and Selectivity of Complex Formation. *J. Org. Chem.* **2008**, *73* (17), 6471–6479.
- (21) Peters, J. A. Interactions between Boric Acid Derivatives and Saccharides in Aqueous Media: Structures and Stabilities of Resulting Esters. *Coord. Chem. Rev.* **2014**, *268*, 1–22.
- (22) Adamczyk-Woźniak, A.; Borys, K. M.; Sporyński, A. Recent Developments in the Chemistry and Biological Applications of Benzoxaboroles. *Chem. Rev.* **2015**, *115*, 5224–5247.
- (23) Liu, C. T.; Tomsho, J. W.; Benkovic, S. J. The Unique Chemistry of Benzoxaboroles: Current and Emerging Applications in Biotechnology and Therapeutic Treatments. *Bioorg. Med. Chem.* **2014**, *22* (16), 4462–4473.
- (24) Kotsuchibashi, Y.; Agustin, R. V. C.; Lu, J.-Y.; Hall, D. G.; Narain, R. Temperature, PH, and Glucose Responsive Gels via Simple Mixing of Boroxole- and Glyco-Based Polymers. *ACS Macro Lett.* **2013**, *2* (3), 260–264.
- (25) Lin, M.; Sun, P.; Chen, G.; Jiang, M. The Glyco-Stereoisomerism Effect on Hydrogelation of Polymers Interacting via Dynamic Covalent Bonds. *Chem Commun* **2014**, *50* (68), 9779–9782.
- (26) Kotsuchibashi, Y.; Ebara, M.; Sato, T.; Wang, Y.; Rajender, R.; Hall, D. G.; Narain, R.; Aoyagi, T. Spatiotemporal Control of Synergistic Gel Disintegration Consisting of Boroxole- and Glyco-Based Polymers via Photoinduced Proton Transfer. *J. Phys. Chem. B* **2015**, *119* (6), 2323–2329.
- (27) Pettignano, A.; Grijalvo, S.; Häring, M.; Eritja, R.; Tanchoux, N.; Quignard, F.; Díaz Díaz, D. Boronic Acid-Modified Alginate Enables Direct Formation of Injectable, Self-Healing and Multistimuli-Responsive Hydrogels. *Chem. Commun.* **2017**, *53* (23), 3350–3353.
- (28) D'Este, M.; Eglin, D.; Alini, M. A Systematic Analysis of DMTMM vs EDC/NHS for Ligation of Amines to Hyaluronan in Water. *Carbohydr. Polym.* **2014**, *108*, 239–246.
- (29) Tomsho, J. W.; Pal, A.; Hall, D. G.; Benkovic, S. J. Ring Structure and Aromatic Substituent Effects on the pK_a of the Benzoxaborole Pharmacophore. *ACS Med. Chem. Lett.* **2012**, *3* (1), 48–52.

- (30) Jay, J. I.; Lai, B. E.; Myszka, D. G.; Mahalingam, A.; Langheinrich, K.; Katz, D. F.; Kiser, P. F. Multivalent Benzoboroxole Functionalized Polymers as Gp120 Glycan Targeted Microbicide Entry Inhibitors. *Mol. Pharm.* **2010**, *7* (1), 116–129.
- (31) Semenov, A.; Charlot, A.; Auzély-Velty, R.; Rinaudo, M. Rheological Properties of Binary Associating Polymers. *Rheol. Acta* **2007**, *46* (5), 541–568.
- (32) Appel, E. A.; Barrio, J. del; Loh, X. J.; Scherman, O. A. Supramolecular Polymeric Hydrogels. *Chem. Soc. Rev.* **2012**, *41* (18), 6195–6214.
- (33) Yu, K.; Xin, A.; Wang, Q. Mechanics of Self-Healing Polymer Networks Crosslinked by Dynamic Bonds. *J. Mech. Phys. Solids* **2018**, *121*, 409–431.
- (34) Jung, M. E.; Piizzi, G. Gem -Disubstituent Effect: Theoretical Basis and Synthetic Applications. *Chem. Rev.* **2005**, *105* (5), 1735–1766.
- (35) frahn, J. L. Paper Electrophoresis of Hydroxycarboxylic Acids as Their Borate Complexes with Special Reference to Viridifloric, Trachelanthic, Lasiocarpic and Heliotric Acids. *J. Chromatogr. A* **1984**, *314*, 167–181.
- (36) Yount, W. C.; Loveless, D. M.; Craig, S. L. Small-Molecule Dynamics and Mechanisms Underlying the Macroscopic Mechanical Properties of Coordinatively Cross-Linked Polymer Networks. *J. Am. Chem. Soc.* **2005**, *127* (41), 14488–14496.
- (37) Cromwell, O. R.; Chung, J.; Guan, Z. Malleable and Self-Healing Covalent Polymer Networks through Tunable Dynamic Boronic Ester Bonds. *J. Am. Chem. Soc.* **2015**, *137* (20), 6492–6495.
- (38) Yount, W. C.; Loveless, D. M.; Craig, S. L. Strong Means Slow: Dynamic Contributions to the Bulk Mechanical Properties of Supramolecular Networks. *Angew. Chem. Int. Ed.* **2005**, *44* (18), 2746–2748.
- (39) Shen, W.; Kornfield, J. A.; Tirrell, D. A. Dynamic Properties of Artificial Protein Hydrogels Assembled through Aggregation of Leucine Zipper Peptide Domains. *Macromolecules* **2007**, *40* (3), 689–692.
- (40) Macosko, C. W. G. *Rheology: Principles, Measurements, and Applications*; VCH Publishers: Weinheim, Germany, 1994.
- (41) Abraham, M. J.; Murtola, T.; Schulz, R.; Páll, S.; Smith, J. C.; Hess, B.; Lindahl, E. GROMACS: High Performance Molecular Simulations through Multi-Level Parallelism from Laptops to Supercomputers. *SoftwareX* **2015**, *1–2*, 19–25.
- (42) Schmid, N.; Eichenberger, A. P.; Choutko, A.; Riniker, S.; Winger, M.; Mark, A. E.; van Gunsteren, W. F. Definition and Testing of the GROMOS Force-Field Versions 54A7 and 54B7. *Eur. Biophys. J.* **2011**, *40* (7), 843.
- (43) Bussi, G.; Donadio, D.; Parrinello, M. Canonical Sampling through Velocity Rescaling. *J. Chem. Phys.* **2007**, *126* (1), 014101.
- (44) Berendsen, H. J. C.; Postma, J. P. M.; van Gunsteren, W. F.; DiNola, A.; Haak, J. R. Molecular Dynamics with Coupling to an External Bath. *J. Chem. Phys.* **1984**, *81* (8), 3684–3690.
- (45) Berendsen, H. J. C.; Postma, J. P. M.; van Gunsteren, W. F.; Hermans, J. Interaction Models for Water in Relation to Protein Hydration. In *Intermolecular Forces*; Springer: Dordrecht, 1981; pp 331–342.

Supporting Information

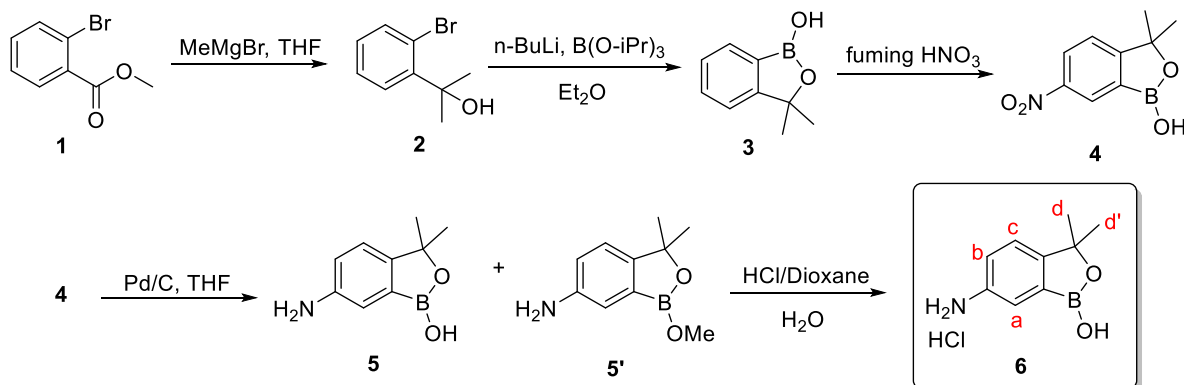
Self-crosslinking smart hydrogels through multivalent interactions between benzoboroxole derivatives and diols from hyaluronic acid

Table of Contents

166	1. Synthesis of aminobenzoboroxole (BOR-NH ₂) compounds
182	2. ¹ H NMR characterization of HA-BOR derivatives synthesized (M _w 100 kg/mol)
191	3. Summary of HA-BOR derivatives synthesized (M _w 360 kg/mol)
191	4. ¹ H NMR characterization of HA-BOR derivatives synthesized (M _w 360 kg/mol)
192	5. Methodology for determining K_a by ¹ H NMR Spectroscopy
194	6. Determination of K_a by ¹ H NMR for 6ABOR and D-fructose
195	7. Determination of K_a by ITC for 6ABOR and D-fructose
196	8. Determination of K_a by ¹ H NMR for DMF6ABOR and D-fructose
197	9. Determination of K_a by ITC for DMF6ABOR and D-fructose
198	10. Determination of K_a by ¹ H NMR for DM7ABOR and D-fructose
199	11. Determination of K_a by ITC for DM7ABOR and D-fructose
200	12. Determination of K_a by ¹ H NMR for DM7ABOR and native HA
201	13. Self-healing characterization of a hydrogel based on HA100-DMF6ABOR
202	14. Determination of the pK_a of free 6ABOR, DMF6ABOR and DM7ABOR derivatives by ¹¹ B NMR spectroscopy
202	15. DMF6ABOR model used for molecular modeling studies
203	16. Investigation of intramolecular hydrogen bond formation between DMF6ABOR by MD simulation
203	17. References

1. Synthesis of aminobenzoboroxole (BOR-NH₂) compounds

3,3-Dimethylbenzo[*c*][1,2]oxaborol-1(3H)-ol (DM6ABOR)



Synthesis of 2:

To a solution of **1** (5.0 g, 23 mmol) in anhydrous THF (80 mL), MeMgBr (23 mL, 3 M) was added dropwise at 0°C and the reaction was allowed to room temperature for 4 h. The mixture was poured by saturated NH₄Cl, extracted with ethyl acetate (3 x 100 mL), washed with brine (2 x 100 mL), dried over Na₂SO₄ and concentrated to yield crude, which was purified by flash column chromatography to give compound **2** (2.6 g, 52 %) as a colorless oil.

Synthesis of 3:

To a solution of n-BuLi (21 mL, 2.5 M) in Et₂O (50 mL) was added dropwise a solution of compound **2** (5.0 g, 23.36 mmol) in Et₂O (50 mL) at -75°C and stirred for 2 h. Triisopropyl borate was added dropwise and the reaction was allowed to room temperature overnight. The mixture was poured by saturated NH₄Cl, extracted with ethyl acetate (3 x 500 mL), washed with brine (2 x 100 mL), dried over Na₂SO₄ and concentrated to yield crude, which was purified by flash column chromatography to give compound **3** (2.0 g, 80 % pure) as a colorless oil, which was used to next step directly.

Synthesis of 4:

A solution of compound **3** in PhNO₃ was added to fuming HNO₃ and stirred at -40°C for 2 h. The mixture was poured onto ice-water and extracted with ethyl acetate (3 x 500 mL), washed with brine (2 x 50 mL), dried over Na₂SO₄ and concentrated to yield crude, which was purified by flash column chromatography (eluent: 10 % to 17 % ethyl acetate) to give compound **4** (0.6 g) as a yellow solid.

Synthesis of 5:

Then, a mixture of compound **4** (120 mg, crude) and Pd/C (50 mg) in THF (10 mL) was stirred at room temperature overnight under H₂ atmosphere. The mixture was filtered and the residue was concentrated to dryness to give crude (300 mg), which was purified by preparative-TLC to give a mixture of compound **5/5'** (70 mg, confirmed by ¹H NMR).

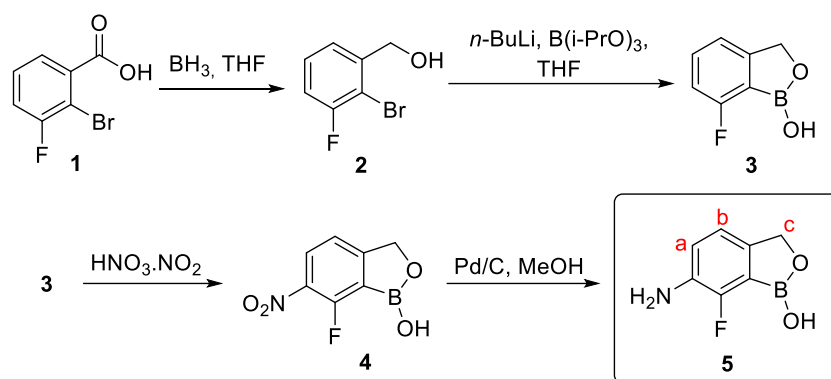
Synthesis of 6 (DM6ABOR):

A mixture of compound **5/5'** (70 mg, crude) in HCl/dioxane and H₂O was stirred at room temperature overnight. The solution was removed under reduced pressure to give compound **6** (80 mg, 98 % pure) as an off white solid.

¹H NMR (400 MHz, DMSO-d₆, 298 K): δ (ppm) 9.32 (br, 1H), 7.63 (s, 1H, **Ha**), 7.53-7.51 (d, 1H, **Hc**), 7.42-7.40 (d, 1H, **Hb**), 1.43 (s, 6H, **Hd-Hd'**).

LC-MS (MS, *m/z*): 178.4 [M+H]⁺.

6-amino-7-fluorobenzo[c][1,2]oxaborol-1(3H)-ol (F6ABOR)



Synthesis of 2:

To a solution of **1** (120 g, 547.9 mmol) in anhydrous THF (1200 mL) was added $\text{BH}_3\cdot\text{THF}$ (1638 mL, 1643.8 mmol, 3.0 eq) at 0 °C. After stirring for 30 min at 0°C, the mixture was warmed to room temperature and stirred for 16 h. HPLC indicated SM was disappeared, the reaction mixture was cooled to 0°C and was carefully quenched with addition of 2000 mL of H_2O . The mixture was then extracted with EtOAc (3 x 400 mL). The organic layer was dried and concentrated in vacuum to give **2** (108 g, crude) as a white solid.

Synthesis of 3:

To a solution of **2** (108 g, 525.7 mmol, 1 eq) and triisopropyl borate (197.7 g, 224.2 mmol, 2 eq) in anhydrous THF (2600 mL) at N_2 atmosphere, $n\text{-BuLi}$ (2.5 M in hexane, 470.7 mL, 1177.7 mmol, 2.2 eq) was added dropwise at -78°C. Then, the mixture was allowed to warm to room temperature and stirred overnight under N_2 . HPLC indicated that the reaction was completed and 1 M HCl (30 mL) was added in the medium followed by extraction with EtOAc (3 x 1000 mL). The organic phase was washed with brine, dried and concentrated under vacuum to give a crude residue, which was purified by silica gel column chromatography to afford **3** (8.0 g, 47 %) as a yellow powder.

$^1\text{H NMR}$ (300 MHz, DMSO-d_6 , 298 K): δ (ppm) 9.25 (br, 1H), 7.57-7.50 (m, 1H), 7.24 (d, $J = 7.2$ Hz, 1H), 7.04 (t, $J = 8.1$ Hz, 1H), 5.01 (s, 2H).

Synthesis of 4:

To a pre-cooled fuming HNO_3 (24 mL), **3** (8.0 g, 52.6 mmol, 1 eq) was added as a solid in portions with the aid of -30 °C cooler. After the completion of addition, the reaction mixture was stirred for 1 h to give a yellow slurry, quenched by the addition of crushed ice (400 g) at the same temperature, and warmed to room temperature slowly. The final yellow suspension was filtrated, washed to pH 6-7 with water to give crude compound **4**, which was purified by silica gel column chromatography to afford **4** (2.7 g, 26.2 %) as a white powder solid.

$^1\text{H NMR}$ (300 MHz, DMSO-d_6 , 298 K): δ (ppm) 8.43-8.24 (m, 1H), 7.48-7.37 (m, 1H), 5.37 (s, 2H).

LC-MS (MS, m/z): 198.1 $[\text{M}+\text{H}]^+$.

Synthesis of 5 (F6ABOR):

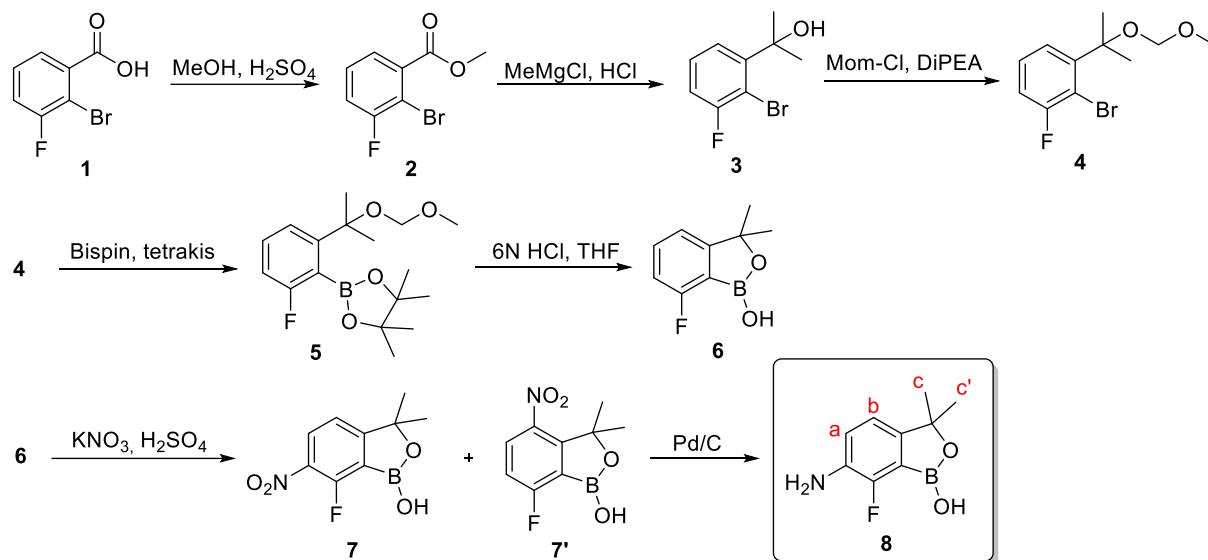
Pd/C (0.27 g) was added to a solution of **4** (2.7 g, 13.7 mmol, 1.0 eq) in THF (27 mL) under N_2 and the suspension was degassed under vacuum and purged with H_2 for three times. The reaction medium was stirred at 25°C for 2 h under H_2 . Thin layer chromatography (eluent: petroleum ether/ethyl acetate 1:1) indicated that the reaction was completed. The reaction

mixture was then filtered to remove Pd/C and the filtrate was concentrated to dryness to give **5** (1.7 g, 77 %).

¹H NMR (300 MHz, DMSO-*d*₆, 298 K): δ (ppm) 9.04 (s, 1H), 6.79-6.73 (m, 1H, **H_b**), 6.68-6.63 (m, 1H, **H_a**), 4.90 (br, 2H), 4.78 (s, 2H, **H_c**).

LC-MS (MS, *m/z*): 168.1 [M+H]⁺.

6-amino-7-fluoro-3,3-dimethylbenzo[*c*][1,2]oxaborol-1(3H)-ol (DMF6ABOR)



Synthesis of 2:

To a stirred solution of **1** (50 g, 0.229 mol) in methanol (500 mL) cooled to 5°C, H₂SO₄ (50 mL) was added dropwise below 10°C under N₂. The reaction mixture was stirred at 85 °C for 16 h and the formation of product was observed by thin layer chromatography. The reaction mixture was completely concentrated and cooled to get solid, diluted with water and stirred for 15 min, filtered and then dried to give 50 g (94 %) of **2** as a white solid.

Synthesis of 3:

To a solution of **2** (50 g, 0.215 mol) in THF (1000 mL) cooled to 5°C, CH₃MgCl (3 M in THF, 287 mL, 0.862 mol) was added dropwise at 10°C under N₂. The mixture was stirred at room temperature for 2 h and quenched with 500 mL of saturated NH₄Cl solution. The mixture was extracted with ethyl acetate and the combined organic layer was washed with brine, dried over sodium sulfate and concentrated under vacuum to provide yellow oil. The crude product was purified by column chromatography (silica gel; eluent: ethyl acetate/hexane, 70:30) to afford 38 g (76 %) of **3** as a colorless liquid.

Synthesis of 4:

To a solution of **3** (38 g, 0.163 mol) in THF (700 mL) DIPEA (84.5 g, 0.655 mol) and MOM-Cl (26.0 g, 0.326 mol) were added successively, followed by reaction mixture heating to 75 °C under stirring for 16 h under N₂. The product formation was observed by TLC. The reaction mixture was concentrated completely, diluted with water (400 mL) and extracted with ethyl acetate (3 x 50 mL). Combined organic layer was dried over anhydrous sodium sulfate, filtered and concentrated to get the crude product, which was purified by column chromatography (silica gel; eluent: ethyl acetate:hexane, 10:90) to afford **4** (30 g, 63%) as a colorless liquid.

Synthesis of 5:

BISPIN (41.2 g, 0.162 mol) and potassium acetate (26.5 g, 0.270 mol) were added to a solution of **4** (30 g, 0.108 mol) in dioxane (600 mL), degassed with argon for 10 min. Pd(PPh₃)₄ (8.78 g, 0.010 mol) was then added the reaction medium was degassed for more 5 min followed by heating to 110°C and stirred for 24 h under N₂. A color change of the reaction mixture from yellow to black indicated the completion of the reaction as observed by TLC. The medium was filtered through celite and the filtrate was concentrated to give **5** (40 g, crude) as a black gum crude which was used directly in the next step without further purification.

Synthesis of 6:

To a solution of **5** (40 g, 0.123 mmol) in THF (200 mL) was added 6 N HCl (200 mL) followed by reaction stirring at room temperature for 4 h. After confirming formation of product by thin layer chromatography, the reaction mixture was concentrated and basified with a NaOH solution until pH 9 and extracted with EtOAc (2 x 200 mL). An aqueous layer was acidified until pH 2 and extracted with ethyl acetate (3 x 50 mL). Combined organic layer was dried over anhydrous sodium sulfate, filtered and concentrated to afford **6** (12 g, 51%, LC-MS 80 %) as a yellow gum.

Synthesis of 7:

KNO₃ (6.73 g, 0.066 mol) was added to a solution of **6** (12 g, 0.066 mol) in H₂SO₄ (100 mL) at 0°C and stirred for 1 h under nitrogen. The reaction mixture was diluted with ice water (400 mL) and extracted with ethyl acetate (3 x 200 mL). Combined organic layer was dried over anhydrous sodium sulfate, filtered and concentrated to give **7/7'** (10 g, 66 %, LC-MS 80 %) as a yellow solid containing a mixture of positional isomers.

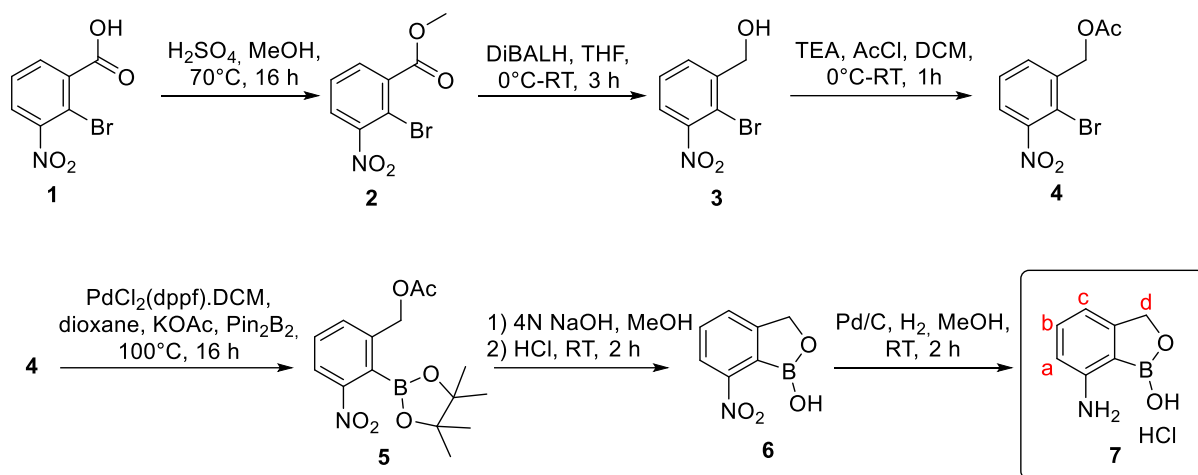
Synthesis of 8 (DMF6ABOR):

To a solution of **7/7'** (8 g, 0.046 mol) in methanol (100 mL) was added 10 % Pd/C (2 g) and stirred at room temperature for 16 h under hydrogen atmosphere. After observation of product formation by thin layer chromatography, the reaction mixture was filtered through celite and the filtrate was concentrated. The crude product was then purified by column chromatography (silica gel; eluent: ethyl acetate:hexane, 25:75) to give **8** (3.0 g, 90 %) as a yellow solid as a mixture of positional isomers purified by preparative HPLC and recovered by lyophilization to afford 1.16 g of an off-white solid.

¹H NMR (400 MHz, DMSO-d₆, 298 K): δ (ppm) 6.90-6.88 (d, 2H, **Hb-Ha**), 4.93 (s, 2H), 1.39 (s, 6H, **Hc-Hc'**).

LC-MS (MS, *m/z*): 195.97 [M+H]⁺.

7-aminobenzo[c][1,2]oxaborol-1(3H)-ol (7ABOR)



Synthesis of 2:

To a stirred solution of **1** (40 g, 162.6 mmol, 1.0 eq) in MeOH (400 mL), H₂SO₄ (20 mL) was added dropwise through addition of funnel at 0°C. After completion of the addition, the medium was heated to 70 °C and stirred for 16 h. The progress of the reaction was monitored by TLC (40 % EtOAc in *n*-hexane). After completion of the reaction, the mixture was fully evaporated under reduced pressure to get a residue. Water (1.5 L) was added to the resulting residue and stirred for 10 min followed by filtration of the solid and drying to get **2** (40.0 g, 94.6 %) as a yellow solid.

¹H NMR (400 MHz, DMSO-*d*₆, 298 K): δ (ppm) 7.85 (dd, *J*=7.6, 1.2 Hz, 1H), 7.76 (dd, *J*=8.0, 1.6 Hz, 1H), 7.52 (t, *J*=8.0 Hz, 1H), 3.98 (s, 3H).

LC-MS (ES, *m/z*): no ionization.

Synthesis of 3:

To a stirred solution of **2** (40 g, 153.82 mmol, 1.0 eq) in THF (400 mL) was added DIBALH (138 mL, 230.73 mmol, 1.5 eq) dropwise at 0°C over a period of 45 minutes. After completion of addition, the reaction mixture was slowly warmed to room temperature and stirred for 3 h. The progress of the reaction was monitored by TLC (40 % EtOAc in *n*-hexane) and, after completion of the reaction, the medium was cooled to 0°C, quenched with saturated ammonium chloride solution (150 mL) and extracted with ethyl acetate (2 x 500 mL). The combined organic layer was washed with saturated brine solution (200 mL), dried over anhydrous sodium sulfate and evaporated under reduced pressure to get crude compound. The crude product was purified by flash column chromatography using 100-200 mesh silica gel, eluted with 20 % ethyl acetate in petroleum ether to afford **3** (35.0 g, 98.06 %) as an off-white solid.

¹H NMR (400 MHz, DMSO-*d*₆, 298 K): δ (ppm) 7.77 (d, *J*=7.6 Hz, 1H), 7.65 (d, *J*=8.4 Hz, 1H), 7.48 (t, *J*=8.0 Hz, 1H), 4.84 (s, 2H), 2.08 (s, 1H, OH).

Synthesis of 4:

TEA (62.5 mL, 452.50 mmol, 3.0 eq) and AcCl (21.5 mL, 301.67 mmol, 2.0 eq) were sequentially added to a stirred solution of **3** (35 g, 150.83 mmol, 1.0 eq) in DCM (350 mL) at 0°C. The reaction mixture was slowly warmed to room temperature and stirred for 1 h. Then, the medium was diluted with DCM (500 mL) and washed with water (500 mL) followed by saturated brine solution (500 mL). The organic layer was dried over sodium sulfate and concentrated under reduced pressure to get a crude compound, which was purified by flash

column chromatography using 100-200 mesh silica gel and eluted with 15 % ethyl acetate in petroleum ether to give **4** (30.0 g, 72.5%) as a pale yellow solid.

¹H NMR (400 MHz, DMSO-*d*₆, 298 K): δ (ppm) 7.67 (d, *J*=7.6 Hz, 1H), 7.62 (d, *J*=7.2 Hz, 1H), 7.47 (d, *J*=8.0 Hz, 1H), 5.26 (s, 2H), 2.17 (s, 3H).

LC-MS (ES, *m/z*): 276.14 [M+H]⁺.

Synthesis of **5**:

Compound **4** (5.0 g, 18.34 mmol, 1.0 eq), Pin₂B₂ (6.94 g, 27.36 mmol, 1.5 eq), AcOK (5.40 g, 55.02 mmol, 3.0 eq) were then taken in 1,4-dioxane (50 mL) degassed with argon for 10 minutes. PdCl₂(dppf)₂ (1.49 g, 1.834 mmol, 0.1 eq) was added to the reaction mixture, degassed for 5 minutes, heated to 100 °C and stirred for 16 h. The progress of the reaction was monitored by TLC (10 % EtOAc in *n*-hexane). The reaction mixture was filtered through celite and the filtrate was evaporated under vacuum to obtain a crude product which was purified by flash column chromatography (silica gel; eluent: 20 % ethyl acetate in petroleum ether) to afford **5** (3.50 g, 59.82 %) as a pale brown solid.

¹H NMR (400 MHz, DMSO-*d*₆, 298 K): δ (ppm) 8.15 (d, *J*=8.4 Hz, 1H), 7.73 (d, *J*=7.6 Hz, 1H), 7.53 (t, *J*=8.0 Hz, 1H), 5.20 (s, 2H), 2.10 (s, 3H), 1.45 (s, 12H).

LC-MS (ES, *m/z*): 322.18 [M+H]⁺.

Synthesis of **6**:

To a solution of **5** (2.5 g, 7.78 mmol, 1.0 eq) in methanol (25 mL), a 4 N NaOH solution was added dropwise at 0 °C. After completion of addition, reaction mixture was warmed to room temperature and stirred for 2 h. The progress of the reaction was monitored by TLC (70 % EtOAc in *n*-hexane) and the completed reaction mixture was cooled to 0 °C followed by adding a 6 N HCl solution (4.5 mL) dropwise. The recovered solid was filtered and dried to give **6** (600 mg, 43.47 %) as a white solid.

¹H NMR (400 MHz, DMSO-*d*₆, 298 K): δ (ppm) 8.94 (s, 1H, OH), 8.02 (d, *J*=8.0 Hz, 1H), 7.82 (d, *J*=7.82 Hz, 1H), 7.75 (t, *J*=7.6 Hz, 1H), 5.09 (s, 2H).

LC-MS (ES, *m/z*): 179.9 [M+H]⁺.

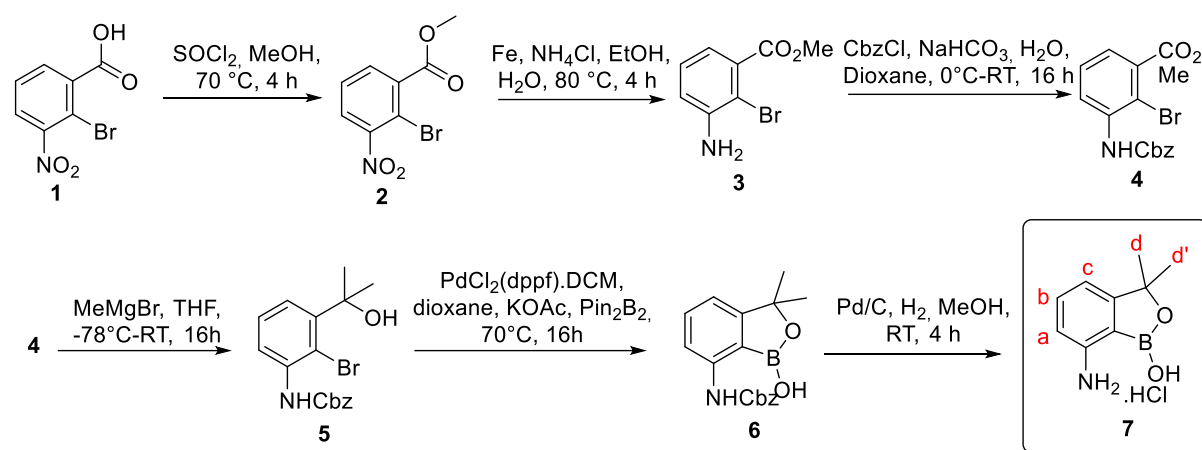
Synthesis of **7** (7ABOR):

Pd/C (2.50 g) was added to a solution of **6** (3.5 g, 19.56 mmol, 1.0 eq) in MeOH (25 mL) under N₂ and the reaction medium was hydrogenated under 50 psi at room temperature for 4 h. The reaction was monitored by TLC (50% EtOAc in hexane). Then, the medium was filtered through celite and washed with MeOH (100 mL). The combined filtrate was evaporated under reduced pressure to afford the final compound as a free amine. This was converted to its corresponding HCl salt in 1,4-dioxane (20 mL) with addition of 4 M HCl in 1,4-dioxane (10 mL) under stirring for 1 h. The reaction mixture was fully evaporated under vacuum to give a crude product which was washed with 50 % ethyl acetate in petroleum ether (100 mL) and filtered the solid to give **7** (2.5 g, 85.91 %) as an off-white solid.

¹H NMR (400 MHz, DMSO-*d*₆, 298 K): δ (ppm) 7.42 (t, *J*=7.6 Hz, 1H, **Hc**), 7.13 (d, *J*=7.2 Hz, 1H, **Hb**), 7.04 (d, *J*=7.6 Hz, 1H, **Ha**), 4.97 (2H, s, **Hd**).

LC-MS (ES, *m/z*): 150.2 [M+H]⁺.

7-amino-3,3-dimethylbenzo[c][1,2]oxaborol-1(3H)-ol (DM7ABOR)



Synthesis of 2:

To a stirred solution of compound **1** (70 g, 284.5 mmol, 1.0 eq) in MeOH (750 mL) was added SOCl_2 (30.97 mL, 426.8 mmol, 1.5 eq) dropwise through addition funnel at 0 °C. The reaction mixture was then heated to 70 °C and stirred for 4 h. The progress of the reaction was monitored by TLC (20 % EtOAc in *n*-hexane). After completion of the reaction, the reaction mixture was fully evaporated under reduced pressure to get residue. Water (1.5 L) was added to the resulting residue with stirring for 10 min. The solid was then filtered and dried to obtain **2** (72.0 g, 97.3%) as an off white solid.

$^1\text{H NMR}$ (400 MHz, DMSO-d_6 , 298 K): δ (ppm) 7.85 (dd, $J=7.6, 1.6$ Hz, 1H), 7.76 (dd, $J=8.0, 1.2$ Hz, 1H), 7.52 (t, $J=8.0$ Hz, 1H), 3.98 (s, 3H).

LC-MS (ES, m/z): no ionization.

Synthesis of 3:

To a stirred solution of compound **2** (72 g, 276.92 mmol, 1.0 eq) in EtOH/water (720 mL, 1:1) were added Fe (77.33 g, 1384.6 mmol, 5.0 eq) and NH_4Cl (118.4 g, 2215 mmol, 8.0 eq) at rt. The reaction medium was heated to 80 °C and stirred for 4 h. The progress of the reaction was monitored by TLC (40 % EtOAc in *n*-hexane). After completion of the reaction, the medium was cooled to rt, filtered through celite bed and the filtrate was evaporated under reduced pressure to give a residue, which was portioned between water (2.0 L) and ethyl acetate (2.0 L). The organic layer was washed with saturated brine solution (500 mL), dried over anhydrous sodium sulfate and evaporated under reduced pressure to give the crude compound **3** (62.0 g, 98.4%) as a brown liquid.

$^1\text{H NMR}$ (400 MHz, DMSO-d_6 , 298 K): δ (ppm) 7.12 (t, $J=8.0$ Hz, 1H), 6.93 (dd, $J=8.0, 1.2$ Hz, 1H), 6.80 (dd, $J=7.6, 1.6$ Hz, 1H), 5.58 (s, 2H), 3.81 (s, 3H).

LC-MS (ES, m/z): 229.8 $[\text{M}+\text{H}]^+$.

Synthesis of 4:

To a stirred solution of **3** (62 g, 271.92 mmol, 1.0 eq) in 1,4-dioxane/water (640 mL, 1:1) were added NaHCO_3 (68.52 g, 815.76 mmol, 3.0 eq) and CbzCl (57.98 mL, 407.88 mmol, 1.5 eq) sequentially at 0 °C, and the reaction mixture was slowly warmed to rt under stirring for 16 h. The progress of the reaction was monitored by TLC (20 % EtOAc in *n*-hexane). After completion of the reaction, the medium was diluted with ethyl acetate (1500 mL) washed with water (1500 mL) followed by saturated brine solution (500 mL). The organic layer was dried over sodium sulfate and concentrated under reduced pressure to get a crude

compound which was purified by flash column chromatography using 100-200 mesh silica gel, eluted with 10 % ethyl acetate in petroleum ether to afford compound **4** (65.0 g, 65.8%) as an off white solid.

¹H NMR (400 MHz, DMSO-*d*₆, 298 K): δ (ppm) 9.25 (s, 1H, NH), 7.67 (dd, *J*=7.6, 2.4 Hz, 1H), 7.49-7.33 (m, 7H), 5.16 (s, 2H), 3.86 (s, 3H).

LC-MS (ES, *m/z*): 365.9 [M+H]⁺.

Synthesis of 5:

To a stirred solution of **4** (40.0 g, 110.19 mmol, 1.0 eq) in THF (400 mL) was added 2.5 M MeMgBr (440.4 mL, 1101 mmol, 10 eq) in diethyl ether dropwise over a period of 30 min at -78 °C (temperature maintained for 1 h). After 1 h, the reaction mixture was slowly warmed to rt and stirred for 16 h. The progress of the reaction was monitored by TLC (40 % EtOAc in *n*-hexane). After completion of the reaction, the medium was quenched with saturated NH₄Cl solution (1000 mL) at 0 °C and extracted with EtOAc (2 x 750 mL). The combined organic layer was washed with saturated brine solution (500 mL), dried over anhydrous sodium sulfate and evaporated under reduced pressure to get a crude compound. The crude product was purified by flash column chromatography using 100-200 mesh silica gel, eluted with 25 % ethyl acetate in petroleum ether to give **5** (24.0 g, 60%) as a brown solid.

¹H NMR (400 MHz, DMSO-*d*₆, 298 K): δ (ppm) 8.98 (m, 1H, NH), 7.71 (dd, *J*=7.2, 2.0 Hz, 1H), 7.41-7.30 (m, 7H), 5.13 (s, 2H), 1.63 (s, 6H).

Synthesis of 6:

Compound **5** (24.0 g, 66.11 mmol, 1.0 eq), Pin2B2 (22.4 g, 99.17 mmol, 1.5 eq) and AcOK (19.46 g, 198.3 mmol, 3.0 eq) were taken in 1,4-dioxane (250 mL) and degassed with argon for 10 minutes. PdCl₂(dppf)₂ (4.83 g, 6.611 mmol, 0.1 eq) was added to the reaction mixture, degassed by additional 5 minutes and then heated to 70 °C under stirring for 16 h. The progress of the reaction was monitored by TLC (40 % EtOAc in *n*-hexane). After completion of the reaction, the medium was filtered through celite pad and the filtrate was evaporated under vacuum to obtain a crude compound, which was purified by flash column chromatography using 100-200 mesh silica gel and eluted with 20 % ethyl acetate in petroleum ether to afford **6** (12.0 g, 58.53%) as a brown solid.

¹H NMR (400 MHz, DMSO-*d*₆, 298 K): δ (ppm) 9.25 (s, 1H, NH), 8.22 (s, 1H, OH), 7.75 (d, *J*=7.6 Hz, 1H), 7.45-7.34 (m, 6H), 7.07 (d, *J*=7.6 Hz, 1H), 5.17 (s, 2H), 1.43 (s, 6H).

LC-MS (ES, *m/z*): 312.14 [M+H]⁺.

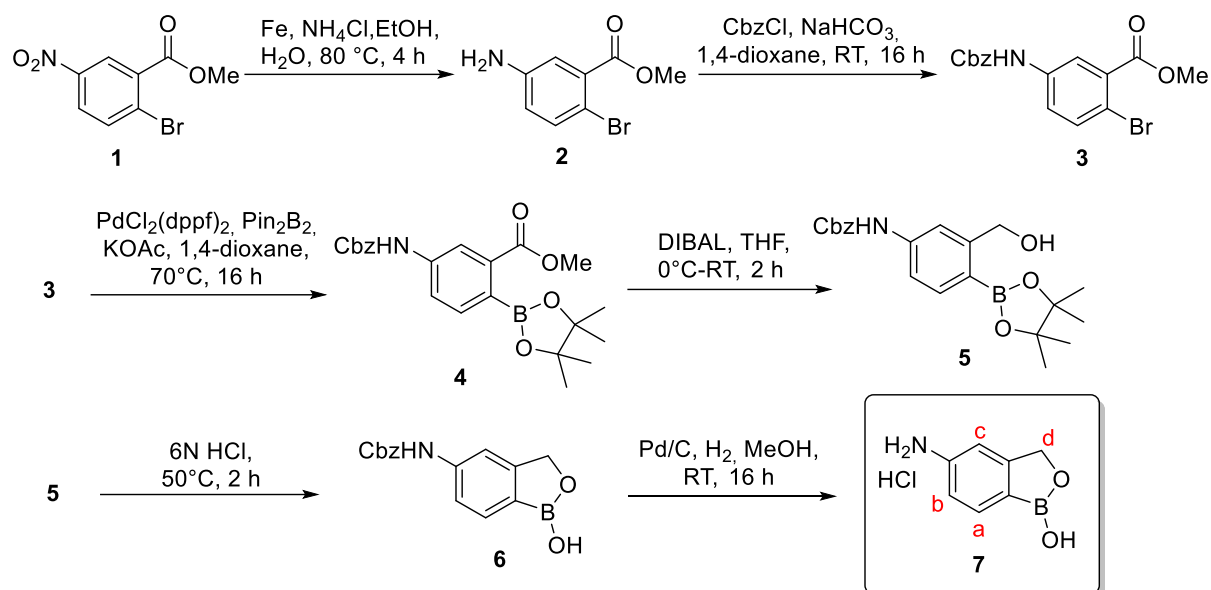
Synthesis of 7 (DM7ABOR):

Pd/C (1.20 g) was added to a solution of compound **6** (12.0 g, 38.58 mmol, 1.0 eq) in MeOH (120 mL) under nitrogen atmosphere, and the reaction mixture was hydrogenated under 50 psi at rt for 4 h. The progress of the reaction was monitored by TLC (50 % EtOAc in *n*-hexane). After completion of the reaction, the medium was filtered through celite pad and washed with MeOH (200 mL). The combined filtrate was evaporated under reduced pressure to afford the final compound as a free amine. The amine was converted to its corresponding HCl by taking the crude compound in DCM (120 mL) with addition of 4M HCl in 1,4-dioxane (120 mL) under stirring for 1 h. The reaction mixture was fully evaporated under reduced pressure to get the crude compound, which was washed with 30 % ethyl acetate in petroleum ether (150 mL) and filtered the solid to give **7** as HCl salt (3.4 g, 41.4%) as an off white solid.

¹H NMR (400 MHz, DMSO-*d*₆, 298 K): δ (ppm) 7.43 (t, *J*=7.6 Hz, 1H, **Hc**), 7.18 (d, *J*=6.8 Hz, 1H, **Hb**), 7.05 (d, *J*=7.6 Hz, 1H, **Ha**), 1.44 (6H, s, **Hd-Hd'**).

LC-MS (ES, m/z): 178.26 [M+H]⁺.

5-aminobenzo[c][1,2]oxaborol-1(3H)-ol (5ABOR)



Synthesis of 2:

To a stirred solution of compound **1** (40 g, 55.03 mmol, 1.0 eq) in EtOH/water (500 mL, 1:1) were added Fe (43.29 g, 775.1 mmol, 5.0 eq) and NH₄Cl (66.34 g, 1240 mmol, 8.0 eq) at rt. The reaction mixture was heated to 80 °C and stirred for 16 h. The progress of the reaction was monitored by TLC (20 % EtOAc in *n*-hexane). After completion of the reaction, the medium was cooled to rt, filtered through celite bed and the filtrate was evaporated under reduced pressure to give a residue. The resulting residue was portioned between water (1.0 L) and ethyl acetate (1.0 L). The organic layer was washed with saturated brine solution (500 mL), dried over anhydrous sodium sulfate and evaporated under reduced pressure to get crude compound **2** (33.0 g, 93.4%) as a brown liquid.

¹H NMR (400 MHz, DMSO-*d*₆, 298 K): δ (ppm) 7.28 (d, *J*=8.8 Hz, 1H), 6.94 (d, *J*=2.4 Hz, 1H), 6.63 (dd, *J*=8.8, 3.2 Hz, 1H), 5.52 (s, 2H, NH₂), 3.80 (s, 3H).

LC-MS (ES, m/z): 231.97 [M+H]⁺.

Synthesis of 3:

To a solution of compound **2** (33 g, 144.12 mmol, 1.0 eq) in THF/water (400 mL, 1:1) were added NaHCO₃ (36.31 g, 432.37 mmol, 3.0 eq) and CbzCl (29.50 g, 172.94 mmol, 1.5 eq) successively at 0 °C. The reaction mixture was slowly warmed to rt and stirred for 16 h. The progress of the reaction was monitored by TLC (20 % EtOAc in *n*-hexane). After completion of the reaction, the medium was diluted with ethyl acetate (1000 mL) and washed with water (1000 mL) followed by saturated brine solution (500 mL). The organic layer was dried over sodium sulfate and concentrated under reduced pressure to obtain a crude compound. The crude product was purified by flash column chromatography using 100-200 mesh silica gel eluted with 10 % ethyl acetate in petroleum ether to give **3** (35.0 g, 67%) as an off white solid.

¹H NMR (400 MHz, DMSO-*d*₆, 298 K): δ (ppm) 10.09 (s, 1H, NH), 7.95 (d, *J*=2.4 Hz, 1H), 7.65 (d, *J*=8.4 Hz, 1H), 7.52 (dd, *J*=8.8, 2.4 Hz, 1H), 7.44-7.34 (m, 5H), 5.16 (s, 2H), 3.85 (s, 3H).

LC-MS (ES, m/z): 362.07 [M+H]⁺.

Synthesis of 4:

Compound **3** (30.0 g, 82.41 mmol, 1.0 eq), Pin₂B₂ (31.1 g, 253.94 mmol, 1.5 eq) and AcOK (24.0 g, 247.25 mmol, 3.0 eq) were taken in 1,4-dioxane (300 mL). The reaction mixture was degassed with argon for 10 minutes. Then, PdCl₂(dppf)₂ (6.69 g, 8.241 mmol, 0.1 eq) was added and the medium was degassed by additional 5 minutes, heated to 70 °C and stirred for 16 h. The progress of the reaction was monitored by TLC (30 % EtOAc in *n*-hexane). After completion of the reaction, the reaction mixture was filtered through celite pad, washed with ethyl acetate (200 mL) and the filtrate was evaporated under vacuum to get a crude compound. This was purified by flash column chromatography using 100-200 mesh silica gel eluted with 20 % ethyl acetate in petroleum ether to afford **4** (30.0 g, 79.43%) as an off white solid.

¹H NMR (400 MHz, DMSO-*d*₆, 298 K): δ (ppm) 10.03 (s, 1H, NH), 8.02 (d, *J*=2.0 Hz, 1H), 7.64 (dd, *J*=8.4, 2.0 Hz, 1H), 7.44-7.32 (m, 6H), 5.16 (s, 2H), 3.82 (s, 3H), 1.29 (s, 12H).

LC-MS (ES, m/z): 412.13 [M+H]⁺.

Synthesis of 5 and 6:

To a solution of **4** (30.0 g, 72.9 mmol, 1.0 eq) in DCM (180 mL) was added 20 % DIBAL in toluene (150 mL) dropwise through addition funnel at 0 °C. After completion of the addition, the medium was slowly warmed to rt and stirred for 2 h. The progress of the reaction was monitored by TLC (40 % EtOAc in *n*-hexane) until formation of **5**. After completion of the reaction, 6 N HCl (200 mL) was added dropwise at 0 °C and the reaction mixture was heated to 50 °C under stirring for 2 h. The reaction medium was then diluted with ethyl acetate (600 mL), washed with water (500 mL) followed by saturated brine solution (200 mL), dried over anhydrous sodium sulfate and evaporated under vacuum to obtain a crude compound. The crude product was purified by flash column chromatography using 100-200 mesh silica gel, eluted with 30 % ethyl acetate in petroleum ether to give compound **6** (13.0 g, 62.95%) as a light brown solid.

¹H NMR (400 MHz, DMSO-*d*₆, 298 K): δ (ppm) 9.92 (s, 1H, NH), 8.98 (s, 1H, OH), 7.61-7.57 (m, 2H), 7.44-7.20 (m, 6H), 5.14 (s, 2H), 4.92 (s, 2H).

LC-MS (ES, m/z): 284.05 [M+H]⁺.

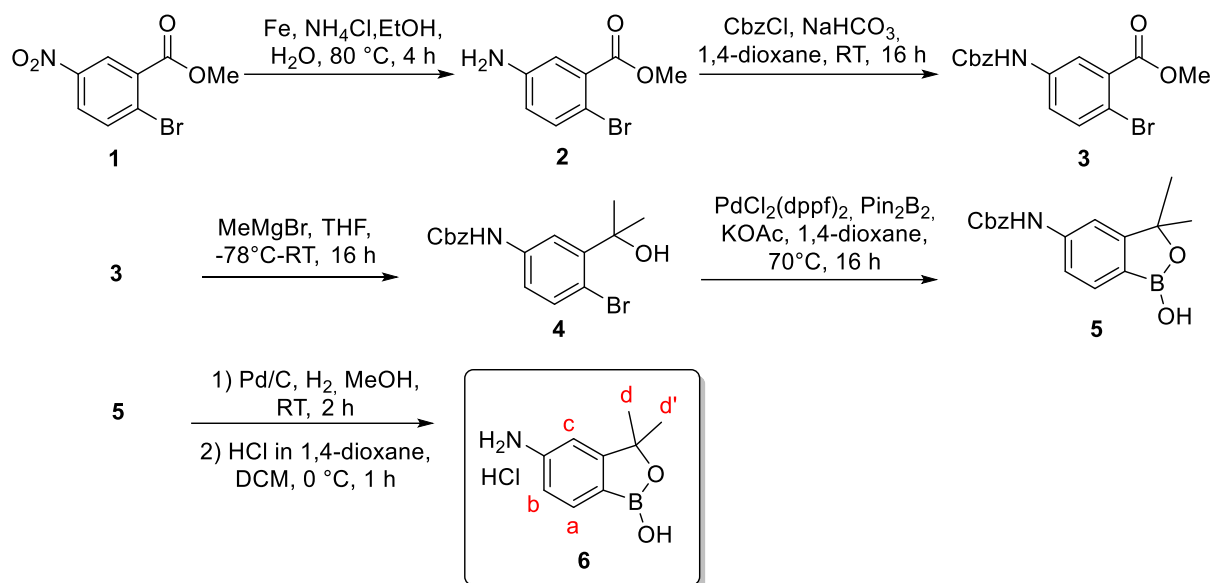
Synthesis of 7 (5ABOR):

Pd/C (13.0 g) was added to a solution of **6** (13.0 g, 45.9 mmol, 1.0 eq) in MeOH (260 mL) under N₂ atmosphere and the reaction mixture was hydrogenated under 50 psi at rt for 16 h. The progress of the reaction was monitored by TLC (50 % EtOAc in hexane). After completion of the reaction, the medium was filtered through celite pad and washed with MeOH (400 mL). The combined filtrate was evaporated under reduced pressure to afford the final compound as free amine. It was converted to the corresponding HCl salt in diethyl ether (100 mL) with addition of 4 M HCl in 1,4-dioxane (100 mL) under stirring for 1 h. The reaction mixture was fully evaporated under reduced pressure to get crude compound. The crude product was washed with 50 % ethyl acetate in diethyl ether (100 mL) and the solid was filtered to give the final compound as HCl salt (4.4 g, 51.82%) as an off white solid.

¹H NMR (400 MHz, DMSO-*d*₆, 298 K): δ (ppm) 7.71 (d, *J*=7.6 Hz, 1H, **Ha**), 7.17 (s, 1H, **Hc**), 7.12 (d, *J*=8.0 Hz, 1H, **Hb**), 4.97 (2H, s, **Hd**).

LC-MS (ES, m/z): 150.2 [M+H]⁺.

5-amino-3,3-dimethylbenzo[c][1,2]oxaborol-1(3H)-ol (DM5ABOR)



Synthesis of 2:

To a stirred solution of **1** (40 g, 55.03 mmol, 1.0 eq) in EtOH/water (500 mL, 1:1), were added Fe (43.29 g, 775.1 mmol, 5.0 eq) and NH_4Cl (66.34 g, 1240 mmol, 8.0 eq) at RT. The reaction mixture was heated to 80 °C and stirred for 16 h. The progress of the reaction was monitored by TLC (20 % EtOAc in *n*-hexane). After completion of the reaction, the medium was cooled to RT, filtered through celite bed and the filtrate was evaporated under reduced pressure to give a residue, which was portioned between water (1.0 L) and ethyl acetate (1.0 L). The organic layer was washed with saturated brine solution (500 mL), dried over anhydrous sodium sulfate and evaporated under reduced pressure to obtain crude compound **2** (33.0 g, 93.4%) as a brown liquid.

$^1\text{H NMR}$ (400 MHz, DMSO- d_6 , 298 K): δ (ppm) 7.28 (d, $J=8.8$ Hz, 1H), 6.94 (d, $J=2.4$ Hz, 1H), 6.63 (dd, $J=8.8, 3.2$ Hz, 1H), 5.52 (s, 2H, NH_2), 3.80 (s, 3H).

LC-MS (ES, m/z): 231.97 $[\text{M}+\text{H}]^+$.

Synthesis of 3:

To a solution of compound **2** (33 g, 144.12 mmol, 1.0 eq) in THF/water (400 mL, 1:1), were added NaHCO_3 (36.31 g, 432.37 mmol, 3.0 eq) and CbzCl (29.50 g, 172.94 mmol, 1.5 eq) successively at 0 °C. The reaction mixture was slowly warmed to RT and stirred for 16 h. The progress of reaction was monitored by TLC (20 % EtOAc in *n*-hexane). After completion of the reaction, the medium was diluted with ethyl acetate (1000 mL) washed with water (1000 mL) followed by saturated brine solution (500 mL). The organic layer was dried over sodium sulfate and concentrated under reduced pressure to get crude compound. Crude product was purified by flash column chromatography using 100-200 mesh silica gel, eluted with 10 % ethyl acetate in petroleum ether to afford **3** (35.0 g, 67%) as an off white solid.

$^1\text{H NMR}$ (400 MHz, DMSO- d_6 , 298 K): δ (ppm) 10.09 (s, 1H, NH), 7.95 (d, $J=2.4$ Hz, 1H), 7.65 (d, $J=8.4$ Hz, 1H), 7.52 (dd, $J=8.8, 2.4$ Hz, 1H), 7.44-7.34 (m, 5H), 5.16 (s, 2H), 3.85 (s, 3H).

LC-MS (ES, m/z): 262.07 $[\text{M}+\text{H}]^+$.

Synthesis of 4:

To a stirred solution of **3** (35.0 g, 96.41 mmol, 1.0 eq) in THF (350 mL) was added 2.5 M MeMgBr (385.6 mL, 964.1 mmol, 10 eq) in diethyl ether dropwise over a period of 30 min at -78 °C (temperature maintained for 1 h). After 1 h, the reaction mixture was slowly warmed to RT and stirred for 16 h. The progress of the reaction was monitored by TLC (40 % EtOAc in *n*-hexane). After completion of the reaction, the medium was quenched with saturated NH₄Cl solution (1000 mL) at 0 °C and extracted with EtOAc (2 x 750 mL). The combined organic layer was washed with saturated brine solution (500 mL), dried over anhydrous sodium sulfate and evaporated under reduced pressure to get crude compound. The crude product was purified by flash column chromatography using 100-200 mesh silica gel, eluted with 25 % ethyl acetate in petroleum ether to give compound **4** (25.0 g, 71.4%) as an off-white solid.

¹H NMR (400 MHz, DMSO-d₆, 298 K): δ (ppm) 9.82 (s, 1H, NH), 7.97 (d, *J*=2.8 Hz, 1H), 7.46-7.30 (m, 7H), 5.19 (s, 1H, OH), 5.15 (s, 2H), 1.58 (s, 6H).

LC-MS (ES, *m/z*): 362.01 [M+H]⁺.

Synthesis of 5:

Compound **4** (25.0 g, 68.87 mmol, 1.0 eq), Pin₂B₂ (26.23 g, 103.3 mmol, 1.5 eq) and AcOK (20.27 g, 206.6 mmol, 3.0 eq) were taken in 1,4-dioxane (250 mL). The reaction medium was degassed with argon for 10 minutes. Then, PdCl₂(dppf)₂ (5.0 g, 6.88 mmol, 0.1 eq) was added, the reaction mixture was degassed by additional 5 minutes, heated to 70 °C and stirred for 16 h. The progress of the reaction was monitored by TLC (40 % EtOAc in *n*-hexane). After completion of the reaction, the medium was filtered through celite pad and the filtrate was evaporated under vacuum to afford a crude compound. The crude product was purified by flash column chromatography using 100-200 mesh silica gel, eluted with 20 % ethyl acetate in petroleum ether to give **5** (17.0 g, 79.43%) as a brown solid.

¹H NMR (400 MHz, DMSO-d₆, 298 K): δ (ppm) 9.95-9.90 (m, 1H, NH), 8.83 (s, 1H, OH), 7.59-7.49 (m, 2H), 7.44-7.29 (m, 6H), 5.16 (s, 2H), 1.40 (s, 6H).

LC-MS (ES, *m/z*): 310.19 [M+H]⁺.

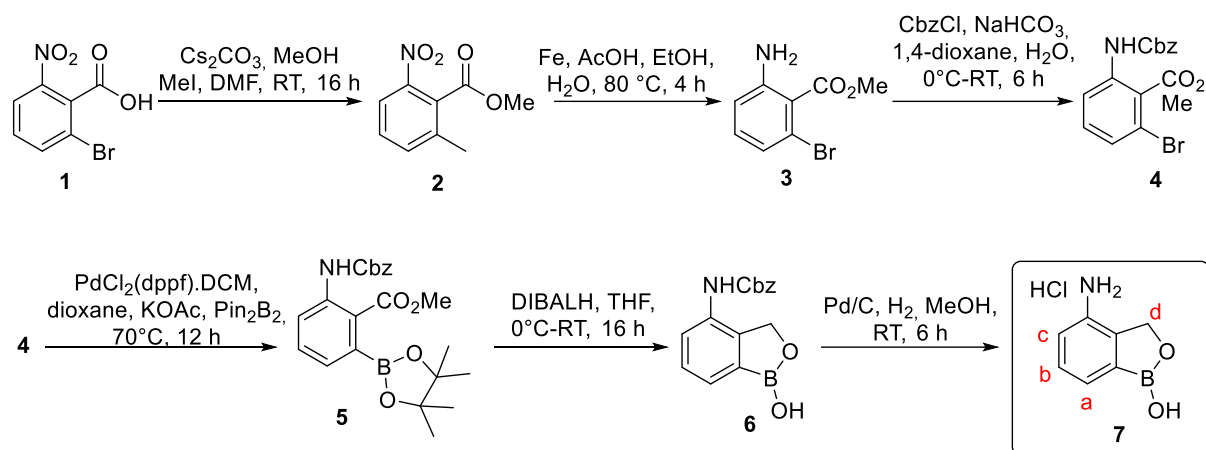
Synthesis of 6 (DM5ABOR):

Pd/C (1.70 g) was added to a solution of **5** (17.0 g, 54.63 mmol, 1.0 eq) in MeOH (200 mL) under N₂ and the reaction was hydrogenated under 50 psi for 16 h. The progress of the reaction was monitored by TLC (50 % EtOAc in *n*-hexane). After completion of the reaction, the medium was filtered through celite pad and washed with MeOH (300 mL). The combined filtrate was evaporated under reduced pressure to afford final compound as free amine. Compound was converted to its corresponding HCl salt in DCM (170 mL) with addition of 4 M HCl in 1,4-dioxane (170 mL) under stirring for 1 h. The reaction mixture was fully evaporated under reduced pressure to obtain a crude compound, which was washed with 30 % ethyl acetate in petroleum ether to give **6** as HCl salt (6.2 g, 53.12%) as an off white solid.

¹H NMR (400 MHz, DMSO-d₆, 298 K): δ (ppm) 7.60 (d, *J*=8.0 Hz, 1H, **Ha**), 7.03 (s, 2H, **Hc-Hb**), 1.42 (6H, s, **Hd-Hd'**).

LC-MS (ES, *m/z*): 178.26 [M+H]⁺.

4-aminobenzo[c][1,2]oxaborol-1(3H)-ol (**4ABOR**)



Synthesis of 2:

To a stirred solution of **1** (110 g, 447.15 mmol, 1.0 eq) in MeOH (1000 mL), Cs₂CO₃ (72.8 g, 223.5 mmol, 0.5 eq) was added at RT under stirring for 30 min. The reaction mixture was fully evaporated under reduced pressure to get a residue. To the resulting residue taken in DMF (1000 mL), was added MeI (33.4 mL, 141.94 mmol, 1.2 eq) dropwise through addition funnel at 0 °C, the reaction mixture was slowly warmed to RT and stirred for 16 h. The progress of the reaction was monitored by TLC (25 % EtOAc in *n*-hexane). After completion of the reaction, the medium was diluted with ice cooled water (1.5 L), the solid was filtered and dried to afford **2** (110 g, 94%) as a white solid.

¹H NMR (400 MHz, DMSO-*d*₆, 298 K): δ (ppm) 8.17 (d, *J*=7.6 Hz, 1H), 7.92 (d, *J*=8.0 Hz, 1H), 7.42 (d, *J*=8.0 Hz, 1H), 4.02 (s, 3H).

LC-MS (ES, *m/z*): 259.92 [M+H]⁺.

Synthesis of 3:

To a solution of compound **2** (110 g, 424.7 mmol, 1.0 eq) in EtOH (2.0 L), were added AcOH (550 mL) followed by Fe (118.1 g, 2123.5 mmol, 5.0 eq) at RT. The reaction mixture was heated to 80 °C and stirred for 4 h. The progress of the reaction was monitored by TLC (25 % EtOAc in *n*-hexane). After completion of the reaction, the medium was fully evaporated under reduced pressure to give a residue. The resulting residue was diluted with water (1.5 L), basified with NaHCO₃ and extracted with ethyl acetate (1 L x 2). The organic layer was dried over anhydrous sodium sulfate and evaporated under reduced pressure to obtain the crude compound **3** (80.0 g, 82.2%) as a brown liquid.

¹H NMR (400 MHz, DMSO-*d*₆, 298 K): δ (ppm) 7.01 (d, *J*=8.0 Hz, 1H), 6.76 (d, *J*=8.0 Hz, 1H), 6.71 (d, *J*=8.0 Hz, 1H), 5.64 (s, 2H, NH₂), 3.82 (s, 3H).

LC-MS (ES, *m/z*): 229.9 [M+H]⁺.

Synthesis of 4:

NaHCO₃ (29.2 g, 349.39 mmol, 2.0 eq) and CbzCl (37.5 mL, 262.04 mmol, 1.5 eq) were sequentially added to a stirred solution of **3** (40 g, 174.69 mmol, 1.0 eq) in THF/water (800 mL, 1:1) at 0 °C. The reaction mixture was slowly warmed to RT and stirred for 6 h. The progress of the reaction was monitored by TLC (20 % EtOAc in *n*-hexane). After completion of the reaction, the medium was diluted with ethyl acetate (1000 mL) and washed with water (1000 mL) followed by saturated brine solution (500 mL). The organic layer was dried over sodium sulfate and concentrated under reduced pressure to get crude compound. Crude

product was purified by flash column chromatography using 100-200 mesh silica gel, eluted with 10 % ethyl acetate in petroleum ether to afford **4** (50.0 g, 78.8%) as a yellow liquid.

¹H NMR (400 MHz, DMSO-*d*₆, 298 K): δ (ppm) 9.57 (s, 1H, NH), 7.48 (d, *J*=8.4 Hz, 2H), 7.40-7.20 (m, 6H), 5.16 (s, 2H), 3.76 (s, 3H).

LC-MS (ES, *m/z*): 362.05 [M+H]⁺.

Synthesis of **5**:

Compound **4** (50.0 g, 137.36 mmol, 1.0 eq), Pin₂B₂ (41.8 g, 164.83 mmol, 1.5 eq) and AcOK (40.3 g, 412.08 mmol, 3.0 eq) were taken in 1,4-dioxane (500 mL). The reaction medium was degassed with argon for 10 min. PdCl₂(dppf)₂.DCM (5.60 g, 6.86 mmol, 0.05 eq) was added to the reaction mixture, degassed by additional 5 minutes, heated to 70 °C and stirred for 12 h. The progress of the reaction was monitored by TLC (30 % EtOAc in *n*-hexane). After completion of the reaction, the medium was filtered through celite pad, washed with ethyl acetate (500 mL) and the filtrate was evaporated under vacuum to give a crude compound. The crude product was purified by flash column chromatography using 100-200 mesh silica gel, eluted with 20 % ethyl acetate in petroleum ether to afford **5** (40.0 g, 70.67%) as an off white solid.

¹H NMR (400 MHz, DMSO-*d*₆, 298 K): δ (ppm) 9.59 (s, 1H, NH), 7.81 (d, *J*=8.0 Hz, 1H), 7.51 (t, *J*=8.0 Hz, 1H), 7.42-7.34 (m, 5H), 7.25-7.23 (m, 1H), 5.14 (s, 2H), 3.75 (s, 3H), 1.28 (s, 12H).

LC-MS (ES, *m/z*): 412.18 [M+H]⁺.

Synthesis of **6**:

To a solution of **5** (40.0 g, 97.32 mmol, 1.0 eq) in DCM (500 mL), was added 20 % DIBALH in toluene (200 mL) dropwise through addition funnel at 0 °C. The reaction mixture was then slowly warmed to RT and stirred for 2 h. The progress of the reaction was monitored by TLC (40 % EtOAc in *n*-hexane). After completion of the reaction, 6 N HCl (200 mL) was added dropwise at 0 °C, and the medium was heated to 50 °C under stirring for 2 h (reaction also monitored by TLC). After completion of the reaction, the medium was diluted with DCM (500 mL), washed with water (500 mL) followed by saturated brine solution (200 mL), dried over anhydrous sodium sulfate and evaporated under vacuum to obtain a crude compound. The crude product was purified by flash column chromatography using 100-200 mesh silica gel, eluted with 40-50 % ethyl acetate in petroleum ether to give **6** (16.0 g, 58.18%) as an off white solid.

¹H NMR (400 MHz, DMSO-*d*₆, 298 K): δ (ppm) 9.32 (s, 1H, NH), 9.14 (s, 1H, OH), 7.62 (d, *J*=8.0 Hz, 1H), 7.48-7.30 (m, 7H), 5.15 (s, 2H), 4.97 (s, 2H).

LC-MS (ES, *m/z*): 284.08 [M+H]⁺.

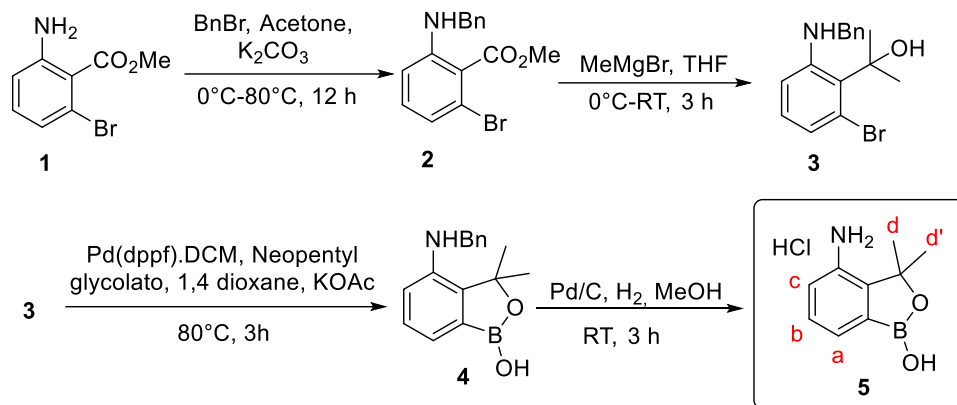
Synthesis of **7 (4ABOR)**:

Pd/C (13.0 g) was added to a solution of **6** (16.0 g, 56.5 mmol, 1.0 eq) in MeOH (300 mL) under nitrogen atmosphere. The reaction mixture was hydrogenated under 50 psi at RT for 6 h. The progress of the reaction was monitored by TLC (50 % EtOAc in *n*-hexane). After completion of the reaction, the medium was filtered through celite pad and washed with MeOH (400 mL). The combined filtrate was evaporated under reduced pressure to afford the final compound as free amine. It was converted to its corresponding HCl salt in diethyl ether (100 mL) with addition of 4 M HCl in 1,4-dioxane (100 mL) under stirring for 1 h. The reaction mixture was fully evaporated under reduced pressure to get crude compound. The crude product was washed with 30 % acetone in ethyl acetate (100 mL) and the solid was filtered to give the final compound **7** as HCl salt (6.1 g, 71.25%) as a white solid.

¹H NMR (400 MHz, DMSO-d₆, 298 K): δ (ppm) 7.61 (d, *J*=7.2 Hz, 1H, **Ha**), 7.41-7.34 (m, 2H, **Hb-Hc**), 5.07 (2H, s, **Hd**).

LC-MS (ES, *m/z*): 150.1 [M+H]⁺.

4-amino-3,3-dimethylbenzo[c][1,2]oxaborol-1(3H)-ol (DM4ABOR)



Synthesis of 2:

K₂CO₃ (57.4 g, 416 mmol) was added to a solution of **1** (48 g, 208 mmol) in acetone (500 mL) and the reaction medium was stirred at RT for 15 min. BnBr (53.35 g, 213 mmol) was then added and the medium was stirred at RT for 12 h. The reaction progress was monitored by TLC (25 % EtOAc in *n*-hexane). After completion of the reaction, the reaction mixture was quenched with water (250 mL) and extracted with ethyl acetate (1 L). Combined organic layers were washed with saturated NaHCO₃ solution (250 mL) and brine solution (250 mL), dried over sodium sulfate and concentrated under reduced pressure to afford the crude compound **2** as a brown gummy. The crude product was purified by silica gel column chromatography (60-120 mesh) initially eluted with 5-7 % ethyl acetate in petroleum ether. The collected fractions were combined and concentrated under reduced pressure to obtain **2** (40 g, 59 %) as a pale yellow liquid.

¹H NMR (400 MHz, DMSO-d₆, 298 K): δ (ppm) 7.32-7.29 (m, 2H), 7.28-7.20 (m, 3H), 7.07-6.98 (m, 1H), 6.91-6.89 (dd, *J* = 7.6 Hz, 0.8 Hz, 1H), 6.56-6.53 (dd, *J* = 7.6 Hz, 0.8 Hz, 1H), 6.15 (s, 1H), 4.36 (s, 2H), 3.92 (s, 3H).

LC-MS (ES, *m/z*): 320.06 [M+H]⁺.

Synthesis of 3:

To a solution of **2** (40 g, 125 mmol) in THF (500 mL) was added MeMgBr (400 mL) dropwise over the period of 30 min at 0 °C. The medium was stirred at 0 °C for 15 min and then at RT for 16 h. The reaction progress was monitored by TLC (25 % EtOAc in *n*-hexane). After completion of the reaction, the reaction mixture was quenched with saturated ammonium chloride solution (600 mL) and extracted with ethyl acetate (3 x 500 mL). The combined organic layers were dried over sodium sulfate and concentrated under reduced pressure to afford crude compound **3**, which was washed with pentane and dried to give **3** (35 g, 87 %) as a white solid.

¹H NMR (400 MHz, DMSO-d₆, 298 K): 7.34-7.26 (m, 5H), 6.96-6.93 (dd, *J* = 8.0 Hz, 1.2 Hz, 1H), 6.84-6.80 (t, *J* = 8.4 Hz, 1H), 6.56-6.54 (d, *J* = 8.4 Hz, 1H), 4.30 (s, 2H), 1.92 (s, 6H).

LC-MS (ES, *m/z*): 320.09 [M+H]⁺.

Synthesis of 4:

To a solution of **3** (35 g, 109 mmol), neopentyl glycolato diborane (37.03 g, 163 mmol) and KOAc (32.1 g, 327 mmol), Pd(dppf)Cl₂.DCM (4.45 g, 5.45 mmol) in 1,4 dioxane (350 mL) was added and heated to 70 °C for 6 h under N₂. The reaction progress was monitored by TLC (25 % EtOAc in *n*-hexane). After completion of the reaction, the medium was filtered through celite bed and washed with ethyl acetate (2 x 200 mL) and the filtrate was evaporated under vacuum to get crude compound **4** as a brown gummy. The crude product was purified by silica gel column chromatography (100-200 mesh) initially eluted with 5-7 % ethyl acetate in petroleum ether and the collected fractions were combined and concentrated under reduced pressure to give **4** (20 g, 68 %) as a pale yellow liquid.

¹H NMR (400 MHz, DMSO-d₆, 298 K): 7.37-7.26 (m, 5H), 7.22-7.16 (m, 1H), 7.10-7.05 (m, 1H), 6.74-6.67 (m, 1H), 4.39 (s, 2H), 1.63 (s, 6H).

LC-MS (ES, *m/z*): 268.22 [M+H]⁺.

Synthesis of 5 (DM4ABOR):

To a stirred solution of **4** (20 g, 74.9 mmol) in methanol (200 mL), was added Pd/C (10 g) in one charge wet with ethyl acetate. The reaction was hydrogenated at 30 psi (balloon pressure). The reaction progress was monitored by TLC (40 % EtOAc in *n*-hexane). After completion of the reaction, the reaction medium was filtered through celite bed, washed with methanol (2 x 100 mL) and the filtrate was evaporated under vacuum to get crude compound **5** as a brown gummy. The crude product was washed with diethyl ether (2 x 200 mL) followed by addition of 4 M HCl in dioxane under stirring for 1 h. The reaction medium was then evaporated under vacuum to afford **5** (12.218 g (77%)) as a white solid

¹H NMR (400 MHz, DMSO-d₆, 298 K): 8.07 (br, 1H), 7.53-7.22 (m, 3H, **Ha-Hb-Hc**), 5.32 (br, 3H), 1.54 (s, 6H, **Hd-Hd'**).

LC-MS (ES, *m/z*): 178.26 [M+H]⁺.

2. ^1H NMR characterization of HA-BOR derivatives synthesized (M_w 100 kg/mol)

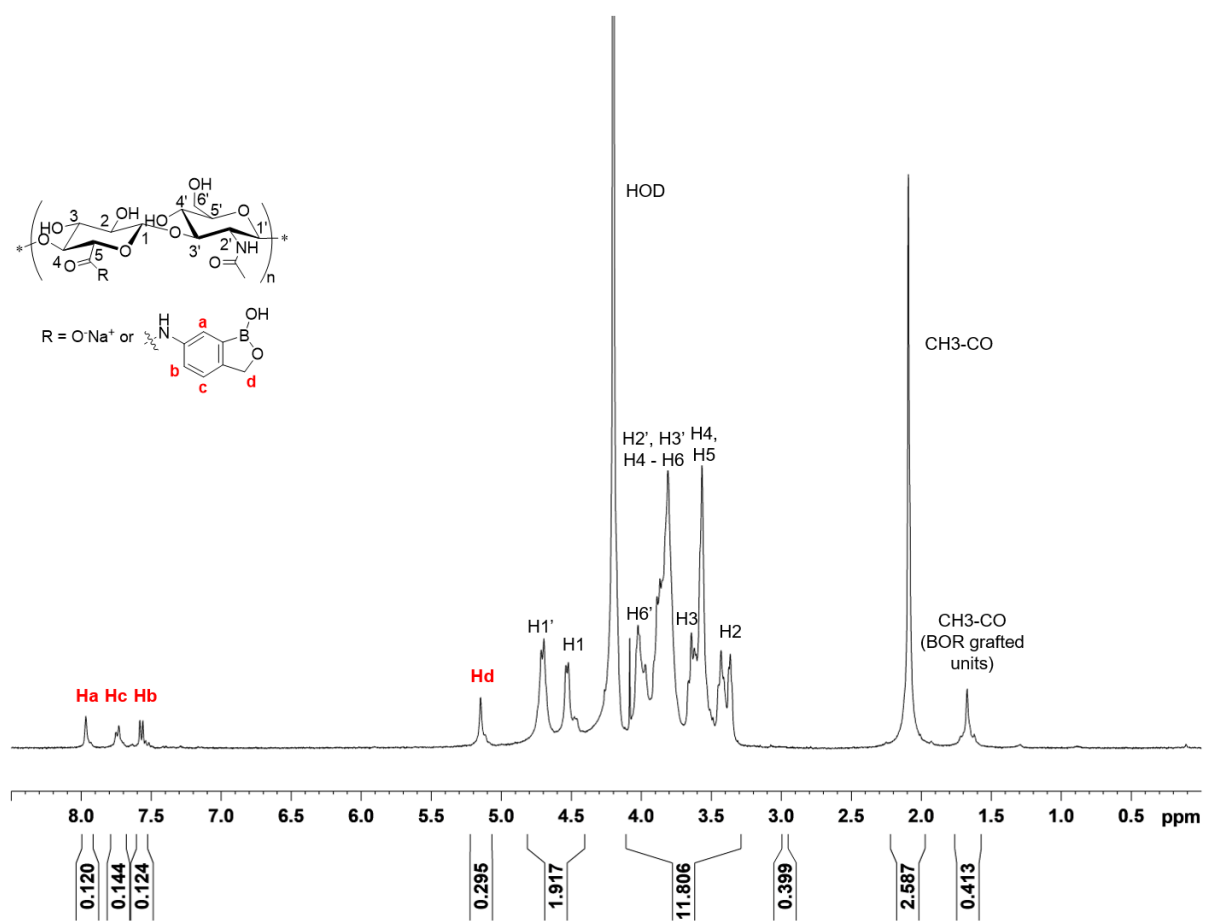


Figure S1. ^1H NMR spectrum (400 MHz, D_2O , $6 \text{ mg}\cdot\text{mL}^{-1}$, 80°C) of HA100-6ABOR.

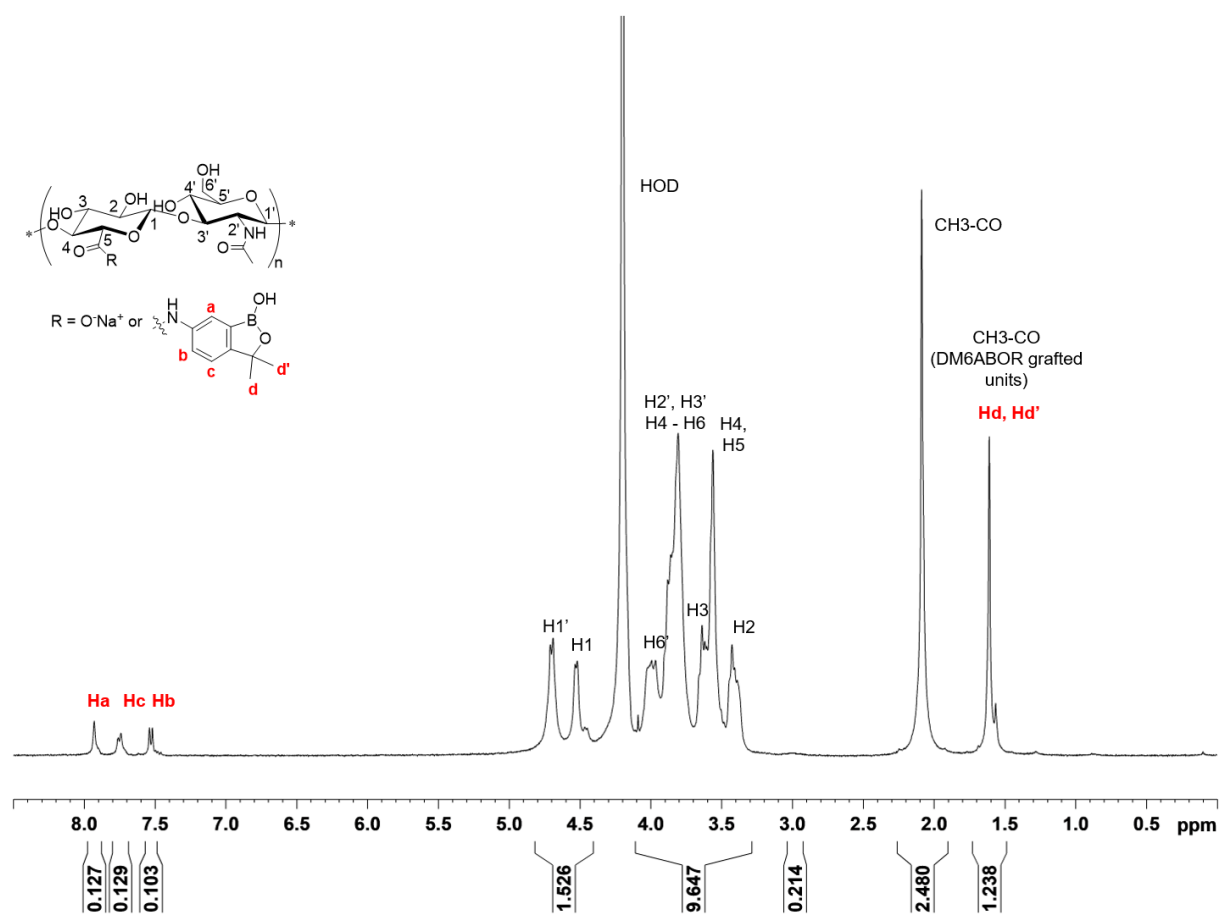


Figure S2. ^1H NMR spectrum (400 MHz, D_2O , $6 \text{ mg}\cdot\text{mL}^{-1}$, 80°C) of HA100-DM6ABOR.

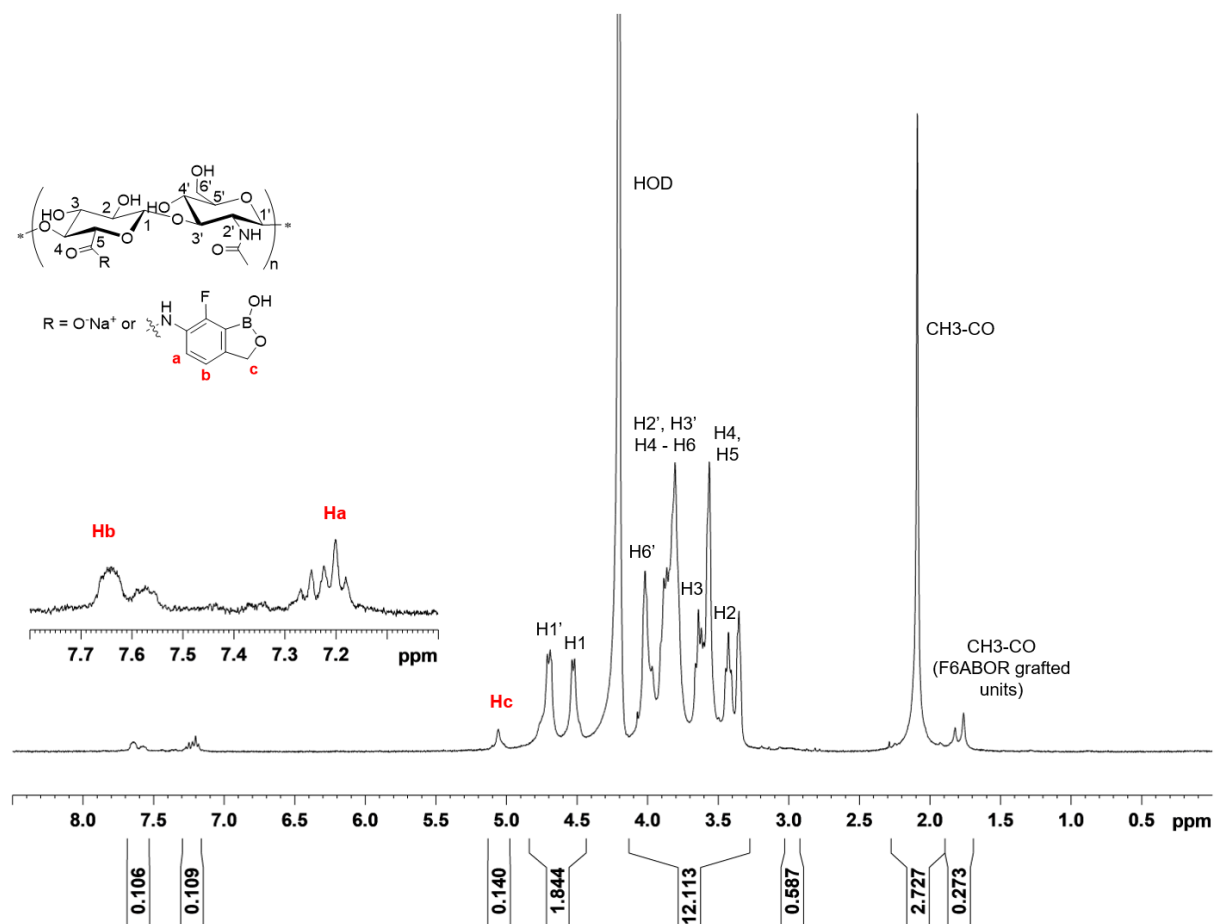


Figure S3. ¹H NMR spectrum (400 MHz, D₂O, 6 mg.mL⁻¹, 80 °C) of HA100-F6ABOR.

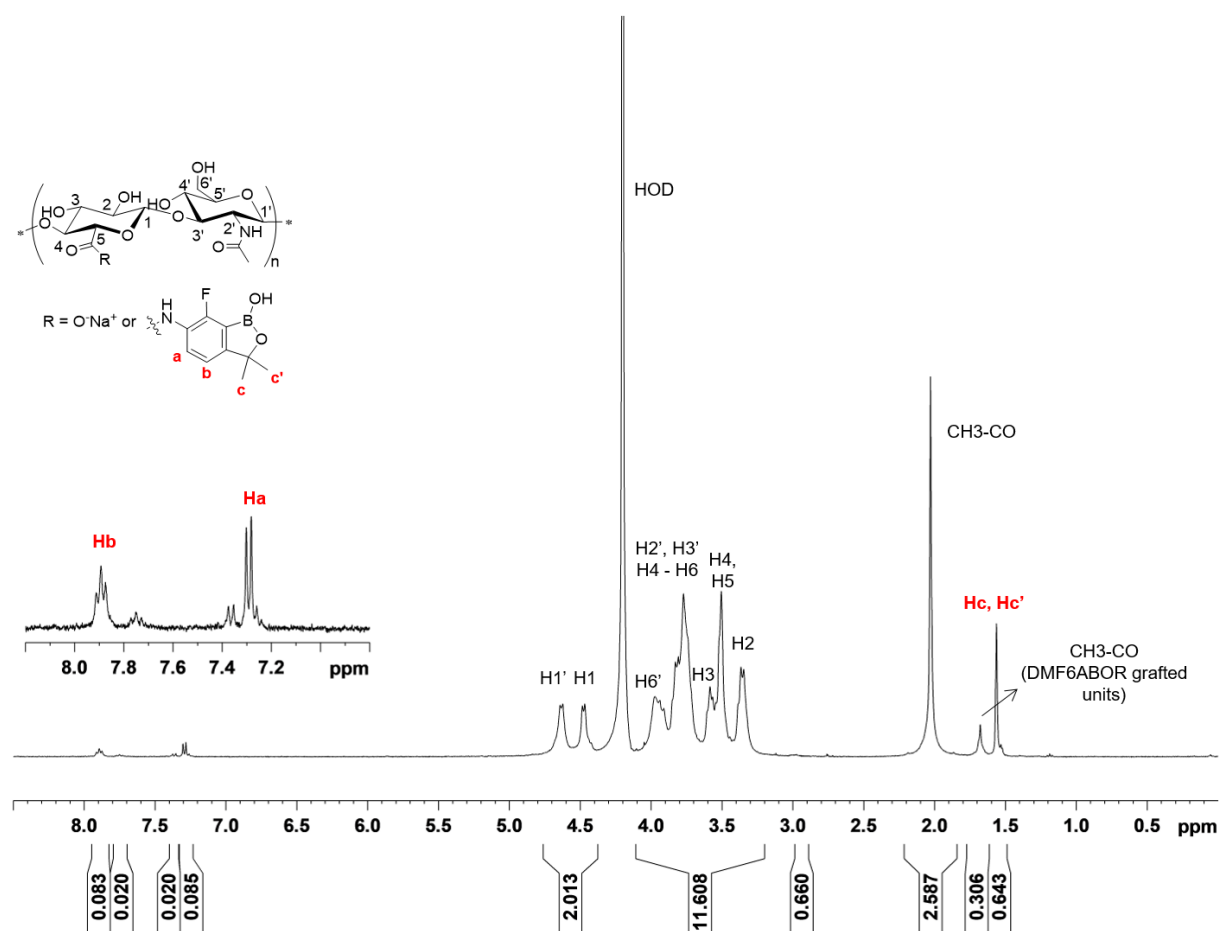


Figure S4. ^1H NMR spectrum (400 MHz, D_2O , $6 \text{ mg}\cdot\text{mL}^{-1}$, 80°C) of HA100-DMF6ABOR.

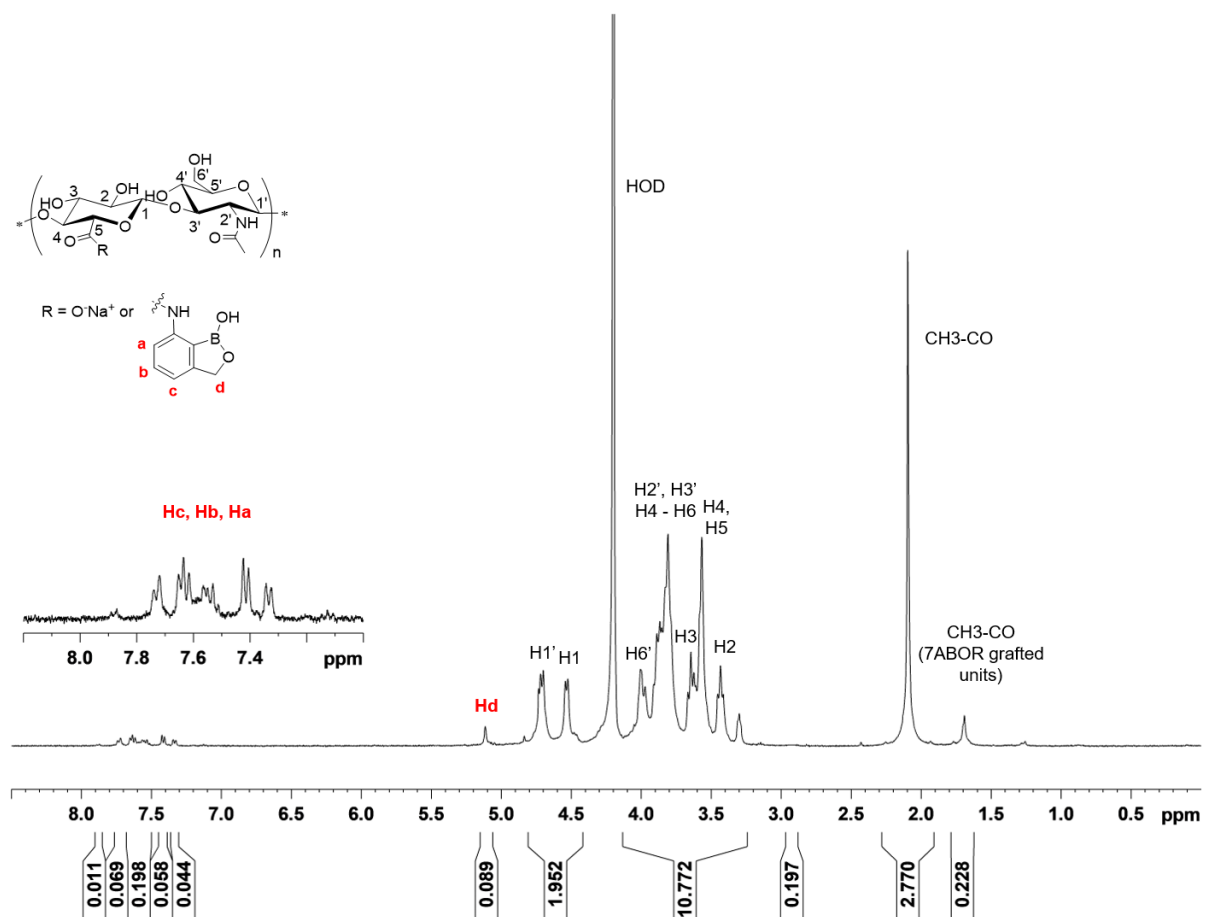


Figure S5. ^1H NMR spectrum (400 MHz, D_2O , $6 \text{ mg}\cdot\text{mL}^{-1}$, 80°C) of HA100-7ABOR.

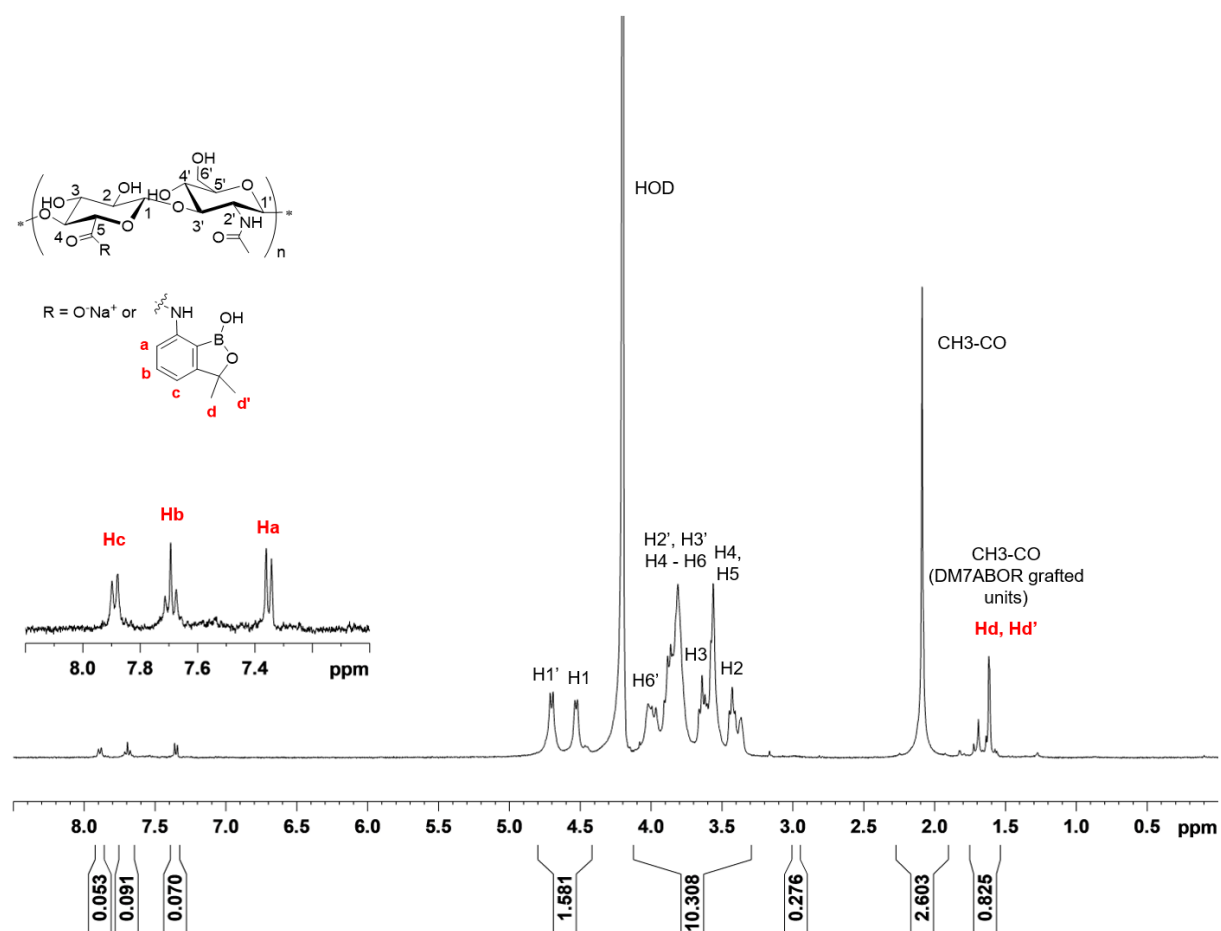


Figure S6. ^1H NMR spectrum (400 MHz, D_2O , 6 $\text{mg}\cdot\text{mL}^{-1}$, 80 °C) of HA100-DM7ABOR.

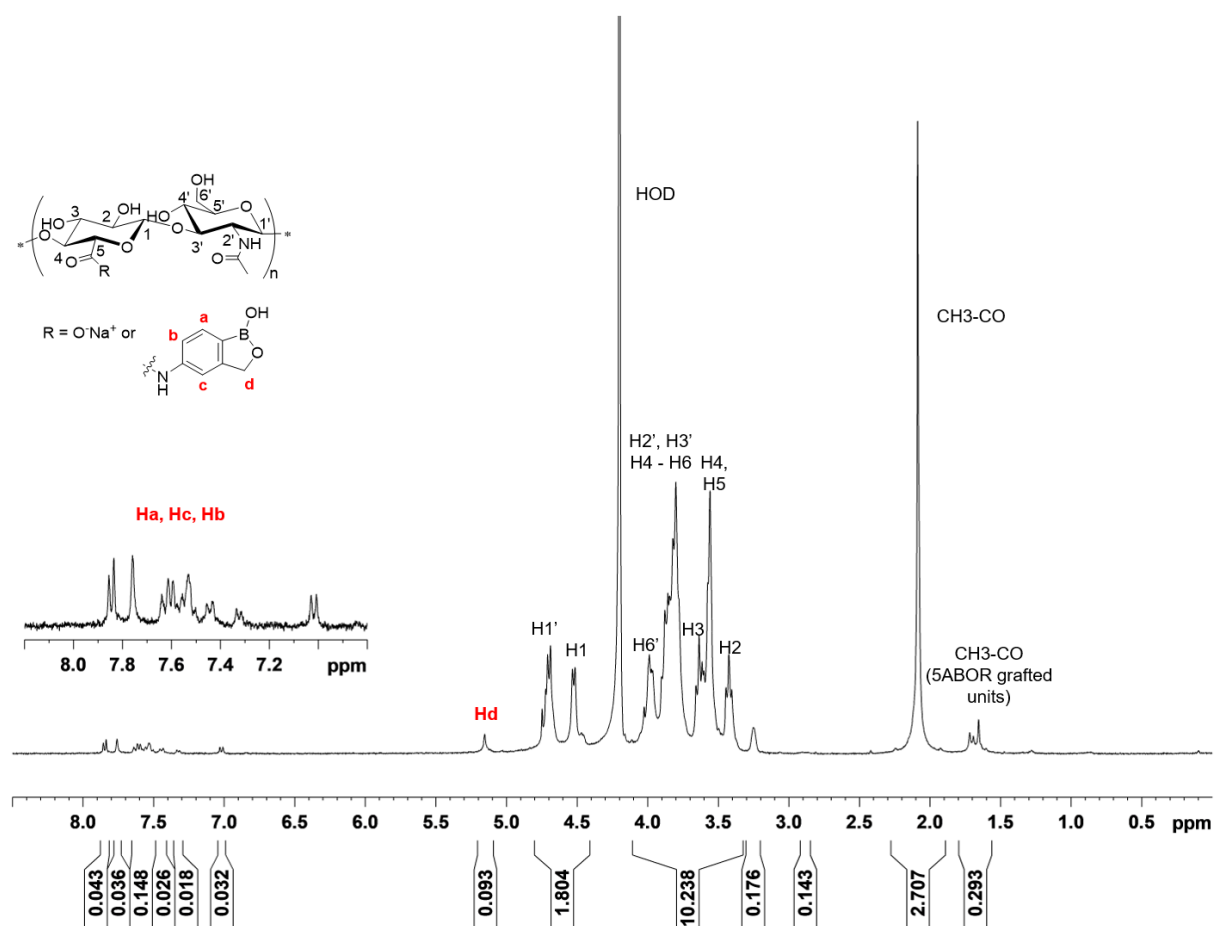


Figure S7. ^1H NMR spectrum (400 MHz, D_2O , $6 \text{ mg}\cdot\text{mL}^{-1}$, 80°C) of HA100-5ABOR.

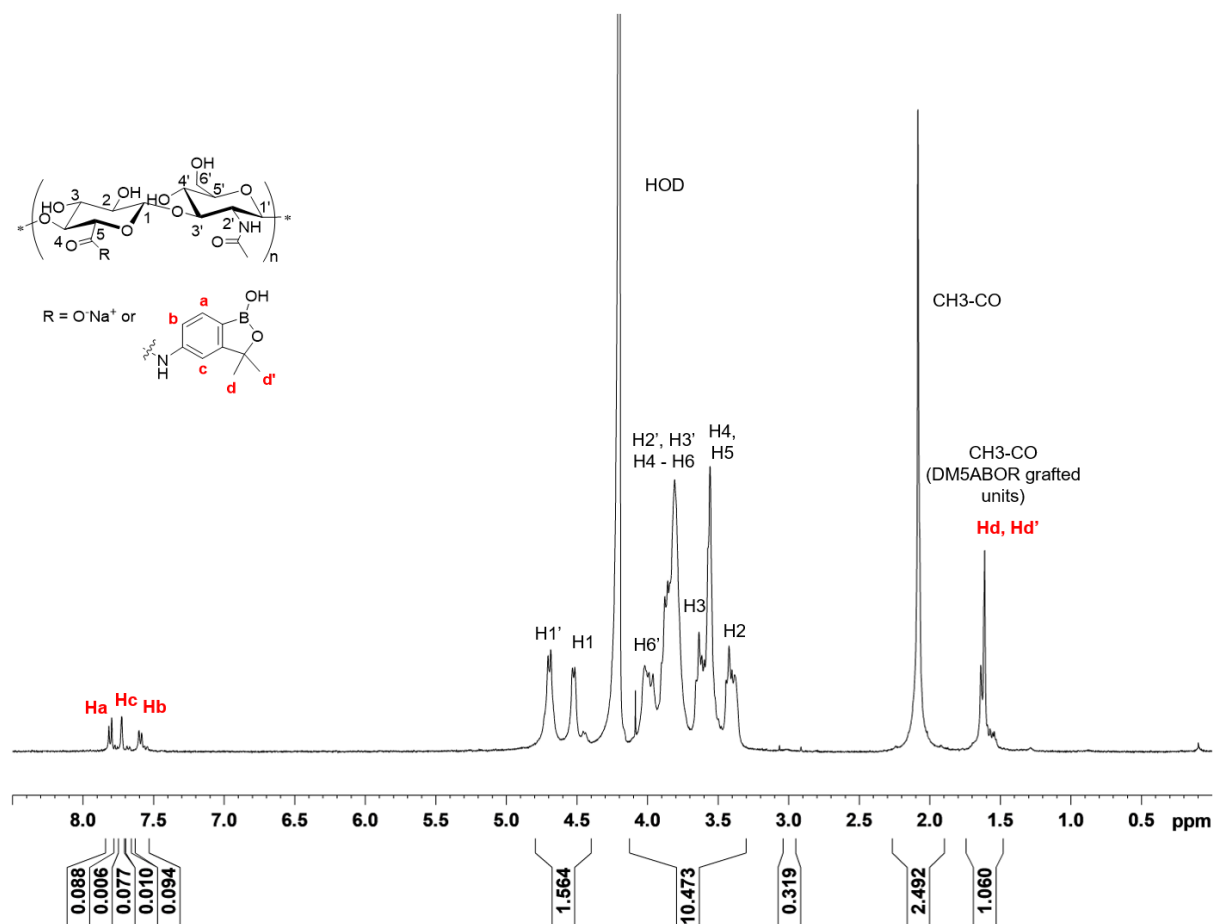


Figure S8. ^1H NMR spectrum (400 MHz, D_2O , $6 \text{ mg}\cdot\text{mL}^{-1}$, 80°C) of HA100-DM5ABOR.

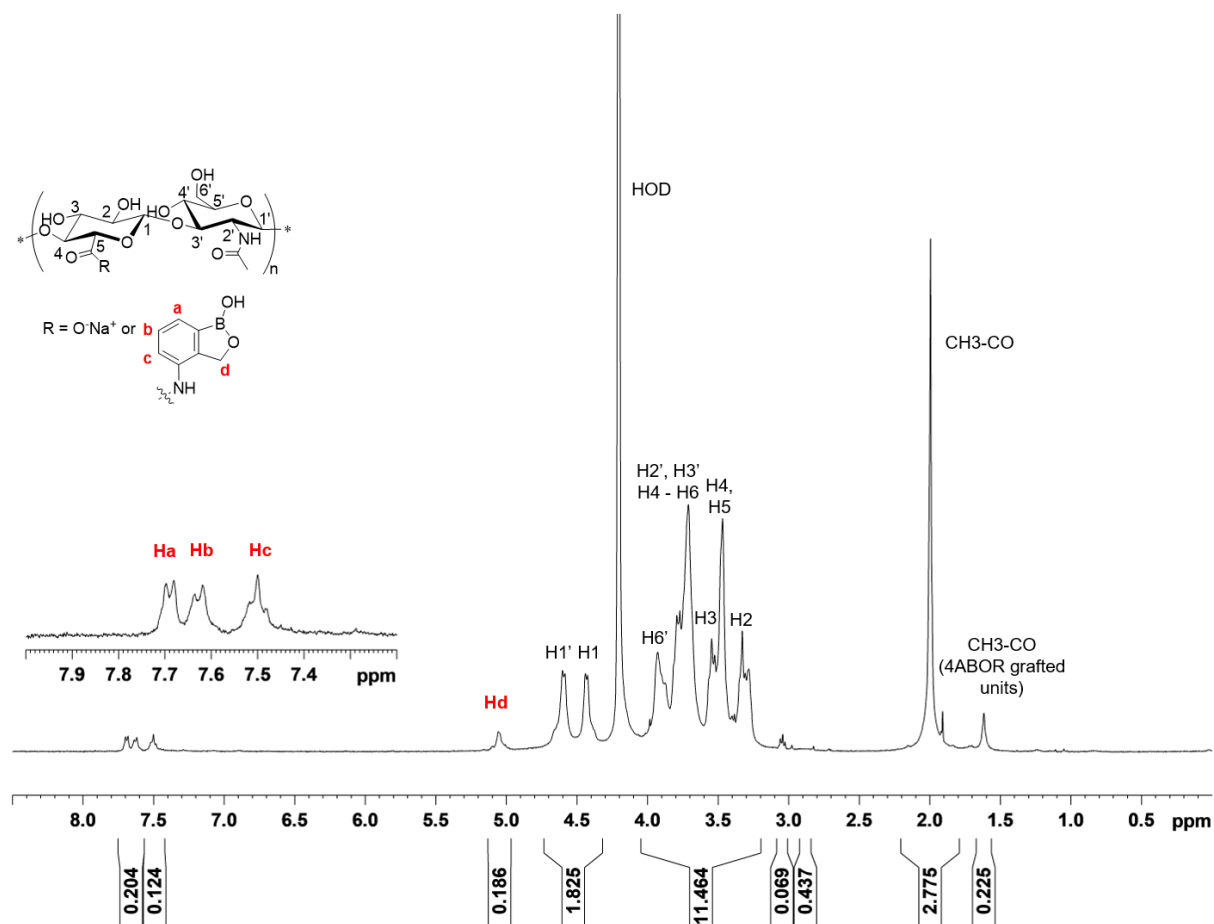


Figure S9. ^1H NMR spectrum (400 MHz, D_2O , $6\text{ mg}\cdot\text{mL}^{-1}$, $80\text{ }^\circ\text{C}$) of HA100-4ABOR.

3. Summary of HA-BOR derivatives synthesized (M_w 360 kg/mol)

TableS1. Summary of the syntheses of HA360-BOR conjugates.

Entry	Derivative	Structure	Time of reaction (h)	DS ^a	Coupling NMR (%)
1	DMF6ABOR		46	0.1	67
2	DM7ABOR		44	0.1	67

^aDetermined by ¹H NMR spectroscopy at 80 °C in D₂O.

4. ¹H NMR characterization of HA-BOR derivatives synthesized (M_w 360 kg/mol)

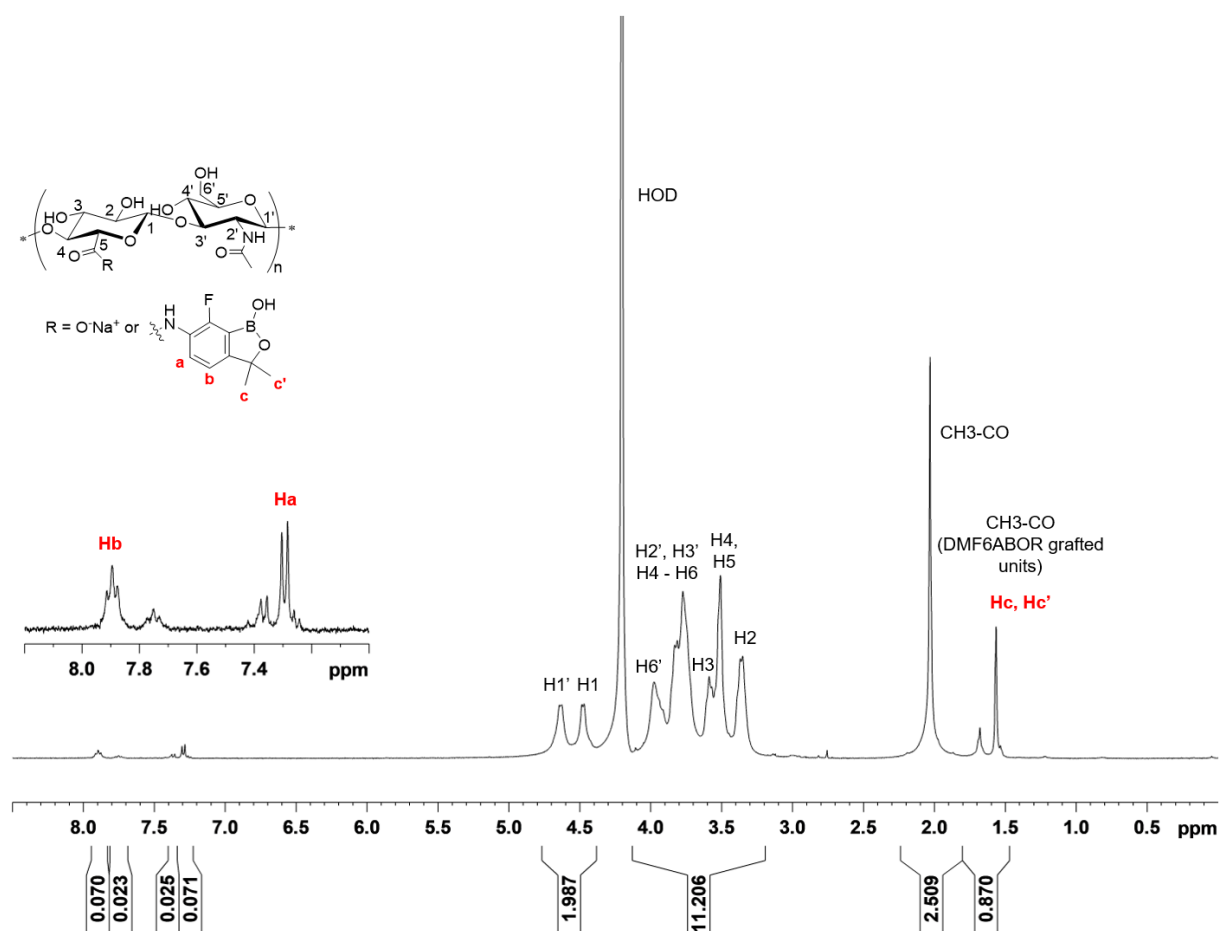


Figure S10. ¹H NMR spectrum (400 MHz, D₂O, 6 mg.mL⁻¹, 80 °C) of the HA360-DMF6ABOR derivative.

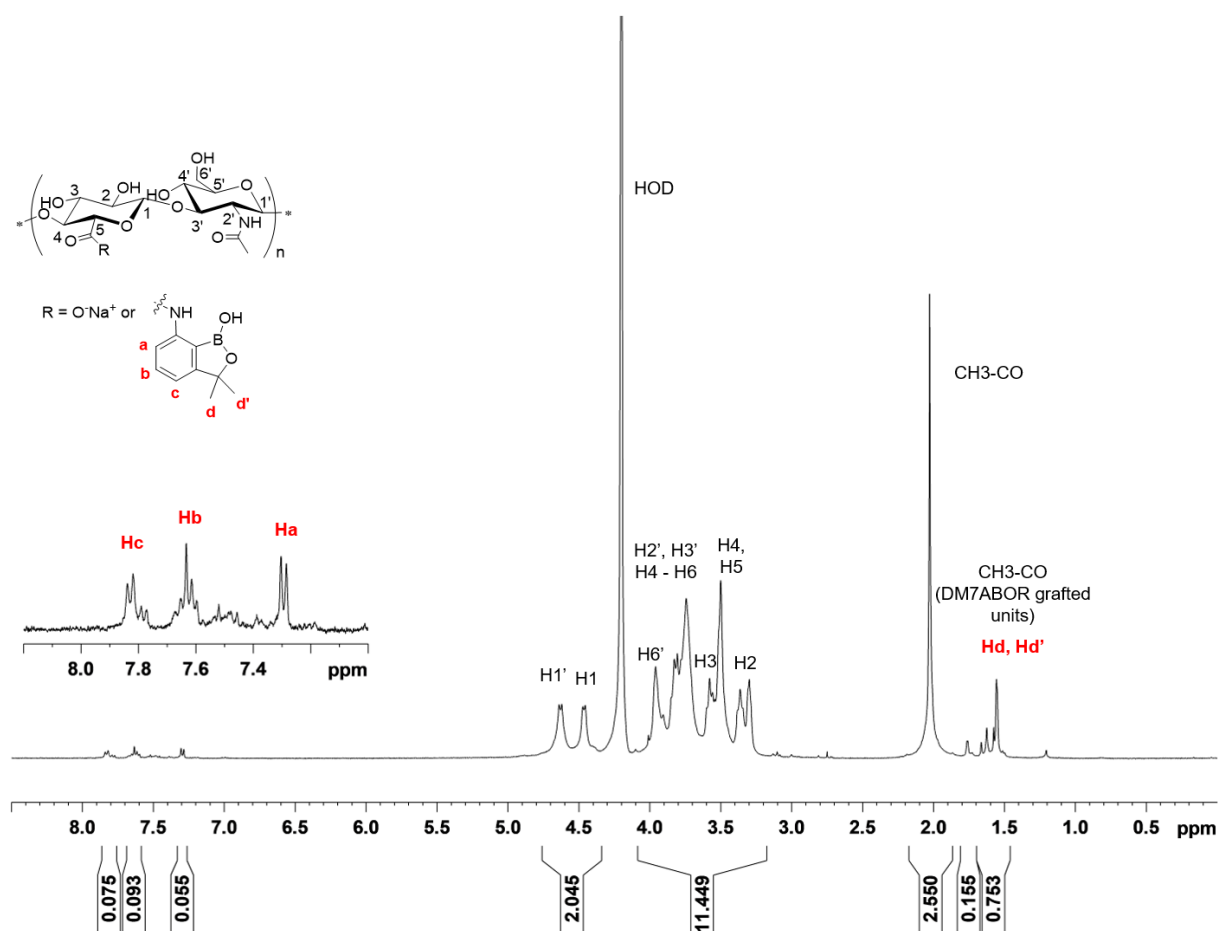
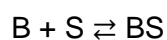


Figure S11. ^1H NMR spectrum (400 MHz, D_2O , $6 \text{ mg}\cdot\text{mL}^{-1}$, $80 \text{ }^\circ\text{C}$) of the HA360-DM7ABOR derivative.

5. Methodology for determining K_a by ^1H NMR Spectroscopy

The procedure to determine values of K_a was adapted from previous studies using free boronic acids and saccharides.^{1,2} This method consisted in assuming that a boronic acid (B) and a saccharide (S) bind in one modality, BS:



$$K_a = \frac{[\text{BS}]}{[\text{B}]\cdot[\text{S}]} \quad (1)$$

Where [B], [S] and [BS] are the molar concentrations of free boronic acid, free saccharide and complex, respectively.

To calculate K_a , the [BS]/[B] ratio was determined by digital integration of aryl protons of the boronic acid/saccharide complex and of the free boronic acid, allowing to calculate [B], [BS] and [S], as follows:

$$[\text{B}] = \frac{[\text{B}]_0}{\frac{[\text{BS}]}{[\text{B}]} + 1} \quad (2)$$

Where $[\text{B}]_0$ is the initial concentration of boronic acid added in the NMR tube, and

$$[\text{BS}] = \frac{[\text{BS}]}{[\text{B}]} [\text{B}] \quad (3)$$

$$[\text{S}] = [\text{S}]_0 - [\text{BS}] \quad (4)$$

Where $[\text{S}]_0$ is the initial concentration of saccharide added in the NMR tube.

Procedure for the preparation of samples for NMR analysis

Stock solutions of free DMF6ABOR (DM7ABOR) and free D-fructose (native HA100) were prepared by solubilization in distilled water. When necessary, the pH was carefully adjusted to 7.4 by adding 1 M NaOH, using a pH-meter, and water was added to get a concentration of 4 mM. Then, the solutions were diluted with 0.02 M PBS pH 7.4 in order to obtain a final concentration of 2 mM DMF6ABOR (DM7ABOR) or D-fructose (native HA100) in 0.01 M PBS at pH 7.4. The solutions of complexes were then prepared by mixing various volumes of a stock solution of DMF6ABOR (DM7ABOR) with a stock solution of D-fructose (native HA100). This generated mixtures of pH 7.4 (± 0.1), with a molar ratio of DMF6ABOR (DM7ABOR)/saccharide at a range of 0.3 to 1.5. Water was removed by freeze-drying and the samples were properly dissolved in D_2O prior to NMR analysis. Each value of K_a was determined from two experiments of titration using freshly prepared solutions. ^1H NMR titration was performed with at least 6 different concentrations at 25 °C.

Procedure for determining the chemical shifts of aryl protons in bound and free boronic acids

^1H NMR spectra of DMF6ABOR and DM7ABOR alone were first recorded (spectra (a) in Figure S12, S14, S16 and S18). Second, ^1H NMR spectra of DMF6ABOR and DM7ABOR in presence of excess free saccharide (D-fructose or native HA100 to induce 100 % complex formation are acquired (spectra (b) in Figure S12, S14, S16 and S18). Comparison of spectra (a) and (b) allows the assignment of the aryl protons in bound and free aminobenzoboroxoles. This analysis was then used to interpret the spectra from the titrations with D-fructose or native HA100; spectra (c) in Figure S12, S14, S16 and S18.

6. Determination of K_a by ^1H NMR for 6ABOR and D-fructose

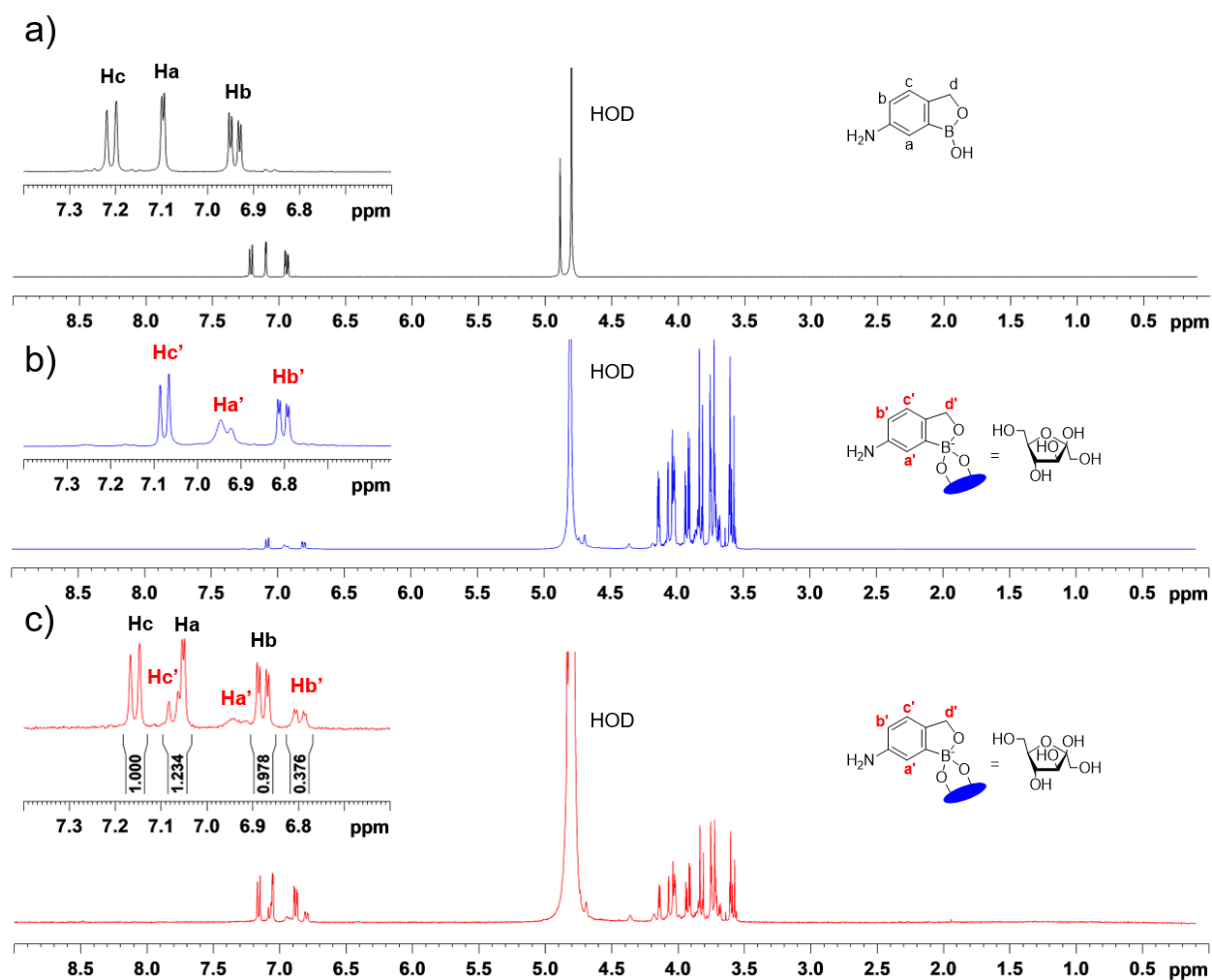


Figure S12. ^1H NMR spectra in 0.01 M deuterated PBS pH 7.4 at 25 °C of ABOR alone (15 mM) (a), ABOR (15 mM) in the presence of excess D-fructose (150 mM) (b) and ABOR (15 mM) with D-fructose (15 mM) (c). The $[\text{BS}]/[\text{B}]$ ratio was calculated from the digital integration of Hc (free ABOR) and Hb' (complexed ABOR) signals.

7. Determination of K_a by ITC for 6ABOR and D-fructose

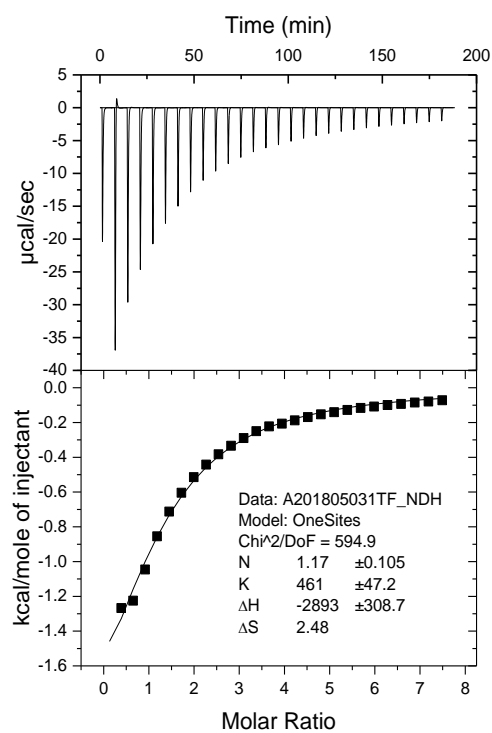


Figure S13. Calorimetric titration of 6ABOR (2 mM) with D-fructose (75 mM) in 0.01 M PBS (pH 7.4, 25 °C).

8. Determination of K_a by ^1H NMR for DMF6ABOR and D-fructose

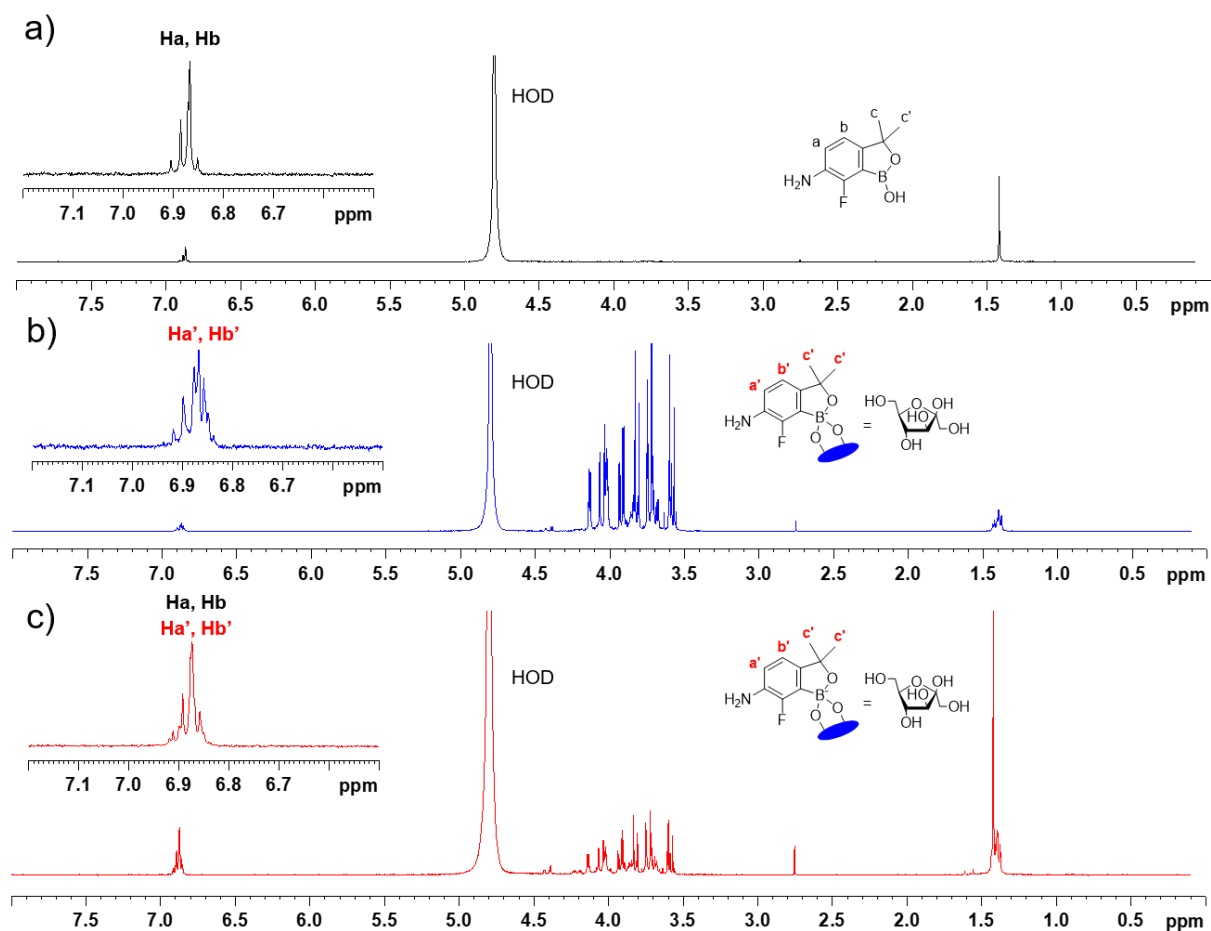


Figure S14. ^1H NMR spectra in 0.01 M deuterated PBS pH 7.4 at 25 °C of DMF6ABOR alone (1 mM) (a), DMF6ABOR (1 mM) in the presence of excess D-fructose (10 mM) (b), and DMF6ABOR (1 mM) with D-fructose (1 mM) (c). K_a was not measured because the aromatic signals (7-8 ppm) of bound and unbound forms of DMF6ABOR were not sufficiently separated to be integrated.

9. Determination of K_a by ITC for DMF6ABOR and D-fructose

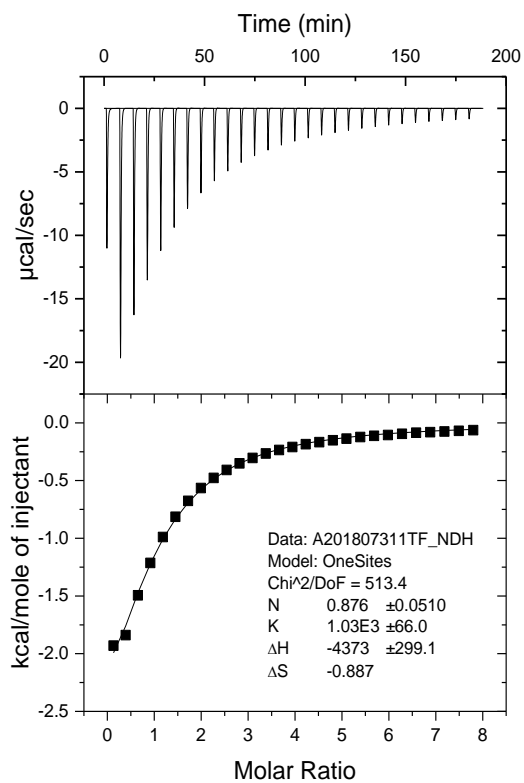


Figure S15. Calorimetric titration of DMF6ABOR (1 mM) with D-fructose (37.5 mM) in 0.01 M PBS (pH 7.4, 25 °C).

10. Determination of K_a by ^1H NMR for DM7ABOR and D-fructose

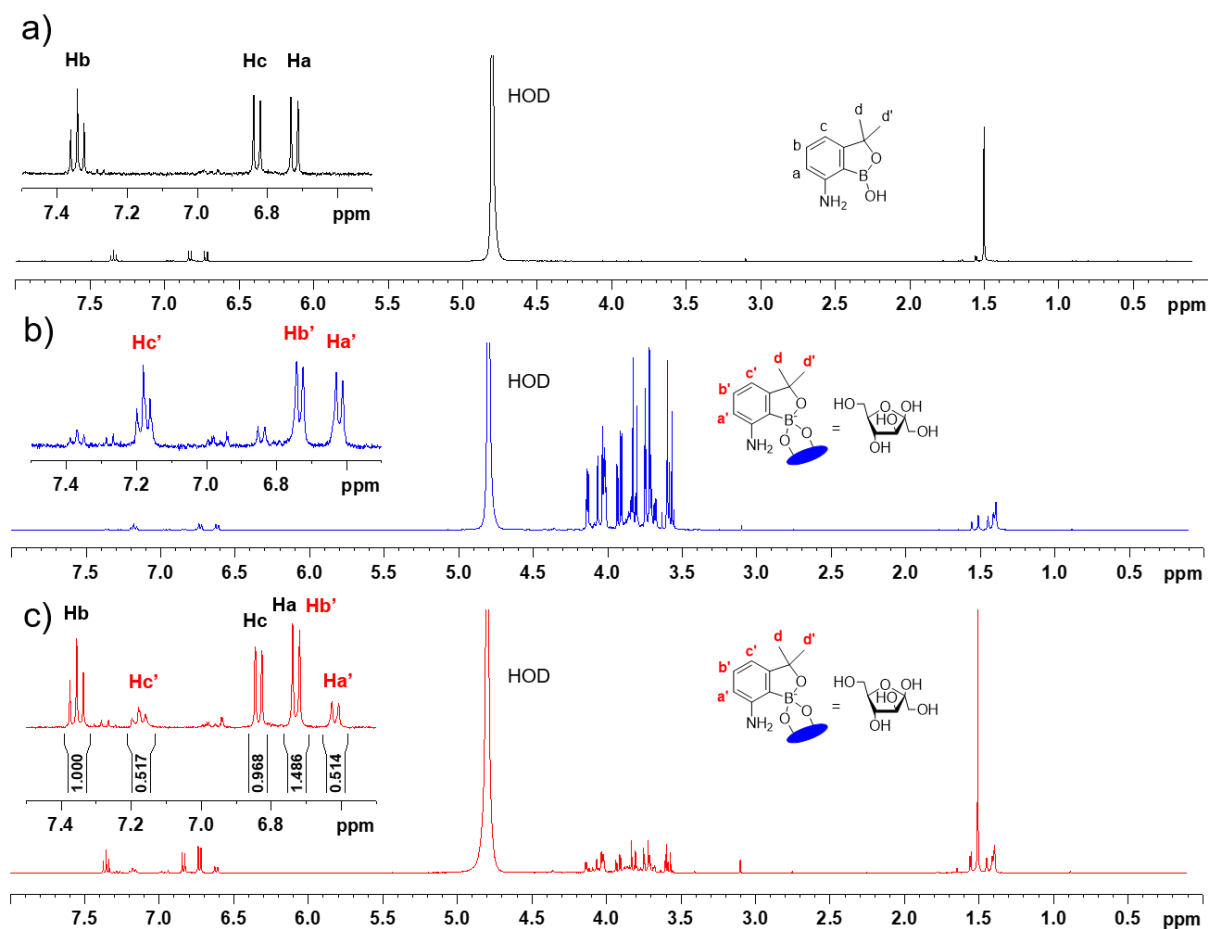


Figure S16. ^1H NMR spectra in 0.01 M deuterated PBS pH 7.4 at 25 °C of DM7ABOR alone (1 mM) (a), DM7ABOR (1 mM) in the presence of excess D-fructose (10 mM) (b), and DM7ABOR (1 mM) with D-fructose (1 mM) (c). The $[\text{BS}]/[\text{B}]$ ratio was calculated from the digital integration of Hb (free DM7ABOR) and Ha' or Hc' (complexed DM7ABOR) signals.

11. Determination of K_a by ITC for DM7ABOR and D-fructose

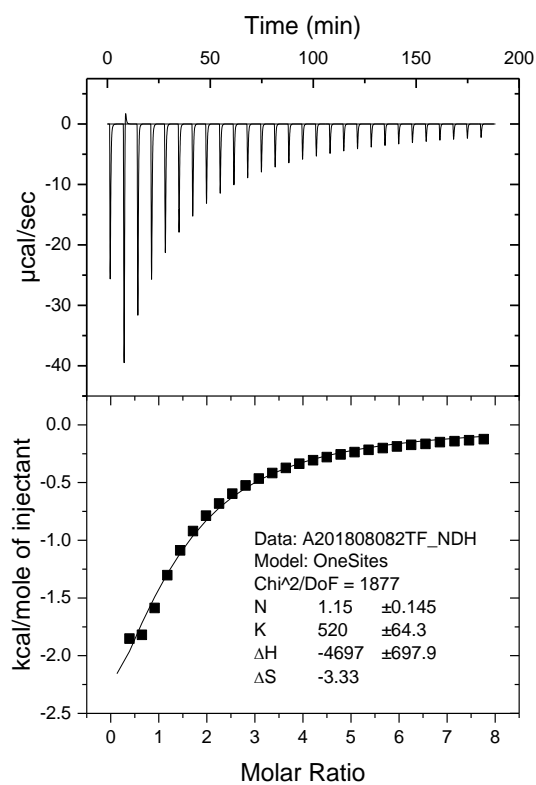


Figure S17. Calorimetric titration of DM7ABOR (1.5 mM) with D-fructose (56 mM) in 0.01 M PBS (pH 7.4, 25 °C).

12. Determination of K_a by ^1H NMR for DM7ABOR and native HA

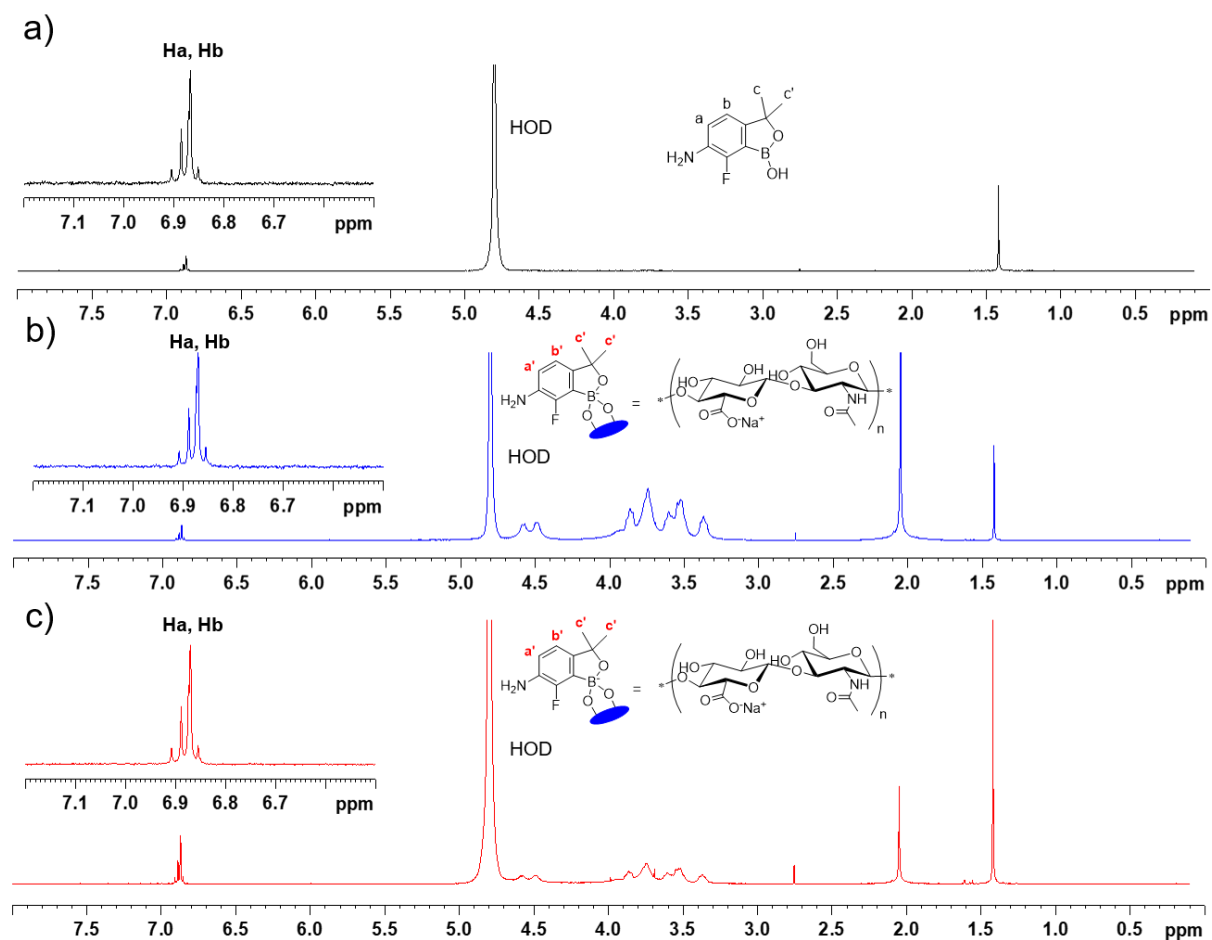


Figure S18. ^1H NMR spectra in 0.01 M deuterated PBS pH 7.4 at 25 °C of DMF6ABOR alone (1 mM) (a), DMF6ABOR (1 mM) in the presence of excess native HA (10 mM of HA disaccharide) (b), and DMF6ABOR (1 mM) with native HA (1 mM of HA disaccharide) (c). K_a was not measured because only the unbound form of DMF6ABOR was observed at 25 °C (rapid exchange dynamics relative to NMR time-scale).

13. Self-healing characterization of a hydrogel based on HA100-DMF6ABOR

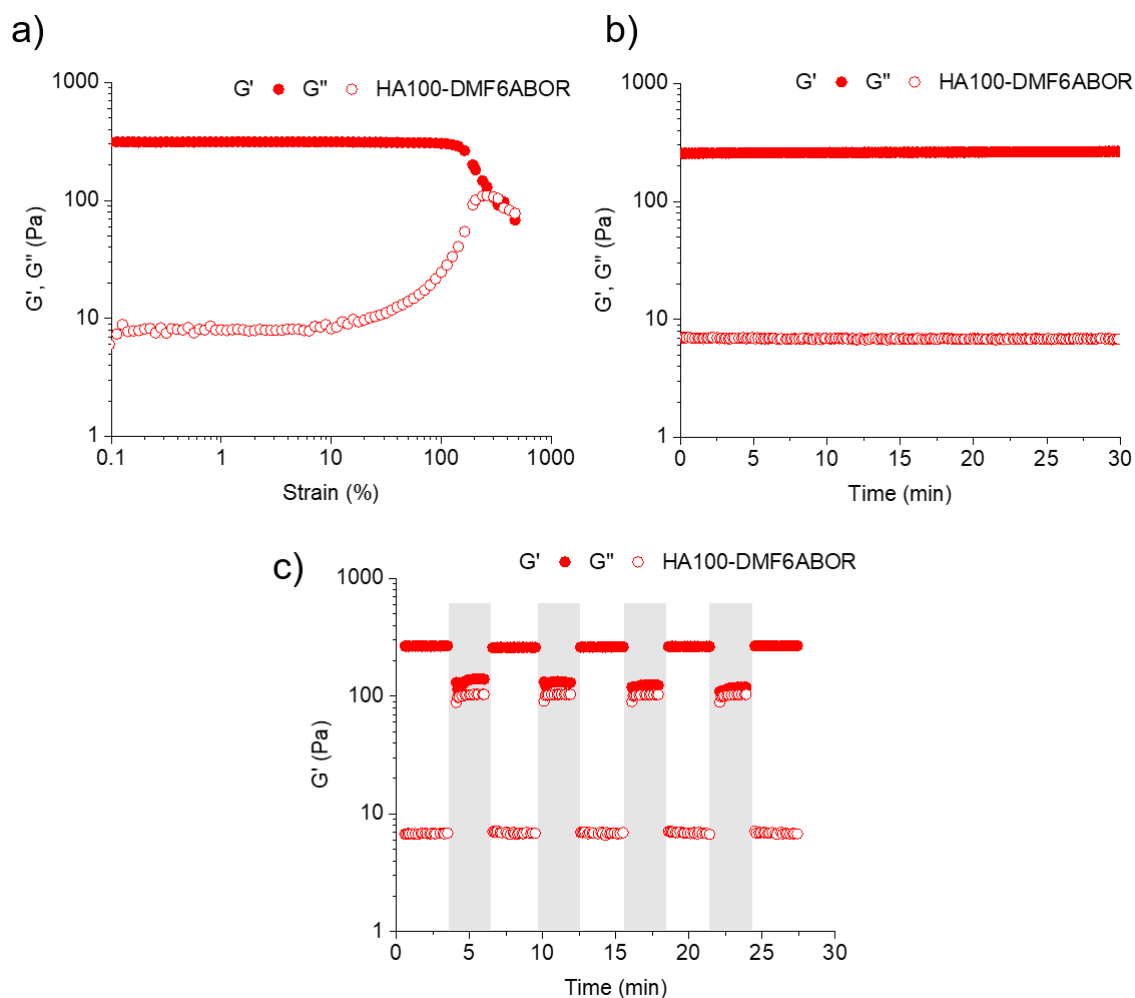


Figure S19. Self-healing of the HA100-DMF6ABOR hydrogel after failure. (a) Variation of G' and G'' when increasing strain, followed by (b) the linear recovery of the moduli when strain was reduced. The gel fractured at a strain of, approximately, 300 % and immediately recovered its moduli when strain was reduced to 5 %. (c) Four cycles of recovery from strain-induced breakdowns at physiological pH: a strain above the linear viscoelastic region (shaded regions, 250 % of strain) was applied for 2 min, followed by linear recovery measurements during 3 min (unshaded regions, 5 % of strain).

14. Determination of the pK_a of free 6ABOR, DMF6ABOR and DM7ABOR derivatives by ^{11}B NMR spectroscopy

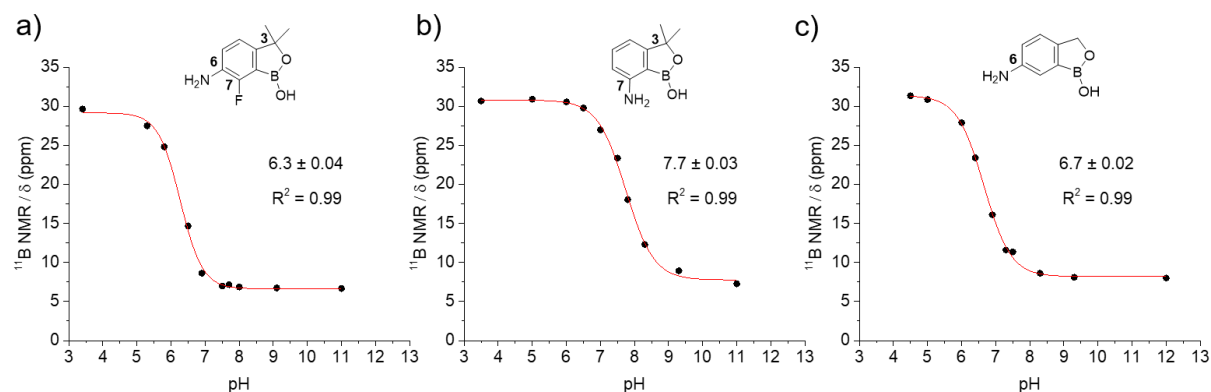


Figure S20. Determination of the pK_a of free (a) 6ABOR, (b) DMF6ABOR and (c) DM7ABOR derivatives by ^{11}B NMR titration as a function of pH (curve fitting using Boltzmann equation).

15. DMF6ABOR model used for molecular modeling studies

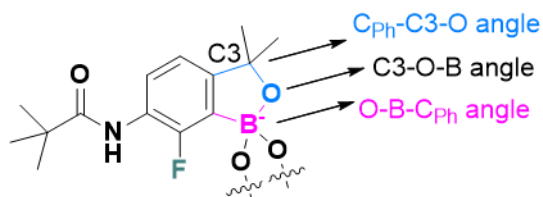


Figure S21. DMF6ABOR model containing a *tert*-butyl group to simulate the HA chain used for MD calculations. The arrows indicate the angles of the oxaborole ring that are impacted by the *gem*-dimethyl group.

16. Investigation of intramolecular hydrogen bond formation between DMF6ABOR by MD simulation

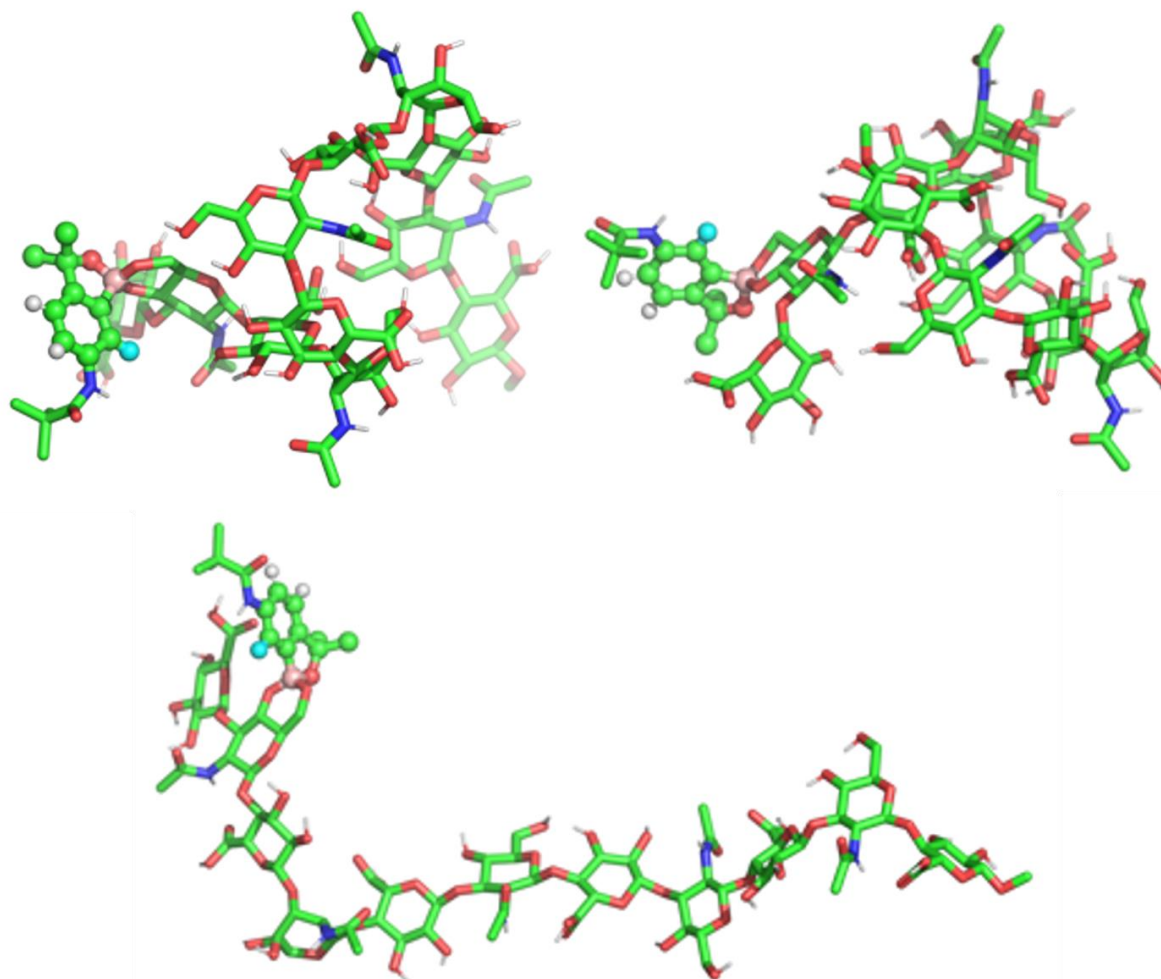


Figure S22. Snapshots of DMF6ABOR complexed with a HA chain (containing 11 saccharide units) during 20-ns by MD simulation. No intramolecular hydrogen bond formation was observed from the simulation.

17. References

- (1) Dowlut, M.; Hall, D. G. An Improved Class of Sugar-Binding Boronic Acids, Soluble and Capable of Complexing Glycosides in Neutral Water. *J. Am. Chem. Soc.* **2006**, *128* (13), 4226–4227.
- (2) Ellis, G. A.; Palte, M. J.; Raines, R. T. Boronate-Mediated Biologic Delivery. *J. Am. Chem. Soc.* **2012**, *134* (8), 3631–3634.

CHAPTER 4

Injectable self-healing hyaluronic acid hydrogels based on boronate ester crosslinks between benzoxaborin derivatives and saccharides

T. Figueiredo, J. Jing, C. Harris, J.-G. Boiteau, T. Gerfaud, J. Olsson, R. Auzély-Velty

Injectable self-healing hyaluronic acid hydrogels based on boronate ester crosslinks between benzoxaborin derivatives and saccharides

1. Introduction

Recent advances in biomaterials research have encouraged the design of new injectable hydrogels showing shear-thinning and self-healing properties. Such gels can be pre-formed into syringes, show viscous flow under shear stress (i.e. shear-thinning) and rapid recovery when the applied stress is removed (i.e. self-healing).¹ These materials have become particularly attractive for clinical uses as they have a great potential to be surgically implanted in patients by minimally invasive methods. Chemically, such hydrogels can be crosslinked via non-covalent interactions (e.g. hydrophobic, hydrogen bonding, ionic, host-guest interactions) or dynamic covalent bonds.²

Injectable hydrogels based on dynamic covalent chemistry have recently been explored due to the reversible nature of their covalent linkages that may confer shear-thinning during injection and self-healing after injection.³ More specifically, gels crosslinked by dynamic boronate ester bonds have emerged as promising injectable biomaterials because of their rapid self-healing capacity.⁴ Moreover, the selective formation of boronate esters offers the possibility to adapt the mechanical properties of hydrogels by tuning the binding strength between their small molecule partners (i.e. by varying the boronic acid and/or the diol (or polyol) crosslinking moieties). Indeed, as the formation of crosslinks in these gels at physiological pH strongly depends on the affinity of the boronic acid towards the diol (K_a) and on their pK_a ,⁵ one possibility for gel optimization is to use arylboronic acids with varied pK_a and diol-binding affinities.

Organoboron compounds have attracted increasing attention in modern chemistry as building blocks for organic synthesis and functional materials, and as unique pharmacophores and chemosensors in medicinal chemistry.⁶ Inspired by studies on the structure-property relationships of small arylboronic acid molecules,⁷⁻¹¹ several boronate-crosslinked hydrogels have been prepared using phenylboronic acid (PBA)¹²⁻¹⁴ and its derivatives, such as PBA substituted with fluorine (as an electron-withdrawing group that can reduce pK_a),^{4,15} and *ortho*-substituted PBA derivatives,¹⁶ in particular *o*-hydroxymethylphenylboronic acid (benzoboroxole, BOR, Figure 1).¹⁷⁻¹⁹ Compared to PBA, BOR has a strained five-membered oxaborole ring, which is a contributing factor explaining its higher acidity (pK_a of 7.3 for BOR⁹ and 8.8 for PBA²⁰) and its exceptional carbohydrate-binding behavior at neutral pH.^{11,21} The capability of this class of arylboronic acids to bind non-reducing saccharides locked in their

pyranose form (glycopyranosides) was first reported by the Hall group.^{10,22} This unique property was successfully used to produce highly elastic hydrogel networks crosslinked via complexation of BOR with mannopyranoside moieties covalently linked to synthetic polymers.¹⁹ Furthermore, we recently demonstrated for the first time the possibility to form reversible hydrogels at neutral pH from benzoboroxole-modified hyaluronic acid (HA) via direct complexation between the custom-made BOR derivatives grafted on HA and the C-4/C-6 diols of the *N*-acetyl-D-glucosamine unit of HA (*cf. chapter 3*). Despite the weak binding affinity of the BOR derivatives towards the C-4/C-6 diol of the polysaccharide, effective crosslinking was observed, leading to the formation of HA networks displaying a viscoelastic behavior (i.e. crossover frequency of G' and G'' seen within the tested frequencies) or gel-like properties ($G' > G''$ in the frequency window explored) due to high affinity molecular recognition through multivalent BOR/HA diol interactions. Besides, we also showed that HA hydrogels with almost identical rheological moduli are obtained when mixing HA bearing PBA or BOR moieties with a HA-fructose conjugate at neutral pH (*cf. chapter 2*). This unexpected similar behavior was found to be related to the unusual formation of a tridentate complex between PBA and grafted fructose promoted by HA, in addition to the previously unobserved binding mode between BOR and fructose, leading to the formation of a monocyclic bidentate adduct instead of a spiro adduct due to the opening of the oxaborole ring (Figure 1).

In addition to benzoboroxole, its six-membered ring homologue, *o*-hydroxyethylphenylboronic acid (benzoxaborin, 2,1-BORIN, Figure 1), has recently been investigated as a synthetic building block for constructing bioactive molecules,^{6,9,23} and as a recognition element for carbohydrate sensing.²² However, in spite of the structural similarities between BOR and 2,1-BORIN, the latter is not able to complex saccharides in the pyranose form at neutral pH.²² Indeed, studies published by Tomsho *et al.* explain the different binding capacities of these derivatives based on their geometrical structures. Regarding 2,1-BORIN, its less strained six-membered ring, compared to the strained five-membered ring of BOR, does not induce a geometrical distortion about the boron atom, which results in a less reactive boronic center and a higher pK_a (8.4).⁹ On the other hand, the slightly higher acidity of 2,1-BORIN in comparison with PBA appears to be related to a reduced flexibility of the intramolecular B-O bond of the former, which increases boron electronic deficiency. Nevertheless, despite increasing attention has been paid to assess the potential of benzoxaborin compounds as sugar-binding agents, no published studies have exploited benzoxaborin-saccharide complexation as a crosslinking strategy to form reversible boronate-crosslinked hydrogels.

The present study is a first demonstration of the applicability of dynamic benzoxaborin-saccharide complexation as a reversible covalent crosslinking method to form HA networks.

Herein, we selected fructose as a saccharide (polyol) partner grafted on HA, for which most of boronic acids exhibit inherent binding selectivity among monosaccharides due to the high abundance in solution of its tautomeric β -D-fructofuranose form (i.e. present at 25 % in D₂O at 31 °C),²⁴ that contains a *syn*-periplanar pair of hydroxyl groups (OH-2 and OH-3) available for complexation.²⁵ To assess the effect of the structure of the arylboronic acid group on the efficiency of boronate crosslinking formation, we compared the rheological properties of HA assemblies based on a HA-fructose conjugate combined with HA bearing 2,1-BORIN or BOR or PBA moieties. Besides, we also investigated a new original derivative containing a six-membered heterocycle like 2,1-BORIN, with the endocyclic oxygen linked to the phenyl ring (named 1,2-benzoxaborin, 1,2-BORIN, Figure 1). This molecule has never been tested and reported as a carbohydrate-binding agent. Nevertheless, this derivative can also show interesting properties to produce hydrogels at neutral pH by formation of boronate ester crosslinks with fructose as its particular structure suggests a more acidic behavior (i.e. lower boronic pK_a) compared to standard 2,1-BORIN.

Herein, we show effective boronate ester crosslinking between HA-1,2-BORIN and HA-fructose derivatives at physiological pH, leading to the formation of hydrogel networks with dynamic rheological properties comparable to those of the HA-PBA (BOR)/HA-fructose assemblies. Their injectable and self-healing properties, which rely on the dynamic boronic acid-fructose interactions, were further studied in detail. This demonstrated potential of these new systems as injectable scaffolds in the biomedical field.

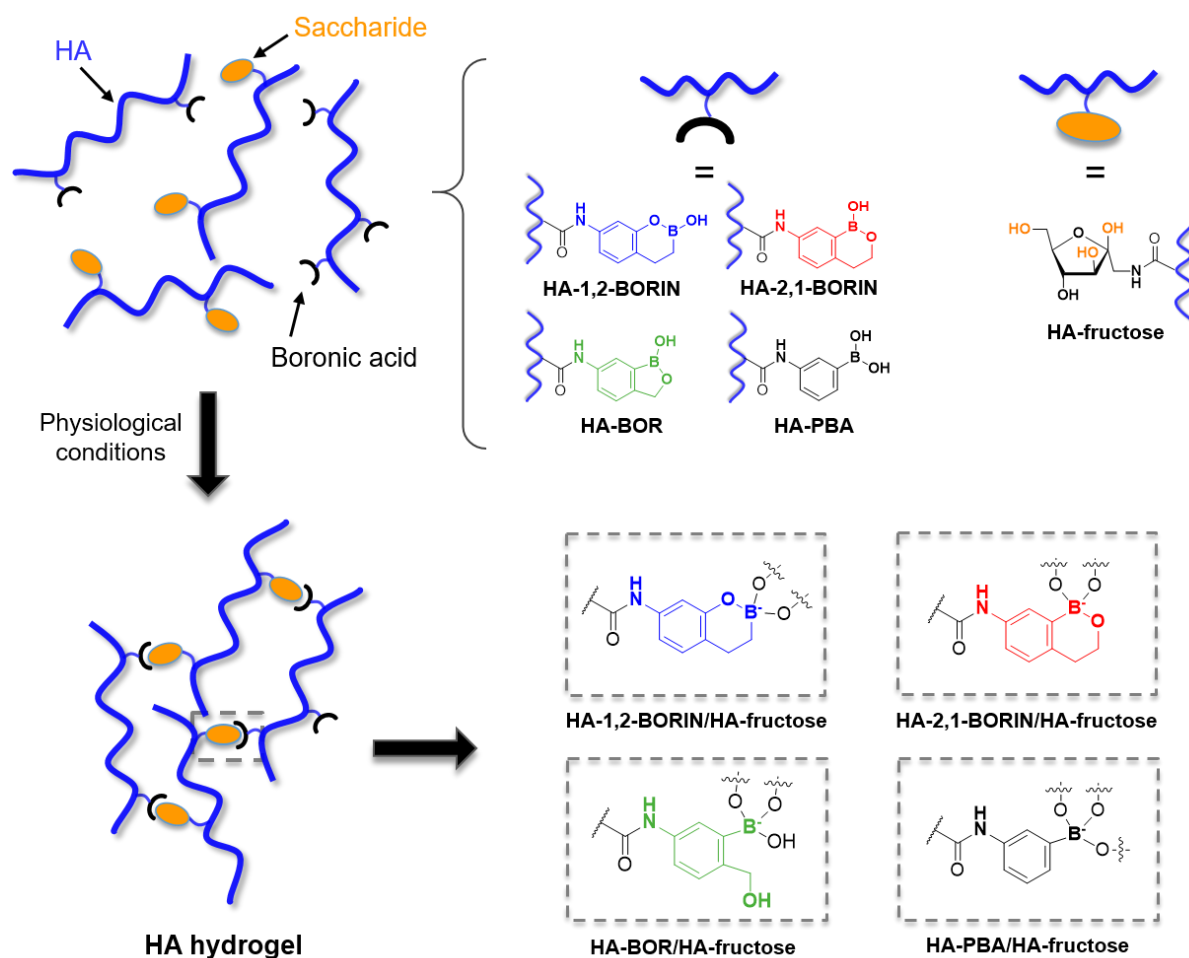
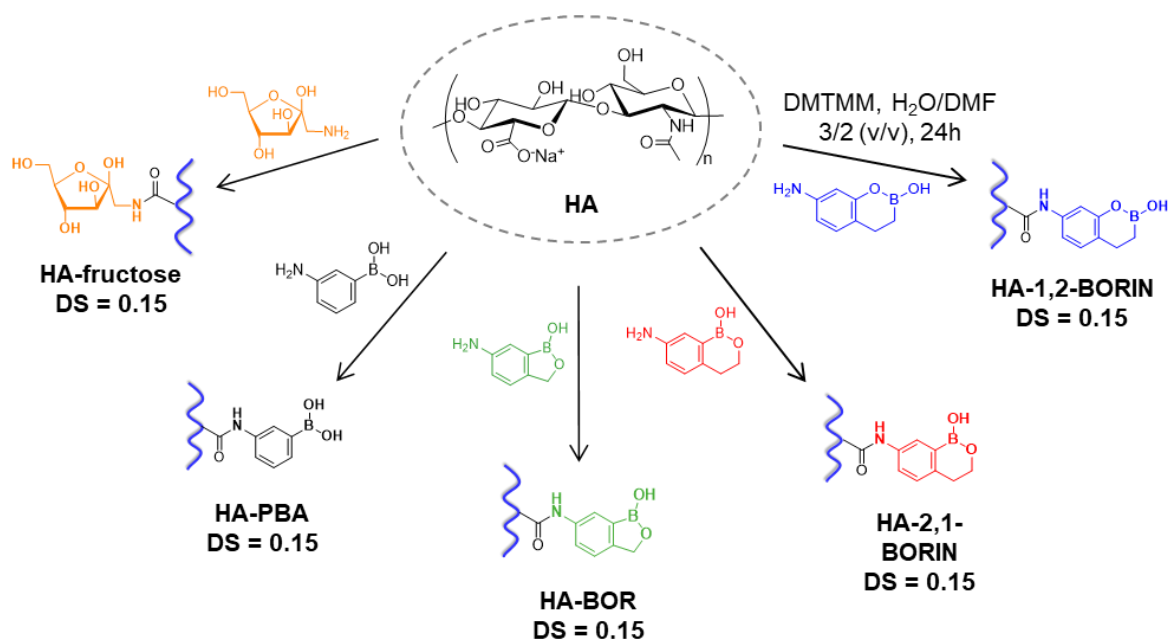


Figure 1. HA hydrogels crosslinked by boronate-fructose complexation at physiological pH. Hydrogel formation is triggered by combining fructose-grafted HA and HA modified with benzoxaborin derivatives, benzoboroxole or phenylboronic acid. Potential binding sites for boronate ester formation in fructose moieties grafted on HA correspond to the *syn*-periplanar hydroxyl pair (OH-2 and OH-3) in addition to OH-6 (highlighted in orange).

2. Results

To properly investigate the effect of the different small molecule crosslinkers on the rheological properties of the HA networks, all HA derivatives were synthesized from the same HA sample, possessing a weight-average molar mass (M_w) of 360 kg/mol (referred to as HA360), and with a similar degree of substitution (DS, average number of substituting group per repeating disaccharide unit). The synthesis of HA-benzoxaborin conjugates required first that of aminobenzoxaborin derivatives (1,2-ABORIN and 2,1-ABORIN, Scheme 1). These custom-made products were synthesized in four- to seven-steps, as described in the Supporting Information, and were isolated with yields comprised between 81 and 92 %. The HA-1,2-BORIN, HA-2,1-BORIN, HA-BOR, HA-PBA and HA-fructose conjugates were prepared by an amide coupling reaction carried out in aqueous solution between 3,4-dihydro-2*H*-benzo[*e*][1,2]oxaborinin-2-ol (1,2-ABORIN), 3,4-dihydro-1*H*-benzo[*c*][1,2]oxaborinin-1-ol

(2,1-ABORIN), 6-aminobenzoxaborole (ABOR), 3-aminophenylboronic acid (APBA) and 1-amino-1-deoxy-D-fructose (fructosamine), respectively, and HA, using 4-(4,6-dimethoxy-1,3,5-triazin-2-yl)-4-methylmorpholinium chloride (DMTMM) as a coupling agent (Scheme 1).²⁶ The DS of the HA conjugates was controlled by the amount of amine to carboxylic acid. Using DMTMM/HA and amine/HA molar ratios of 1 and 0.15, respectively, we obtained HA derivatives with a DS of 0.1-0.15 from ¹H NMR analysis (Figure S1-S4). In the case of HA-fructose, successful grafting was confirmed by 2D HSQC NMR analysis (Figure S5), and a DS of 0.15 was estimated from the reaction kinetics performed using 2,4,6-Trinitrobenzene Sulfonic Acid (TNBS) to quantify the free primary amines in the reaction medium as a function of time (Figure S6).²⁷



Scheme 1. Synthetic scheme for the preparation of HA derivatives via amide coupling reaction.

The different HA-based networks were then produced by mixing thoroughly aqueous solutions of HA-1,2-BORIN (or HA-2,1-BORIN or HA-BOR or HA-PBA) and HA-fructose at physiological pH (0.01 M HEPES buffer, 0.15 M NaCl), at a total polymer concentration ($C_p = 15$ g/L) higher than the overlap concentration of initial HA360 ($C^* \approx 1$ g/L), and with a molar ratio of 1,2-BORIN (2,1-BORIN or BOR or PBA)-to-grafted fructose of 1. Dynamic rheological analyses revealed a gel-like behavior ($G' > G''$) within the frequency window explored for the mixtures based on HA-1,2-BORIN (PBA) (BOR) and HA-fructose (Figure 2). A comparison between these three formulations showed that the elastic modulus at the plateau region is higher for the HA-PBA/HA-fructose assembly ($G'_{\text{plateau}} = 424$ Pa), than for the HA-1,2-BORIN/HA-fructose and HA-BOR-HA-fructose networks ($G'_{\text{plateau}} = 266$ Pa and 156 Pa,

respectively). A larger discrepancy between G' and G'' was also observed for the HA-PBA/HA-fructose mixture, indicating a higher resistance to flow. By contrast, the assembly based on HA-2,1-BORIN showed a viscoelastic behavior (crossover of G' and G'' seen within the tested frequencies) with a G' value at the plateau region of 20 Pa.

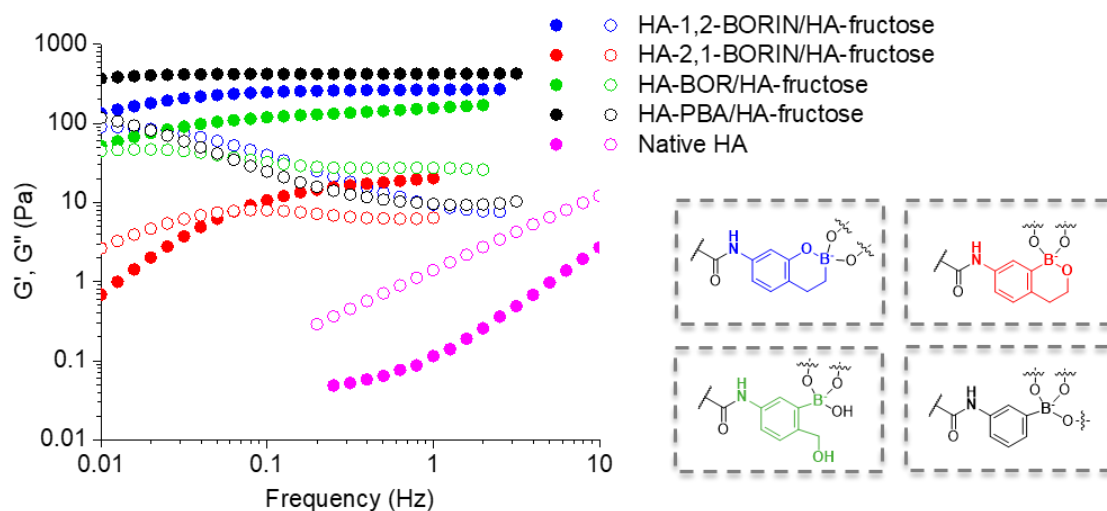
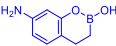
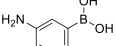


Figure 2. Dynamic rheological behavior of HA networks (M_w HA = 360 kg/mol) based on arylboronic acid/fructose crosslinks. Frequency dependence of the storage modulus (G' , filled symbols) and loss modulus (G'' , empty symbols) of formulations based on HA-fructose mixed with HA-1,2-BORIN or HA-2,1-BORIN or HA-BOR or HA-PBA at pH 7.4 (1,2-BORIN or 2,1-BORIN or BOR or PBA/fructose molar ratio of 1).

On the basis of these observations, we investigated the relationships between the macroscopic mechanical properties and the small molecule crosslinkers by analyzing the thermodynamics of boronic acid-fructose complexation. As the bound and unbound forms of these boronic acid derivatives in the presence of fructose are distinguishable by ^1H NMR spectroscopy,^{10,28} we used this technique to measure their affinities for free/grafted fructose (Table 1, Figure S7-S14). The values of K_a for free D-fructose were also examined by Isothermal Titration Calorimetry (ITC) and were in the same order of magnitude as the values derived from ^1H NMR (Table 1, Figure S15-S18).

Table 1. Binding constants of complexes based on 1,2-ABORIN (2,1-ABORIN or ABOR or APBA) with free D-fructose or grafted fructose (HA-fructose).

Entry	Derivative	Saccharide	K_a^a NMR (M ⁻¹)	K_a^b ITC (M ⁻¹)	n^b (n saccharide : 1 boronic acid)	ΔH^b (kJ.mol ⁻¹)	ΔS^b (J.mol ⁻¹ .K ⁻¹)
1	1,2-ABORIN 	D-fructose	487 ± 49	531 ± 40	1.07 ± 0.05	-10.3 ± 0.6	18
		HA-fructose	- ^c				
2	2,1-ABORIN 	D-fructose	87 ± 13	74 ± 17	n fixed at 1 ^d	-16.7 ± 0.4	-20
		HA-fructose	179 ± 67				
3	ABOR 	D-fructose	461 ± 73	484 ± 50	1.24 ± 0.1	-11.7 ± 1.2	12.1
		HA-fructose	545 ± 28				
4	APBA 	D-fructose	201 ± 5	112 ± 16	1.3 ± 0.3	-11.2 ± 2.8	1.6
		HA-fructose	503 ± 18				

^aMeasured from at least two ¹H NMR experiments; ^bmeasured from at least two ITC experiments; ^cnot determined because the bound and unbound forms of 1,2-ABORIN are not sufficiently separated to be properly integrated; ^dcalorimetric curve fitting by applying a fixed value of $n = 1$.

From Table 1, we observe that relatively close values of K_a (in the same order of magnitude) were determined for 1,2-ABORIN (ABOR) with free and grafted fructose as well as for APBA with grafted fructose (Table 1, entries 1, 3 and 4). These results are consistent with the gel-like behavior observed for the HA mixtures based on these derivatives (Figure 2). Regarding complexation with APBA, a 2-fold increase of K_a was observed for HA-fructose compared to D-fructose (Table 1, entry 4). As mentioned earlier, we previously explained this result by the special binding mode of APBA towards grafted fructose, resulting in a trivalent complex (*cf. chapter 2*). Moreover, despite the close values of K_a found for the complexation of APBA (ABOR) with fructose grafted on HA, a lower elastic modulus is measured for the HA-BOR/HA-fructose mixture. This may be ascribed to competitive interactions between BOR and HA saccharides as demonstrated by steady shear flow and dynamic rheology experiments performed on HA-1,2-BORIN (2,1-BORIN) (PBA) and initial HA360 alone at pH 7.4 (Figure S19). Indeed, these measurements showed that the HA-BOR solution stands out with increased moduli and an increased viscosity compared to native HA360, indicating formation of crosslinks between BOR moieties and HA (Figure S19). Moreover, ¹H NMR analysis of this conjugate at neutral pH provided another evidence of the selective binding of benzoboroxole moieties to HA. This indeed showed additional ¹H signals in the aromatic region of grafted BOR moieties, suggesting the presence of free and complexed BOR species which are in slow

exchange on the NMR timescale (Figure S3). Regarding the interaction of 2,1-ABORIN with free/grafted fructose, the low K_a measured for these couples in comparison to the other pairs correlates with the low G' value at the plateau and faster dynamics of the HA-2,1-BORIN/HA-fructose mixture (Table 1, entry 2).

Taken together, these results demonstrate that the macroscopic rheological behavior of the HA assemblies are directly related to the binding affinities of their small molecule crosslinkers. Considering that all mixtures only differ in the nature of their boronic acid partner, the binding mechanism allowing boronate ester formation may strongly depend on the structure and physico-chemical properties of each derivative used. While the mechanism of crosslinking in HA networks based on the interaction of PBA (BOR) with fructose has previously been assessed, the different behavior of HA assemblies including 1,2-BORIN (2,1-BORIN)/fructose complexation remains unclear. In these systems, one determinant factor that may affect K_a and boronate crosslinking formation is the pK_a of the boronic acid group. Surprisingly, in the case of complexation between PBA (BOR) and HA-fructose, boronate esters were formed with similar affinities in spite of their different structures and values of pK_a (8.8 for PBA²⁰ and 7.3 for BOR⁹).

Regarding the 2,1-BORIN derivative, the weak interaction with fructose may be partially related to its relatively high pK_a (8.4), which is due to its structure containing a less strained six-membered heterocycle compared to benzoboroxole.⁹ By contrast, the disposition of the endocyclic B-O bond in 1,2-BORIN, with the oxygen atom between the phenyl ring and boron, suggests a more electron-deficient character of the boronic center and, therefore, a higher acidity. Indeed, values of pK_a of 6.17 and 8.59 were determined for free 1,2-ABORIN and free 2,1-ABORIN, respectively, by ¹¹B NMR titration^{10,22} (Figure 3d and 3e). Interestingly, the dynamic rheological properties of the HA-1,2-BORIN (HA-2,1-BORIN)/HA-fructose networks at a pH range of 6-9 are consistent with the values of pK_a measured for the free derivatives. As demonstrated in Figure 3a, formation of crosslinks in the HA-1,2-BORIN/HA-fructose system was observed in this pH range. This assembly showed a remarkable increase of the elastic modulus at pH 7 and a gel-like behavior from pH 7.4. By contrast, crosslinking in HA-2,1-BORIN/HA-fructose was effective only from pH 7.4, and a pH value around 9 is required to achieve a gel-like behavior (Figure 3b). The higher cross-linking efficiency of HA-1,2-BORIN/HA-fructose at physiological pH can be related to the lower pK_a of 1,2-ABORIN (6.17), than that of 2,1-ABORIN (8.59) (Figure 3c, 3d and 3e). Collectively, these results indicate that the contrasting acidities of these benzoxaborin compounds are a main factor determining the different rheological properties of the HA mixtures.

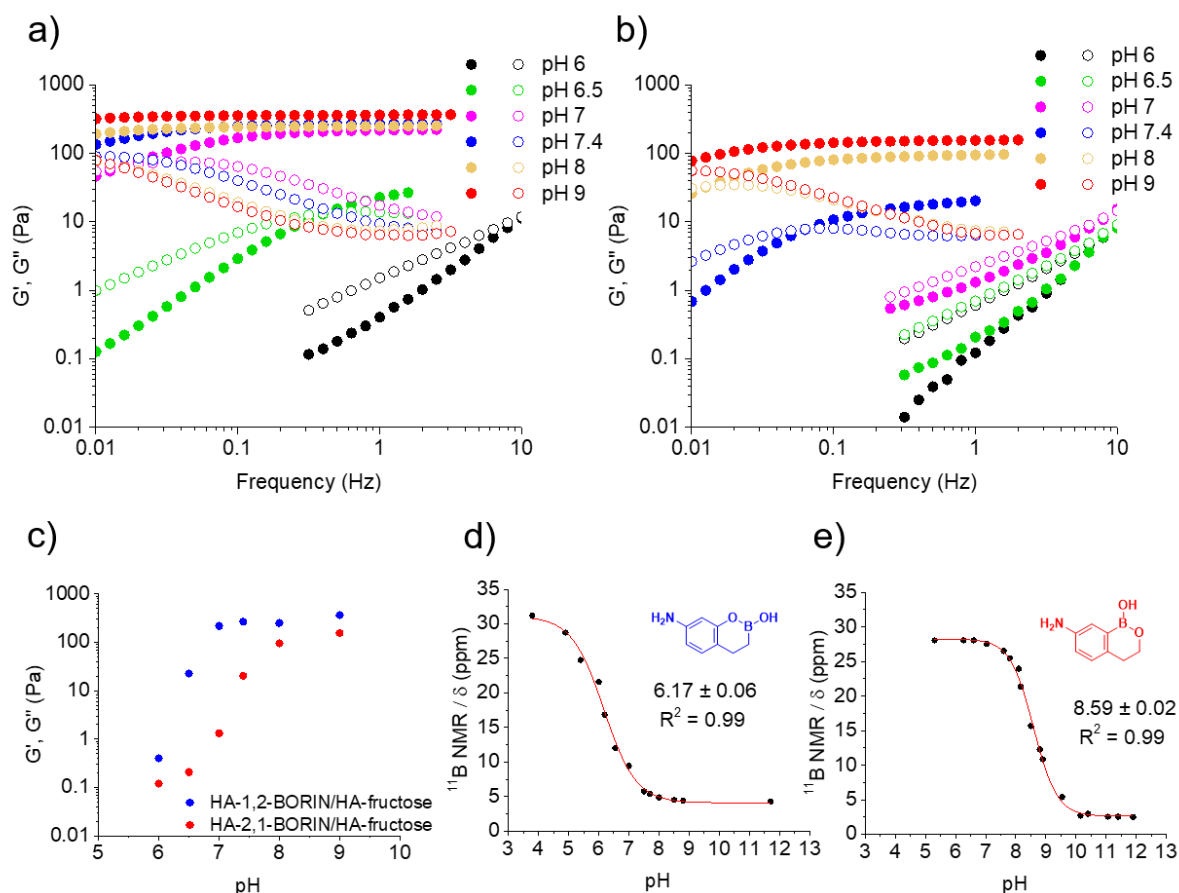


Figure 3. Dynamic rheological properties of the HA-1,2-BORIN (2,1-BORIN)/HA-fructose networks by varying the pH of the medium from 6 to 9: frequency dependence of G' (filled symbols) and G'' (empty symbols) of (a) HA-1,2-BORIN/HA-fructose and (b) HA-2,1-BORIN/HA-fructose; (c) variation of G' at a frequency of 1 Hz as a function of pH for the mixtures based on HA-fructose and HA-1,2-BORIN (2,1-BORIN). Values of pK_a determined for (d) free 1,2-ABORIN and (e) free 2,1-ABORIN by ^{11}B NMR spectroscopy.

To gain more insight into the macroscopic mechanical properties of the HA-1,2-BORIN/HA-fructose assembly, we investigated the binding mode of 1,2-BORIN to fructose by ^1H NMR spectroscopy. As previously reported for the complexation of ABOR with fructose, careful analysis of ^1H NMR spectra of ABOR alone and in the presence of free/granted fructose revealed that complexation is accompanied by the breaking of the endocyclic B-O bond of ABOR, resulting in the formation of a vicinal cyclic boronic ester with the *syn*-periplanar anomeric hydroxyl pair (C2–C3), similar to APBA/free fructose (Figure 1). It was speculated that an energetic advantage can be achieved by the opening of the oxaborole ring to relieve ring strain and thereby, to form a monocyclic adduct with the *syn*-1,2-diol pair of fructofuranose instead of a spiro adduct (*cf. chapter 2*). This was observed by comparing the ^1H NMR spectra of ABOR alone in the open form (i.e. at pD 11-12)²² and in the closed form (at pD 7.4), as well as of ABOR in the presence of free/granted fructose at pD 7.4 (Figure S20a). The upshift observed for the CH_2O group of ABOR in the presence of free/granted fructose similar to that

of ABOR alone at alkaline pH indeed provided evidence of the opening of the oxaborole ring. This observation raised the question of whether the complexation of 1,2-BORIN with fructose also leads to the formation of a monocyclic adduct via the opening of the endocyclic B-O bond. Following the same approach, ^1H NMR experiments were thus carried out to compare the resonances of the CH_2B group of 1,2-ABORIN alone at pD 11-12 and 7.4, and in the presence of free/grafted fructose at pD 7.4 (Figure S20b). Unfortunately, no clear evidence of the possible opening of the intramolecular B-O bond was revealed for the complexation of 1,2-ABORIN with fructose. Indeed, no significant differences were observed in the ^1H NMR spectra of 1,2-ABORIN alone at pD 11-12 and 7.4 as well as in those of 1,2-ABORIN in the presence of free/grafted fructose.

Although additional NMR experiments are warranted to address the exact mode of complexation between the 1,2-BORIN derivative and fructose, we cannot exclude that the strong affinity of 1,2-ABORIN towards this sugar could be associated with the opening of its endocyclic B-O bond similar to ABOR. Curiously, the increased entropy revealed by a positive value of ΔS determined from the calorimetric titration of 1,2-ABORIN with D-fructose may reflect this possible opening of the heterocycle due to complex formation (Table 1, entry 1). Indeed, it is important to note that the calorimetric parameters obtained for this couple follow a similar trend than that of ABOR with fructose (Table 1, entry 3).

Finally, we investigated the self-healing and injectable properties of this original BORIN/HA-fructose network. As shown in Figure 4a, strain-dependent oscillatory measurements displayed a broad linear viscoelastic region with network failure at high strain (700 %). The network was then found to immediately recover its rheological properties when the strain was reduced to 5 %. Then, the gel was exposed to a series of four cycles of breaking and reforming, which consisted in applying high strains (350 %) for 3 min, intercalated with low strains (5 %) for 2 min (Figure 4b). After this series of four cycles, the hydrogel was able to recover its initial rheological moduli, demonstrating its self-healing property. Although dynamic rheological moduli and self-healing capacity are important parameters for determining injectability, quantification of the viscosity and yield stress,²⁹ as well as the injection force required to extrude a gel through a needle, are also important to determine whether or not it is relevant for injection uses.³ Therefore, we evaluated the yield stress and viscosity of the new HA-1,2-BORIN/HA-fructose hydrogel in comparison to the HA assemblies based on HA-PBA (BOR)/HA-fructose. The yield stress is defined as the stress at which the network starts to flow, indicated as the first read-out of viscosity on the rheometer. As illustrated in Figure 4c, the viscosity of the three HA assemblies increased with increasing shear stress. As expected, a higher viscosity was observed for the HA-PBA/HA-fructose hydrogel (η_{max} of approximately 30000 Pa.s) compared to the HA-1,2-BORIN (BOR)/HA-fructose networks (η_{max} of 8000 and

3000 Pa.s, respectively). The yield stress for these formulations were found to be 940, 1650 and 677 Pa, respectively. Moreover, values of injection force close to 10 and 6 N were required to extrude HA-1,2-BORIN (PBA)/HA-fructose and HA-BOR/HA-fructose, respectively, from a 1 mL plastic syringe with a 27 G needle at a flow rate of 1 mm/min (Figure 4d). Despite the fact that the injection force of a gel depends on several factors such as flow rate, needle gauge and needle length, clinically relevant values are often below 20 N.³ These experiments thus indicate that the three networks are promising candidates as injectable scaffolds for regenerative medicine and drug delivery.

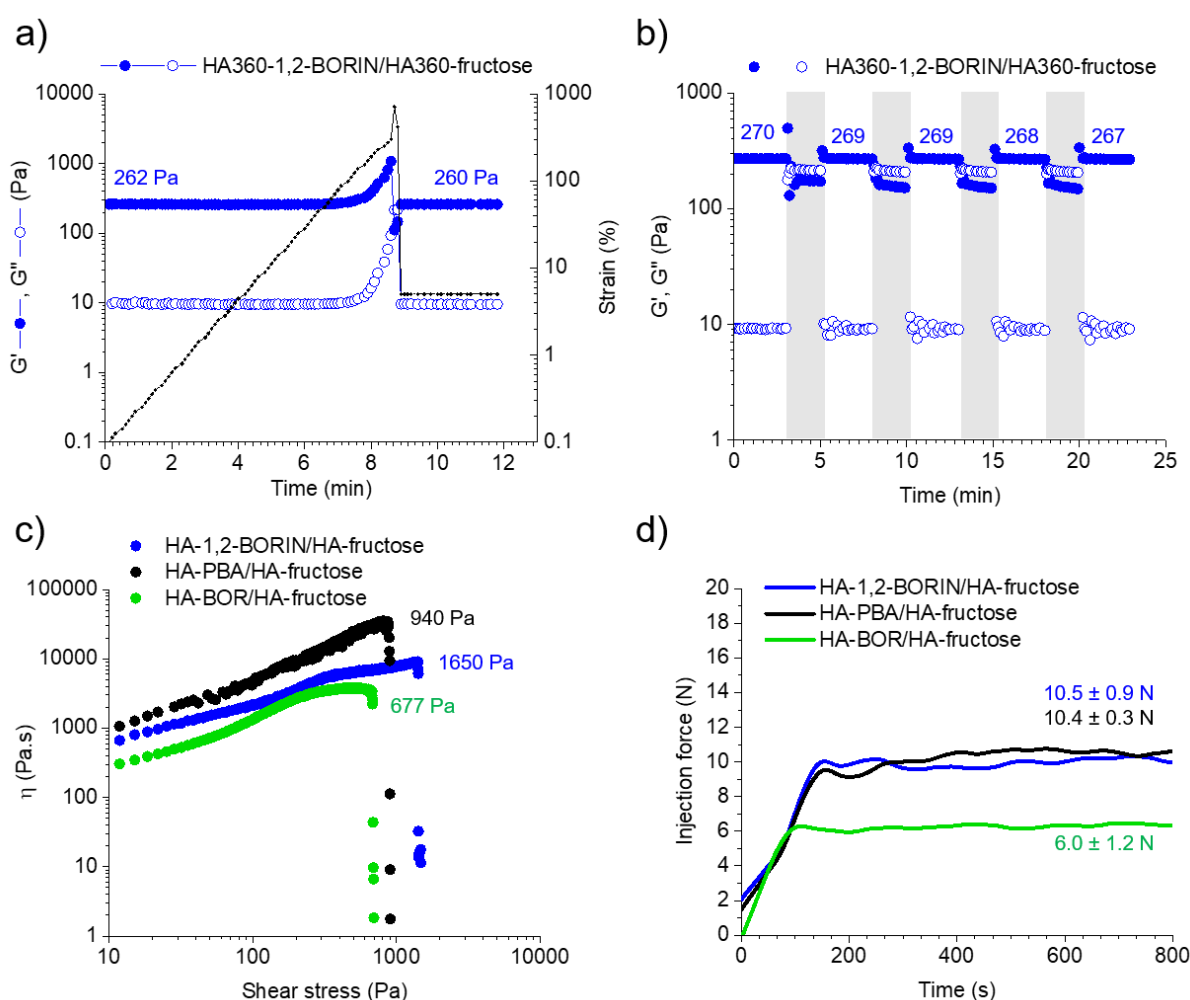


Figure 4. Self-healing ability of the new HA-1,2-BORIN/HA-fructose gel: (a) dynamic rheological behavior of G' (filled symbols) and G'' (empty symbols) at failure under increasing strain application (approximately 700 %), followed by the immediate recovery of the rheological moduli at a strain of 5 % (linear viscoelastic region); and (b) self-recovery of the gel after four cycles of strain-induced breakdowns, by applying a value of strain above the linear viscoelastic region (shaded regions, 350 %) for 2 min, followed by linear recovery measurements for 3 min (unshaded regions, strain of 5 %). Injectability of the HA-1,2-BORIN/HA-fructose hydrogel compared to the HA-PBA (BOR)/HA-fructose assemblies: (c) yield stress and viscosity of the three assemblies (average values of yield stress from at least two identical measurements); and (d) injection force measurements over time for the three

formulations injected from a 1 mL syringe with a 27 G needle, at a flow rate of 1 mm/min (average values of extrusion force determined from triplicates).

3. Conclusion

In this work, we demonstrated the feasibility of HA hydrogel formation at physiological pH through complexation of an original benzoxaborin derivative (1,2-BORIN) grafted on HA with a second HA conjugate modified with fructose moieties. This new hydrogel exhibited rheological properties similar to the previously studied HA-PBA (BOR)/HA-fructose networks. By contrast, the use of HA modified with conventional benzoxaborin (2,1-BORIN) as boronic acid partner of HA-fructose only allowed formation of a viscoelastic solution with a low elastic modulus. The different macroscopic rheological properties observed for the mixtures based on HA-1,2-BORIN (2,1-BORIN) and HA-fructose were found to be closely linked to the different structure and pK_a values of these arylboronic acid derivatives. Indeed, the former showed polymer association at lower pH correlating with the low pK_a of free 1,2-ABORIN, whereas the latter exhibited viscoelastic properties only at basic pH due to its higher pK_a . These results suggest a binding mode of 1,2-BORIN towards fructose similar to that of BOR, which involves the opening of the endocyclic B-O bond. However, further studies are still needed to elucidate the exact binding mode of this new derivative with fructose and other saccharides. Besides, continued investigation of the applicability of these HA hydrogels as promising injectable scaffolds for encapsulation of cells or bioactive molecules will expand their application in many innovative biomedical fields.

4. Experimental section

Materials. Sodium hyaluronate (HA) possessing a weight-average molar mass (M_w) of 360 kg/mol was donated by Galderma-Nestlé Skin Health. The molar mass distribution and the weight-average molar mass of these samples were determined by size exclusion chromatography using a Waters GPC Alliance chromatograph (USA) equipped with a differential refractometer and a light scattering detector (MALLS) from Wyatt (USA); the solution was injected at a concentration of 1×10^{-3} g/mL in 0.1 M NaNO₃, at a flow rate of 0.5 mL/min and at a column temperature of 30 °C. The dispersity (D) of the samples are $M_w/M_n \approx 1.5-2$. The overlap concentration C^* for the HA sample in buffer at 25 °C is around 1 g/L. This value was derived from the intrinsic viscosity assuming that $C^*[\eta]$ is about unity.³⁰ A HA sample with a lower M_w (5 kg/mol), purchased from the same supplier, was used to synthesize HA derivatives for NMR studies (determination of binding constants). This low M_w HA sample was used to circumvent limitations due to the high viscosity of concentrated solutions of high M_w

HA. 5-amino-2-hydroxymethylphenylboronic acid (6-aminobenzoboroxole, ABOR) was purchased from Combi-Blocks. 1-Amino-1-deoxy-D-fructose hydrochloride (fructosamine) was supplied by Carbosynth. 3-Aminophenylboronic acid hemisulfate salt (APBA), 4-(4,6-dimethoxy-1,3,5-triazin-2-yl)-4-methylmorpholinium chloride (DMTMM), picrylsulfonic acid solution (TNBS), 4-(2-hydroxyethyl)piperazine-1-ethanesulfonic acid (HEPES), phosphate buffered saline (PBS) and other chemicals were purchased from Sigma-Aldrich-Fluka and were used without further purification.

Methods.

NMR spectroscopy. ^1H , ^{13}C and ^{11}B NMR spectra were recorded at 25 °C or 80 °C using a Bruker AVANCE III HD spectrometer operating at 400.13 MHz (^1H), 100.61 MHz (^{13}C) and 128.38 MHz (^{11}B). ^1H NMR spectra were recorded by applying a 90° tip angle for the excitation pulse, and a 10 s recycle delay for accurate integration of the proton signals. ^{13}C NMR spectra were recorded by applying a 90° tip angle for the excitation pulse and a 2 s recycle delay. Deuterium oxide (D_2O) was obtained from Euriso-top (Saint-Aubin, France). Chemical shifts (δ in ppm) are given relative to external tetramethylsilane (TMS = 0 ppm) and calibration was performed using the signal of the residual protons of the solvent as a secondary reference. All NMR spectra were analyzed with Topspin 3.1 software from Bruker AXS.

Determination of the $\text{p}K_a$ of 1,2-ABORIN, 2,1-ABORIN and ABOR by ^{11}B NMR spectroscopy. ^{11}B NMR chemical shifts of the aminobenzoxaborin compounds were determined with increasing pH (10 % D_2O in H_2O , 16 mM in 0.01 M phosphate buffer). Chemical shifts (δ in ppm) for each ^{11}B spectrum were given relative to external $\text{Et}_2\text{O}\text{-BF}_3$ in deuterated chloroform as zero. The values of $\text{p}K_a$ were determined from the curve fitting of the variation of δ (in ppm) with the pH using the Boltzmann equation (Figures 3d, 3e and S21).

Synthesis of HA derivatives. HA-1,2-BORIN, HA-2,1-BORIN, HA-PBA, HA-BOR and HA-fructose were synthesized by an amide coupling reaction from 1,2-ABORIN, 2,1-ABORIN, APBA, ABOR and fructosamine (containing free primary amine groups), respectively. To this end, 1,2-ABORIN (0.026 g, 0.12 mmol) or 2,1-ABORIN (0.0205 g, 0.12 mmol) or APBA (0.022 g, 0.12 mmol) or ABOR (0.025 g, 0.135 mmol) or fructosamine (0.024 g, 0.112 mmol) was added to a water/DMF (3/2, v/v) mixture containing DMTMM (0.207 g, 0.75 mmol) and HA (0.3 g, 0.75 mmol) and the pH was adjusted to 6.5 using 0.5 M aqueous NaOH. After stirring for 24 h at room temperature, the different HA derivatives were purified by ultrafiltration using deionized water and the products were recovered by freeze-drying (Table 2). The DS of the HA derivatives were found to be 0.1-0.15 from ^1H NMR analyses (Figure S1-S4) or from the

reaction kinetics using the TNBS method (Figure S6). The HA-gluconamide conjugate with a DS of 0.1 was synthesized as previously reported (*cf. chapter 2*).

Table 2. Reaction conditions for the synthesis of HA360 conjugates.

HA derivative	R-NH ₂ /HA molar ratio	DS	Coupling (%)	Yield (%)
HA-1,2-BORIN	0.16	0.15 ^a	94	81
HA-2,1-BORIN	0.16	0.15 ^a	94	90
HA-BOR	0.16	0.1 ^a	75	91
HA-PBA	0.16	0.15 ^a	94	98
HA-fructose	0.15	0.15 ^b	100	96

^aDS by ¹H NMR (10 % of accuracy).

^bDS estimated from the reaction kinetics using TNBS.

Preparation of HA-1,2-BORIN (HA-2,1-BORIN or HA-BOR or HA-PBA) and HA-fructose mixtures. The different HA derivatives were solubilized in 0.01 M HEPES buffer containing 0.15 M NaCl pH 7.4. The dissolution time was at least 12 h at 4 °C. The solutions of HA-1,2-BORIN or HA-2,1-BORIN or HA-BOR or HA-PBA and of HA-fructose were mixed under vigorous stirring at room temperature, at a total polymer concentration of 15 g/L and with boronic acid/sugar molar ratio of 1. The mixtures were then allowed to rest at 4 °C overnight before rheological analysis. To study the rheological properties of HA hydrogels as a function of pH, the same buffer was prepared at pH values adjusted to 6, 6.5, 7, 8 and 9.

Rheology. Oscillatory shear experiments were performed with a cone-plate rheometer (AR2000EX from TA Instruments). All the dynamic rheological data were checked as a function of strain amplitude to ensure that the measurements were performed in the linear viscoelastic region. The cone used for viscoelastic samples has a diameter of 2 cm and an angle of 4°, whereas viscous solutions were analyzed using a cone of 6 cm of diameter and an angle of 1°. To prevent water evaporation, the measuring system was surrounded with a low-viscosity silicon oil (50 mPa.s) carefully added to the edges of the cone.

Injection force measurements. Hydrogel injection forces were measured using a mechanical testing machine (SHIMADZU EZ-SX). A “homemade” support was used to fix and stabilize the syringe during the test. This base was used as a stage with no accompaniments. The measurements were made using the tensile extension mode, at a flow rate of 1 mm/mL. Hydrogels were prepared by as previously described and loaded into 1 mL syringes. The loaded syringes were kept at 4 °C overnight before analysis at room temperature. Hydrogel injection forces were measured over time using a 27 gauge needle.

Determination of K_a by ITC. Calorimetric titration experiments were carried out on a Microcal VP-ITC titration microcalorimeter (Northampton, U.S.A.). All titrations were performed using solutions of 1,2-ABORIN (2,1-ABORIN or ABOR or APBA) and free D-fructose solubilized in

0.01 M PBS, with pH adjusted to 7.4 (± 0.1) using a pH-meter, by carefully adding 1 M NaOH when necessary. The reaction cell ($V = 1.4478$ mL) contained a solution of “molecule 2” (Table 3). A series of 28 injections of 5 or 10 μL of a solution of “molecule 1” was made from a computer-controlled 300 μL microsyringe at an interval of 400 s into the solution contained in the reaction cell, while stirring at 300 rpm at 25°C. The raw experimental data were reported as the amount of heat produced after each injection of boronic acid as a function of time. The amount of heat produced per injection was calculated by integration of the area under individual peaks by the instrument software, after taking into account heat of dilution. The data were analyzed using the one set of site fitting model (Origin 7.0 software package). Table 3 summarizes the experimental conditions used for the ITC measurements.

Table 3. Experimental conditions of the calorimetric titrations.

Entry	Molecule 1 in syringe	[Molecule 1] (mM)	Molecule 2 in cell	[Molecule 2] (mM)
1	D-fructose	75	1,2-ABORIN	2
2	D-fructose	125	2,1-ABORIN	3.5
3	D-fructose	175	APBA	5
4	D-fructose	75	ABOR	2

5. References

- (1) Loebel, C.; Rodell, C. B.; Chen, M. H.; Burdick, J. A. Shear-Thinning and Self-Healing Hydrogels as Injectable Therapeutics and for 3D-Printing. *Nat. Protoc.* **2017**, *12* (8), 1521–1541.
- (2) Wei, Z.; Yang, J. H.; Zhou, J.; Xu, F.; Zrínyi, M.; Dussault, P. H.; Osada, Y.; Chen, Y. M. Self-Healing Gels Based on Constitutional Dynamic Chemistry and Their Potential Applications. *Chem Soc Rev* **2014**, *43* (23), 8114–8131.
- (3) Chen, M. H.; Wang, L. L.; Chung, J. J.; Kim, Y.-H.; Atluri, P.; Burdick, J. A. Methods To Assess Shear-Thinning Hydrogels for Application As Injectable Biomaterials. *ACS Biomater. Sci. Eng.* **2017**, *3* (12), 3146–3160.
- (4) Tang, S.; Ma, H.; Tu, H.-C.; Wang, H.-R.; Lin, P.-C.; Anseth, K. S. Adaptable Fast Relaxing Boronate-Based Hydrogels for Probing Cell-Matrix Interactions. *Adv. Sci.* **2018**, 1800638.
- (5) Yan, J.; Springsteen, G.; Deeter, S.; Wang, B. The Relationship among PKa, PH, and Binding Constants in the Interactions between Boronic Acids and Diols—It Is Not as Simple as It Appears. *Tetrahedron* **2004**, *60* (49), 11205–11209.
- (6) Sumida, Y.; Harada, R.; Kato-Sumida, T.; Johmoto, K.; Uekusa, H.; Hosoya, T. Boron-Selective Biaryl Coupling Approach to Versatile Dibenzoxaborins and Application to Concise Synthesis of Defucogilvocarcin M. *Org. Lett.* **2014**, *16* (23), 6240–6243.
- (7) Mulla, H. R.; Agard, N. J.; Basu, A. 3-Methoxycarbonyl-5-Nitrophenyl Boronic Acid: High Affinity Diol Recognition at Neutral PH. *Bioorg. Med. Chem. Lett.* **2004**, *14* (1), 25–27.
- (8) Zhang, C.; Losego, M. D.; Braun, P. V. Hydrogel-Based Glucose Sensors: Effects of Phenylboronic Acid Chemical Structure on Response. *Chem. Mater.* **2013**, *25* (15), 3239–3250.

- (9) Tomsho, J. W.; Pal, A.; Hall, D. G.; Benkovic, S. J. Ring Structure and Aromatic Substituent Effects on the pK_a of the Benzoxaborole Pharmacophore. *ACS Med. Chem. Lett.* **2012**, 3 (1), 48–52.
- (10) Dowlut, M.; Hall, D. G. An Improved Class of Sugar-Binding Boronic Acids, Soluble and Capable of Complexing Glycosides in Neutral Water. *J. Am. Chem. Soc.* **2006**, 128 (13), 4226–4227.
- (11) Adamczyk-Woźniak, A.; Borys, K. M.; Sporzyński, A. Recent Developments in the Chemistry and Biological Applications of Benzoxaboroles. *Chem. Rev.* **2015**, 115, 5224–5247.
- (12) Dong, Y.; Wang, W.; Veisoh, O.; Appel, E. A.; Xue, K.; Webber, M. J.; Tang, B. C.; Yang, X.-W.; Weir, G. C.; Langer, R.; et al. Injectable and Glucose-Responsive Hydrogels Based on Boronic Acid–Glucose Complexation. *Langmuir* **2016**, 32 (34), 8743–8747.
- (13) Roberts, M. C.; Hanson, M. C.; Massey, A. P.; Karren, E. A.; Kiser, P. F. Dynamically Restructuring Hydrogel Networks Formed with Reversible Covalent Crosslinks. *Adv. Mater.* **2007**, 19 (18), 2503–2507.
- (14) Tarus, D.; Hachet, E.; Messenger, L.; Catargi, B.; Ravaine, V.; Auzély-Velty, R. Readily Prepared Dynamic Hydrogels by Combining Phenyl Boronic Acid- and Maltose-Modified Anionic Polysaccharides at Neutral pH. *Macromol. Rapid Commun.* **2014**, 35 (24), 2089–2095.
- (15) Yesilyurt, V.; Webber, M. J.; Appel, E. A.; Godwin, C.; Langer, R.; Anderson, D. G. Injectable Self-Healing Glucose-Responsive Hydrogels with pH-Regulated Mechanical Properties. *Adv. Mater.* **2016**, 28 (1), 86–91.
- (16) Deng, C. C.; Brooks, W. L. A.; Abboud, K. A.; Sumerlin, B. S. Boronic Acid-Based Hydrogels Undergo Self-Healing at Neutral and Acidic pH. *ACS Macro Lett.* **2015**, 4 (2), 220–224.
- (17) Chen, Y.; Wang, W.; Wu, D.; Nagao, M.; Hall, D. G.; Thundat, T.; Narain, R. Injectable Self-Healing Zwitterionic Hydrogels Based on Dynamic Benzoxaborole–Sugar Interactions with Tunable Mechanical Properties. *Biomacromolecules* **2018**, 19 (2), 596–605.
- (18) Chen, Y.; Diaz-Dussan, D.; Wu, D.; Wang, W.; Peng, Y.-Y.; Asha, A. B.; Hall, D. G.; Ishihara, K.; Narain, R. Bioinspired Self-Healing Hydrogel Based on Benzoxaborole-Catechol Dynamic Covalent Chemistry for 3D Cell Encapsulation. *ACS Macro Lett.* **2018**, 7 (8), 904–908.
- (19) Lin, M.; Sun, P.; Chen, G.; Jiang, M. The Glyco-Stereoisomerism Effect on Hydrogelation of Polymers Interacting via Dynamic Covalent Bonds. *Chem Commun* **2014**, 50 (68), 9779–9782.
- (20) Springsteen, G.; Wang, B. A Detailed Examination of Boronic Acid–Diol Complexation. *Tetrahedron* **2002**, 58 (26), 5291–5300.
- (21) Liu, C. T.; Tomsho, J. W.; Benkovic, S. J. The Unique Chemistry of Benzoxaboroles: Current and Emerging Applications in Biotechnology and Therapeutic Treatments. *Bioorg. Med. Chem.* **2014**, 22 (16), 4462–4473.
- (22) Bérubé, M.; Dowlut, M.; Hall, D. G. Benzoboroxoles as Efficient Glycopyranoside-Binding Agents in Physiological Conditions: Structure and Selectivity of Complex Formation. *J. Org. Chem.* **2008**, 73 (17), 6471–6479.
- (23) Saito, H.; Otsuka, S.; Nogi, K.; Yorimitsu, H. Nickel-Catalyzed Boron Insertion into the C2–O Bond of Benzofurans. *J. Am. Chem. Soc.* **2016**, 138 (47), 15315–15318.

- (24) Angyal, S. J. The Composition of Reducing Sugars in Solution. In *Advances in Carbohydrate Chemistry and Biochemistry*; Tipson, R. S., Horton, D., Eds.; Academic Press, 1984; Vol. 42, pp 15–68.
- (25) Wu, X.; Li, Z.; Chen, X.-X.; Fossey, J. S.; James, T. D.; Jiang, Y.-B. Selective Sensing of Saccharides Using Simple Boronic Acids and Their Aggregates. *Chem. Soc. Rev.* **2013**, *42* (20), 8032.
- (26) D'Este, M.; Eglin, D.; Alini, M. A Systematic Analysis of DMTMM vs EDC/NHS for Ligation of Amines to Hyaluronan in Water. *Carbohydr. Polym.* **2014**, *108*, 239–246.
- (27) Cayot, P.; Tainturier, G. The Quantification of Protein Amino Groups by the Trinitrobenzenesulfonic Acid Method: A Reexamination. *Anal. Biochem.* **1997**, *249* (2), 184–200.
- (28) Ellis, G. A.; Palte, M. J.; Raines, R. T. Boronate-Mediated Biologic Delivery. *J. Am. Chem. Soc.* **2012**, *134* (8), 3631–3634.
- (29) Mouser, V. H. M.; Melchels, F. P. W.; Visser, J.; Dhert, W. J. A.; Gawlitta, D.; Malda, J. Yield Stress Determines Bioprintability of Hydrogels Based on Gelatin-Methacryloyl and Gellan Gum for Cartilage Bioprinting. *Biofabrication* **2016**, *8* (3), 035003.
- (30) Macosko, C. W. G. *Rheology: Principles, Measurements, and Applications*; VCH Publishers: Weinheim, Germany, 1994.

Supporting Information

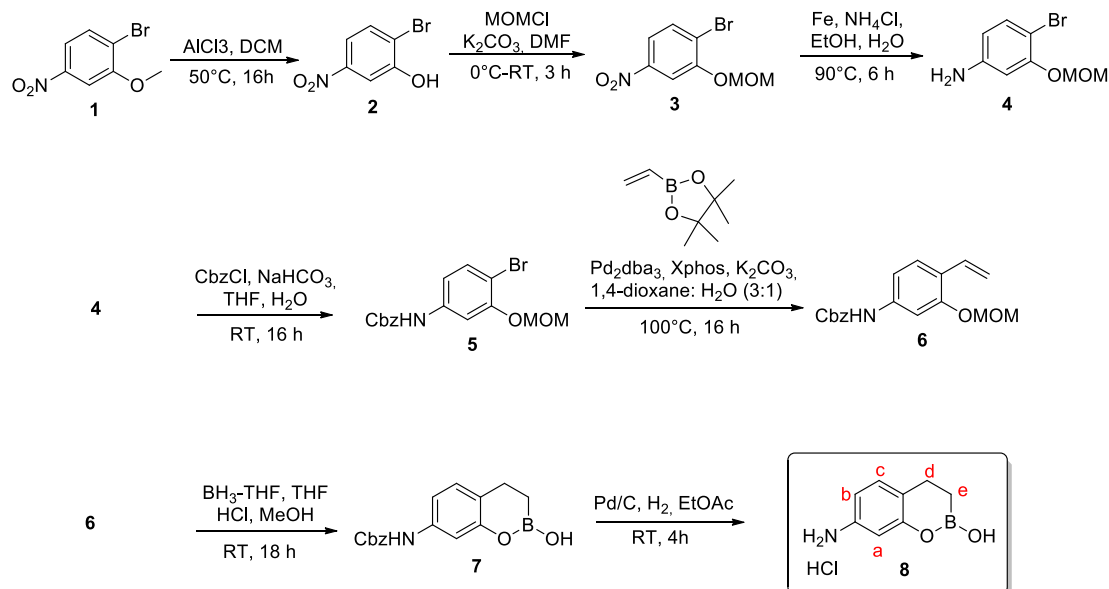
Injectable self-healing hyaluronic acid hydrogels based on boronate ester crosslinks between benzoxaborin derivatives and saccharides

Table of Contents

224	1. Synthesis of aminobenzoxaborin (ABORIN) compounds
228	2. ^1H NMR spectra of HA-1,2-BORIN, HA-2,1-BORIN, HA-BOR and HA-PBA derivatives synthesized by amide coupling reaction (M_w HA = 360 kg/mol)
231	3. 2D HSQC NMR characterization of HA-fructose conjugate synthesized by amide coupling reaction (M_w HA = 360 kg/mol)
232	4. Determination of the degree of substitution (DS) of HA-fructose from the kinetics of the amide coupling reaction (M_w HA = 360 kg/mol)
233	5. Methodology for K_a measurements by ^1H NMR spectroscopy
235	6. Determination of K_a by ^1H NMR for 1,2-ABORIN (2,1-ABORIN) and fructose (free fructose and HA-fructose)
238	7. Determination of K_a by ^1H NMR for APBA (ABOR) and fructose (free fructose and HA-fructose)
241	8. Calorimetric titration of 1,2-ABORIN (2,1-ABORIN) with free D-fructose
242	9. Calorimetric titration of APBA (ABOR) with free D-fructose
243	10. Rheological analysis of the HA-1,2-BORIN (2,1-BORIN, BOR or PBA) alone at pH 7.4 (M_w HA = 360 g/mol)
244	11. Investigation of the opening of the endocyclic B-O bond of 1,2-ABORIN (ABOR) in complexation with free/grafted fructose
245	12. Determination of the pK_a of free ABOR by ^{11}B NMR spectroscopy
245	13. References

1. Synthesis of aminobenzoxaborin (ABORIN) compounds

7-amino-3,4-dihydro-2H-benzo[e][1,2]oxaborinin-2-ol (1,2-ABORIN)



Synthesis of 2:

To a stirred solution of **1** (200 g, 862 mmol) in DCM (600 mL), AlCl_3 (334 g, 2586 mmol) was added at RT. The reaction mixture was heated to 50°C for 16 h under N_2 . The reaction was monitored by TLC (30 % EtOAc in *n*-hexanes). After completion of the reaction, the reaction mixture was cooled to RT and quenched with ice (2 kg). The pH was adjusted to ~ 4 with ammonium chloride and the aqueous layer was extracted with DCM (3 L). The organic layer was separated and washed with brine solution (1.5 L), dried over Na_2SO_4 and evaporated under vacuum to get **2** as a yellow solid (130 g, 70 %).

$^1\text{H NMR}$ (400 MHz, DMSO-d_6 , 298 K): 11.33 (s, 1H), 7.81-7.79 (d, $J = 8.8$ Hz, 1H), 7.73-7.72 (d, $J = 2.4$ Hz, 1H), 7.61-7.58 (dd, $J = 8.8$ Hz, 2.8 Hz, 1H).

LC-MS (ES, m/z): 216.28 $[\text{M}+\text{H}]^+$.

Synthesis of 3:

To a stirred solution of compound **2** (130 g, 596 mmol) in DMF (400 mL), was added K_2CO_3 (206.03 g, 1490 mmol) at RT under stirring for 10 min, followed by addition of MOM-Cl (96 g, 1192 mmol). The reaction mixture was stirred at RT for 16 h under N_2 . The reaction was monitored by TLC (30 % ethyl acetate in *n*-hexanes). After completion of the reaction, the reaction mixture was quenched with ice (1 kg). The solids observed were filtered through Buchner funnel, washed with cold water (1 L) and dried under vacuum to yield **3** as a brown solid (98 g, 62 %).

$^1\text{H NMR}$ (400 MHz, DMSO-d_6 , 298 K): δ (ppm) 8.01-8.00 (d, 1H), 7.79-7.71 (m, 2H), 5.35 (s, 2H), 3.54 (s, 3H).

LC-MS (ES, m/z): 215.89 $[\text{M}+\text{H}]^+$.

Synthesis of 4:

To a stirred solution of **3** in a mixture of ethanol and water, iron powder was added followed by ammonium chloride at RT. The reaction mixture was heated to 90°C for 6 h. The reaction progress was monitored by TLC (40 % ethyl acetate in *n*-hexanes). After completion of the

reaction, the medium was cooled to RT, filtered through celite bed and the filtrate was concentrated under vacuum to get a crude residue. The crude residue was portioned between ethyl acetate and water; the organic layer was dried and evaporated under vacuum to afford compound **4** as a sticky liquid (80 g, 93 %).

¹H NMR (400 MHz, DMSO-*d*₆, 298 K): δ (ppm) 7.13-7.11 (d, *J* = 8.4 Hz, 1H), 6.44-6.43 (d, *J* = 2.4 Hz, 1H), 6.18-6.16 (dd, *J* = 2.4 Hz, 8.4 Hz, 1H), 5.28 (s, 2H), 5.14 (s, 2H), 3.39 (s, 3H).

LC-MS (ES, *m/z*): 232 [M+H]⁺.

Synthesis of 5:

To a stirred solution of **4** (80 g, 346 mmol) in THF (900 mL), a solution of NaHCO₃ (49.45 g, 588 mmol) in water (800 mL) was added, followed by Cbz-Cl (117.6 g, 692 mmol) at 0 °C. The reaction mixture was stirred at RT for 6 h. The reaction progress was monitored by TLC (40 % ethyl acetate in *n*-hexanes). After completion of the reaction, the medium was filtered and the filtrate was evaporated under vacuum to get a residue, which was diluted with ethyl acetate (1000 mL) and water (400 mL). The organic layer was separated and washed with water (2 x 500 mL) and brine (250 mL), dried over sodium sulfate and concentrated under reduced pressure to afford crude compound **5** as a white solid (75 g).

¹H NMR (400 MHz, DMSO-*d*₆, 298 K): δ (ppm) 7.44-7.26 (m, 8H), 6.91 (br, 1H), 6.68 (br, 1H), 5.231 (s, 2H), 5.18 (s, 2H), 3.51 (s, 3H).

LC-MS (ES, *m/z*): 364 [M+H]⁺.

Synthesis of 6:

To a stirred solution containing **5** (65 g, 177 mmol) in dioxane (650 mL) and water (400 mL), K₂CO₃ (73.59 g, 531 mmol) and 4,4,5,5-tetramethyl-2-vinyl-1,3,2-dioxaborolane (44.47 g, 301.9 mmol) were added. The reaction mixture was purged with N₂ gas for 30 min, followed by addition of Pd₂(dba)₃ (16.25 g, 17.7 mmol) and X-phos (8.45 g, 17.7 mmol). The reaction mixture was heated to 100 °C for 16 h. The reaction progress was monitored by TLC (30 % ethyl acetate in *n*-hexanes). After completion of the reaction, the medium was filtered through celite bed and washed with EtOAc (500 mL). The filtrate was evaporated under vacuum to get crude residue **6** as a thick brown syrup (100 g, crude). The crude product was purified by column using 60-120 silica gel. The product was eluted at 15 % EtOAc in petroleum ether, and the combined fraction was evaporated under vacuum to yield **6** as a brown solid (38 g, 69 %).

¹H NMR (400 MHz, DMSO-*d*₆, 298 K): δ (ppm) 7.39-7.34 (m, 5H), 7.02-6.95 (m, 2H), 6.67 (br, 1H), 5.69-5.64 (d, *J* = 17.6 Hz, 1H), 5.22-5.19 (m, 5H), 3.49 (s, 3H).

LC-MS (ES, *m/z*): 314.19 [M+H]⁺.

Synthesis of 7:

To a stirred solution of compound **6** in THF (400 mL), was added BH₃-THF in THF at 0 °C. The reaction mixture was stirred for 3 h at RT. The reaction progress was monitored by TLC (40% EtOAc in *n*-hexanes). Then, the medium was cooled to 0 °C, quenched with cold water (250 mL) and stirred for 30 min. Volatiles were evaporated under vacuum to get crude, diluted with methanol (250 mL) and 6 N HCl (190 mL) at 0 °C and stirred at RT for 16 h. The reaction mixture was concentrated under reduced pressure. The residue was portioned between water (500 mL) and EtOAc (1000 mL); the organic layer was separated and washed with water (500 mL) and brine (250 mL), dried over sodium sulfate and concentrated under reduced pressure to afford crude compound **7** as a thick colourless syrup (40 g, crude). The crude product was then purified by column using 60-120 silica gel. The product was eluted at 20 % EtOAc in petroleum ether, and the combined fraction was evaporated under vacuum to get **7** as a white solid (9.5 g, 26 %).

¹H NMR (400 MHz, DMSO-d₆, 298 K): δ (ppm) 9.66 (s, 1H), 8.91 (s, 1H), 7.43-7.34 (m, 5H), 7.06-6.99 (m, 3H), 5.13 (s, 2H), 2.66-2.62 (t, *J* = 7.6 Hz, 2H), 1.01-0.97 (t, *J* = 8.0 Hz, 2H).

LC-MS (ES, *m/z*): 298.15 [M+H]⁺.

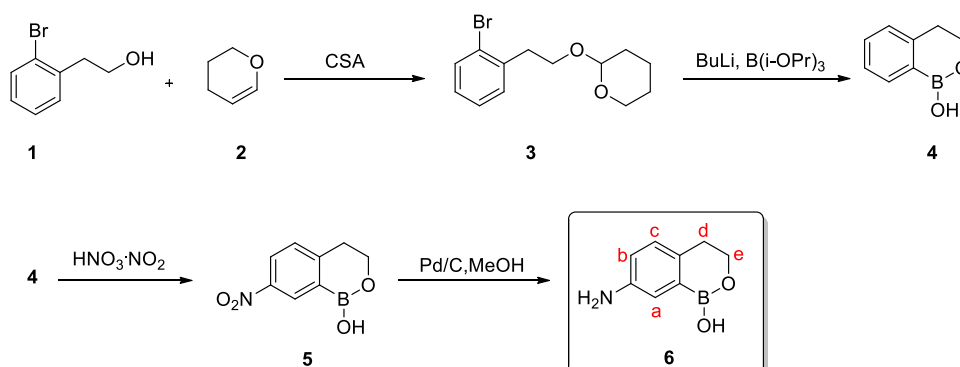
Synthesis of 8 (1,2-ABORIN):

Pd/C (10% Wt) (940 mg) was added to a stirred solution of **7** (9.4 g, 316 mmol) in EtOAc (180 mL). The reaction mixture was hydrogenated under balloon pressure at room temperature for 4 h. The reaction progress was monitored by TLC (50 % ethyl acetate in *n*-hexanes). After completion of the reaction, the medium was filtered through celite bed and washed with EtOAc (500 mL). The filtrate was evaporated to 1/3 part the cooled 0 °C, and 4 M HCl in dioxane was added under stirring for 1 h at RT. Then, the reaction mixture was concentrated under reduced pressure to afford **8** as an off-white solid (5.2 g, 82 %).

¹H NMR (400 MHz, DMSO-d₆, 298 K): δ (ppm) 10.00 (br, 4H), 7.19-7.18 (d, *J* = 12.8 Hz, 1H, **Ha**), 6.89-6.86 (m, 2H, **Hb-Hc**), 2.74-2.70 (t, *J* = 7.6 Hz, 2H, **Hd**), 1.05-1.01 (t, *J* = 8.0 Hz, 2H, **He**).

LC-MS (ES, *m/z*): 164.1 [M+H]⁺.

7-amino-3,4-dihydro-1*H*-benzo[*c*][1,2]oxaborinin-1-ol (2,1-ABORIN)



Synthesis of 3:

To a solution of compound **1** (20 g, 100.0 mmol, 1.0 eq) in DCM (400 mL) was added compound **2** (13.6 mL, 150 mmol, 1.5 eq), followed by camphor sulfonic acid (CSA, 400 mg, 0.02 eq). The mixture was stirred at room temperature for 2 h. HPLC indicated that the reaction was completed. After adding K₂CO₃ (1.2 g), the mixture was filtered to remove the precipitate, the filtrate was washed with H₂O (200 mL) and brine (200 mL). Then, the organic phase was dried, filtered and the filtrate was concentrated under reduced pressure. The oily residue was applied to silica chromatography eluting with EtOAc/Heptanes (0:100 to 50:50) to give compound **3** as a yellow liquid (26.4 g, not pure).

Synthesis of 4:

To a solution of **3** (26.0 g, 91.0 mmol, 1.0 eq.) in THF (500 mL) at -78 °C, was slowly added *n*-BuLi (2.5 M in hexane, 73 mL, 182 mmol, 2.0 eq) under nitrogen atmosphere. Triisopropyl borate (68.6 g, 364 mmol, 4.0 eq) was then added and stirred at -78 °C for 30 min. The mixture was allowed to warm to room temperature gradually and stirred overnight. HPLC indicated that the reaction was completed. After carefully adding HCl (260 mL, 6 N), the yellowish solution was stirred at room temperature for another 1 h and then poured into a mixture of EtOAc (600 mL) and H₂O (300 mL). The layers were separated, and the aqueous phase was extracted

with EtOAc (3 x 200 mL). Combined organic extracts was washed with H₂O (200 mL), brine (200 mL), dried over MgSO₄, filtered and the filtrate was concentrated under reduced pressure. The oily residue was applied to silica chromatography (petroleum ether/ethyl acetate 5:1) to give compound **4** (11.5 g, 88 %) as a light-yellow solid.

¹H NMR (300 MHz, DMSO-d₆, 298 K): δ (ppm) 8.40 (br, 1H), 7.68 (d, *J* = 7.2 Hz, 1H), 7.38-7.36 (m, 1H), 7.25-7.18 (m, 2H), 4.07 (t, *J* = 6.0 Hz, 2H), 2.86 (t, *J* = 6.0 Hz, 2H).

Synthesis of 5:

To 100 mL fuming HNO₃ at -45 °C, compound **4** (13.2 g, 89.1 mmol) was added in small portions while maintaining the reaction temperature between -40 to -45°C. Once the addition was completed, the resulting solution was allowed to stir at -45°C for additional 10 min before poured into crushed ice (500 g). The ice mixture was allowed to warm up to room temperature gradually and the precipitate was collected by filtration and washed with H₂O to afford **5** (4.5 g, 26 %) as a white powder.

¹H NMR (300 MHz, DMSO-d₆, 298 K): δ (ppm) 8.48 (d, *J* = 2.1 Hz, 1H), 8.25 (dd, *J* = 2.4, 8.4 Hz, 1H), 7.52 (d, *J* = 8.4 Hz, 1H), 4.12 (t, *J* = 6.0 Hz, 2H), 3.02 (t, *J* = 5.7 Hz, 2H).

Synthesis of 6 (2,1-ABORIN):

To a solution of compound **5** (2.5 g, 12.9 mmol, 1 eq) in MeOH (25 mL), was added Pd/C (0.25 g) under N₂. Then, the suspension was degassed under vacuum and purged with H₂ for three times. The reaction mixture was stirred at 40 °C for 5 h under H₂. TLC (petroleum ether/ethyl acetate 7:3) indicated that the reaction was completed. The reaction mixture was filtered to remove Pd/C and the filtrate was concentrated to dryness to give **6** (1.7 g, 81 %).

¹H NMR (400 MHz, CDCl₃, 298 K): δ (ppm) 7.11-6.97 (m, 2H, **Ha-Hc**), 6.79-6.73 (m, 1H, **Hb**), 4.23-4.18 (m, 2H, **He**), 2.88-2.82 (m, 2H, **Hd**).

LC-MS (MS, *m/z*): 164.1 [M+H]⁺.

2. ^1H NMR spectra of HA-1,2-BORIN, HA-2,1-BORIN, HA-BOR and HA-PBA derivatives synthesized by amide coupling reaction (M_w HA = 360 kg/mol)

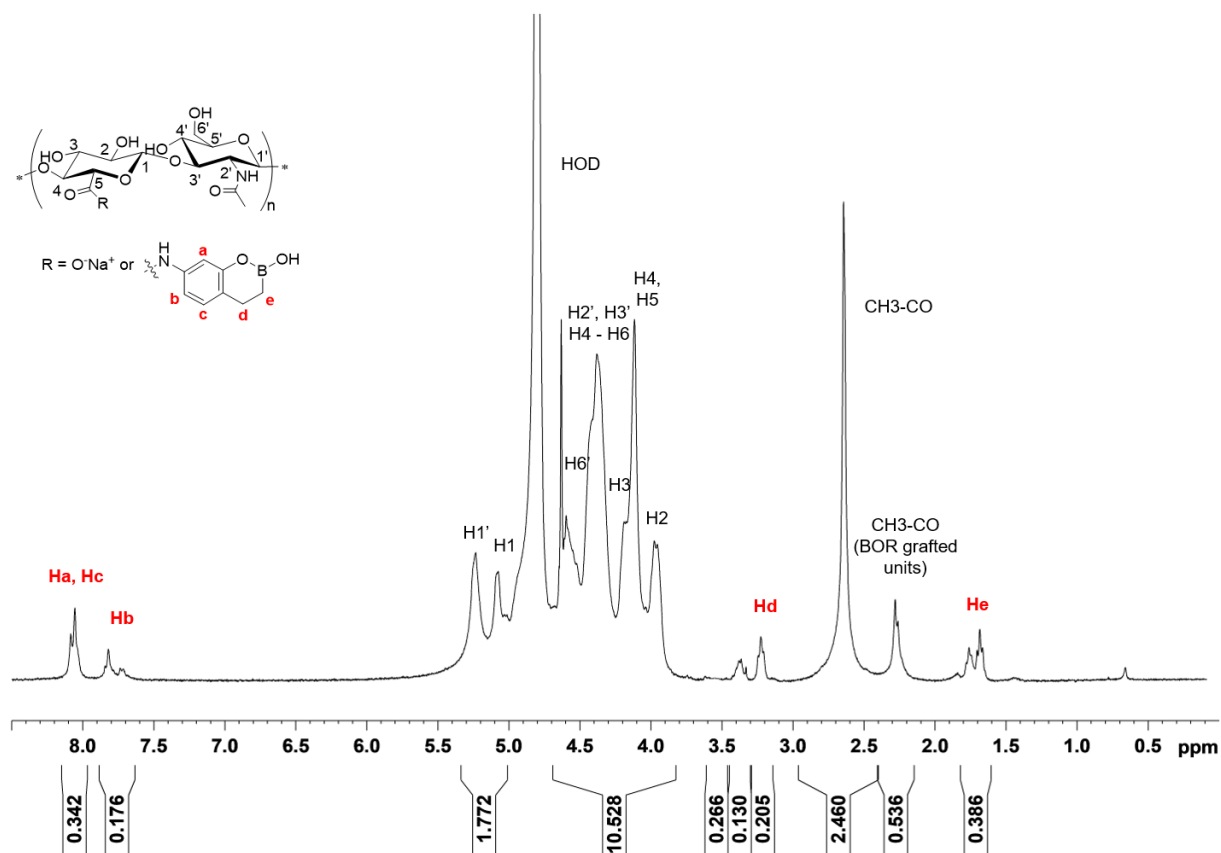


Figure S1. ^1H NMR spectrum (400 MHz, D_2O , 6 mg·mL $^{-1}$, 80 °C) of HA360-1,2-BORIN.

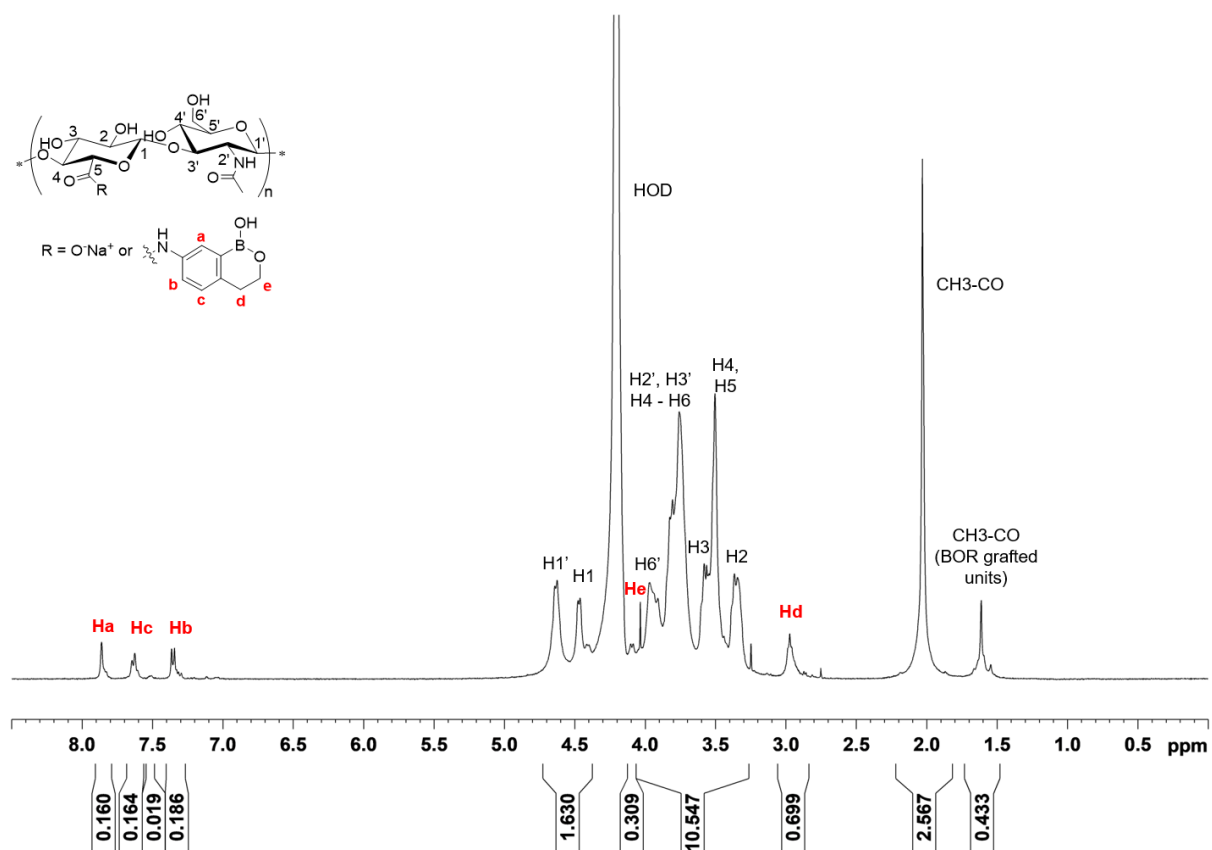


Figure S2. ^1H NMR spectrum (400 MHz, D_2O , $6 \text{ mg}\cdot\text{mL}^{-1}$, $80 \text{ }^\circ\text{C}$) of HA360-2,1-BORIN.

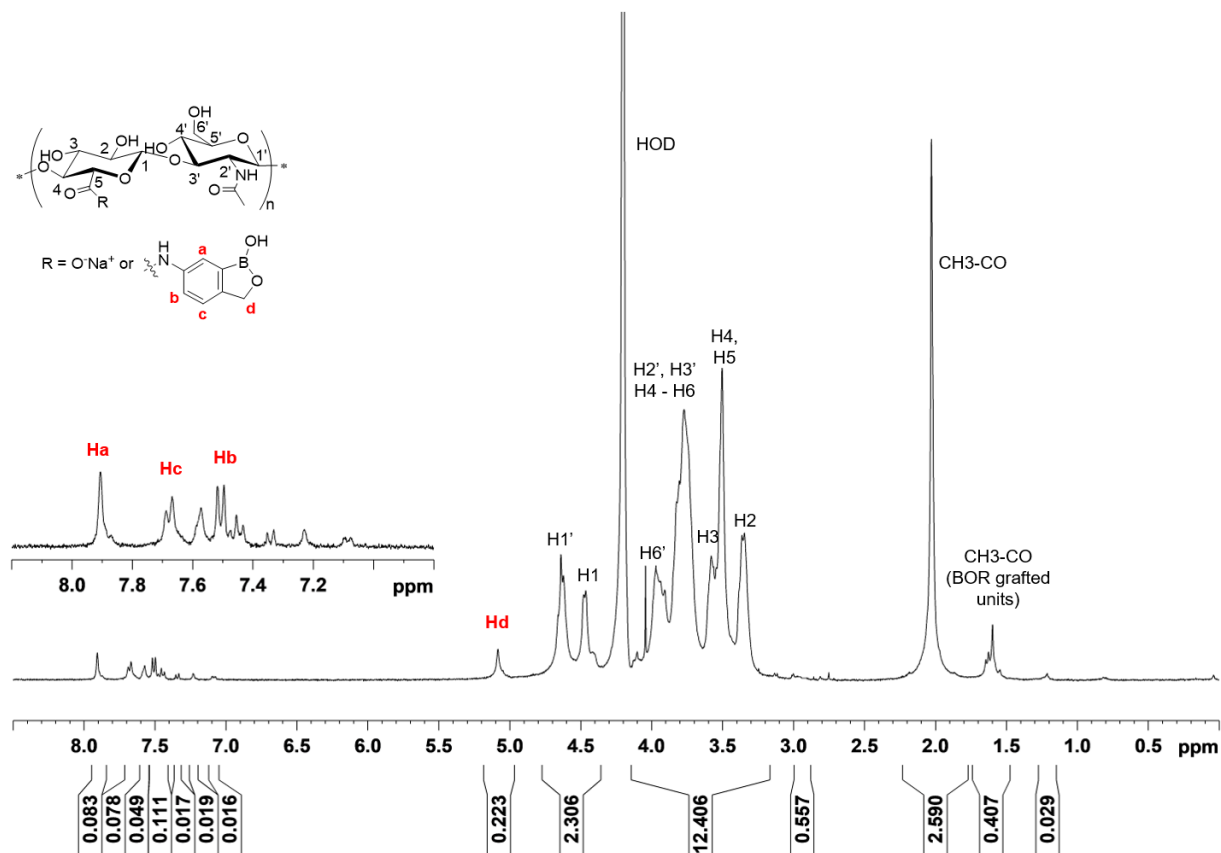


Figure S3. ^1H NMR spectrum (400 MHz, D_2O , $6 \text{ mg}\cdot\text{mL}^{-1}$, $80 \text{ }^\circ\text{C}$) of HA360-BOR.

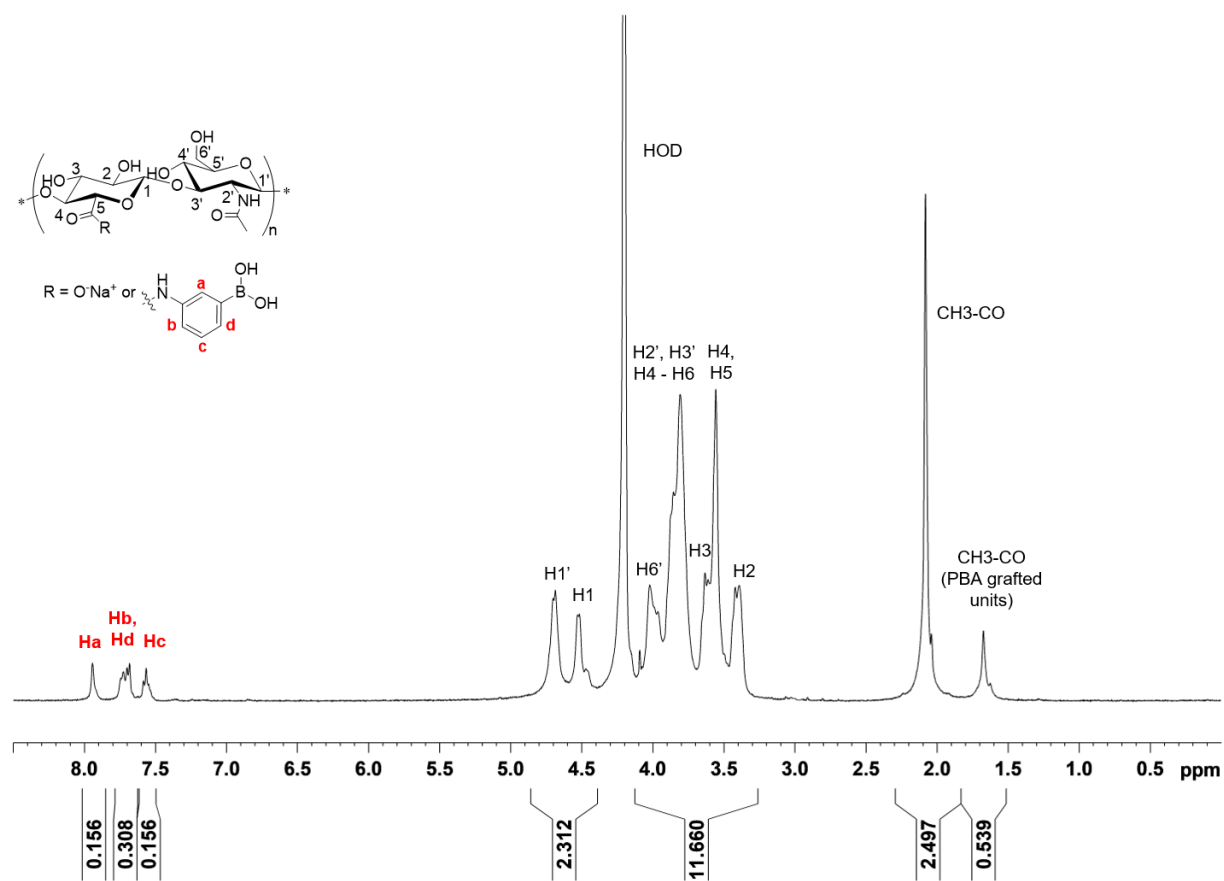
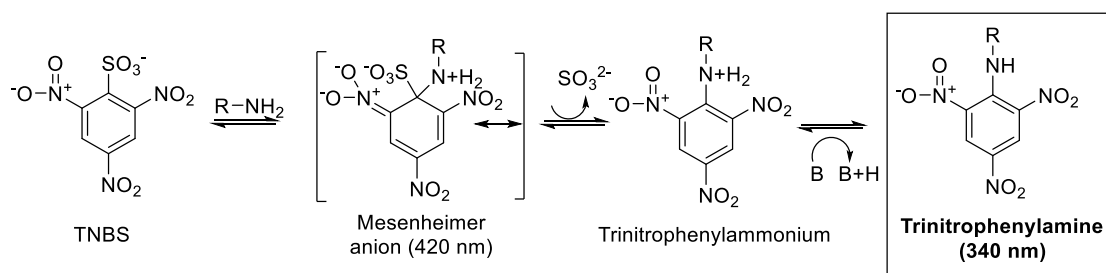


Figure S4. ¹H NMR spectrum (400 MHz, D₂O, 6 mg.mL⁻¹, 80 °C) of HA360-PBA.

4. Determination of the degree of substitution (DS) of HA-fructose from the kinetics of the amide coupling reaction (M_w HA = 360 kg/mol)

As the superposition of ^1H signals of HA and grafted fructose moieties precluded determination of the DS of HA-fructose by ^1H NMR, their DS were estimated from the kinetics of their syntheses, by quantifying the free primary amines in the reaction medium as a function of time. This was based on the reaction of fructosamine with 2,4,6-Trinitrobenzene Sulfonic Acid (TNBS), which gives an orange-colored final product (trinitrophenylamine) that absorbs in the UV region, at around 340 nm (Scheme 1).^{1,2}



Scheme 1. Trinitrophenylation of primary amines with TNBS.

Procedure for the reaction kinetics by quantifying primary amines with TNBS

The methodology to quantify primary amines with TNBS was adapted from a procedure previously described.³ Standard curves of fructosamine were prepared by diluting 1 mg/mL stock solutions in 0.1 M sodium bicarbonate buffer pH 8.5 at known concentrations of amine (10 to 50 $\mu\text{g/mL}$). Various volumes of a fresh solution of 0.01 % TNBS (w/v) in the same buffer were added in each solution, in order to get a molar ratio of TNBS/amine of 1, and samples were incubated at 37 °C for 2 h. Then, the product of reaction between the amine and TNBS was analyzed by UV spectroscopy (from 580 to 280 nm) after addition of a small volume of 1 M HCl (150 μL) in the samples. The same procedure was used to quantify amines during the amide coupling reactions with HA, by taking small aliquots of the reaction medium as a function of time.

Procedure for determining the DS from the kinetics of amide coupling reactions

From the UV spectra recorded for fructosamine-TNB derivatives, a standard curve was plotted with the maximal absorbance values (curve (a) in Figure S6). It is important to note that the wavelength of the maximal absorbance depends on the primary amines. This allowed us to determine the amount of unreacted primary amines during the amide coupling reaction with HA using a fructosamine/HA molar ratio of 0.15. From the kinetic curve, we estimated approximately 100 % of conversion for HA-fructose within 24 h, which gave a value of DS of 0.15 (curve (b) in Figure S6).

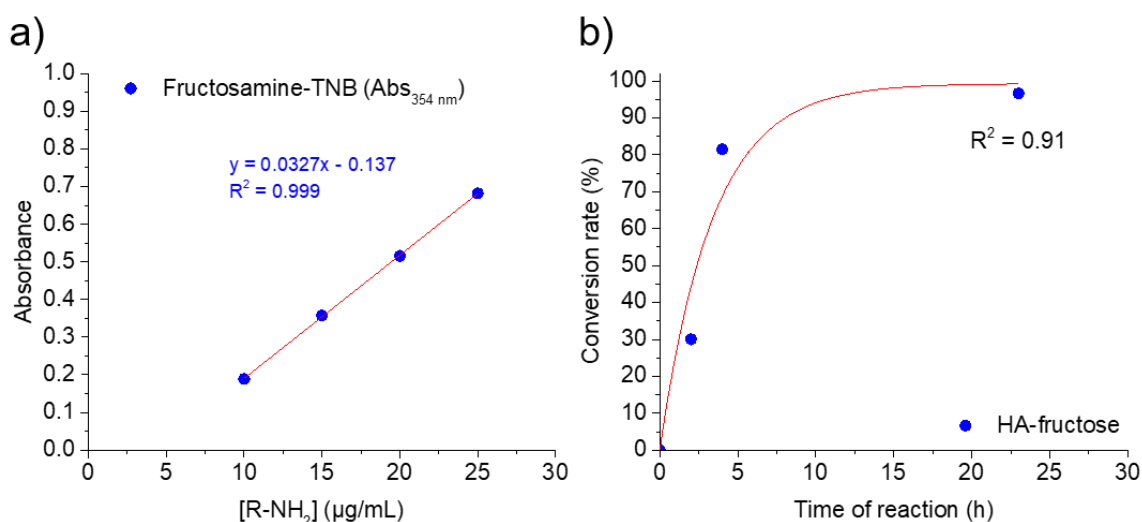


Figure S6. Reaction kinetics for the synthesis of HA360-fructose. Standard curve with the equation used to quantify free fructosamine (a), and kinetic curve plotted for the coupling reaction of fructosamine with HA360 (curve fitting by non-linear fit model using Origin 2015 software).

5. Methodology for K_a measurements by ^1H NMR spectroscopy

The procedure to determine the K_a values was adapted from previous studies using free boronic acids and saccharides.^{4,5} This method consisted in assuming that a boronic acid (B) and a saccharide (S) bind in one modality, BS:



$$K_a = \frac{[\text{BS}]}{[\text{B}][\text{S}]} \quad (1)$$

Where [B], [S] and [BS] are the molar concentrations of the free boronic acid, the free saccharide and the complex, respectively.

To calculate K_a , the [BS]/[B] ratio was determined by digital integration of the aryl protons of the boronic acid/saccharide complex and of the free boronic acid. This allowed calculation of [B], [BS] and [S], as follows:

$$[\text{B}] = \frac{[\text{B}]_0}{\frac{[\text{BS}]}{[\text{B}]} + 1} \quad (2)$$

Where $[\text{B}]_0$ is the initial concentration of boronic acid added in the NMR tube, and

$$[\text{BS}] = \frac{[\text{BS}]}{[\text{B}]} [\text{B}] \quad (3)$$

$$[\text{S}] = [\text{S}]_0 - [\text{BS}] \quad (4)$$

Where $[\text{S}]_0$ is the initial concentration of saccharide added in the NMR tube.

Procedure for the preparation of samples for NMR analysis

Stock solutions of 1,2-ABORIN (2,1-ABORIN or APBA or ABOR) and free (grafted) fructose (HA-fructose) were prepared by solubilization in distilled water. When necessary, the pH was carefully adjusted to 7.4 by adding 1 M NaOH, using a pH-meter, and water was added to get concentrations ranging from 4 to 60 mM. Then, the solutions were diluted with 0.02 M PBS pH 7.4 in order to obtain final concentrations of 2 to 30 mM boronic acid or saccharide in 0.01 M PBS at pH 7.4. The solutions of complexes were then prepared by mixing various volumes of a stock solution of 1,2-ABORIN (2,1-ABORIN or APBA or ABOR) with a stock solution of free D-fructose or HA-fructose. This generated mixtures at pH 7.4 (± 0.1), with a boronic acid/fructose molar ratio ranging from 0.3 to 1.5. Water was removed by freeze-drying and the samples were properly dissolved in D₂O prior to NMR analysis. Each value of K_a was determined from two experiments of titration using freshly prepared solutions. ¹H NMR titration was performed with at least 6 different concentrations at 25 °C.

Procedure for determining the chemical shifts of aryl protons of bound and free boronic acids

¹H NMR spectra of 1,2-ABORIN, 2,1-ABORIN, APBA and ABOR alone were first recorded (spectra (a) in Figure S7-S14). Second, ¹H NMR spectra of the boronic acid derivatives in the presence of excess free D-fructose to induce 100 % complex formation are acquired (spectra (b) in Figure S7-S8 and S11-S12). Comparison of spectra (a) and (b) allows the assignment of the aryl protons of bound and free boronic acids. This analysis was then used to interpret the spectra from the titrations with fructose (free in solution or grafted on HA; spectra (c) in Figure S7-S8 and S11-S12 or spectra (b) in Figure S9-S10 and S13-S14).

6. Determination of K_a by ^1H NMR for 1,2-ABORIN (2,1-ABORIN) and fructose (free fructose and HA-fructose)

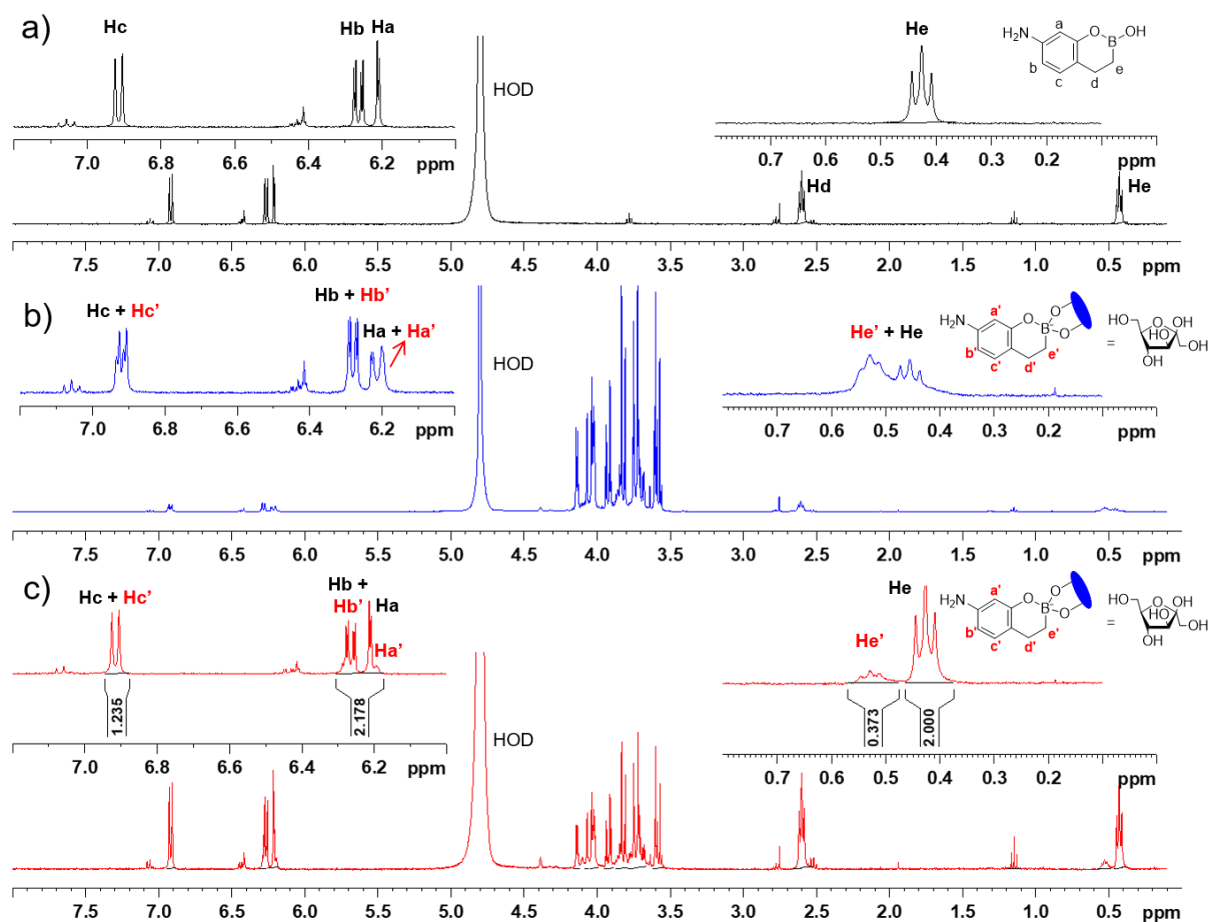


Figure S7. ^1H NMR spectra in 0.01 M deuterated PBS pH 7.4 at 25 °C of 1,2-ABORIN alone (1 mM) (a), 1,2-ABORIN (1 mM) in the presence of excess D-fructose (10 mM) (b) and 1,2-ABORIN (1 mM) with D-fructose (1 mM) (c). The $[\text{BS}]/[\text{B}]$ ratio was calculated from the digital integration of He (free 1,2-ABORIN) and He' (complexed 1,2-ABORIN) signals. Of note, the position of the oxygen of the intramolecular B-O bond between the phenyl ring and the boron atom precluded observation of ^1H signals in the aromatic region corresponding to bound and unbound forms of 1,2-ABORIN.

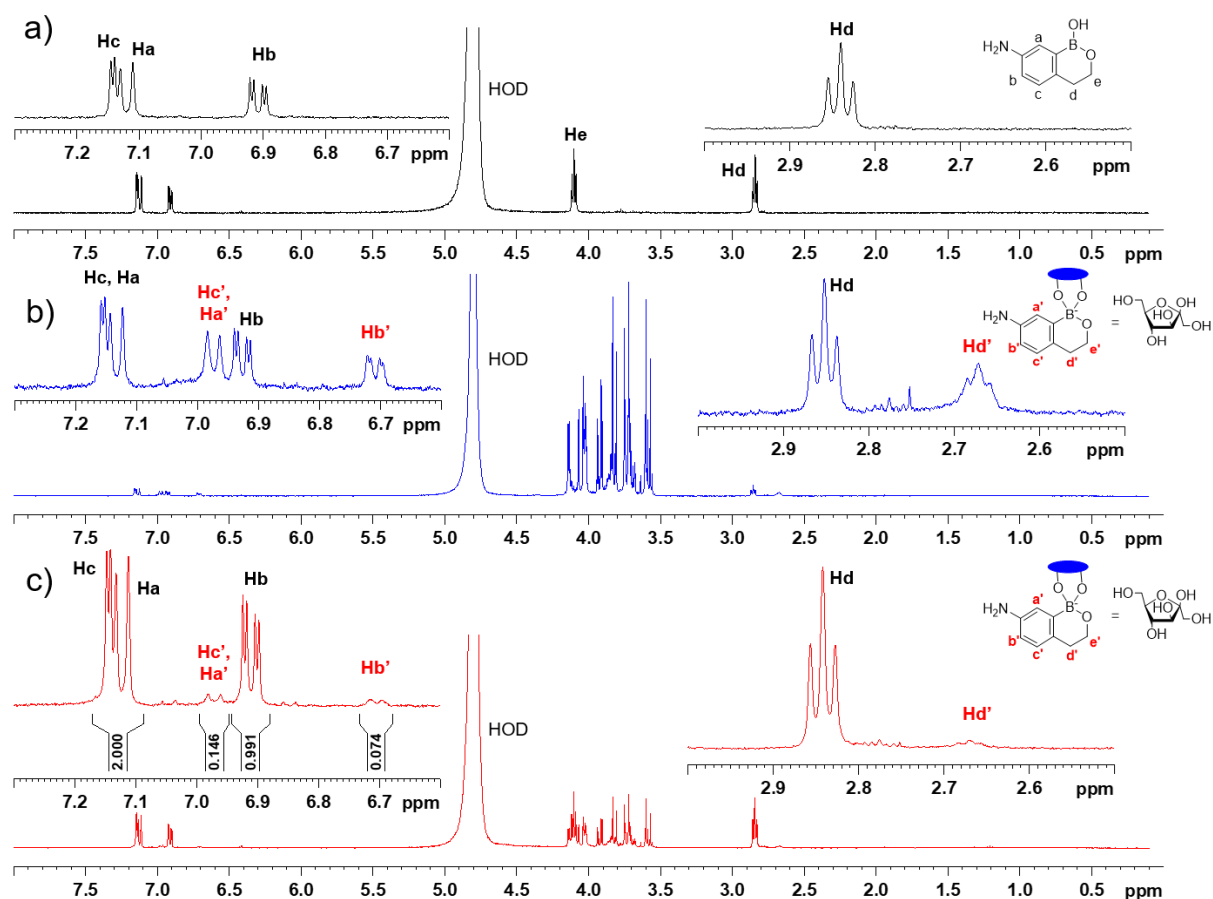


Figure S8. ^1H NMR spectra in 0.01 M deuterated PBS pH 7.4 at 25 °C of 2,1-ABORIN alone (1 mM) (a), 2,1-ABORIN (1 mM) in the presence of excess D-fructose (10 mM) (b) and 2,1-ABORIN (1 mM) with D-fructose (1 mM) (c). The [BS]/[B] ratio was calculated from the digital integration of Hc, Ha (free 2,1-ABORIN) and Hb' (complexed 2,1-ABORIN) signals.

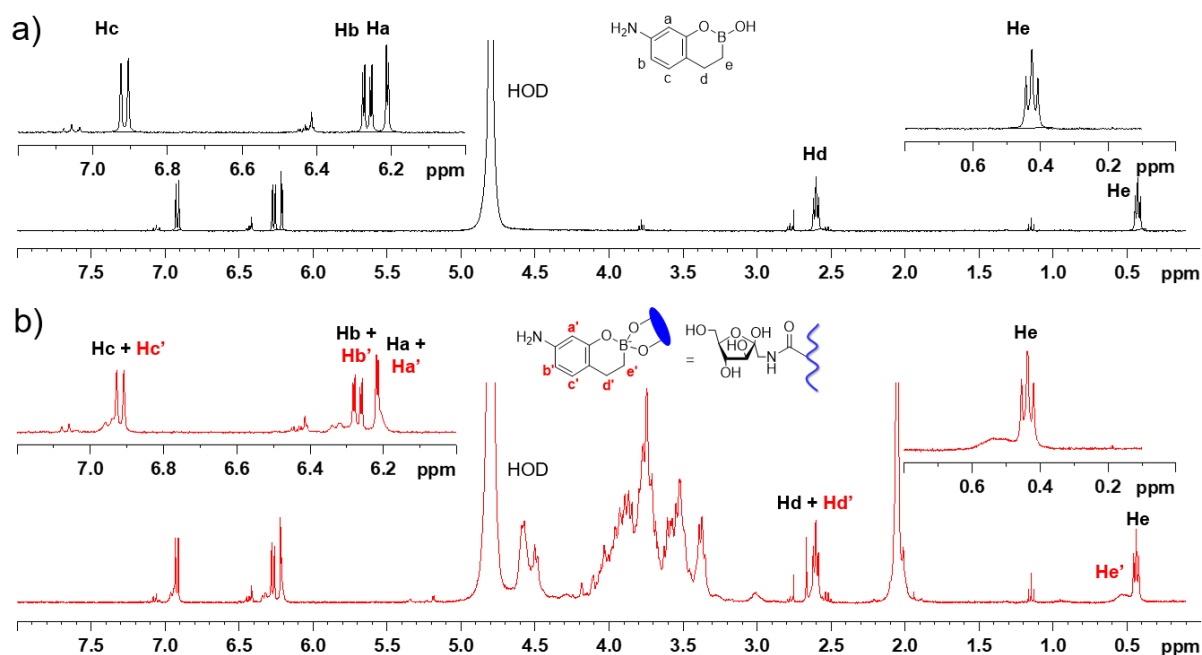


Figure S9. ¹H NMR spectra in 0.01 M deuterated PBS pH 7.4 at 25 °C of 1,2-ABORIN alone (1 mM) (a) and 1,2-ABORIN (1 mM) with HA-fructose (1 mM of grafted fructose) (b). K_a was not measured because ¹H signals corresponding to free and complexed 1,2-ABORIN were not sufficiently separated to be integrated.

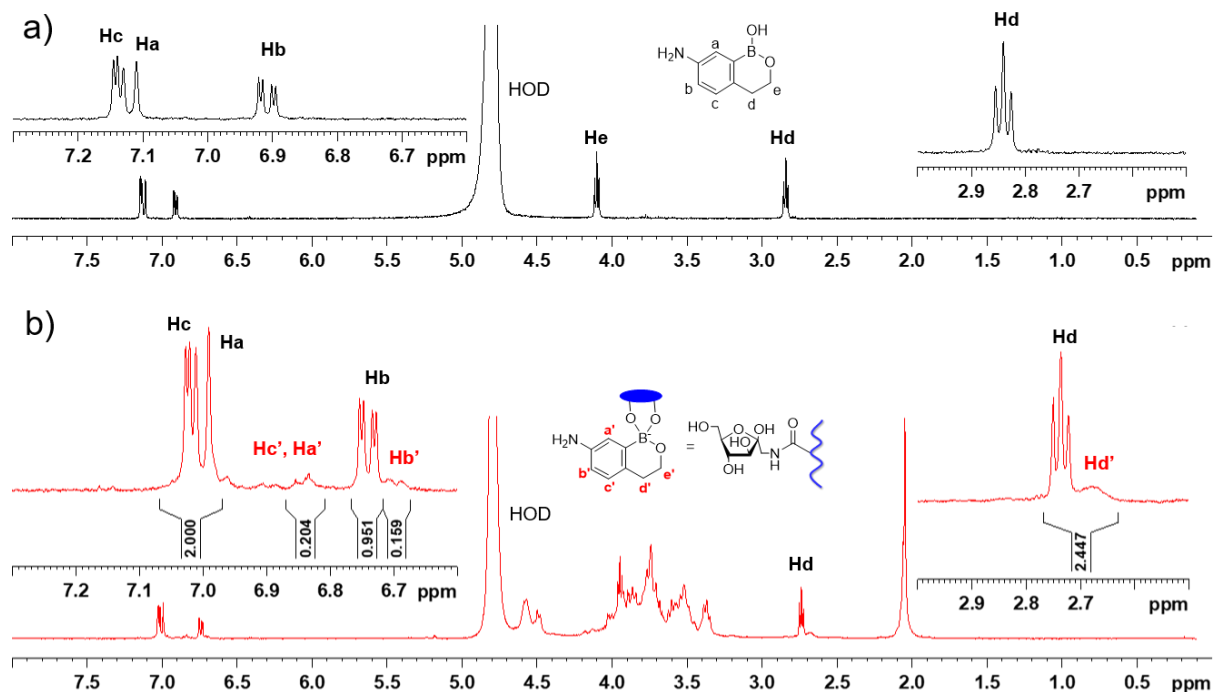


Figure S10. ¹H NMR spectra in 0.01 M deuterated PBS pH 7.4 at 25 °C of 2,1-ABORIN alone (1 mM) (a) and 2,1-ABORIN (1 mM) with HA-fructose (1 mM of grafted fructose) (b). The [BS]/[B] ratio was calculated from the digital integration of Hc, Ha (free 2,1-ABORIN) and Hd, Hd' (4H, free and complexed 2,1-ABORIN) signals.

7. Determination of K_a by ^1H NMR for APBA (ABOR) and fructose (free fructose and HA-fructose)

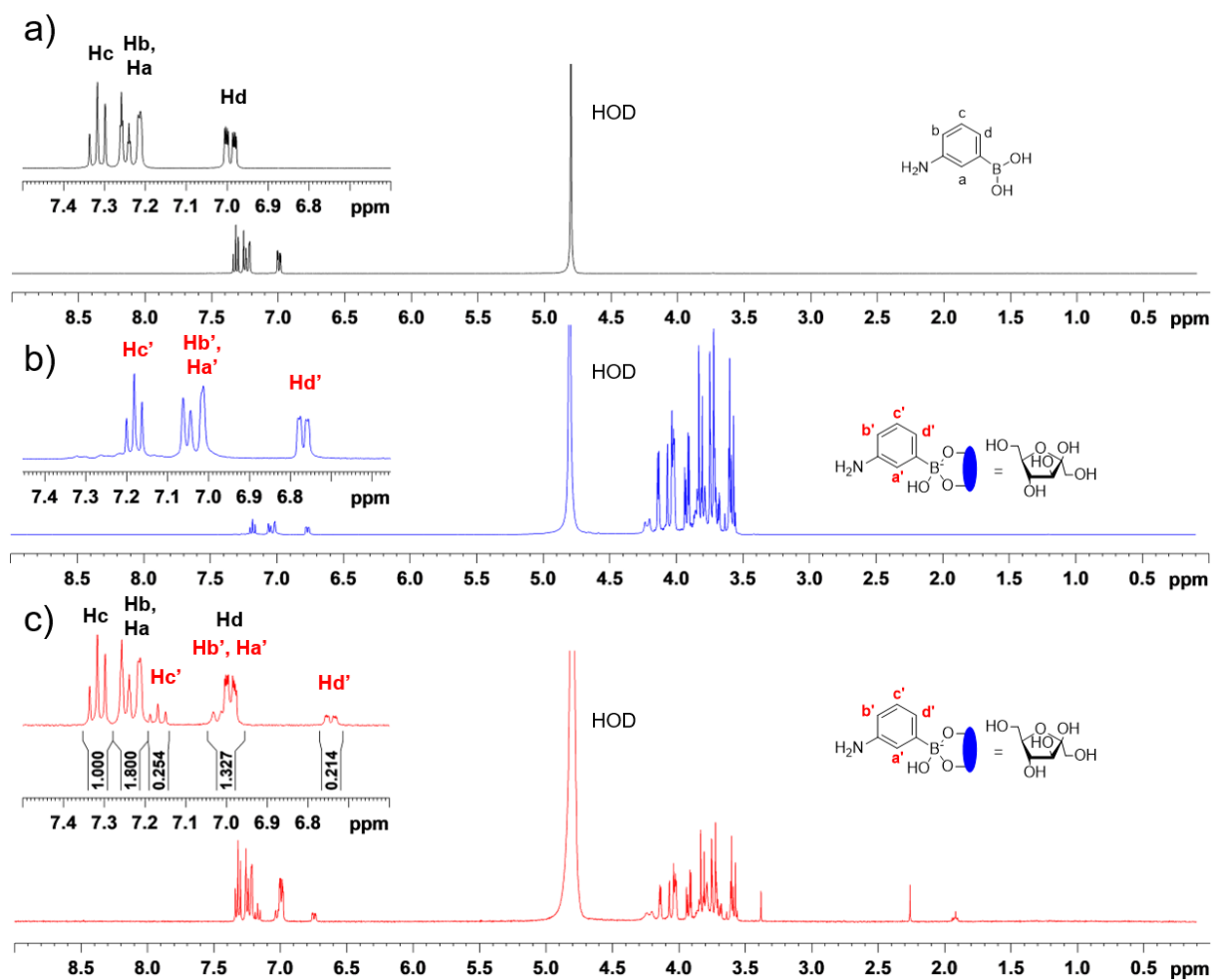


Figure S11. ^1H NMR spectra in 0.01 M deuterated PBS pH 7.4 at 25 °C of APBA alone (15 mM) (a), APBA (15 mM) in the presence of excess D-fructose (150 mM) (b) and APBA (15 mM) with D-fructose (15 mM) (c). The $[\text{BS}]/[\text{B}]$ ratio was calculated from the digital integration of Hc (free APBA) and Hd' (complexed APBA) signals.

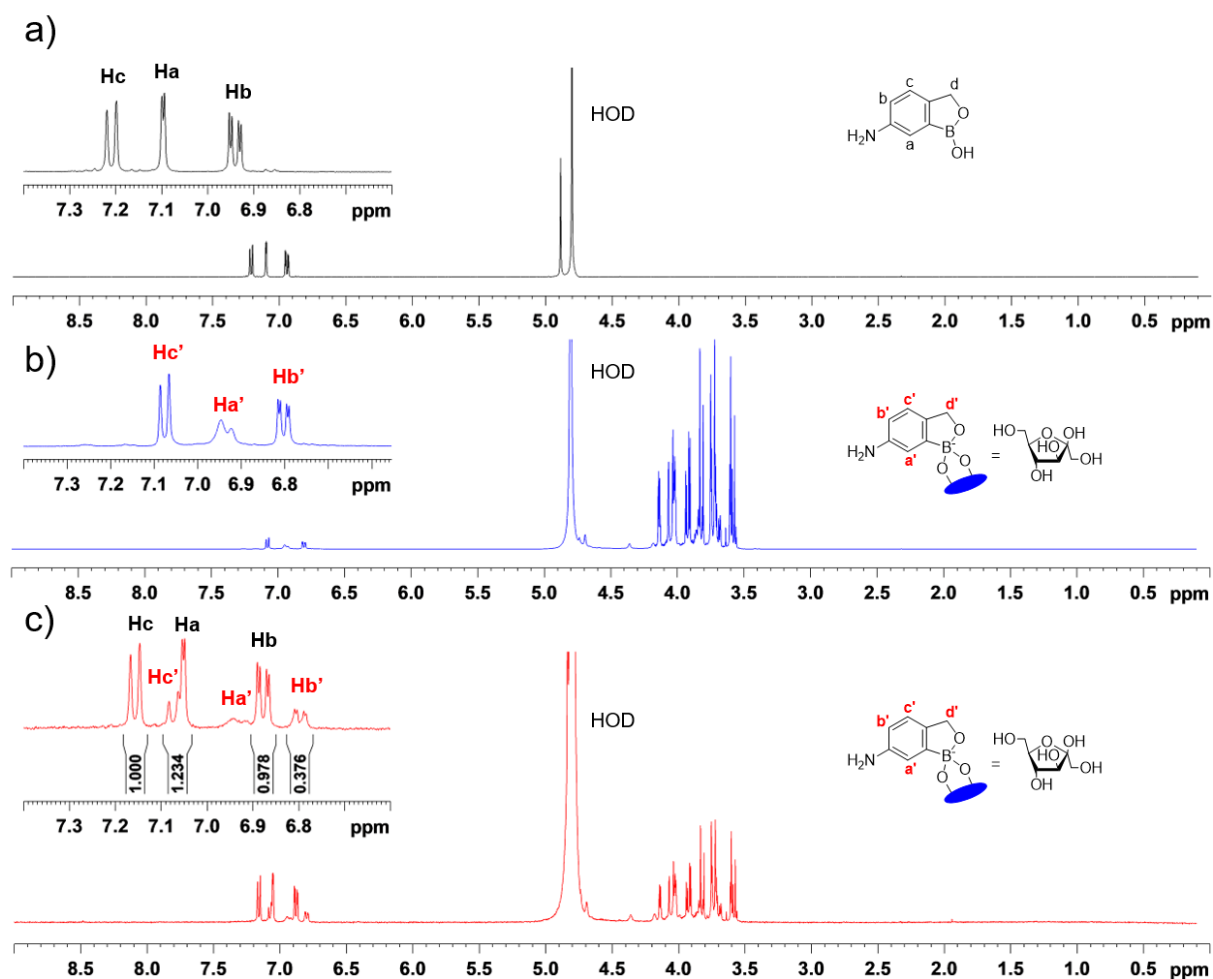


Figure S12. ^1H NMR spectra in 0.01 M deuterated PBS pH 7.4 at 25 °C of ABOR alone (15 mM) (a), ABOR (15mM) in the presence of excess D-fructose (150 mM) (b) and ABOR (15 mM) with D-fructose (15 mM) (c). The [BS]/[B] ratio was calculated from the digital integration of Hc (free ABOR) and Hb' (complexed ABOR) signals.

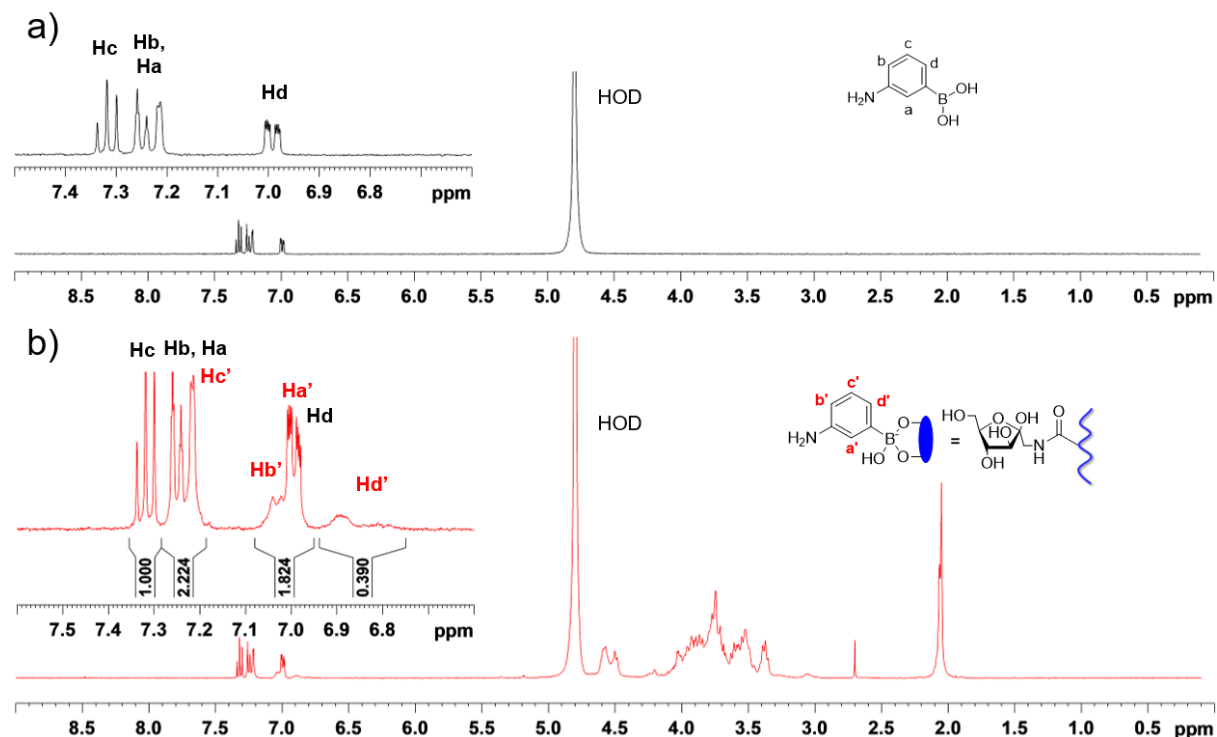


Figure S13. ¹H NMR spectra in 0.01 M deuterated PBS pH 7.4 at 25 °C of APBA alone (1 mM) (a) and APBA (1 mM) with D-fructose (1 mM of grafted fructose) (b). Similar to free D-fructose, the [BS]/[B] ratio was calculated from the digital integration of Hc (free APBA) and Hd' (complexed APBA) signals.

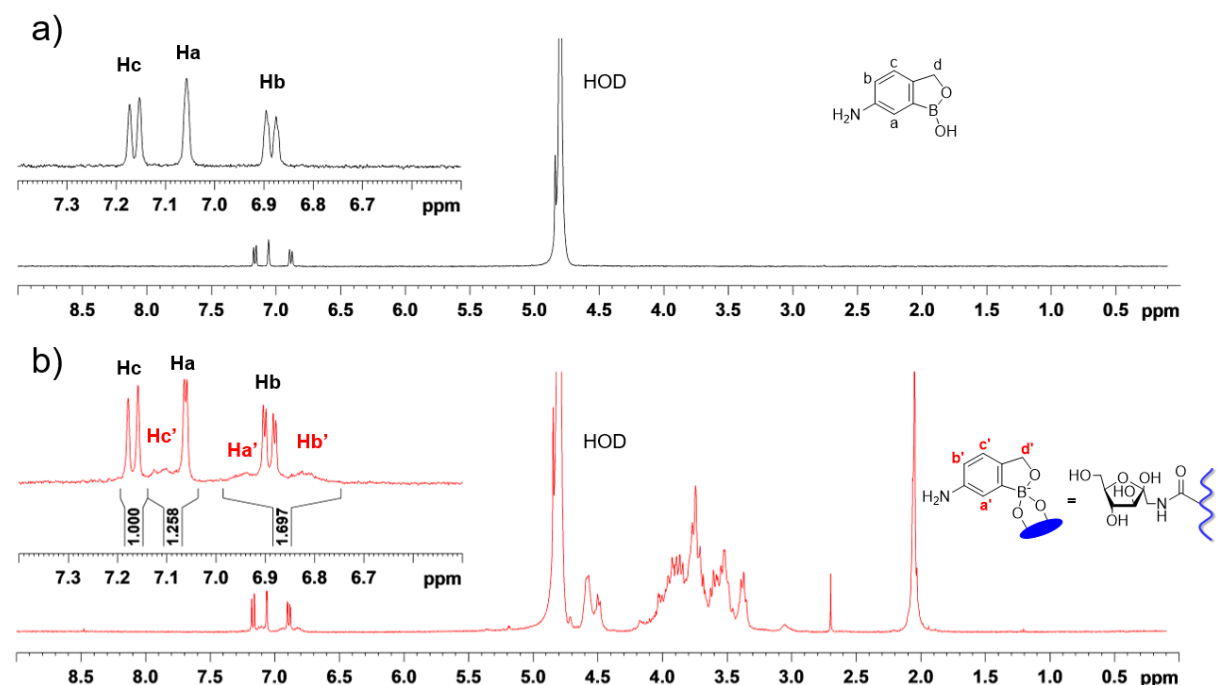


Figure S14. ¹H NMR spectra in 0.01 M deuterated PBS pH 7.4 at 25 °C of ABOR alone (1 mM) (a) and ABOR (1 mM) with HA-fructose (1 mM of grafted fructose) (b). Similar to free D-fructose, the [BS]/[B] ratio was calculated from the digital integration of Hc (free ABOR) and Hb, Ha', Hb' (3H, free and complexed ABOR) signals.

8. Calorimetric titration of 1,2-ABORIN (2,1-ABORIN) with free D-fructose

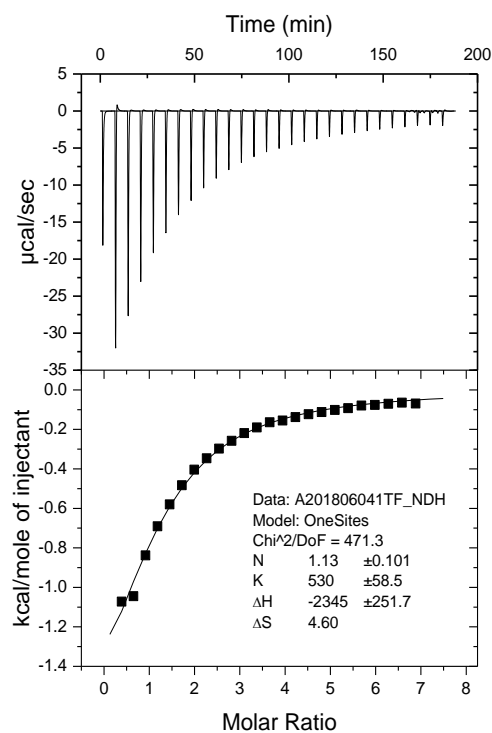


Figure S15. Calorimetric titration of 1,2-ABORIN (2 mM) with D-fructose (75 mM) in 0.01 M PBS (pH 7.4, 25 °C).

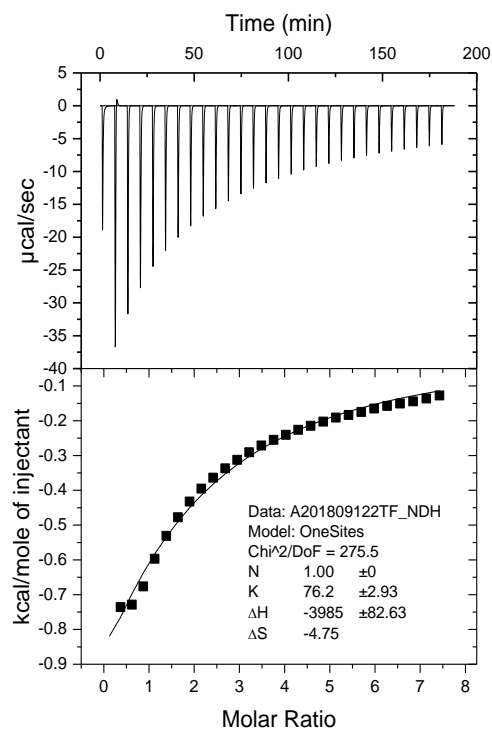


Figure S16. Calorimetric titration of 2,1-ABORIN (3.5 mM) with D-fructose (125 mM) in 0.01 M PBS (pH 7.4, 25 °C).

9. Calorimetric titration of APBA (ABOR) with free D-fructose

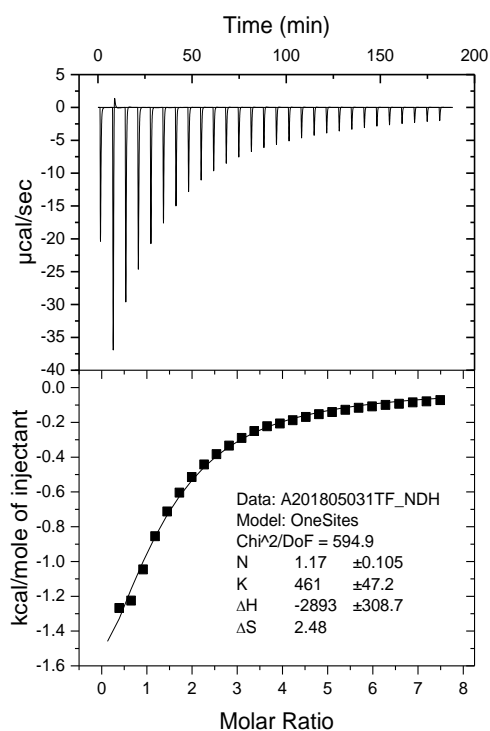


Figure S17. Calorimetric titration of ABOR (2 mM) with D-fructose (75 Mm) in 0.01 M PBS (pH 7.4, 25 °C).

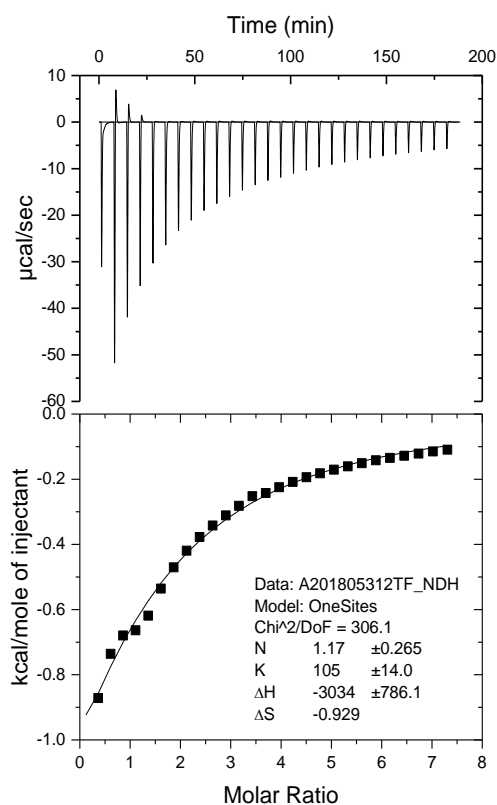


Figure S18. Calorimetric titration of APBA (5 mM) with D-fructose (175 mM) in 0.01 M PBS (pH 7.4, 25 °C).

10. Rheological analysis of the HA-1,2-BORIN (2,1-BORIN, BOR or PBA) alone at pH 7.4 (M_w HA = 360 g/mol)

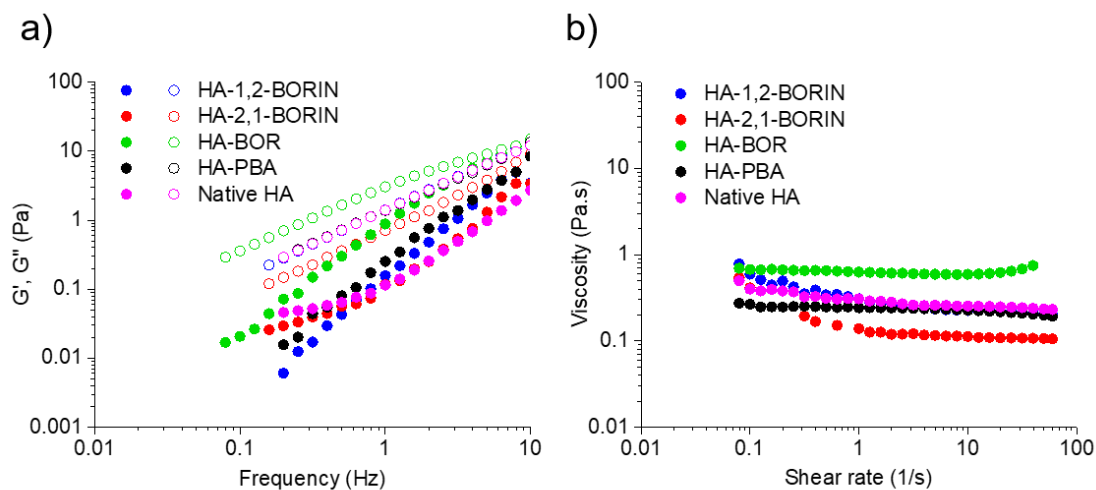


Figure S19. Rheological behavior of the HA360-1,2-BORIN, HA360-2,1-BORIN, HA360-BOR and HA360-PBA conjugates alone at pH 7.4 ($C_p = 15$ g/L): (a) frequency dependence of the storage modulus (G' , filled symbols) and loss modulus (G'' , empty symbols), and (b) viscosity .

11. Investigation of the opening of the endocyclic B-O bond of 1,2-ABORIN (ABOR) in complexation with free/grafted fructose

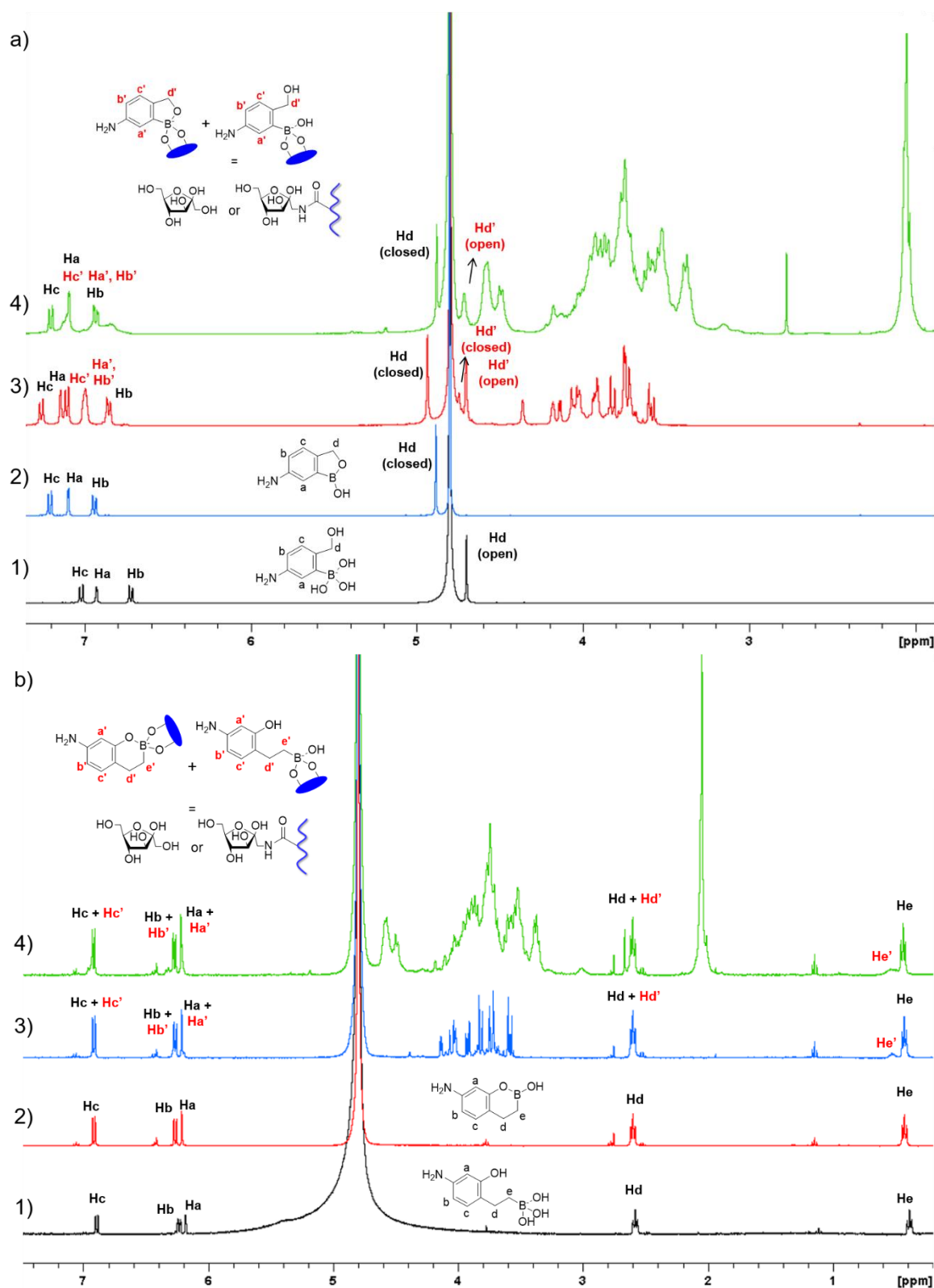


Figure S20. (a) ¹H NMR spectra of ABOR alone at pD 11-12 (1), at pD 7.4 (2), and ABOR in the presence of D-fructose (3) and of HA-fructose (4) at pD 7.4. (b) ¹H NMR spectra of 1,2-ABORIN alone at pD 11-12 (1), at pD 7.4 (2), and 1,2-ABORIN in the presence of D-fructose (3) and HA-fructose (4) at pD 7.4 (ABOR or 1,2-ABORIN/fructose molar ratio of 1:1). 1,2-

ABORIN is also represented in its open form despite no clear evidence of the opening of its endocyclic B-O bond was observed in its ^1H NMR spectra alone at pD 11-12 and in the presence of free/granted fructose.

12. Determination of the pK_a of free ABOR by ^{11}B NMR spectroscopy

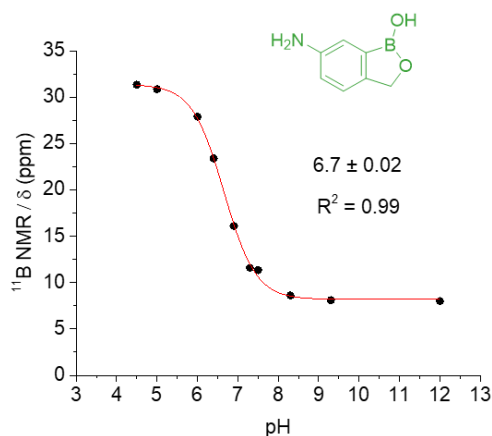


Figure S21. Determination of the pK_a of free ABOR by ^{11}B NMR titration as a function of pH (curve fitting using Boltzmann equation).

13. References

- (1) Cayot, P.; Tainturier, G. The Quantification of Protein Amino Groups by the Trinitrobenzenesulfonic Acid Method: A Reexamination. *Anal. Biochem.* **1997**, *249* (2), 184–200.
- (2) Sashidhar, R. B.; Capoor, A. K.; Ramana, D. Quantitation of E-Amino Group Using Amino Acids as Reference Standards by Trinitrobenzene Sulfonic Acid. *J. Immunol. Methods* **1994**, *167*, 121–127.
- (3) Hermanson, G. Bioconjugate Techniques - 3rd Edition. In *Bioconjugate Techniques*; Academic Press: San Diego, California, 1996; pp 112–113.
- (4) Ellis, G. A.; Palte, M. J.; Raines, R. T. Boronate-Mediated Biologic Delivery. *J. Am. Chem. Soc.* **2012**, *134* (8), 3631–3634.
- (5) Dowlut, M.; Hall, D. G. An Improved Class of Sugar-Binding Boronic Acids, Soluble and Capable of Complexing Glycosides in Neutral Water. *J. Am. Chem. Soc.* **2006**, *128* (13), 4226–4227.

GENERAL CONCLUSIONS AND
PERSPECTIVES

General conclusions and perspectives

This thesis was constructed on the concept of designing injectable self-healing hydrogels based on hyaluronic acid (HA) crosslinked by arylboronate ester bonds for aesthetic and other biomedical applications.

Here, we demonstrated the possibility to synthesize adaptable HA hydrogels with tunable properties by varying the nature of the small molecule crosslinkers, i.e. the arylboronic acid moiety as well as the sugar molecule grafted onto the HA backbone.

A careful analysis of the dynamic rheological behavior of HA networks crosslinked via phenylboronic acid (PBA)-saccharide or benzoboroxole (BOR)-saccharide complexation revealed that the hydrogel bulk properties are closely linked to the dynamics and thermodynamics of the small molecular crosslinkers. Surprisingly, a strikingly high affinity was found for PBA with maltose and gluconamide derivatives (possessing a glucose unit in the ring-opened form) grafted onto HA, as well as fructose. These stronger associations enable formation of hydrogel networks with slower dynamics and higher elastic moduli compared to those based on BOR-saccharide crosslinks. Indeed, despite BOR is known for its efficient binding capability at physiological pH compared to PBA, the dynamics of the HA-BOR/HA-maltose (gluconamide) networks appeared to be much faster and the elastic moduli, lower than the HA-PBA-based networks and the HA-BOR/HA-fructose assembly. A structural study revealed that these differences are related to the binding modes of BOR and PBA toward the different saccharides grafted on HA. Regarding PBA-saccharide complexes, we demonstrated that the slow relaxation time and high elastic moduli of the HA assemblies are due to the original and previously unobserved formation of stable tridentate complexes with PBA grafted on HA. Besides, in the case of the networks based on HA-BOR, the formation of a monocyclic ester with fructose leads to the formation of hydrogel networks with slow relaxation dynamics, whereas the faster dynamics of the other assemblies including glucose-derivatives grafted on HA were found to be related to the formation of spiro adducts.

Together, these findings demonstrate that understanding of the binding mode between boronic acid and polyol moieties is crucial for the rational design of adaptable boronic acid-based hydrogels.

In addition, we also reported in this thesis on the feasibility of a new class of self-crosslinking HA hydrogels based on the multivalent complexation between custom-made benzoboroxole derivatives and the C-4/C-6 diol of the HA D-GlcNAc unit. Indeed, hydrogels with extremely slow dynamics and with pH- and carbohydrate-responsive properties were prepared from a single component based on HA modified with benzoboroxole derivatives (i.e. DMF6ABOR or DM7ABOR). These hydrogels are the first examples of polysaccharide derivatives showing self-crosslinking properties via boronate-diol complexation at

General conclusions and perspectives

physiological pH. In these HA networks, we found that the ability of DMF6ABOR and DM7ABOR moieties to selectively complex the C-4/C-6 diols from the polysaccharide chains is strongly related to the *gem*-dimethyl group in their heterocycle and the *ortho*-substituent in their phenyl ring. Indeed, in these BOR derivatives, the presence of fluorine or the amide moiety on the *ortho*-position relative to the boronic center may result in complexes stabilized via additional hydrogen bonds with hydroxyl groups of HA. Furthermore, despite the weak binding affinity of single BOR derivatives towards HA diols, the formation of junction zones based on multivalent complexation is an important factor contributing to the mechanism of gel formation. Very interestingly, these hydrogels showed a glucose-responsive behavior together with self-healing properties due to the reversible nature of the crosslinks, illustrating their potential of application in many biomedical fields, including in glucose-sensing and insulin-delivery.

Finally, in addition to benzoboroxole, we demonstrated the applicability of its six-membered ring homologue, benzoxaborin (2,1-BORIN), as well as a new original benzoxaborin-like derivative (1,2-BORIN) as new carbohydrate binding sites for the formation of reversible HA networks. With this study, a hydrogel was obtained at physiological pH by combining a HA-1,2-BORIN conjugate and HA modified with fructose moieties (HA-fructose). This new hydrogel exhibited rheological properties comparable to those shown by the previously studied networks based on HA-PBA (BOR)/HA-fructose. By contrast, only viscoelastic properties were found when using HA modified with conventional 2,1-BORIN, suggesting a weak binding of this derivative towards fructose moieties. In these networks, the different macroscopic rheological properties observed were found to be closely linked to the pK_a of the two arylboronic acids. Despite further studies are warranted to elucidate the exact binding mode of 1,2-BORIN with fructose, we cannot exclude the possibility that the slow dynamics of this complex is linked to the opening of the endocyclic B-O bond of 1,2-BORIN, similar to that observed for benzoboroxole. Besides, continued investigation of the applicability of these HA hydrogels as promising injectable scaffolds for encapsulation of cells or bioactive molecules will expand their application in many innovative biomedical fields.

These unique features together with the injectability of these materials open the door to many innovative applications in the biomedical field. In this regard, they led to the joint registration of three patents in August 2016 by Galderma/Nestlé Skin Health and CERMAV-CNRS:

General conclusions and perspectives

- Auzély-Velty, R.; Figueiredo, T.; Jing, J.; Harris, C.; Boiteau J.-G.; Gerfaud T.; Tomas L. Method of crosslinking glycosaminoglycans (Galderma/CNRS/Université Grenoble Alpes), WO 2018024795;
- Auzély-Velty, R.; Figueiredo, T.; Jing, J.; Harris, C.; Boiteau J.-G.; Gerfaud T.; Tomas L. Method of crosslinking glycosaminoglycans (Galderma/CNRS/Université Grenoble Alpes), WO 2018024793;
- Auzély-Velty, R.; Figueiredo, T.; Jing, J.; Harris, C.; Boiteau J.-G.; Gerfaud T.; Tomas L. Double crosslinked glycosaminoglycans (Galderma/CNRS/Université Grenoble Alpes), WO 2018024794.

Moreover, in the framework of a collaboration between CERMAV and the Grenoble Institute of Neurosciences (GIN), studies on the potential of these hydrogels as injectable scaffolds for cell therapy in the treatment of stroke are underway (Figure 1a). The main challenge is the implantation of a cell-laden hydrogel in a minimally invasive manner to improve cell survival in the hostile environment associated with the stroke cavity. *In vitro* studies (Live-Dead) showed the ability of these gels to efficiently entrap human stem cells (mesenchymal stem cells, MSCs) in 3D, without inducing significant cytotoxic effects to the encapsulated cells (Figure 1b). Moreover, these hydrogels also could be easily injected in intracerebral (Figure 1c) and subcutaneous (Figure 1d) rat tissues, without inducing important inflammatory responses and stayed localized at the site of introduction.

General conclusions and perspectives

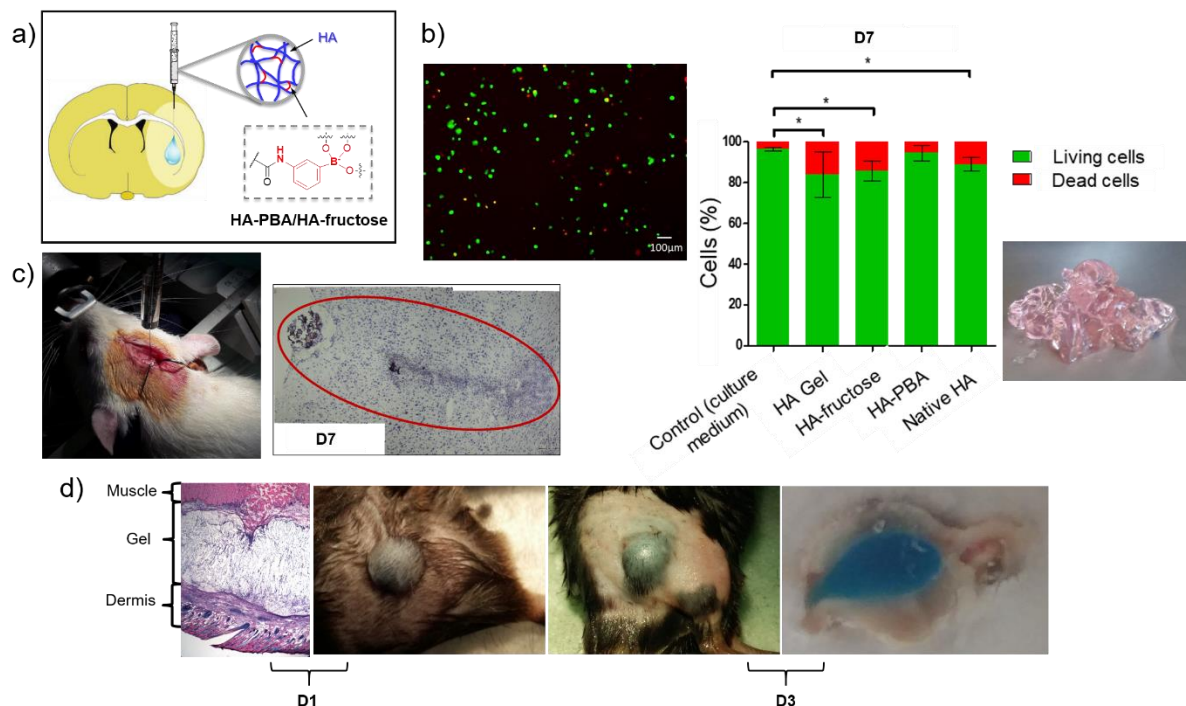


Figure 1. (a) Applicability of a boronate-crosslinked HA hydrogel (HA-PBA/HA-fructose) as an injectable scaffold for cell therapy in the treatment of stroke. (b) Live/Dead assay 3D image of MSCs encapsulated within the HA gel in culture medium, and cell viability in the hydrogel and in solutions of the HA precursors after 7 days. Cells were stained with calcein AM (green, live) and ethidium homodimer (red, dead); scale bar is 100 μm (epifluorescence inverted microscope); statistical analyses from Mann-Whitney U test, * indicating $p < 0.05$. The picture illustrates the hydrogel prepared in the culture medium. Injection of the HA gel in different tissues. (c) Injection of 10 μL of hydrogel in the intracerebral rat tissue, being observed within 7 days after injection. (d) Subcutaneous injection of 250 μL of gel in thighs of mice (from left to right): immunohistology of skin-muscle section within 24 h (hematoxylin and eosin staining); pictures illustrating that the hydrogel stayed localized in the injected area within 3 days; muscle section containing the gel stained with cresyl violet.

Collectively, these features demonstrate that these biomaterials are indeed promising candidates for clinical use. It is also important to note that the possibility of hydrogel formation in culture media and the capacity of these gels to successfully entrap cells in 3D further indicate their applicability for *in vitro* cell culture tests. Continued investigation on boronate-crosslinked hydrogels based on HA as well as other polysaccharides will open doors to address the challenge of injectable hydrogels and expand their application space in the biomedical field.

List of Abbreviations

1,2-ABORIN: 3,4-dihydro-2*H*-benzo[*e*][1,2]oxaborinin-2-ol

2,1-ABORIN: 3,4-dihydro-1*H*-benzo[*c*][1,2]oxaborinin-1-ol

2APBA: 2-acrylamidophenylboronic acid

27G (needle): 27 gauge

3APBA: 3-aminophenylboronic acid

3T3 (fibroblasts): "3-day transfer, inoculum 3×10^5 cells"

4ABOR: 4-aminobenzoboroxole

5ABOR: 5-aminobenzoboroxole

6ABOR: 6-aminobenzoxaborole

7ABOR: 7-aminobenzoboroxole

AA: acrylic acid

ABOR: 6-aminobenzoxaborole

AD: adamantine

AIBN: azobis-(isobutyronitrile)

AMPS: 2-Acrylamido-2-methyl-1-propanesulfonic acid

ANOVA: analysis of variance

APBA: 3-aminophenylboronic acid

ATP: adenosine triphosphate

BDBA: 1,3-benzenediboronic acid

BDDE: 1,4-butanediol diglycidyl ether

Boc-DOOA: boc-1-amino-3,6-dioxa-8-octanamine

BOR: benzoboroxole

BOR-NH₂: aminobenzoboroxole

BSA: bovine serum albumine

BX: benzoboroxole

C*: overlap polymer concentration

CAL-27: "Centre Antoine Lacassagne-27" cell line

Calcein-AM: calcein acetoxymethyl

CAT: catechol

CMC: carboxymethylcellulose

C_p: polymer concentration

D₂O: deuterium oxide

DFT: density functional theory

D-Glc: D-glucuronic acid

D-GlcNac: *N*-acetyl-D-glucosamine

Appendix

DIC: *N,N'*-diisopropylcarbodiimide
DMABOR: amino-3,3-*gem*-dimethylbenzoboroxole
DM4ABOR: 4-amino-3,3-*gem*-dimethylbenzoboroxole
DM5ABOR: 5-amino-3,3-*gem*-dimethylbenzoboroxole
DM6ABOR: 6-amino-3,3-*gem*-dimethylbenzoboroxole
DM7ABOR: 7-amino-3,3-*gem*-dimethylbenzoboroxole
DMEM: Dulbecco's modified eagle's medium
DMF: dimethylformamide
DMF6ABOR: 7-fluoro-6-amino-3,3-*gem*-dimethylbenzoboroxole
DMSO: dimethylsulfoxide
DMTMM: 4-(4,6-dimethoxy-1,3,5-triazin-2-yl)-4-methylmorpholinium chloride
DOP: dopamine
DS: degree of substitution
EA: ellagic acid
ECM: extracellular matrix
EGCG: epigallocatechin gallate
EXSY: exchange spectroscopy
F6ABOR: 7-fluoro-6-aminobenzoboroxole
FBS: fetal bovine serum
FPBA: 2-fluorophenylboronic acid
Fructosamine: 1-amino-1-deoxy-D-fructose
G': storage (elastic) modulus
G'_{1Hz}: storage (elastic) modulus at a frequency of 1 Hz
G'': loss (viscous) modulus
GAG: glycosaminoglycan
GAPMA: 3-gluconamidopropyl methacrylamide
GPC: gel permeation chromatography
HA: hyaluronic acid
HeLa: "Henrietta Lacks" cell line
HEPES: 4-(2-hydroxyethyl)piperazine-1-ethanesulfonic acid
HG: host-guest
hMSC: human mesenchymal stem cell
HOBT: 1-hydroxybenzotriazole
HPMA: 2-hydroxypropylmethacrylamide
HPLC: high pressure liquid chromatography
HSQC: heteronuclear single quantum coherence spectroscopy
HUVEC: human umbilical vein endothelial cell

Appendix

IgG: globulin G

IPN: interpenetrating polymer network

ITC: isothermal titration calorimetry

K_a : binding (affinity) constant

k_{ex} : exchange rate constant

MAAmBO: 5-methacrylamido-1,2-benzoxaborole

MALLS: multi-angle light scattering

Maltose-COOH: maltose functionalized with a terminal COOH group

Maltose-disulfide: maltose dimer functionalized with cystamine

Maltose-thiol: maltose-disulfide reduced in a thiol derivative

MD: molecular dynamics

MPC: 2-methacryloyloxyethyl phosphorylcholine

M_w : weight-average molar mass

n : stoichiometry

ND: nitro-dopamine

NIPAAm: *N*-isopropylacrylamide

PBA: phenylboronic acid

PBS: phosphate buffered saline

PBOB: benzoboroxole-based copolymer

PEG: poly(ethylene glycol)

PGal: synthetic glycopolymer bearing pendent galactopyranoside

PGlc: synthetic glycopolymer bearing pendent glucopyranoside

PLGA: poly(lactic-co-glycolic acid)

PMan: synthetic glycopolymer bearing pendent mannopyranoside

PVA: poly(vinyl alcohol)

RAFT: reversible addition-fragmentation chain-transfer polymerization

SEC: size exclusion chromatography

SEM: scanning electron microscopy

SHA: salicylhydroxamic acid

SMD: solvent model density

SPAAC: strain-promoted alkyne-azide cycloaddition

$\tan\delta$: loss modulus/storage modulus (G''/G')

TCEP: tris(2-carboxyethyl)phosphine hydrochloride

TFA: trifluoroacetic acid

TNBS: 2,4,6-trinitrobenzene sulfonic acid (picrylsulfonic acid)

WBA: Wulff-type-like boronic acid

β -CD: β -cyclodextrin

Appendix

η : viscosity

ω_c : crossover frequency

τ : relaxation time

ΔH : enthalpy

ΔS : entropy

Abstract

Injectable and self-healing hydrogels have recently drawn great attention in the fields of tissue engineering and regenerative medicine. Such gels can be pre-formed into syringes, be extruded under shear stress and show rapid recovery when the applied stress is removed due to the dynamic nature of their crosslinks. Given the exciting potential benefit of using boronic acid-containing polymers to construct dynamic covalent hydrogels, we explored this attractive strategy to design injectable boronate-crosslinked hydrogels based on hyaluronic acid (HA) for aesthetic and other biomedical applications. To design hydrogels with optimized properties, we investigated the effect of the nature of the boronic acid moiety as well as the sugar molecule grafted onto the HA backbone on the gel properties. Among arylboronic acid derivatives, benzoboroxole (BOR) was selected in addition to phenylboronic acid (PBA) as the binding site for sugar moieties grafted on HA. This choice was based on the efficient binding capability of BOR at neutral pH compared to PBA, and on its ability to complex glycopyranosides. With this study, we demonstrated that the dynamic rheological properties of the HA networks based on BOR- or PBA-saccharide complexation are closely linked to the molecular exchange dynamics and thermodynamics of the small molecule crosslinkers. Besides, we also established for the first time the feasibility of self-crosslinking HA hydrogels with extremely slow dynamics at physiological pH through multivalent interactions between BOR derivatives grafted on HA and diols from the polysaccharide chains. Finally, in addition to BOR, we demonstrated the unprecedented capacity of its six-membered ring homologue, benzoxaborin, and a new original benzoxaborin-like derivative as new carbohydrate binding sites for the formation of reversible HA networks. Taking into account the injectable, self-healing and stimuli-responsive properties showed by these new HA hydrogels, these biomaterials appear as promising injectable scaffolds for many innovative applications in the biomedical field, including in tissue engineering and cell therapy.

Résumé

Les hydrogels injectables et auto-réparants suscitent un intérêt particulier dans les domaines de l'ingénierie tissulaire et de la médecine régénératrice. En raison de la nature dynamique de leurs réticulations, ces gels peuvent être pré-formés dans des seringues, extrudés sous cisaillement et s'auto-réparer spontanément après arrêt de la déformation mécanique. Au vu du potentiel que peuvent offrir les polymères fonctionnalisés par des acides boroniques pour la fabrication de gels covalents réversibles, nous avons développé des hydrogels injectables d'acide hyaluronique (HA) réticulés par des liaisons esters boronates pour des applications esthétiques et biomédicales. Pour élaborer de tels gels avec des propriétés optimisées, nous avons exploré l'effet de la nature du dérivé d'acide boronique ainsi que du motif saccharidique greffés sur le HA sur les propriétés rhéologiques dynamiques des gels. Parmi les différents dérivés d'acide boronique, le benzoboroxole (BOR) a été choisi en plus de l'acide phénylboronique (PBA) pour complexer différents motifs saccharidiques greffés sur le HA. Comparé au PBA, le dérivé BOR est, en effet, capable de se complexer de manière plus efficace à pH neutre et avec une plus grande variété de composés saccharidiques, en particulier les glycopyranosides. Cette étude a démontré que les propriétés rhéologiques dynamiques des assemblages de HA formés par complexation des unités de BOR ou PBA avec les différents sucres sont étroitement liées à la dynamique des échanges moléculaires et à la thermodynamique des pontages. En outre, nous avons également établi pour la première fois la possibilité d'obtenir des hydrogels de HA auto-réticulants à pH physiologique via des interactions multivalentes entre les unités de BOR greffées sur le HA et des groupements diols se répétant sur la chaîne polysaccharidique. Outre le BOR, la capacité de son homologue cyclique à six chaînons, la benzoxaborine, et d'un nouveau dérivé original similaire à ce composé a été explorée en tant que nouveaux sites de complexation de saccharides pour la formation de réseaux de HA réversibles. Compte-tenu des propriétés injectables, d'auto-réparation et de réponse à différents stimuli démontrées par ces nouveaux hydrogels de HA, ces biomatériaux apparaissent comme des candidats prometteurs pour de nombreuses applications innovantes dans le domaine biomédical, notamment pour l'ingénierie tissulaire et la thérapie cellulaire.